DEVELOPMENT OF FATIGUE LOADING SPECTRA

Potter/Watanabe, editors

ASTM

STP 1006

STP 1006

Development of Fatigue Loading Spectra

John M. Potter and Roy T. Watanabe

ASTM
1916 Race Street
Philadelphia, PA 19103

Library of Congress Cataloging-in-Publication Data

Development of fatigue loading spectra.

(ASTM special technical publication; 1006)
"ASTM publication code number 04-010060-30."
Includes bibliographies and index.
1. Materials—Fatigue—Testing. I. Potter,
John M., 1943- . II. Watanabe, Roy T.
III. Series.
TA418.38.D48 1989 620.1'123 88-35065
ISBN 0-8031-1185-1

NOTE

The Society is not responsible, as a body,
for the statements and opinions
advanced in this publication.

Peer Review Policy

Each paper published in this volume was evaluated by three peer reviewers. The authors addressed all of the reviewers' comments to the satisfaction of both the technical editor(s) and the ASTM Committee on Publications.

The quality of the papers in this publication reflects not only the obvious efforts of the authors and the technical editor(s), but also the work of these peer reviewers. The ASTM Committee on Publications acknowledges with appreciation their dedication and contribution of time and effort on behalf of ASTM.

Printed in Ann Arbor, MI
February 1989

Foreword

The symposium on Development of Fatigue Loading Spectra was held in Cincinnati, Ohio, 29 April 1987. ASTM Committee E-9 on Fatigue and SAE Committee on Fatigue Design and Evaluation sponsored the symposium. John M. Potter, Wright Patterson Air Force Base, and Roy T. Watanabe, Boeing Commercial Airplane Company, served as symposium cochairman and coeditors of this publication.

Contents

STP1006-EB/Feb. 1989

Overview

The continuing guest for efficient mechanical and structural designs has caused a steady rise in operating stresses as a proportion of design stresses and has placed long life requirements on the articles. Therefore, the cyclic stresses resulting from normal loading have become an important consideration in the design, analysis, and testing process. Similarly, there is ample evidence that loading variables such as amplitude, frequency, sequence, and phasing have a significant effect on fatigue crack initiation and propagation.

In order to review the latest developments in the analytical treatment of fatigue loads, a one-day symposium was held in Cincinnati, Ohio, on 29 April 1987. The symposium was jointly sponsored by ASTM Committee E-9 on Fatigue and the Society of Automotive Engineers (SAE) Fatigue Design and Evaluation Committee to review the state of art in characterizing and standardizing cyclic loads that are experienced by structures in service. This symposium is a sequel to the ASTM sponsored symposia on the Effect of Load Spectrum Variables on Fatigue Crack Initiation and Propagation (STP 714) held on 21 May 1979 in San Francisco, California, and Service Fatigue Loads Monitoring, Simulation, and Analysis (STP 671) presented in Atlanta, Georgia, 14–15 November 1977.

The authors addressed two broad areas of interest; (1) characterization of measured loads and (2) development of analytical and test load spectra from condensed data. The information in this volume should be useful to engineers responsible for collection and evaluation of service loads and to those involved in analyzing and testing structures subjected to repeating loads.

A large number of people contributed their time and energy to make the symposium a success. The editors would like to thank the authors for their contributions and the reviewers for their diligent editing of the manuscripts. We are also indebted to K. H. Donaldson and M. R. Mitchell, from the SAE-Fatigue Design and Evaluation Committee who served on the symposium planning committee and arranged reviewer support. The editors would like to thank symposium session chairmen A. L. Conle and J. W. Fash for their efforts.

J. M. Potter
AFWAL/STS, Wright-Patterson Air Force Base, OH 45433; symposium cochairman and coeditor.

R. T. Watanabe
Boeing Commercial Airplanes, Seattle, WA 98124; symposium cochairman and coeditor.

Walter Schütz[1]

Standardized Stress-Time Histories—An Overview

REFERENCE: Schütz, W., "**Standardized Stress-Time Histories—An Overview,**" *Development of Fatigue Loading Spectra, ASTM STP 1006*, J. M. Potter and R. T. Watanabe, Eds., American Society for Testing and Materials, Philadelphia, 1989, pp. 3–16.

ABSTRACT: After a short historical introduction, the reasons why standardized stress-time histories are necessary and useful are given. A standardized stress-time history must be based on several, preferably many, stress measurements in service. It must also be a fixed stress sequence, not just a spectrum for which an infinite number of stress-time histories are possible. It must be based on a cooperative effort of several competent laboratories, preferably from different countries. It must also be generally applicable to the structure or component in question. The truncation or omission levels, if any, must be clearly stated and must be substantiated by tests. A reasonable return period or block length must be also selected. Preferably, standardized stress-time histories should be used for:

1. comparison of materials, production processes, and design details as well as cooperative (round robin) test programs;
2. investigation of the scatter of fatigue life; and
3. producing preliminary fatigue design data for components etc.;

if the service loads on the component in question are of variable amplitude.

Five standardized stress-time histories available at present (Twist, FALSTAFF, Gauss, Helix-Felix, and Cold TURBISTAN) are briefly described as well as the six at present in progress (WASH, WALZ, WISPER, ENSTAFF, Carlos and hot TURBISTAN).

KEY WORDS: fatigue strength under variable amplitudes, standardized stress-time histories, truncation and omission levels, fatigue (materials), testing, fatigue testing

As soon as one leaves the constant-amplitude fatigue test (which is completely defined by two numbers, that is, stress amplitude and mean stress), in principle an infinite number of different stress-time histories is possible—even for the same spectrum shape—and much more so for different spectrum shapes. It is therefore not surprising that many experts have recommended the development and use of standardized stress-time histories, among them Barrois [*1*] and Schijve [*2*], both for aircraft purposes.

Long before that time, the eight-step blocked program test of Gassner in 1939 [*3*] was the first standardized stress-time history; considering the capabilities of the test machines of that time, nothing more complex was attainable. The computer-controlled servohydraulic test machines [*4*] introduced in the late 1960s and early 1970s had the big advantage that there was no limitation whatever on the stress-time histories possible; but that was also their main disadvantage. Many different stress-time histories have been employed indiscriminately, sometimes even without a sufficient description. Therefore, the results were not

[1] Department head, Industrieanlagen-Betriebsgesellschaft (IABG), D-8012 Ottobrunn, Einsteinstrasse 20, West Germany.

usable for anyone but the author himself; moreover, the results of different test programs were not comparable.

This may not be of importance in ad hoc type tests, but for general fatigue investigations it will produce a confusing situation or, worse, it may even result in qualitatively wrong conclusions.

Requirements to be Met by a Standardized Stress-Time History

The basis of a meaningful standardized stress-time history are strain or load measurements in service, preferably from a considerable number of similar structures; for example, several transport aircraft types. From these many measurements, common features must be extracted; that is, their spectrum shapes must be similar. What constitutes "similarity" in this respect is a difficult question. However, one measurement alone is not enough, as just this one structure may have some special feature, resulting in a spectrum dissimilar to those of all the others. Assuming stress spectra for several or many structures *are* available, an "average" spectrum must then be selected and a logical sequence of individual cycles must be decided upon; for example, a flight always begins with taxiing, followed by the ground-to-air cycle, and so on.

In some cases, the comparison of several measurements may not show a sufficient similarity. It will then be necessary to use two (or at most three) different spectra and, consequently also two (or at most three) different stress-time histories. This has happened with Helix and Felix for helicopters and Cold TURBISTAN and Hot TURBISTAN for gas turbines (see later discussion). A larger number of different stress-time histories would run contrary to the objective of standardization.

Reasons for requiring a stress-time history and not just a spectrum were previously given. Only if the position and size of each and every cycle is fixed in the sequence will the results be really comparable. If only the spectrum were fixed, an infinite number of stress-time histories could be synthesized (reconstituted) from this one spectrum, possibly resulting in different fatigue lives.

Exceptions to this requirement may be necessary. For example, the WASH working group [5] chaired by the author may decide to recommend one or two specific stress histories as the standardized ones, yet leave the option open to potential users to synthesize different sequences for their special purpose, if they have good reasons for it.

Another requirement is that a standardized stress-time history must be a cooperative effort of several laboratories and firms, preferably from different countries. The reasons for this requirement are both technical and psychological: stress measurements from several structures should be available as just explained, and they are often not available from just one laboratory. In the case of tactical aircraft, for example, one country may fly only one type and if this would result in a standardized stress-time history, for example, for the F-5, it would be a contradiction in itself. This would also preclude its use by other laboratories. Also, not many laboratories in the world have the expertise necessary to develop a reasonable and meaningful standardized stress-time history all by themselves.

There have been several attempts at standardizing stress-time histories by individual laboratories—the author is aware of two in Germany, one in Great Britain, and one in the United States (for different structures), but they have been singularly unsuccessful.

Another requirement must be general applicability of the standardized stress-time history for the type of structure in question. If a sufficient similarity of spectra cannot be established, that is, if the stress measurements on several different tactical aircraft gave very dissimilar spectra, a standardized stress history will not be possible. Up to now, this has never been the case for transport aircraft (Twist) [*6–8*], for tactical aircraft (FALSTAFF) [*9–11*], for helicopters (Helix and Felix) [*12–14*], and for disks of gas turbine compressors (Cold TURBISTAN) [*15*]. It was sometimes necessary to limit the applicability of the standardized stress-time history to specific sections of the structure in question; for example Helix and Felix are *strictly* representative only for helicopter rotors in the vicinity of the hub and FALSTAFF for the wing lower surface stresses near the wing-fuselage joint of tactical aircraft.

The last, but not least, requirement concerns the selection of correct truncation and omission levels and return period lengths. Large but infrequent tensile maximum stresses may actually prolong fatigue life due to the beneficial residual stresses they cause. Thus, if the test is carried out with these too high infrequent tensile stresses, the fatigue life in test will most probably be unconservative. So the correct choice of the highest stress amplitude to be employed in the standardized stress-time history, the so-called "truncation dilemma" [*16*], is an important decision. Some experts have suggested that the highest stress amplitudes in the stress-time history should occur not less than ten times [*17*] before failure.

Long-life structures, like oil rigs, ships, trucks, automobiles etc., see more than 10^8 cycles during their service life, too many for an economically feasible standardized stress-time history. So the question is how best to decrease this large number of cycles. In a typical wave spectrum for instance, a reduction of the number of cycles by one order of magnitude means that all stress amplitudes lower than 15% of the maximum amplitude are omitted. Usually, this is below 50% of the fatigue limit, which has been shown to be a reasonable omission criterion [*18*] for normal specimens. For rivetted joints, this omission level may already be too high, as the experience with Minitwist shows (see discussion on presently available programs).

If the number of test cycles has to be reduced still further (for example, if a low test frequency is thought to be necessary, as in some corrosion fatigue tests), further omission may run into the problem of the "omission dilemma" [*16*] where the stress amplitudes left out may be near or above the fatigue limit and the resulting fatigue life in test will be different.

Nevertheless, the allowable omission level should be determined by test. That is one complete stress-time history and one in which one or more low stress levels are omitted must be used to determine by test if the two fatigue lives are identical.

The requirement that the exact sequence of stress cycles must be fixed in the stress-time history means that the sequence must be repeated after a certain number of cycles. The length of this so-called return period is critical. On the one hand, it has to be repeated several times until failure occurs; otherwise, the full variety of stress amplitudes is not contained in the standardized stress-time history in their correct percentages. On the other hand, too short a return period means that infrequent but high-stress amplitudes are not contained in the stress-time history, while they do occur in service and will affect fatigue life. That is a kind of "truncation dilemma in reverse." The load spectrum applied in test is thus quite different from that in service.

The effect is shown in Fig. 1: Assuming a service stress spectrum of 10^8 cycles, a return period of 10^4 cycles has to be repeated 10^4 times in test. Thus, a test spectrum will have been applied in which all stress amplitudes above 50% of the maximum stress amplitudes occurring in service have been truncated. Such a test will most certainly not give the correct result.

With respect to the return period length, the international literature is full of serious errors, one example being the well-known Society of Automotive Engineers (SAE) program

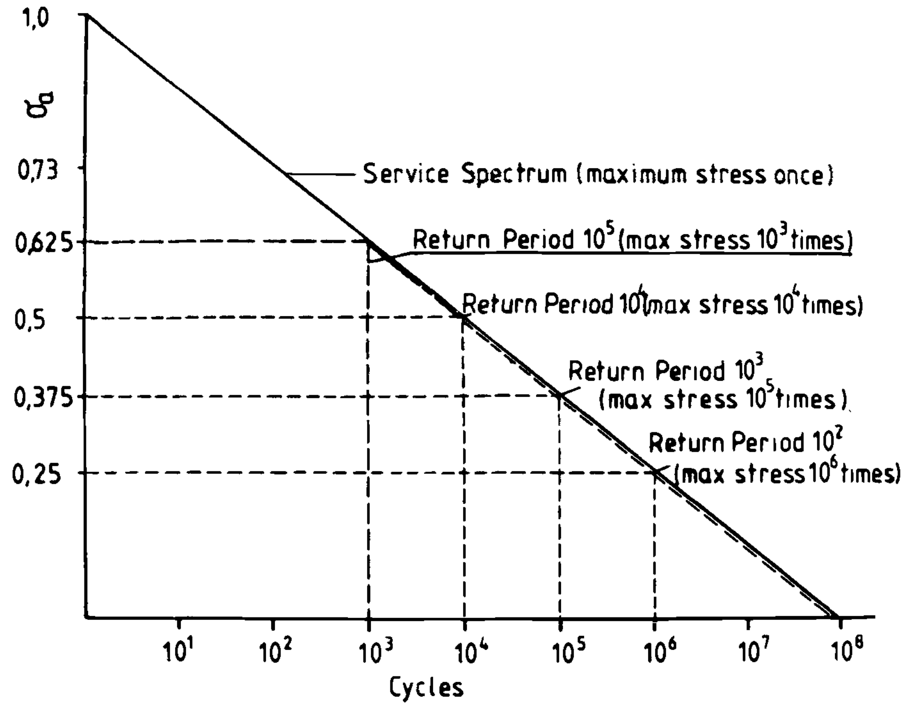

FIG. 1—*The spectrum shape at long fatigue lives under return periods that were too short.*

[*19*]. The return periods of 1500 to 4000 cycles that were used because of the limitations of the computers of that time [*20*] are just not long enough, as can be seen in Fig. 1: for a required fatigue life of 10^8 cycles to failure, a spectrum shape as shown in Fig. 1 and a return period of 10^3 cycles, the highest stress amplitude, occurs 10^5 times. This is practically a constant-amplitude test with this stress amplitude. Moreover, all stresses above 37.5% of the maximum stress amplitude are truncated with the attendant consequences discussed previously. The fatigue life prediction models developed in this program gave especially unconservative results [*20*], when employed for predicting the life under the standardized stress-time history Gauss [*21–23*], which has a return period length of 10^6 cycles. Another SAE program is now in progress with more reasonable return period lengths [*24*].

In some cases, the length of the return period can be decided quite simply. For instance, tactical aircraft in peacetime are flown in a similar manner year by year for training purposes. So a logical return period is one year, and this was chosen for the FALSTAFF sequence [*11*].

Also, some decisions will have to be made, for example, when the maximum stress amplitude should occur in the stress-time history. It is, for example, highly improbable for transport aircraft that this event should happen right at the beginning of the return period.

In the standardized stress-time history Gauss developed by Laboratorium für Betriebsfestigkeit (LBF) and Industrieanlagen-Betriebsgesellschaft (IABG) [*21–23*], it is applied at the middle of the return period of 10^6 cycles, that is after about 5×10^5 cycles. Deterministic or abuse events (like hitting a curbstone) may also need to be added by individual users.

Applications for Standardized Stress-Time Histories

Standardized stress-time histories can be used to advantage in many cases such as:

1. Evaluation of the fatigue strength of notched specimens as well as actual components, especially components made from different materials.
2. Evaluation of fatigue data for preliminary design of components.
3. Evaluation of the scatter of fatigue life data.
4. Determination of permissible stresses for preliminary fatigue design of components (combination of Points 2 and 3).
5. Assessment of models for the prediction of fatigue and crack propagation life by calculation, like Miner's rule.
6. Comparison of design details, like the effect of fillet radius sizes or of different fastener systems.
7. Investigation of processes for improving fatigue life, like shot peening, heat treatment, etc.
8. Round-robin programs on general fatigue or crack propagation problems in which several laboratories participate.

According to Edwards and Darts [*14*],

> The development of standardized stress-time histories has arisen from the fact that, often, life prediction methods are not accurate enough to predict fatigue lives or crack rates adequately under service (variable amplitude loading) conditions. Therefore when making a fatigue assessment of, for instance, a new detail, fastening system or method of life improvement, variable amplitude loading has to be used. Often such tests are not tied specifically to any particular project, but are for more general application. In this case a standard sequence, provided a relevant one exists, is often the best choice for the test loading. The advantage of using standard sequences in this situation is that any resulting data can be compared directly with any other obtained using the same standard as well as being capable of being used as design data.
>
> Experience has shown that, following the definition of a standard sequence, a wealth of relevant data accumulates quickly, negating the need for some tests and giving extensive comparative data for others. This can greatly increase the technical value of individual test results and reduce the amount of expensive fatigue testing. Large evaluation programs using standard sequences can be shared more readily between different organisations and countries because the test results of the program will be compatible with each organisation's own standard data.

Standardized Stress-Time Histories Available at Present

Most of the standardized stress-time histories available at present are shown in the upper division of Table 1, those in progress at the moment are listed in the center of Table 1, and abbreviated versions of some of the available programs are shown in the lower part. The table also shows the laboratories and companies that cooperated in these efforts as well as their respective start and final report dates.

Twist (transport wing standard) [*6–8*] was the first cooperative program; it was developed by the LBF in Germany together with National Aerospace Laboratory (NLR) in the Netherlands. The return period length is 4000 flights, and the corresponding number of cycles is about 400 000. It contains ten different flights, four of which are displayed in the lower half of Fig. 2. The upper half of Fig. 2 shows the spectrum for 40 000 flights based on a level crossing count of gust load cycles, the ground-to-air-to-ground cycle, and taxi load

TABLE 1—*Standardized stress-time histories.*

Name	Purpose	Participants	Finished
Twist	transport Wing Standard	LBF, NLR	1973
Gauss	Gaussian sequence with $i = N_0/N_i =$ 0.99, 0.7, 0.33	LBF, IABG	1975
FALSTAFF	fatigue loading standard for fighters	NLR, F+W Emmen, LBF, IABG	1976
Helix and Felix	helicopter loading standard for fixed (Felix) and hinged (Helix) rotors	NLR, LBF, RAE, IABG, MBB	1984
Cold TURBISTAN	cold compressor disk loading standard	RR, Snecma, LBF, IABG, RAE,	1987
Hot TURBISTAN	Hot compressor and turbine disk loading standard	Technical University of Aachen; CEAT, MTU, University of Utah; NLR	start in 1986
WASH	offshore structures loading standard	LBF, NEL, IABG, University College, GL, University of Waterloo, SINTEF, University of Pisa, IFREMER, Riso Labs	start in 1984
Walz	steel-mill drive loading standard	LBF, IABG, BFI, University of Karlsruhe, University of Clausthal	start in 1986
Wisper	wind turbine loading standard	BAe,[a] IABG; GL, DFVLR Stuttgart, NLR, Riso Labs, ECN, FFA, etc.	start in 1985
ENSTAFF	environmental FALSTAFF	LBF, IABG, RAE, CEAT, F+W Emmen, NLR	start in 1983
Carlos	car component loading standard	LBF, IABG, Opel, Porsche, BMW, Daimler Benz, Audi, Volvo, Fiat, Peugeot	start in 1987
Minitwist	shortened twist	NLR, LBF	1979
Short FALSTAFF	shortened FALSTAFF	CEAT	about 1980
Mini Helix and Felix	shortened Helix and Felix	as for Helix and Felix	1985

[a] British Aerospace.

cycles. In the standardized stress-time history, the taxi loads were omitted, because they were assumed not to contribute any fatigue damage.

Twist is based on center of gravity measurements on DC-9, Boeing 737, BAC 1-11 and, "Transall" aircraft and on the theoretical frequency distributions of DC-10, F-27, and F-28 aircraft.

The Twist stress-time history has been used for several test programs in Europe and in the United States. The corresponding software for the computer control of servohydraulic test machines is availabe from all major test machine manufacturers.

The LBF and NLR also cooperated in developing a shortened version of Twist, called Minitwist [25], as the number of cycles were considered to be too large for some applications.

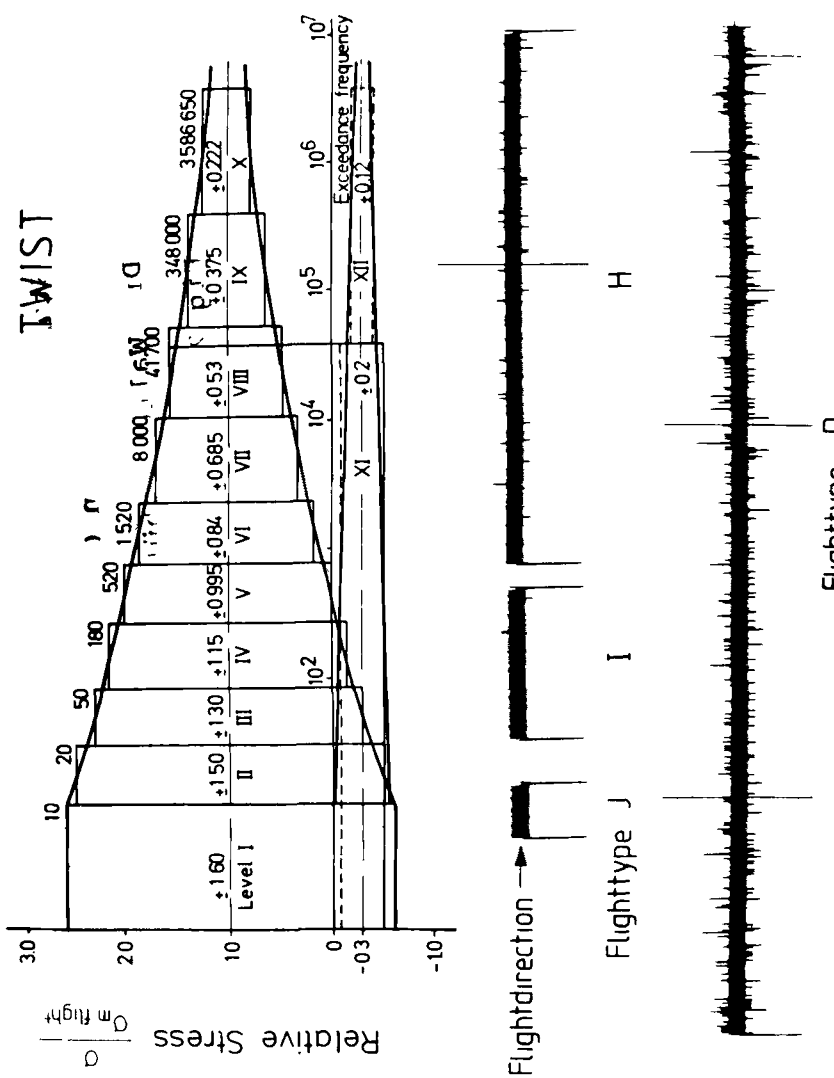

FIG. 2—*Spectrum and a section of the stress-time history for Twist.*

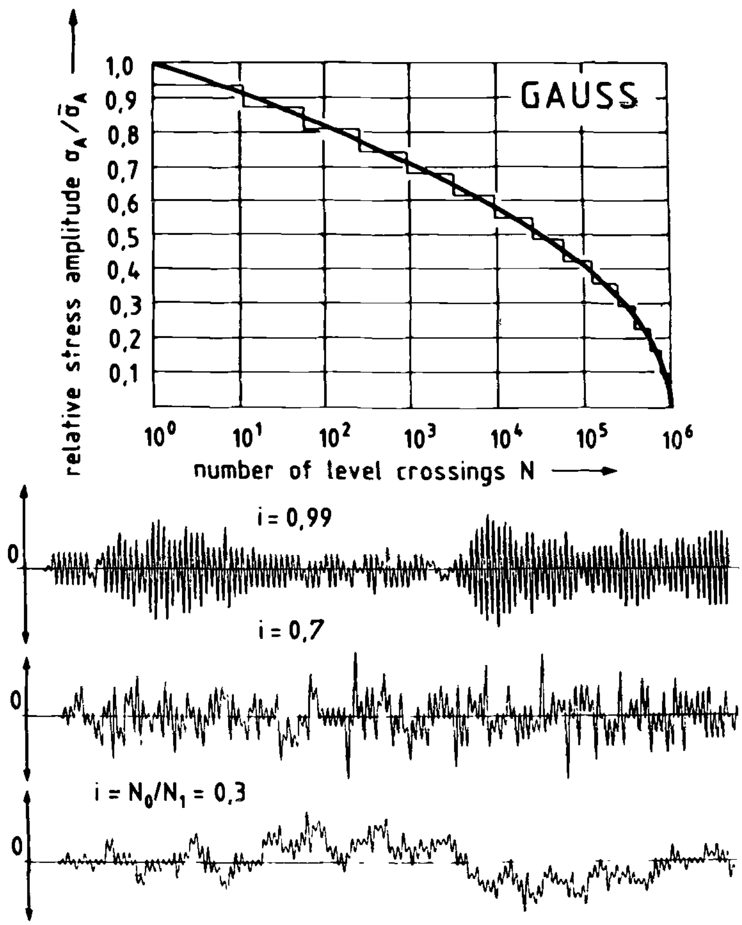

FIG. 3—*Spectrum and three sections of the stress-time history with different irregularity factors for Gauss.*

In testing small components, a life at 100 000 to 200 000 flights to failure is required, which corresponds to 10^7 to 2×10^7 cycles. In the Minitwist stress-time history, the average number of cycles per flight was reduced from 100 to 15. Somewhat unexpectedly, this reduction increased the fatigue and crack propagation life by a factor of about two [*25–28*].

Historically, the next standardized stress-time history was Gauss [*16–18*], developed by IABG and LFB. It was *not* based on specific stress measurements, but on the general experience from extensive measurements carried out by the LBF on automobile components in service, which revealed that roads of similar surface conditions result in nearly stationary Gaussian processes. Therefore, it was decided to standardize the exactly defined Gaussian process for this stress-time history. The level crossing-counted spectrum is shown in Fig. 3. It can be obtained by an infinite number of different stress-time histories with different irregularity factors. Two extremes (i = 0.3 and 0.99) and a medium one (i = 0.7) were chosen to cover the wide field of practical cases. The return period is 10^6 cycles, corresponding to about 3.000 to 10.000 road kilometres for automobiles. Gauss is to be employed for general fatigue investigations; for example, the assessment of fatigue life prediction models in the crack initiation and propagation phases, comparison of different materials, and so on.

Gauss has found wide acceptance in Germany, especially for automotive fatigue programs. It was also used in other countries [20], and is being used at present in an Advisory Group for Aerospace Research and Development (AGARD) round-robin program on short cracks by laboratories in Germany, the Netherlands, Great Britain, and the United States. The corresponding software is available from all the major test machine manufacturers.

The FALSTAFF (Fighter Aircraft Loading Standard for Fatigue) [9–11] stress-time history has found the greatest acceptance of them all. For example, it has been employed over the last ten years in many AGARD round-robin programs on corrosion fatigue, critically loaded holes, rivetted joints, short cracks, and fatigue rated fasteners, in which a large number of laboratories in Europe and North America participated. Moreover, to the author's knowledge it has been used in every western country capable of running computer-controlled servohydraulic tests.

It is based on load factor and stress measurements of F 104 G, Fiat G-91, Northrop

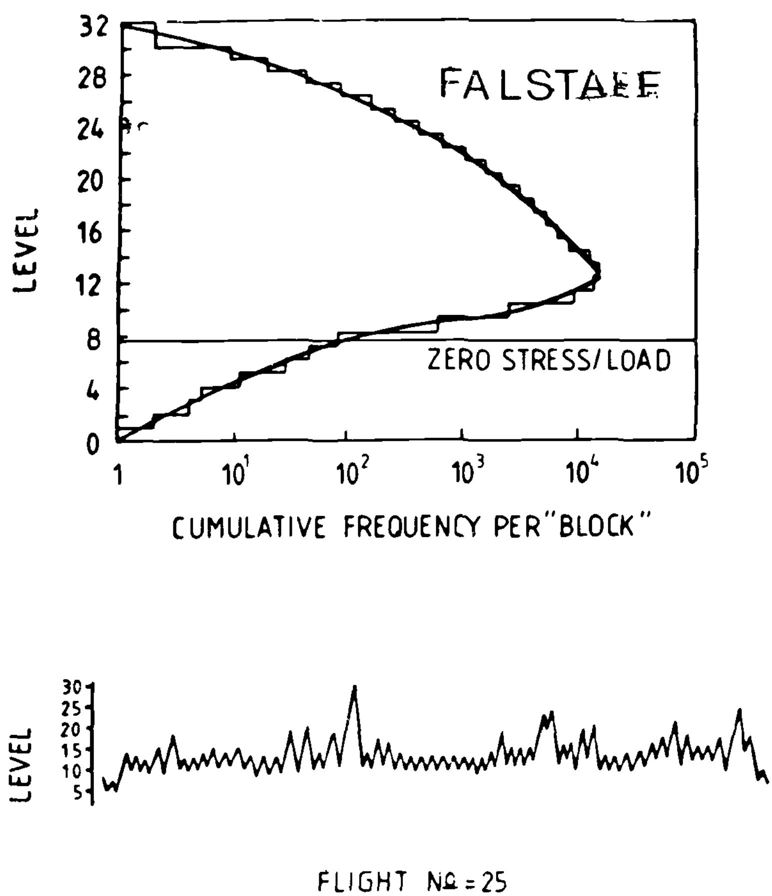

FIG. 4—*Spectrum and Flight No. 25 of the stress-time history FALSTAFF.*

NF-5A, and Dassault Mirage III fighter aircraft contributed by the four cooperating laboratories NLR, LBF, Flugzeugwerke Emmen (F+W Emmen) (Switzerland), and IABG.

The length of the return period is 200 flights, corresponding to one year of service. This resulted in roughly 16 000 cycles. The FALSTAFF stress-time history contains 200 different flights. The level crossing-counted spectrum and one typical flight are shown in Fig. 4.

The software is again obtainable from the major fatigue test machine makers.

Short-FALSTAFF was developed by Centre d'Essais Aeronautique de Toulouse (CEAT) around 1980, because their control computers at that time had insufficient storage capacity [*29*]. The average number of cycles per flight was decreased from 90 to 45. Contrary to the experience with Minitwist, practically no effect of this reduction on fatigue and crack propagation life was found [*27,30*].

Helix (for hinged or articulated rotors) and Felix (for fixed or semirigid rotors) of helicopters came next [*12–14*]. Four laboratories (LBF, IABG, NLR, and the Royal Aircraft Establishment (RAE)) and one manufacturer (Messerschmidt-Bölkow-Blohm [MBB]) cooperated. Operational data and stress measurements data were evaluated from two helicopters with hinged rotors, namely, the Westland Sea King and the Sikorsky CH-53 D/G, and two helicopters with fixed rotors, the Westland Lynx and the MBB Bo-105. It became apparent quite early in the program that the spectra for the two different rotor designs were

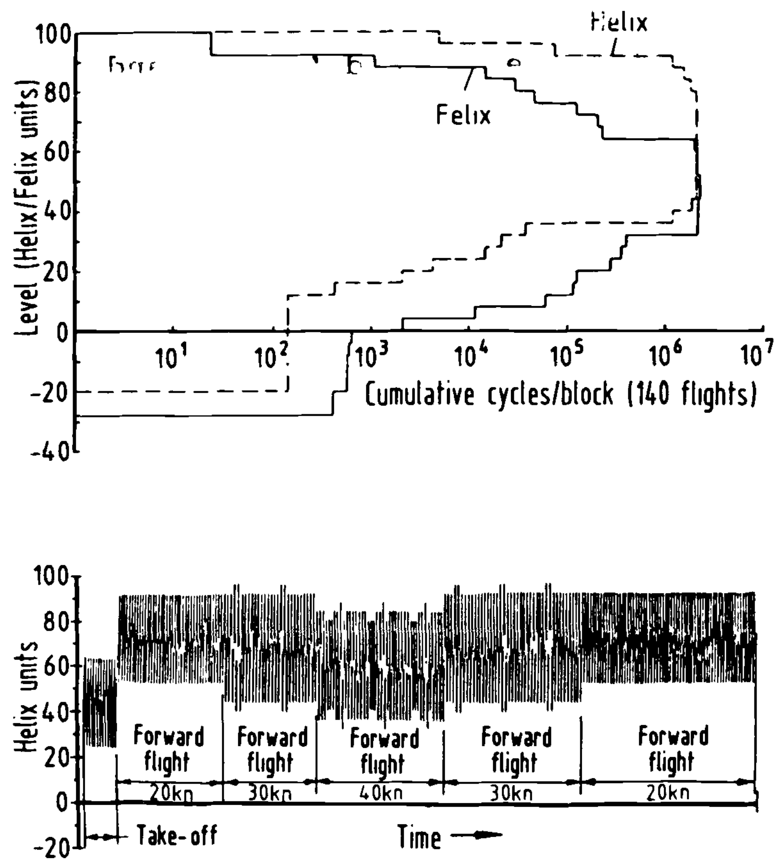

FIG. 5—*Spectra Helix and Felix and one typical Helix-flight.*

fundamentally different, and that two standardized stress-time histories would be needed. The resulting two level-crossing counted spectra are shown in Fig. 5, together with a Helix training flight. The return period length is 140 flights, where 12 different flights are employed, consisting of four different flight types (training, transport, Anti-Submarine Warfare, and Search and Rescue) and of three different lengths each.

Due to the high-frequency loading of helicopter rotors in service, the number of cycles for the 140 flights is more than two million, resulting in formidable testing times. To reduce these, shortened versions were developed and are included in the original report [*14*]; they give a reduction in return period length of 93% for both Helix and Felix, albeit at a two to four times longer fatigue life.

As Helix and Felix are comperatively new, the author is not aware of its employment

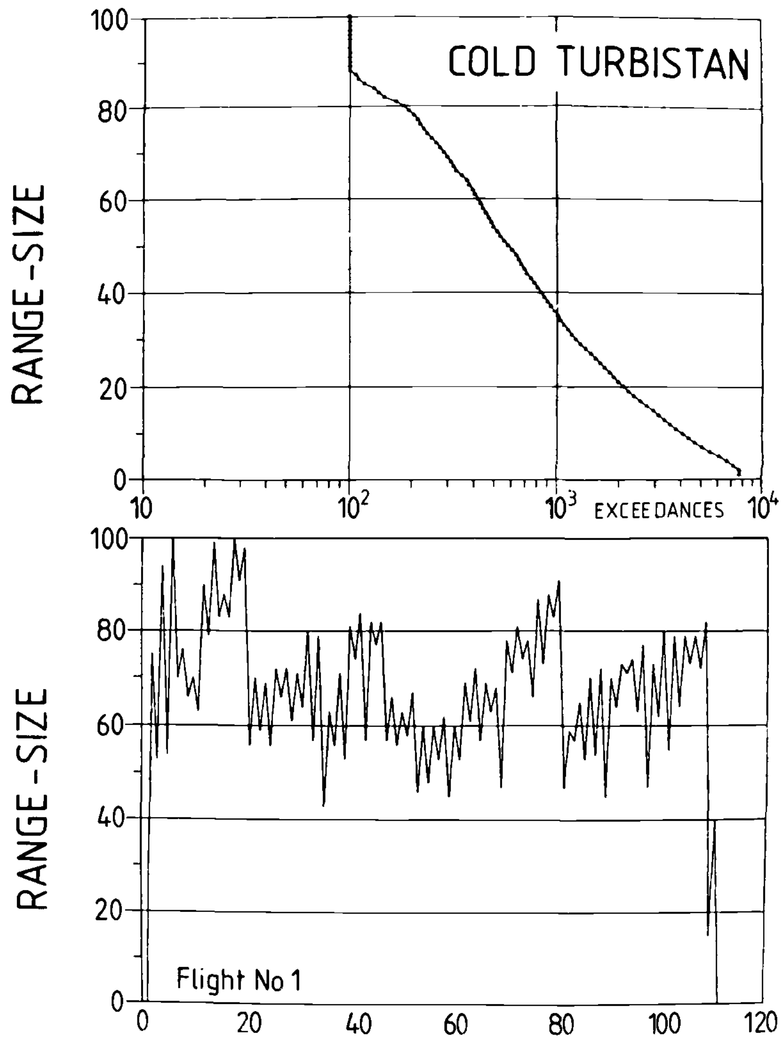

FIG. 6—*Spectrum and Flight No. 1 of the stress-time history Cold TURBISTAN.*

outside of his own department, except for the tests carried out during the development.

The cooperative program for Cold TURBISTAN [15] for cold (low pressure) compressor disks of gas turbines of tactical aircraft terminated in 1986. The final report was published in 1987; however, a comprehensive paper was given at this symposium [31]. Measured rpm-data from five different gas turbines in service in European Airforces were the basis. Ten laboratories (one of them in North America, two from gas turbine manufacturers) cooperated. The rainflow-counted spectrum, plotted with the mean stresses deleted is shown in Fig. 6, as well as one typical flight. The return period length is 100 flights, which are all different, and the number of cycles is 7726.

Due to its newness, to the author's knowledge only the author's department has used Cold TURBISTAN up to now. However, the AGARD Engine Disk Material Cooperative Program, in which at least nine European and North American laboratories are involved, does employ the Cold TURBISTAN stress-time history.

Standardized Stress-Time Histories under Development

After the success of some standardized stress-time histories for aircraft structures, it was only natural that other applications for this idea were sought.

The first one was WASH (Wave Action Standard History). First contacts with other laboratories date back to 1979, but due to lack of funds, the work actually started in 1984. Ten laboratories, one of them in Canada, are cooperating, see Table 1. More details have been presented by Pook at this symposium [5]. Measured stress-time histories from a number of platforms are available, more will probably be forthcoming. There will be at least two standardized stress-time histories. Potential users will also probably have the option to generate (from the same spectrum) other stress-time histories, which then cannot be called standardized.

The growing use of carbon fiber reinforced composites in aircraft with their susceptibility to moist environments led to the formation of the ENSTAFF (environmental FALSTAFF) working group, consisting of six European laboratories, see Table 1. ENSTAFF is the FALSTAFF stress-time history combined with a humidity-temperature time history derived from typical European meterorological data. More details were presented at the 1987 ICAF-symposium in Ottawa [32], the final report was scheduled for the end of 1987.

Hot TURBISTAN for disks of gas turbines, which see thermal strains and stresses (as well as mechanical ones), is being developed by the same working group as Cold TURBISTAN. The work has just started. More details were presented in two other papers of this symposium [31,32].

Severe fatigue problems, some of them catastrophic, with practically every wind turbine type with steel blades, led to the formation of the WISPER (wind turbine spectrum reference) working group. The laboratories involved are shown in Table 1. Stress measurements from no less than eleven wind turbines with rotor diameters of 12 to 100 m are available. More details will be presented at this symposium by ten Have [33].

In Germany, like in many other countries, the steel production industry has had a large number of fatigue failures. Their explanation and prevention is difficult, due, among other things, to the large size of the components, which cannot be tested in the laboratory. Usually Miner's rule is used to derive allowable stresses for design. The required *S-N* curves are based on small specimen data with a reduction to allow for the size effect.

A German working group was formed in 1986 under the preliminary name of Walz. One or more standardized stress-time histories will be developed for steel-mill drive systems by the five participating laboratories. At least 14 service stress measurements are already available.

The automobile industry in Germany has employed variable-amplitude testing for decades. Except for the eight-step blocked program test of Gassner [3], which was the first standardized stress-time history, it has very often used actual service stress measurements to control its servohydraulic test machines; that is, it has typically run ad-hoc tests.

However, in 1985 a working group was formed to develop standardized stress-time histories for typical automobile components. Due to nontechnical reasons, this proved to be a false start and a new group was formed in early 1987, consisting of LBF, IABG, and the German manufacturers mentioned in Table 1. Membership, however, is open to all other automobile firms; some European ones have already joined, see Table 1.

References

[1] Barrois, W., Symposium on Random Load Fatigue, AGARD-CP-118, Advisory Group for Aerospace Research and Development, Lyngby, Denmark, 1972.

[2] Schijve, J., Symposium on Random Load Fatigue, AGARD-CP-118, Advisory Group for Aerospace Research and Development, Lyngby, Denmark, 1972.

[3] Gassner, E., Festigkeitsversuche mit wiederholter Beansprunchung im Flugzeugbau, Deutsche Luftwacht, Ausgabe Luftwissen, Feb. 1939.

[4] Schütz, W. and Weber, R., *Materialprüfung*, No. 11, 1970, pp. 369–372.

[5] Pook, L. P. and Dover, W. D., "Progress in the Development of a Wave Action Standard History (WASH) for Fatigue Testing Relevant to Tubular Structures in the North Sea," in this volume, pp. 99–120.

[6] Schütz, D., *Proceedings*, Seventh ICAF Symposium, International Committee of Aeronautical Fatigue, Vol. 2, 1973, pp. 3.4/1–3.4/34.

[7] Schütz, D., Technische Mitteilungen, Laboratorium für Betriebsfestigkeit, TM No. 55/70, 1972.

[8] Schütz, D., Lowak, H., De Jonge, J. B., and Schijve, J., "Standardisierter Einzelflug-Belastungsablauf für Schwingfestigkeitsversuche an Tragflächenbauteilen von Transportflugzeugen," NLR Report TR 73, LBF Bericht No. FB-106, National Aerospace Laboratory, The Netherlands, 1973.

[9] Van Dijk, G. M. and De Jonge, J. B. in *Proceedings*, 8th ICAF Symposium, International Committee on Aeronautical Fatigue, Lausanne, 1975, pp. 3.61/1–3.61/39.

[10] Hück, M. and Schütz, W. in *Proceedings*, 8th ICAF Symposium, International Committee on Aeronautical Fatigue, Lausanne, 1975, pp. 3.62/1–3.62/23.

[11] Aicher, W., Branger, J., Van Dijk, G. M., Ertelt, J., Hück, M., De Jonge, J., Lowak, H., Rhomberg, H., Schütz, D., and Schütz, W., "Description of a Fighter Aircraft Loading Standard for Fatigue Evaluation "FALSTAFF"," Common Report of F+W Emmen, LBF, NLR, IABG, March 1976.

[12] Schütz, D., Köbler, H.-G., Schütz, W., and Hück, M., *Helicopter Fatigue Life Assessment*, AGARD-CP-297, Advisory Group for Aerospace Research and Development, 1981, pp. 16.1–16.7.

[13] Darts, J. and Schütz, D., *Helicopter Fatigue Life Assessment*, AGARD-CP-297, Advisory Group for Aerospace Research and Development, 1981, pp. 16.1–16.38.

[14] Edwards, P. R. and Darts, J., "Standardized Fatigue Loading Sequence for Helicopter Rotors (Helix and Felix)," RAE TR 84084, Royal Aircraft Establishment, Parts 1 and 2, Aug. 1984.

[15] Mom, A. J. A., Evans, W. J., and ten Have, A. A., *Damage Tolerance Concepts for Critical Engine Components*, AGARD-CP-393, Advisory Group for Aerospace Research and Development, 1985, pp. 20.01–20.11.

[16] Crichlow, W., *On Fatigue Analysis and Testing for the Design of the Airframe*, AGARD-LS-62, Advisory Group for Aerospace Research and Development, 1973.

[17] Schijve, J., "The Significance of Flight-Simulation Fatigue Tests," Delft University of Technology, Report LR-466, June 1985.

[18] Heuler, P. and Seeger, T., *International Journal of Fatigue*, No. 4, 1986, pp. 225–230.

[19] Wetzel, R. M., *Fatigue Under Complex Loading: Analysis and Experiments*, Society of Automotive Engineers, 1977.

[20] Fash, J., *SEECO '83, Digital Techniques in Fatigue,* Society of Environmental Engineers, 1983.
[21] Haibach, E., Fischer, R., Schütz, W., and Hück, M., *Fatigue Testing and Design, SEE Proceedings,* Society of Environmental Engineers, April 1976, pp. 29.1–29.21.
[22] Fischer, R., Köbler, H.-G., Schütz, W., and Huck, M., "Kriterien für die Bewertung der Schwingfestigkeit von Werkstoffen and Bauteilen für laufende und zukünftige Projekte," IABG-Bericht No. 142 246 01, Industrieanlagen-Betriebsgesellschaft, 1975, LBF-Bericht No. 2909, 1975.
[23] Fischer, R., Hück, M., Köbler, H.-G., and Schütz, W., "Eine dem stationären Gaußprozeß verwandte Beanspruchungs-Zeit-Funktion für Betriebsfestigkeitsversuche," Düsseldorf, VDI-Forschungsberichte, Reihe 5, Nr. 30, 1977.
[24] Personal information given to the author by Prof. Socie in 1985 at the International Committee of Aeronautical Fatigue meeting, Pisa, Italy.
[25] Lowak, H., De Jonge, J. B., Franz, T., and Schütz, D., "Minitwist, a shortened version of Twist," LBF-Report TB 146, NLR-Report MP 79018 U, Laboratorium für Betriebsfestigkeit, 1979.
[26] Ichsan, "Fatigue crack propagation in 2024-T3 aluminum alloy sheet material under different types of loading," thesis, Delft University of Technology, 1983.
[27] Schijve, J., Vlutters, A. M., Ichsan, and Provokluit, I. C., "Crack growth in aluminium alloy sheet material under flight simulation loading: A comparison between 'Twist' and 'Minitwist', 'FALSTAFF' and 'short FALSTAFF'," Delft University of Technology, Report LR-441, 1984.
[28] De Jonge, J. B. and Van Nederveen, A., "The Effect of Gust Alleviation on Fatigue and Crack Growth in Alclad 2024-T3," *Effect of Load Variables on Fatigue Crack Initiation and Propagation, ASTM STP 714,* Bryan and Potter, Eds., American Society for Testing and Materials, Philadelphia, 1980.
[29] CEAT Report M 7 681 900, Centre d'Essais Aeronautique de Toulouse, 1980.
[30] Vlutters, A. M., "Crack Growth Flight Simulation Tests with FALSTAFF and a Shortened Version, Mini-FALSTAFF at Two Design Stress Levels," thesis, Department of Aerospace Engineering, Delft University of Technology, 1982.
[31] Breitkopf, G. E., "Basic Approach in the Development of TURBISTAN, a Loading Standard for Fighter Aircraft Engine Disks" in this volume, pp. 65–78.
[32] Schütz, D. and Gerharz, J. J., *Proceedings* 14th ICAF Symposium in Ottawa, International Committee of Aeronautical Fatigue, June 1987, Engineering Materials Advisory Services.
[33] ten Have, A. A., "European Approaches in Standard Spectrum Development" in this volume, pp. 75–35.

Aalt A. ten Have[1]

European Approaches in Standard Spectrum Development

REFERENCE: ten Have, A. A., **"European Approaches in Standard Spectrum Development,"** *Development of Fatigue Loading Spectra, ASTM STP 1006,* J. M. Potter and R. T. Watanabe, Eds., American Society for Testing and Materials, Philadelphia, 1989, pp. 17–35.

ABSTRACT: Typical characteristics of various types of service loading are presented as they were discussed during the establishment of standardized test load sequences. Counting methods are reviewed and a simple and powerful algorithm is given to perform rainflow counting and to store the counting results afterwards. Synthesis procedures are discussed that generate rainflow consistent load sequences from matrix-based counting results.

KEY WORDS: fatigue load spectra, loading standards, counting methods, rainflow analysis, Markov matrix, rainflow synthesis, fatigue (materials), testing

At present, it is generally accepted that fatigue tests under constant amplitude or blocked loading insufficiently represent the interaction effects between individual load cycles of a more realistic type of loading. Together with developments in data processing methods and testing capabilities this has caused variable-amplitude loading is now widely appreciated in fatigue testing.

In order to produce reliable fatigue life or crack growth data for a specific structure, test loads are required that simulate the anticipated loading for that structure as accurately as possible. If, on the other hand, the aim is to evaluate materials, fabrication techniques, design solutions, surface treatments, analytical prediction methods, etc., the demand for similarity between service loading and test loading is not as stringent. In these cases, test loading is required that adequately represents the common type of loading on those kinds of structures by incorporating each fatigue-related parameter according to its respective relevancy. By standardizing the test load sequences in these cases, it becomes possible to exchange and compare variable-amplitude test results of various origins while also a data bank may be built up containing many spectrum reference data.

Some 20 years ago, this was realized within some of the European aeronautical institutes. Since then a number of international working groups have been acting, which has led to the definition of loading standards for:

1. fighter aircraft lower wing skins (FALSTAFF),
2. transport aircraft lower wing skins (TWIST, MiniTWIST),
3. helicopter rotor blades (Helix, Felix),
4. tactical aircraft cold-end engine disks (Cold TURBISTAN), and
5. tactical aircraft wing skin composites (ENSTAFF),

[1] Research engineer, National Aerospace Laboratory NLR, Amsterdam, The Netherlands.

while loading standards are currently being developed for:

1. tactical aircraft hot-end engine disks (Hot TURBISTAN),
2. horizontal axis wind turbine blades (WISPER), and
3. off-shore structures (WASH).

When considering these programs, a common approach may become evident with respect to the subsequent development steps. It is the intention of this paper to highlight what might be called the common European approach in the definition of a loading standard and to discuss the data handling techniques that are currently in use.

Loading Characteristics

A general description of fatigue loading is: the ensemble of individually occurring structural load variations having a certain magnitude and, above all, appearing in a certain sequence. Depending on the material used and its structural application, there will be a set of underlying parameters determining the damaging effect of the loading. In most cases, this leads to time domain techniques that are required to evaluate fatigue loading, that is, counting techniques that search for occurrences of load extremes, exceedings or crossings of specific load levels, and occurrences of load variations or ranges of specific size. Similar techniques are needed to use counting results for reconstruction of test load sequences again.

In terms of time domain parameters, the structure of any type of service loading can be described as a sequence of separate modes of operation. Such a mode is the major building stone of the loading and is either a flight (aerospace application), a continuous period of operation (wind turbine), or a sea-state (off-shore structure). Within each mode the subsequent load reversals occur, which are the smallest elements of the loading. In cases where grouping of load reversals occurs that are in some way interrelated, a loading element of intermediate level can be distinguished, called an event. Typical events are flight phases (cruise, approach, etc.), maneuvers, single operational procedures (emergency stop), or periods under stationary conditions (constant average wind speed). In Fig. 1, this structural build-up of fatigue loading is shown schematically. A loading standard will have to reflect these characteristics in the same way. To illustrate this, the present loading standards are

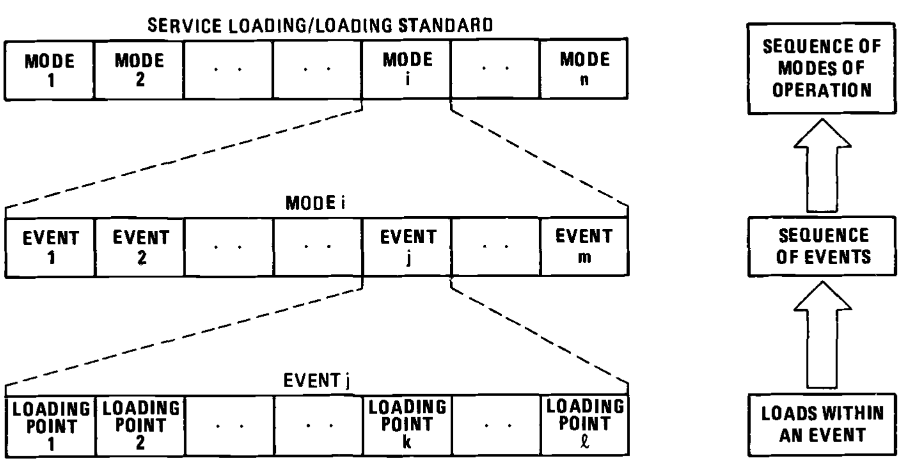

FIG. 1—*Schematic of the loading.*

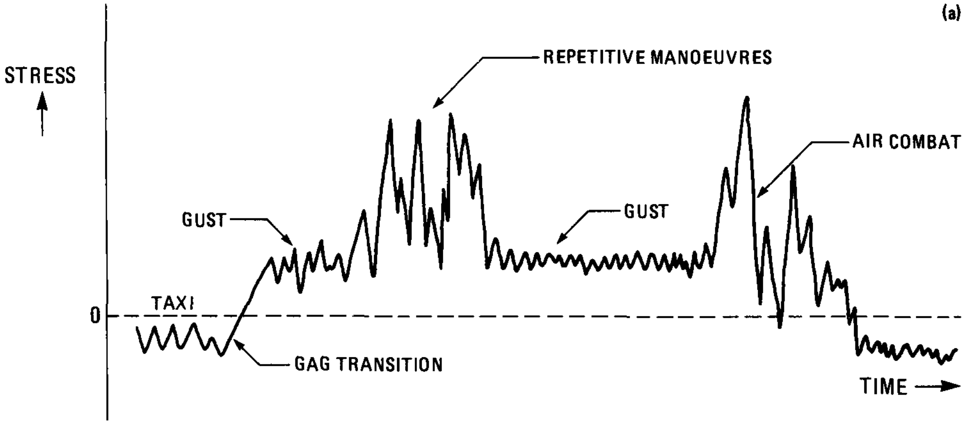

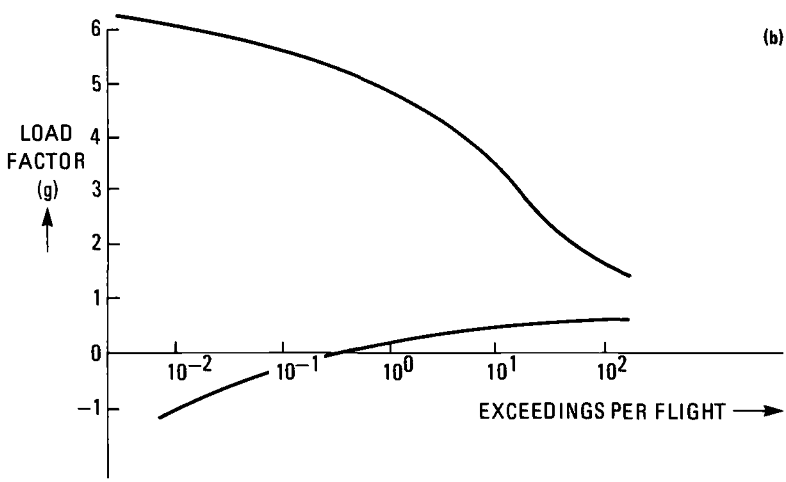

FIG. 2—*Typical fighter aircraft-wing load history* (a) *and load spectrum shape* (b).

reviewed and typifying elements within the various types of service loading are briefly discussed.

Tactical Aircraft

A fatigue critical location is the lower wing root area. Flight loading is primarily due to maneuvers causing upward bending moments. The high load factor capability of a fighter results in a relatively low mean flight load level. Compared to flight loads, the downward bending moment variations during ground handling are significant and may be enhanced by external stores. The aircraft configuration also results in a relatively small Ground-Air-Ground (GAG) transition. Often, the subsequent maneuver loads appear in a systematic manner, contrary to the random character of a gust type of loading. A typical fighter lower-wing-skin loading pattern is schematically shown in Fig. 2 [*1*], together with the overall load spectrum. The spectrum is distinctly asymmetric with the positive part having a convex shape. Loading spectra derived for different fighters usually have this shape, but differ in severity. Each flight is a different mode of operation. The mission type is then considered. Characteristic loading patterns will depend on the operational task that is to be performed during the mission. Also, mission length is important because the interaction between the tensile flight loads and the compressive ground loads is relevant. An air force will operate according to some annual training program, thereby exhibiting a recurrence period for the loading of one year. With respect to events, the parameters maneuver type (a mission may contain logical sequences of different exercises) and aircraft configuration are to be considered.

A loading standard representing fighter aircraft lower-wing loading has been defined, called FALSTAFF (Fighter Aircraft Loading STAndard For Fatigue evaluation) [*2–4*]. The loading standard contains three different mission types, three mission durations per mission type, and two aircraft configurations while the sequence represents 200 missions. The sequence length is about 36 000 loading points yielding 90 cycles per mission, at average. Although this type of loading is known to be maneuver-oriented, individual maneuvers have not been identified during the definition of FALSTAFF. Since the basis of the standard is a set of actual flown load-factor time histories, in which the occurrence of individual maneuvers or events is expected to be representative for common operational usage, the inability to handle separate maneuvers was accepted.

FALSTAFF has been developed primarily for evaluating metals and metal structures. A need was felt to define a similar loading standard for evaluating composite materials, called ENSTAFF (ENvironmental fighter aircraft loading STAndard For Fatigue evaluation). Additional features that should be reflected for this application are humidity and temperature. The first topic is handled by specification of preconditioning procedures, the second by association of simplified temperature profiles to each of the missions of FALSTAFF. It should be noted that elements of mechanical loading, as contained within FALSTAFF, are included in ENSTAFF without modification. Publication of ENSTAFF was realized in end 1987 [*5*].

A third area for loading standardization in a fighter aircraft is the engine disk. Current design practice employs very simplified mission cycles to simulate service loading. The loading in a gas turbine engine disk depends very much on the location within the engine and differentiation between cold-section components and hot-section components is required. Cold-section components are loaded by centrifugal forces that depend linearly on the square of the rotor speed. Hot-section components are loaded in a far more complex way due to the combined effect of centrifugal forces, material temperature, and time. A picture of both cold- and hot-section loading is given in Fig. 3. The cold-section loading is rather constant at a high load level frequently reaching the maximum load level. Due to maneuvering, irregular dips in the loading occur that do not go below a certain flight-idle level. A ground-idle level can be distinguished that may show sudden load peaks due to ground-handling procedures. Compressive loads to not occur. The peak load spectrum for cold-section loading exhibits a flat upper part and a linearly rising lower part. Cold-section disk loading is maneuver based and may contain rather deterministic elements with respect to sequencing of individual load cycles within each maneuver or event. The sequencing of events within a flight may also show deterministic features. The elements to consider when breaking down this type of loading are mission type, maneuver type, and mission duration. For hot-section loading, the engine type is a parameter also. The mechanical and thermal response varies from engine to engine due to differences in material and structural design and may lead to compressive loads. A loading standard representative for cold-section engine-disk loading has been defined, called Cold TURBISTAN (gas TURBIne engine

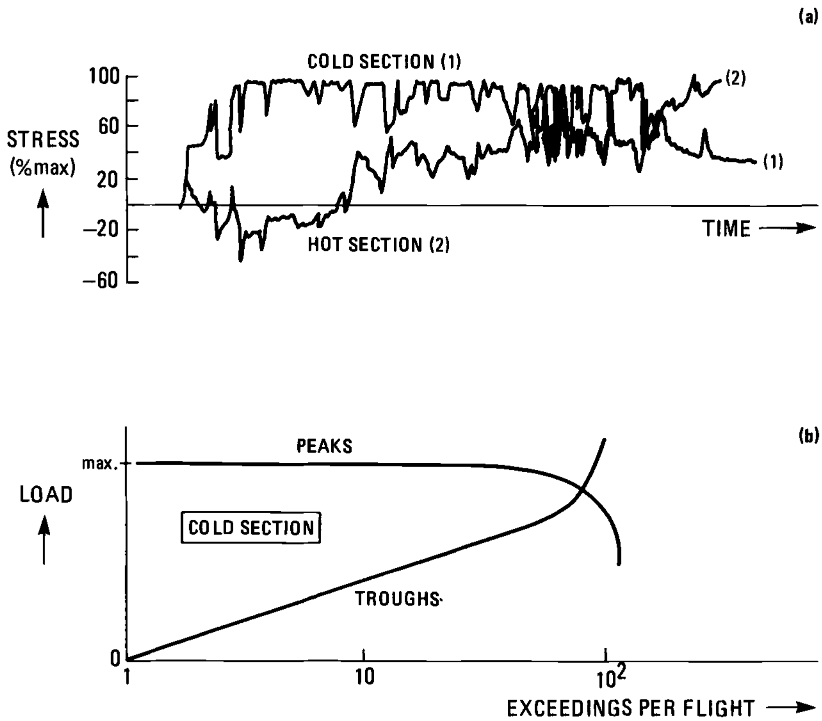

FIG. 3—*Typical fighter engine disk rim load history* (a) *and cold-section load-spectrum shape* (b).

loading STANdard) [*6,7*]. It recognizes four different mission types of variable length and nine different maneuver types. One block contains 15 452 loading points representing 100 flights, giving an average flight length of about 75 cycles. A loading standard representing hot-section component loading is currently being developed and is named Hot TURBISTAN. The problem here is to define an isothermal loading sequence that adequately represents the effects of fatigue and creep damage felt by the material under varying mechanical and thermal conditions. Hot TURBISTAN is expected to be available in end 1988.

Transport Aircraft

The loading on transport aircraft lower-wing skins is mainly considered gust dominated. Flight load cycles are superimposed on a tensile 1-*g* flight stress level. Taxi load cycles are superimposed on a compressive ground stress level, giving rise to a pronounced GAG cycle. Figure 4 shows a typical loading pattern for this type of loading. The spectrum shape shown is symmetric around the mean flight respective mean ground level and is rather concave. To evaluate this loading type the 1-*g* level is important. Load cycle amplitudes due to gust must be referenced to undisturbed flight under cruise conditions. The spectrum in Fig. 4 is normalized with respect to the mean stress level in flight. The load experience will depend on meteorological conditions, ranging from very smooth flights to extremely rough flights. Therefore, different flight types with different load intensity have to be discriminated. Each flight will contain subsequent flight phases or events, that is, ground phase with taxiing,

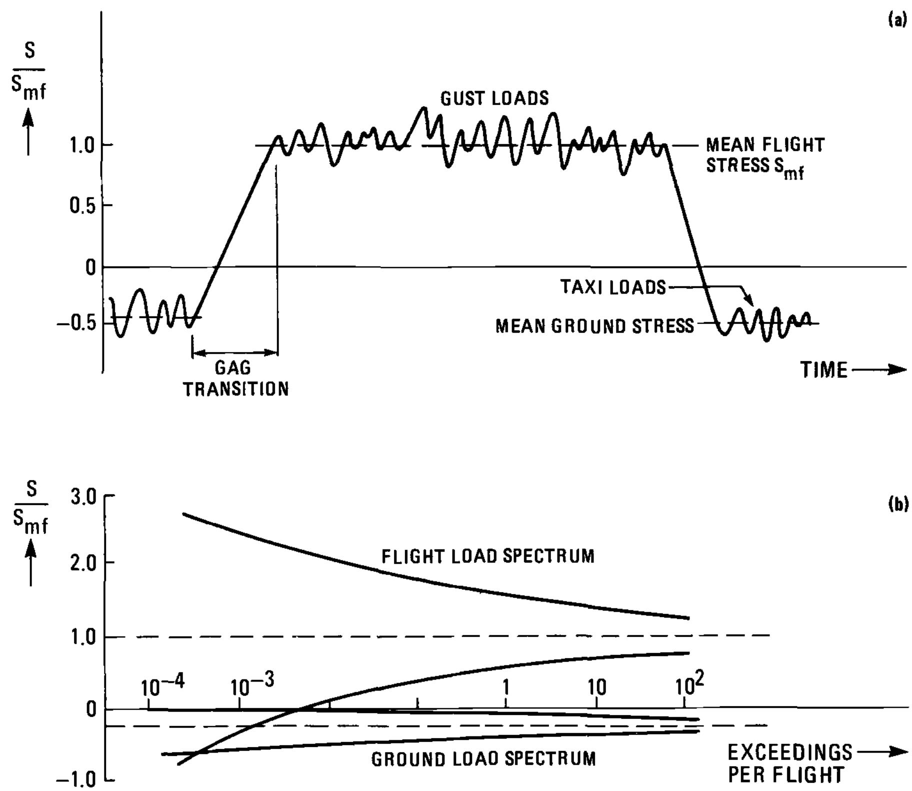

FIG. 4—*Typical transport aircraft-wing load history* (a) *and load-spectrum shape* (b).

take-off, climb, cruise, descent, approach, and landing. Average design life of modern transport aircraft is in the order of 100 000 flights. This utilization must also be taken into account. For this application TWIST (Transport WIng STandard) has been developed [*8*]. The standard defines ten different flight types and ten different gust amplitude levels, but does not discriminate between different flight phases. The ground load spectrum has been simplified to a single GAG cycle on the basis that TWIST was primarily meant for evaluating metallic materials. The omission of compressive ground load cycles that should be interspersed between the tensile flight load levels should be realized when using TWIST for testing composites. TWIST is a sequence of 717 330 loading points representing 4000 flights and, thus, the average flight length is 90 cycles. A shortened version of TWIST, called MiniTWIST, has been defined for all cases where testing time is to be minimized [*9*]. Here, only the number of load cycles with the smallest amplitude is reduced and, by doing so, the average flight length changes from 90 to about 15 cycles per flight.

Helicopters

The topic of helicopter blade loading has been subject to standardization. The loading is coupled to the rotating movement giving one basic load cycle per rotor revolution. The cyclic frequency is rather high, when compared with other types of fatigue loading. Rotor speeds are in the order of three to seven cycles per second yielding 10 to 25 thousand cycles per hour. The forces acting on a rotor blade are lift, drag, and centrifugal force that give the loading pattern the character of a large number of flight load cycles with relatively small amplitude that are superimposed on a constant tensile load due to the centrifugal force. Compared to rotor speed, the amplitude of these cycles varies slowly so that a sample of a load time trace has the appearance of a sequence of different blocks representing periods spent in discrete maneuvers. Each of those blocks contains cycles of relatively constant amplitude. In Fig. 5 a blade loading pattern is shown with peak load spectra for hinged and fixed rotors, respectively. Between the flights, pronounced GAG cycles occur associated with rotor stop and downward bending of the blades. Differences are made between hinged (articulated) and fixed (semi-rigid) rotor types. Near the rotor head, the flapping bending moment in the hinged blade is zero, whereas the rigid rotor bending moment still has some value there. At half span radius, the dynamic loading may not be too different for both

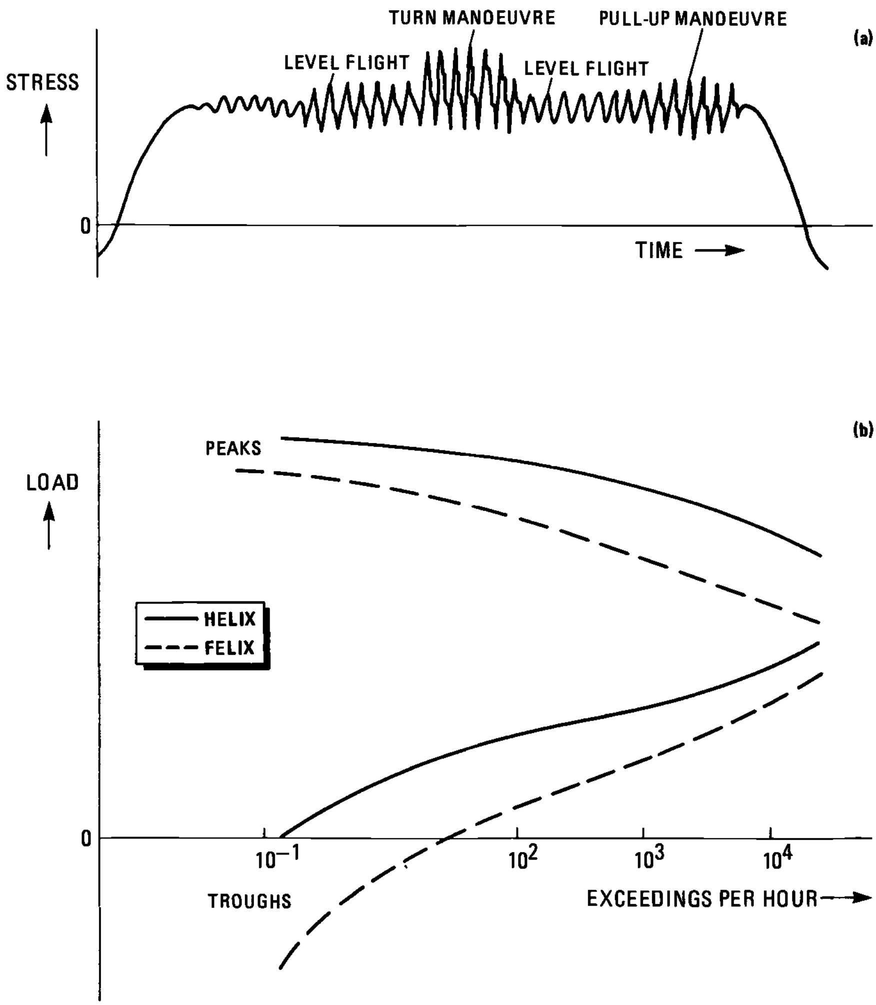

FIG. 5—*Typical helicopter-blade load history* (a) *and load-spectrum shape* (b).

types. From flight measurements, it appeared that load cycle amplitudes and variations in mean stress were larger for the rigid rotor type, while the absolute mean stress level is generally higher for the hinged rotor blade. Also, it was expected that maneuvers significant to fatigue in a hinged rotor would not necessarily be significant for the rigid rotor type and vice versa. The parameters to be considered here are mission type, maneuver type, mission duration, and rotor type. The resulting loading standards are called Helix and Felix, representing hinged and fixed rotor types, respectively [*10–13*]. The standards contain four different mission types, three flight lengths per mission type, and discriminate between more than 20 different maneuvers. Helix and Felix are relatively long with more than two million cycles for representing 140 missions, that is, about 15 000 cycles per flight. With a testing frequency of 20 Hz, application of one block of 140 flights lasts more than 30 h. With this in mind, shortened versions have also been defined, cutting down the sequence lengths more than 90%.

Horizontal Axis Wind Turbines

A nonaeronautical structural area where a common load basis exists is a horizontal axis wind turbine blade. In general, the root area of a fixed blade will be a circular circumference connecting the blade to the hub. The loading in this fatigue critical component is a function of location along the circumference; that is, the position relative to the rotorplane will determine the loading contributions of blade weight due to gravity and aerodynamical force, respectively. Typical loading patterns for in-plane and out-of-plane bending moments at a blade root are shown in Fig. 6. For a heavy blade, the in-plane loading resembles pure constant-amplitude loading resulting in a range spectrum of rectangular shape. Perpendicular to this direction, the blade weight is not felt and the wind-induced loads are of a more random nature. The range spectrum for out-of-plane loading is of triangular shape. Wind turbine blade loading obviously depends on wind statistics. The wind regime will determine the basic blade loading, and this applies both to wind speed and wind direction. The yawing movement is a relevant event with respect to fatigue loads generation. The wind turbine geometry is important because blade weight determines the in-plane loading. For large and heavy blades, this loading element is more severe than for small and light blades. The combination of in-plane and out-of-plane loading for a critical location somewhere on a circular circumference is, consequently, a function of geometry. The control system regulating the wind turbine performance greatly influences the loading environment. Changes in wind velocity and wind direction will lead to changes in operation. For example, at cut-in wind speed, the turbine will start operating; at cut-out wind speed, it will be stopped; through the yawing mechanism, it will follow wind direction; an emergency stop may occur; etc. If the control system employs electrical braking through the generator, different blade loading will be experienced as compared with a system using tip devices that stop rotational speed. Also, handling statistics have to be considered. For this application a mode is associated with a continuous period of operation. Apart from starting and stopping due to meteorological reasons, having a more or less random basis, more deterministic events may take place such as inspections and repairs. A loading standard for this application is under development, called WISPER (WInd turbine reference SPEctRum).

Off-Shore Structures

The sources of fatigue loading in an off-shore structure are wind, current, and wave action, the latter being predominant. Waves, in turn, occur as an interaction between wind and water. This leads to a loading system that may be described as a series of continuously

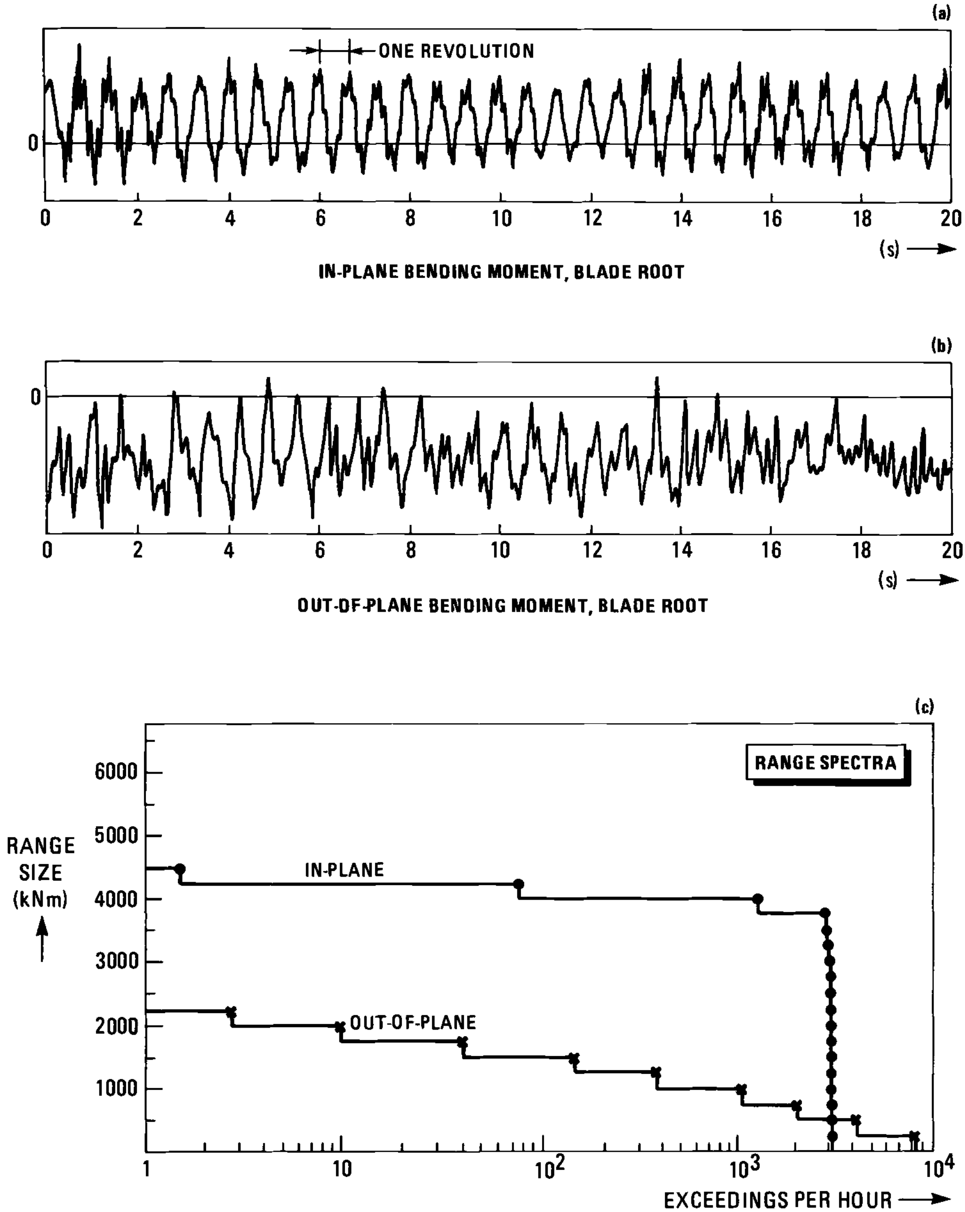

FIG. 6—*Typical horizontal-axis wind-turbine load histories* (a), (b) *and range spectrum* (c).

varying sea-states. For rigid structures, the response to this input is rather direct, and for tall slender platforms, the dynamic response may yield a very different fatigue environment. Not only the type of structure determines the loading, but also weather conditions will influence the wave action, consequently, geographical location is also relevant. A loading standard representative for off-shore structures is being developed, called WASH (Wave Action Standard History) [*14*].

So far, only time-related parameters were used to describe fatigue loading. Since many physical systems may be considered as random processes, they are well described by frequency domain parameters. A theory has been developed to link this kind of information to properties that are directly related to fatigue damage accumulation. Rice [*15*] has formulated relationships that turn frequency domain data into numbers of level crossings and numbers of peaks and troughs of various levels. These formulae are most effective if the Power Spectral Density (PSD) function characterizes narrow-band random loading, but the calculation of fatigue-related parameters is much less satisfactory for wide-band excitations.

Kowalewski [*16*] developed a tool to derive the joint probability distribution of peaks and troughs for a stationary Gaussian process with given PSD function. Based on this theory, a loading standard named GAUSSIAN STANDARD was defined in Germany in 1976 [*17*]. It defines a set of three relatively long test-load sequences with 10^6 positive zero level crossings having a narrow-band, a medium-wide-band, and wide-band characteristics. The standard is used for those random load tests in which a load sequence with fixed statistical properties is required.

Loading Standard Basics

Various types of fatigue loading have just been described for which standard spectra have been or are being defined. The conditions that must be met to successfully construct a useful loading standard are summarized here:

(*a*) the loading must exhibit a spectrum shape that is characteristic for the type of structure that is considered;
(*b*) the loading must contain interaction properties that are, at least partly, understood and means must be found to incorporate this interaction "signature" in the resulting standard; and
(*c*) the standard must comply with certain applicability requirements, for example, simple structure, clear generation procedure (that must be simple also if the generation effort is to be performed by each potential user), and it must be fully documented.

The resulting steps in a loading standard development program are: (1) identification of structural application, (2) feasibility study to investigate the common type of loading for this application, (3) compilation of usage data, (4) determination of fatigue-related parameters, (5) development of analysis tools adequately recognizing these parameters, (6) data analysis, (7) evaluation of analysis results, (8) development of synthesis tools that also comply with the underlying spectrum basics and, finally, (9) the actual synthesis procedure. In view of this list of development steps, the following choices must be made.

Sequence Length—Opposing criteria are to be considered. The sequence must be short enough to guarantee a sufficiently large number of repetitions in the fatigue tests, but it must also be long enough to avoid "flattening" of the spectrum by applying the same sequence too often.

Extreme Value—Maximum load levels found in usage data are, in general, a function of measurement duration. If short-term measurements are performed, proper extreme values have to be determined through extrapolation.

Truncation Level—Due to retardation effects, high loads can have a beneficial effect on fatigue damage accumulation in metallic materials. From measurements or calculations, the highest load levels (extreme values) expected in service will be known. But due to usage variability, not all structures in service will experience the same high loads. To adjust for this, truncation of high loads in a loading standard may avoid unconservative test results. However, truncation does not affect fatigue damage accumulation in a very straightforward way, but the effect will depend on spectrum shape. To illustrate this, a schematic comparison between a transport aircraft spectrum and a fighter spectrum is shown in Fig. 7 [*18*]. An arbitrary truncation at the "ten times per aircraft life" level effects the transport aircraft spectrum much more than the fighter spectrum because of its steeper curve in the high-load-amplitude region. In other words, truncating a relatively flat spectrum will less drastically lead to more conservative test results.

Another aspect is the material that is considered. The retardation effect of high loads is known to exist in metals, whereas the situation in composite materials is different, and infrequent high loads may very well cause sudden damage growth. Truncation means conservatism in metals, however, it produces unconservative test results in composites.

Omission Level—Large reductions of testing time can be obtained by omitting low-amplitude cycles from the spectrum. The acceptable degree of reduction will depend on the spectrum type. Comparing both spectrum shapes in Fig. 7 in the low-amplitude region, the steeper fighter spectrum curve indicates a lower sensitivity to low-cycle omission than does the transport aircraft spectrum. A chosen omission level is not necessarily near the endurance limit. Since a loading standard is used for comparative tests, omission of cycles is acceptable if its effect on different test results is known to be similar. It is noted here that Schijve [*18*] has published a comprehensive overview of spectrum parameters and their influence in flight simulation testing. Test results of many fatigue evaluation programs have been compiled in this report. Similar to truncation, the effect of omission depends on the material. Small

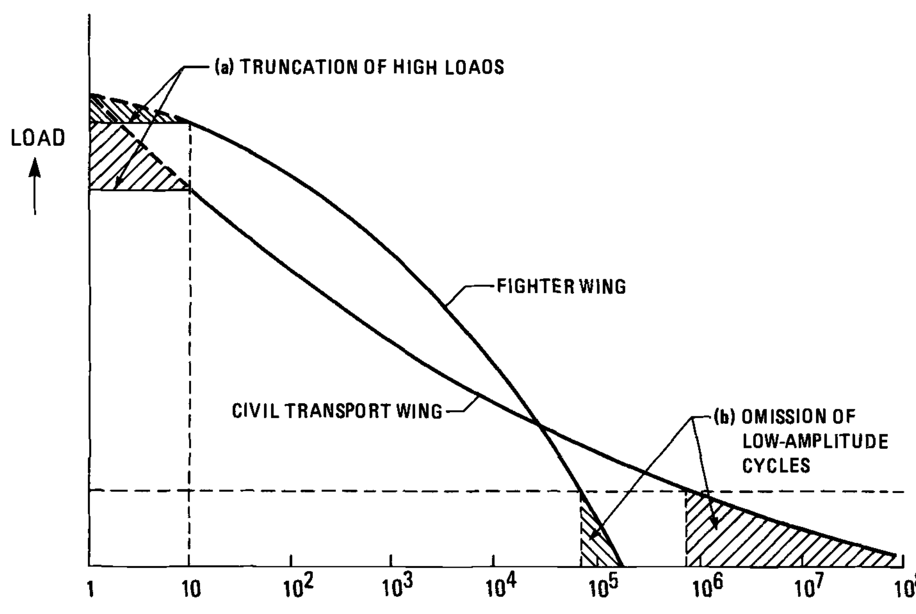

FIG. 7—*The effect of spectrum shape on* (a) *truncation and* (b) *omission.*

compressive load cycles are insignificant for metals but will contribute to damage accumulation in composite materials.

Level Definition—A loading standard is a sequence of load reversals being defined as either relative or absolute levels. In TWIST and MiniTWIST, 22 different load levels appear that are expressed as deviations from the mean flight stress level and, thus, its choice determines the absolute load extremes during a test. Other loading standards employ absolute arbitrary loading units with various degrees of sophistication. The number of different levels varies from 120 (Helix, Felix), through 100 (TURBISTAN) to 32 (FALSTAFF, ENSTAFF). The choice of level definition will depend on loading type, testing facilities, and numerical procedures adopted during data processing.

Data Analysis Techniques

Means must be found to process time-domain usage data from various origins in such a way that properties causing fatigue are properly analyzed in a quantitative way. These properties have already been indicated as occurrences of load extremes, level crossings, and load variations. The counting methods that are associated with the three categories may be summarized as follows.

Peak Counting Methods—The turning points in a load-time trace are administrated according to their load level.

Level Crossing Counting Methods—This counts the number of times a load-time trace crosses a certain level, either in a positive or negative direction. Peak counting and level crossing counting are related: the number of positive level crossings is equal to the number of peaks above a level minus the number of troughs above that level. This implies that the result of a level crossing counting can be derived from a peak counting result. As the opposite is not true, level crossing counting is considered to be of a lower order than peak counting.

Range Counting Methods—It appears logical to count load variations directly because fatigue damage accumulation comes from variations in load rather than from individual peaks and troughs. Ranges may be counted as either single ranges or as range pairs. The counting of single ranges, usually indicated as range count, is a straightforward counting of all subsequent load ranges in their order of occurrence. This principle splits up a loading trace at any occurrence of a load reversal. The range-pair counting avoids this sensitivity. Rather than splitting up a loading trace, it searches for full-load cycles that are contained within main load variations.

The counting methods just mentioned consider single features. It is also possible to look for the simultaneous or subsequent occurrence of two features. Such counting methods are indicated as two dimensional. An example of such a combination is a peak at level j followed by a trough at level i, which can be presented as element $a(i,j)$ in a so-called Markov From/To Matrix A, see Fig. 8. Instead of a From/To Matrix $A[i,j]$ the information may be stored in a range-mean Matrix $M[r,m]$, where r gives the range magnitude and m gives the mean of range r.

Rainflow or Range-Pair-Range Counting Method

Some 20 years ago in Japan, a counting method was defined that became known as the Rainflow or Pagoda-roof method [*19*]. In Europe at the same time and independently, a counting method was developed that was later called the range-pair-range counting method

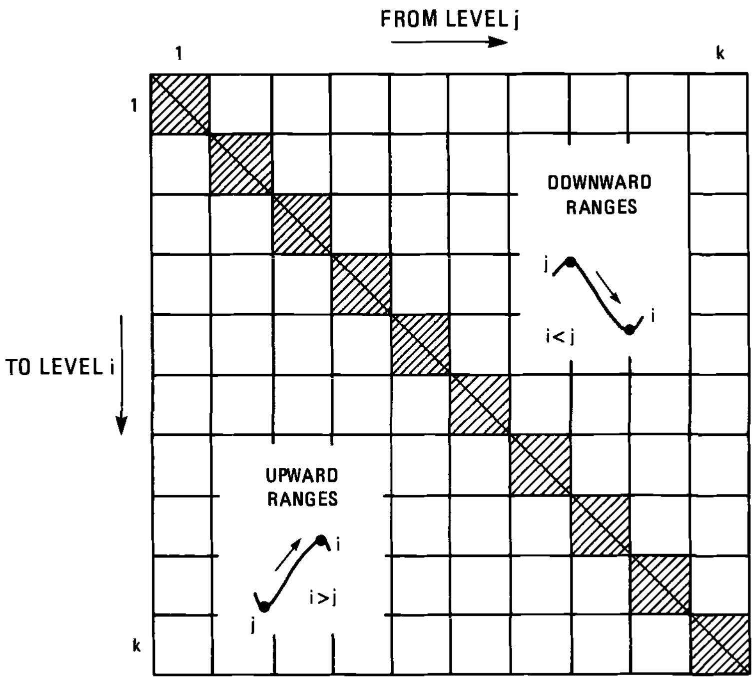

FIG. 8—*Markov From/To Matrix A of size (kxk). Range size is ABS* (i − j), *range mean is* $(i + j)/2$.

[*20,21*]. Although the descriptions of both sources are very different, both yield the same result, that is, they extract the same range pairs and single ranges from the load.

Rainflow counting techniques have been accepted widely and associated software has been implemented at numerous institutes. However, a large variety of algorithms now exist that are sometimes badly understood with respect to details. Because the original rainflow description is a set of rather artificial rules instead of a physically understandable feature, preference is given to the range-pair-range description in the standardization programs. The principles of the algorithm, which are easily accessible to programming, will be briefly discussed.

The algorithm simplifies to three elements:

1. *Classification of Extremes*—The continuous signal is searched for peaks and troughs. Each peak and trough is attributed to a certain class level. A range filter of certain size may be applied to suppress the lowest amplitudes.
2. *Full-Cycle Recognition*—Employing a four-point check, the series of integer class levels is searched for full cycles that are contained within major single ranges. A full cycle is found if the load levels of the two inner points fall within the load range between the first and fourth loading point, see Fig. 9. The full cycle found is deleted from the four-point sequence and a new four-point sequence is evaluated "moving backwards" two points. If this criterion is not met, one step forward is taken, and so on. The successive full cycles found are stored in a matrix.
3. *Residue Handling*—After having omitted all full cycles from the sequence as depicted Point 2, a "residue" of single load ranges remains that generally has a diverging-converging shape. As seen in Fig. 10, the residue contains the largest load variation

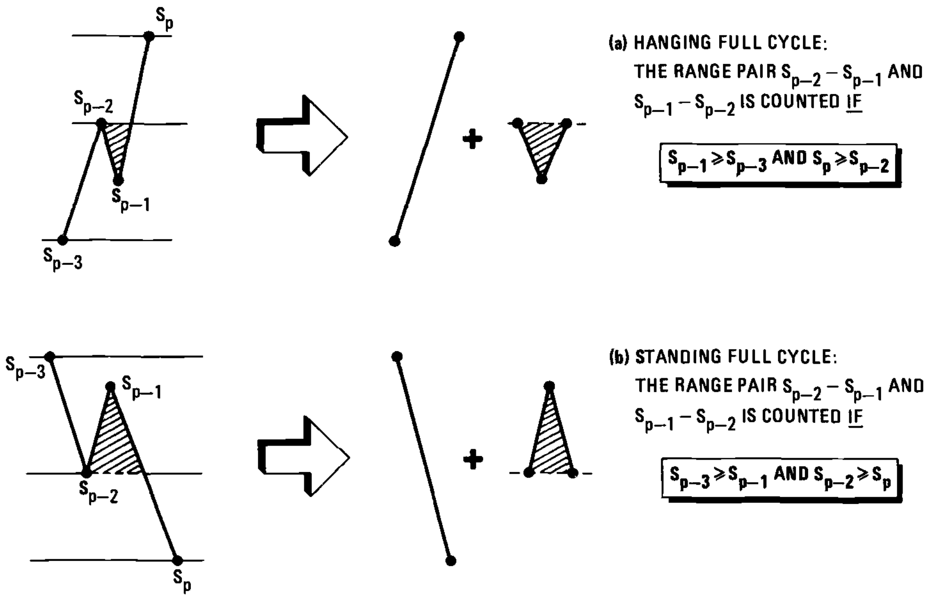

FIG. 9—*Rainflow (range-pair-range) counting criterion.*

present within the signal. The single load ranges are stored in the From/To matrix in addition to the already-existing full-cycle content.

The way of storing full cycles and single ranges in a matrix can be done in different ways, see Fig. 11. If it is the intention to maintain information on load direction, an entire matrix of size (kxk) is used. A full cycle, consisting of a rising and a falling range, is stored by increasing the corresponding matrix elements above and below the main diagonal with one. A single range is stored in the associated matrix-element, either above or below the main diagonal depending on its direction. This storage method is shown in Fig. 11*a* for one full cycle found within one major loading range. Three matrix elements are changed here, one for each load excursion 3-2 and 2-3 of the full cycle 3-2-3, and 1-5 for the residue. This way of storing has the advantage that all one-dimensional counting results can be derived from the matrix directly, that is, the peak/trough counting result, the level crossing counting result, and the range-mean counting result [*22*]. By distributing these types of matrices, the

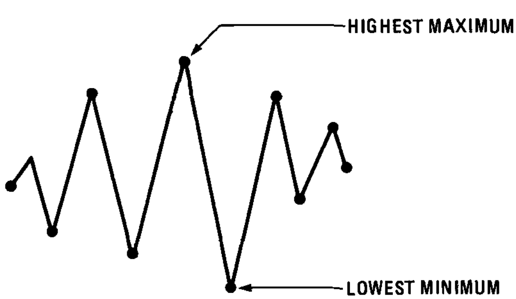

FIG. 10—*Typical residue shape.*

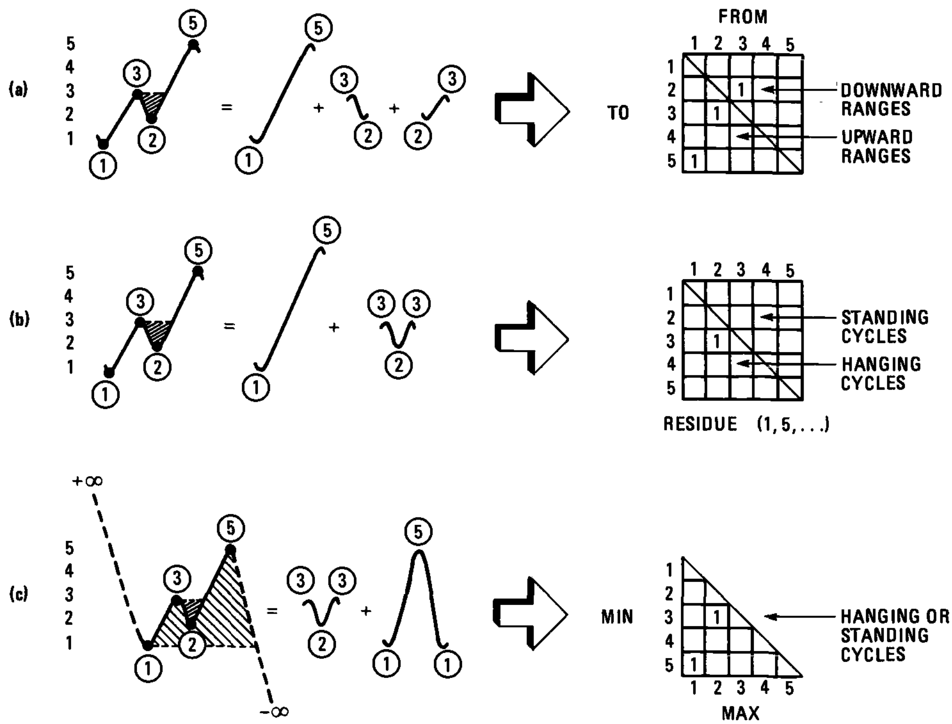

FIG. 11—*Storage of rainflow counting results.*

result of different usage data can be easily shared. Another way of storing the cyclic content is shown in Fig. 11*b* in which the residue is stored separately from the matrix. On one side from the main diagonal, all cycles are stored that were found within a falling major load variation and are indicated as "standing" cycles. In the other matrix-half, the "hanging" cycles are stored. A third storage method is presented in Fig. 11*c* that is characterized by two elements: the residue is modified to a set of full cycles, and no distinction is to be made with respect to loading direction. This method has the advantage that only half a storage matrix is necessary to record the counting result. It is therefore frequently used in those cases where memory capacity is limited.

Synthesis Procedures

The structure of a loading standard has been presented as a series of modes. Each mode may be built up by a series of events that contain the actual loading points. The generation of a loading standard is, in fact, the subsequent generation of loading points within each event, the generation of events to construct one mode of operation, and the generation of the modes to give the final sequence. This sequence may contain both deterministic and random elements. The nature of deterministic events cause them to be generated or situated within the overall sequence by hand, whereas random events need some kind of random drawing technique to reproduce the cyclic loading. Thus, after having compiled, counted, and evaluated time-domain usage data, there will be a demand to turn schematizations or counting results of certain type into load-time sequences again. Generally, these schematizations are in the form of tables, exceedance curves, or From/To (range/mean) matrices. Load-time data generation from matrix-based rainflow counting results is extensively used in the synthesis of loading standards and has gained and is still gaining much interest in other fatigue programs. Because of its relevancy, some basic principles of load-time data generation will be discussed.

Rainflow analysis means counting the number and magnitude of full-load cycles. At the end, a residue remains from which no full cycles can be extracted anymore. The reconstruction task is to make a valid load-time history out of these results that, if being rainflow counted again, produce the same counting result as the initial one. In Fig. 9, sketches are shown of a peak/trough pair constituting a complete loading cycle within an increasing and a decreasing major load range, respectively. Now, a schematic counting result is considered in Fig. 12*a*, being a hanging cycle, X-Y-X, and a residue range, A-B. Constituting a load-time trace from this result gives A-X-Y-B as the only possibility. In Fig. 12*b*, a counting result is given with the same full cycle, X-Y-X, and with a somewhat larger residue, A-B-C-D-E. The hanging cycle, X-Y-X, can be located in either one of the rising load ranges, A-B or C-D, giving possible load-time solutions, A-X-Y-B-C-D-E and A-B-C-X-Y-D-E, respectively. If the condition is neglected that a hanging loop is to be superimposed on a rising range or vice versa, two more possibilities exist to constitute a valid load-time trace,

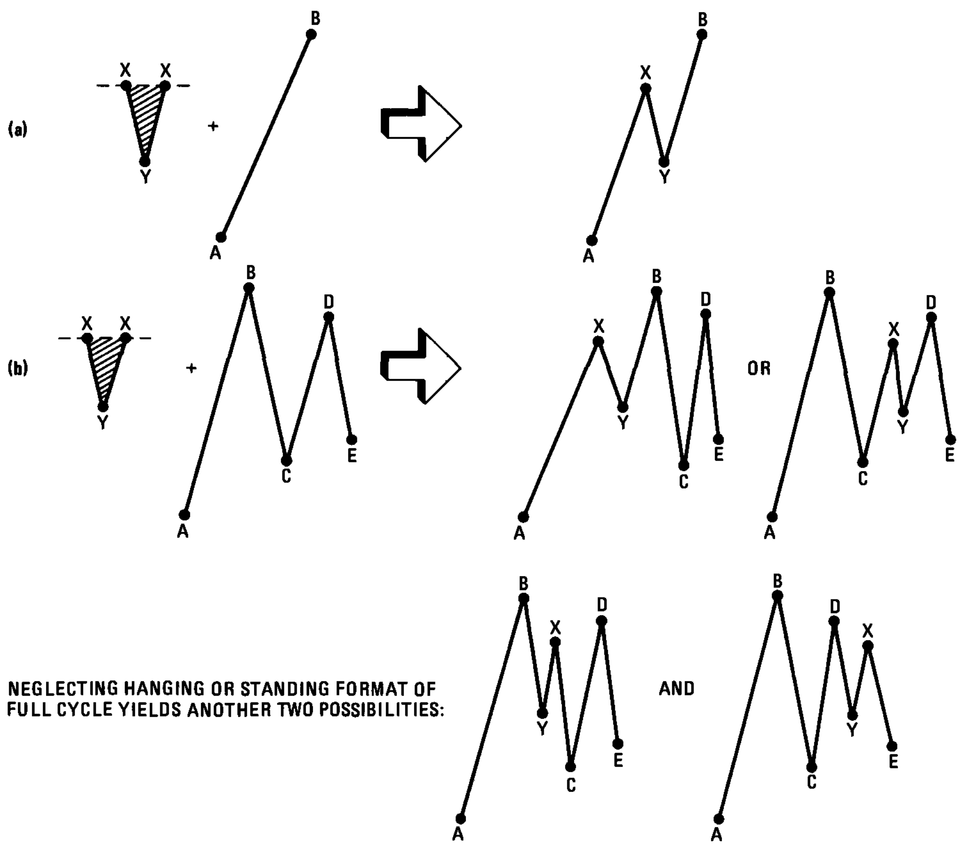

FIG. 12—*Reconstruction of a load sequence.*

that is, A-B-Y-X-C-D-E and A-B-C-D-Y-X-E. The full cycle can now be located within any larger loading range.

A counting result is considered according to the storage method of Fig. 11*c* that only handles full cycles, see Fig. 13. Five different load levels are defined, and the sum of all matrix elements of the half-matrix is six. These cycles can also be presented in the absolute stress field as a set of individually standing cycles. Keeping in mind the rainflow condition, it is immediately seen which cycles can be interspersed within other ones to maintain rainflow consistency. Cycle A represents the largest cycle of all and lies at the greatest distance from the main diagonal. This Cycle A is, in fact, the modified residue spanning the major load range that contains all other cycles from the matrix. Cycle D can be contained within Cycle A and Cycle B. Obviously, given a minimum/maximum Matrix A of size (kxk), a cycle that is defined as element $a(m,n)$ can contain all matrix elements

$$a(i,j) \quad \text{with} \quad i = m - p \quad \text{and} \quad j = n \quad \text{to} \quad (i - 1)$$

$$\text{for} \quad p = 0,1,2,3\ldots, k - 1 \quad \text{and} \quad i \geqq n$$

The area within the matrix that is associated with these conditions is indicated by the shaded area in Fig. 14. The same principle is valid for each of the matrix elements within the shaded area, of course. This means that by looking at a half-matrix counting result, it can immediately be seen which cycles are candidates for containing smaller cycles. For example, Cycle A in Fig. 13 is the initial and largest cycle to start with consisting of a rising and a falling part. Cycle B can be placed in either the rising of falling part of Cycle A, and a random drawing procedure choosing one out of two possibilities has to be performed. Next, Cycle C is considered lying in the shade of Cycle A and Cycle B, which means that Cycle C can be situated in the rising or falling part of two large cycles. Four possibilities exist to locate Cycle C. Within Cycle C, no other cycles have to be generated because its shaded area is empty. Now, four cycles remain to be "eaten up": Cycle D and three Cycles E. Cycle D is in the shade of Cycles B and A, and, consequently, four vacancies are available to replace it. Finally, the three Cycles E can only be contained within Cycle A with its two branches and the generation task is to spread three cycles at two possible positions.

It will be clear that the entire matrix content can be handled element-by-element in the preceding way. In this iterative process, the resulting rainflow consistent load time sequence grows cycle by cycle until the matrix is empty. The number of iterative steps is determined by the sum of all matrix elements, and this may require considerable data processing time

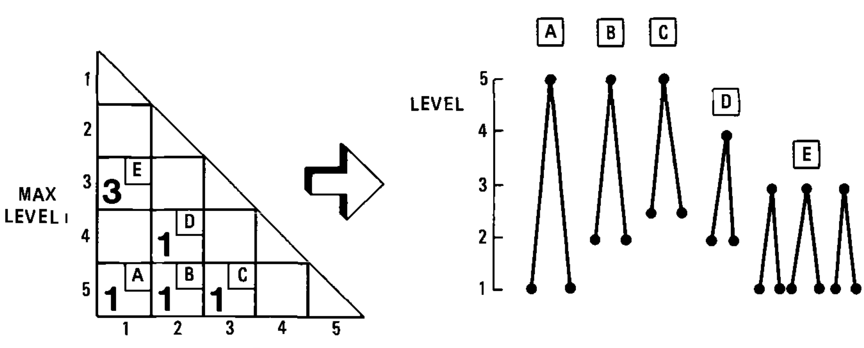

FIG. 13—*Rainflow counting result schematized for load sequence reconstruction.*

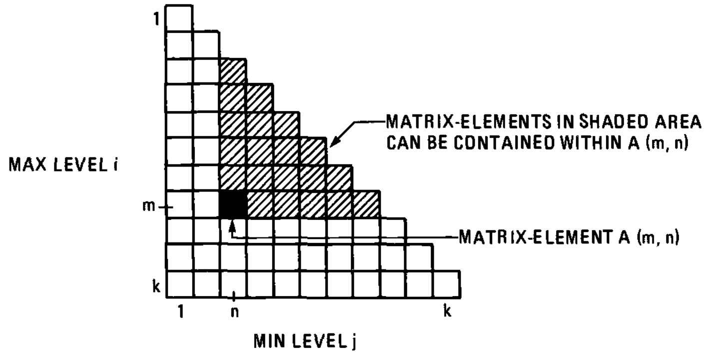

FIG. 14—*Condition with respect to rainflow consistency.*

and memory capacity to store the growing sequence. Therefore, methods have been developed to generate valid load sequences on an on-line basis [*23*]. From the very start, the algorithm gives out loading point-by-loading point in such a way that rainflow consistency is guaranteed and a statistically sound randomization is achieved. Such an algorithm is particularly useful for on-line control of variable-amplitude test equipment.

It is worth noting that the preceding algorithms also exist for the more sophisticated counting result storage methods that take into account load cycle direction.

Summary and Outlook

Major histories of European fatigue load standardization programs were reviewed. Apart from the obvious result that a set of useful loading standards now exist, and a few more will be available shortly, the work has accomplished beneficial technical agreement between the various cooperating institutes. This applies in particular to the topic of quantitative data handling procedures for fatigue evaluation purposes.

Apart from new structural applications (aircraft landing gear, aircraft vertical tail structure), future work may lay in updating or modifying existing loading standards in order to increase their validity or to extend their applicability.

References

[*1*] de Jonge, J. B., "The Use of Standardized Fatigue Load Sequences in Coupon and Component Tests," NLR MP 80001 U, National Aerospace Laboratory, Amsterdam, The Netherlands, Jan. 1980.

[*2*] Van Dijk, G. M., "Introduction to a Fighter Aircraft Loading Standard for Fatigue Evaluation FALSTAFF," NLR MP 75017 U, National Aerospace Laboratory, Amsterdam, The Netherlands, 1975.

[*3*] "FALSTAFF, Description of a Fighter Aircraft Loading Standard for Fatigue Evaluation," joint publication of Flugzeugwerke Emmen, Switzerland; Laboratorium für Betriebsfestigkeit (LBF), Germany; National Aerospace Laboratory (NLR), The Netherlands; and Industrie-Anlagen-Betriebsgesellschaft mbH (IABG), West Germany, 1976.

[*4*] de Jonge, J. B., "Additional Information about FALSTAFF," NLR TR 79056 U, National Aerospace Laboratory, Amsterdam, The Netherlands, ICAF Doc. No. 1133, June 1979.

[*5*] "Standardised Environmental Fatigue Sequence for the Evaluation of Composite Components in Combat Aircraft, called ENSTAFF," Report No. FB-179 (1987), Fraunhofer-Institut für Betriebsfestigkeit (LBF), Darmstadt, West Germany, 1987 (Also published as IABG-Report No. B-TF2194 (1987), NLR-Report No. TR87053 U, and RAE-Report No. TR 87048.).

[6] Mom, A. J. A., Evans, W. J., and ten Have, A. A., "TURBISTAN: a Standard Load Sequence for Aircraft Engine Discs," *Damage Tolerance Concepts for Critical Engine Components, AGARD CP 393, Advisory Group for Aerospace Research and Development, 1985, pp. 20.1–20.11.*
[7] Breitkopf, G. E., "Basic Approach in the Development of TURBISTAN, a Loading Standard for Fighter Aircraft Engine Disks," in this volume, pp. 65–78.
[8] de Jonge, J. B., Schuetz, D., Lowak, H., and Schijve, J., "A Standardised Load Sequence for Flight Simulation Tests on Transport Aircraft Wing Structures," LBF-Bericht TB-106, NLR TR 73029 U, National Aerospace Laboratory, Amsterdam, The Netherlands, March 1973.
[9] Lowak, H., de Jonge, J. B., Franz, J., and Schuetz, D., "MiniTWIST, a Shortened Version of TWIST," LBF-Bericht TB-146, NLR MP 79018 U, National Aerospace Laboratory, Amsterdam, The Netherlands, May 1979.
[10] ten Have, A. A., "Helix and Felix: Loading Standards for Use in the Fatigue Evaluation of Helicopter Rotor Components," *Helicopter Fatigue Design Guide,* AGARDograph No. 292, Advisory Group for Aerospace Research and Development, 1983, pp. 249–270.
[11] Edwards, P. R., "A Description of Helix and Felix, Standard Fatigue Loading Sequences for Helicopters, and of Related Fatigue Tests Used to Assess Them," Ninth European Rotorcraft Forum, Paper No. 95, Stresa, Italy, Sept. 1983.
[12] Edwards, P. R. and Darts, J., "Standardised Fatigue Loading Sequences for Helicopter Rotors (Helix and Felix). Part 1: Background and Fatigue Evaluation," RAE TR 84084, Royal Aircraft Establishment, Farnborough, U.K., Aug. 1982.
[13] Edwards, P. R. and Darts, J., "Standardised Fatigue Loading Sequences for Helicopter Rotors (Helix and Felix). Part 2: Final Definition of Helix and Felix," RAE TR 84085, Royal Aircraft Establishment, Farnborough, U.K., Aug. 1982.
[14] Pook, L. P. and Dover, W. D., "Progress in the Development of a Wave Action Standard History (WASH) for Fatigue Testing Relevant to Tubular Structures in the North Sea," in this volume, pp. 99–120.
[15] Rice, S. D., "Mathematical Analysis of Noise," in *Bell Systems Technical Journal,* Vol., 23, 1944 and Vol. 24, 1945; reprinted in *Selected Papers on Noise and Stochastic Processes,* Nelson Wax, Dover Publications, New York, 1954.
[16] Kowalewski, J., "Beschreibung Regelloser Vorgaenge," Fortschritt Bericht VDI-Z, Reihe 5, No. 7, pp. 7–28, VDI-Verlag GmbH, Duesseldorf, West Germany, 1969, in German.
[17] Hueck, M., Schuetz, W., Fischer, R., and Koebler, H. G., "A Standard Random Load Sequence of Gaussian Type Recommended for General Application in Fatigue Testing," LBF-Report No. 2909, Darmstadt, West Germany, April 1976.
[18] Schijve, J., "The Significance of Flight-Simulation Fatigue Tests," Report LR-466, Delft University of Technology, Delft, The Netherlands, June 1985.
[19] Matsuiski, M. and Endo, T., "Fatigue of Metals Subjected to Varying Stress," paper presented at the Kyushu District Meeting of the Japan Society of Mechanical Engineers, No. 68-2, Fukuoka, Japan, March 1968, pp. 37–40, in Japanese.
[20] de Jonge, J. B., "Fatigue Load Monitoring of Tactical Aircraft," NLR TR 69063 U, National Aerospace Laboratory, Amsterdam, The Netherlands, July 1969.
[21] de Jonge, J. B., "The Monitoring of Fatigue Loads," paper presented at the 7th ICAS Congress, Rome, 14–18 Sept. 1970; also published as NLR MP 70010 U, National Aerospace Laboratory, Amsterdam, The Netherlands, 1970.
[22] de Jonge, J. B., "The Analysis of Load-Time Histories by Means of Counting Methods," *Helicopter Fatigue Design Guide,* AGARDograph No. 292, Advisory Group for Aerospace Research and Development, 1983, pp. 89–105.
[23] Krueger, W., Scheutzow, M., Beste, A., and Petersen, J., "Markov- und Rainflow-Rekonstruktionen Stochastischer Beanspruchungs Zeitfunktionen," Fortschritt Bericht VDI, Reihe 18, No. 22, VDI-Verlag GmbH, Duesseldorf, West Germany, 1985, in German.

Kevin R. Fowler[1] *and Roy T. Watanabe*[1]

Development of Jet Transport Airframe Fatigue Test Spectra

REFERENCE: Fowler, K. R. and Watanabe, R. T., **"Development of Jet Transport Airframe Fatigue Test Spectra,"** *Development of Fatigue Loading Spectra, ASTM STP 1006*, J. M. Potter and R. T. Watanabe, Eds., American Society for Testing and Materials, Philadelphia, 1989, pp. 36–64.

ABSTRACT: Aircraft development programs commonly employ large tests to substantiate new design features. Full-scale airframe static and fatigue tests are conducted to demonstrate that the structure has sufficient strength and will be economical to maintain in service. Full-scale fatigue testing is accelerated relative to actual usage so that areas that exhibit early fatigue problems can be located and corrected in a timely manner.

Development of the airframe fatigue test spectra for two new jet transport models is described. These test spectra were based on the concept of applying loads as realistically as possible while conforming to program schedule and test equipment limitations. The frequency and magnitudes of loads were determined to meet observed statistical criteria without relying on damage model assumptions. Test loads were applied in blocks of 5000 flights using five different flight types. Each flight type employed up to 25 flight segments with five load levels for nine major gust and maneuver segments. Test time objectives were met by tailoring the spectra truncation levels. Ancillary panel tests were conducted to evaluate the impact of spectrum variables. The mixture of flights was constructed such that unique fracture face marking would result to simplify subsequent optical microscopy.

KEY WORDS: fatigue (materials), full-scale testing, spectrum loads, testing

The development of a new aircraft type generally embodies the latest in available technology. Innovative construction methods, advanced materials and processes, and highly refined structural analysis techniques are combined to produce a vehicle with performance that surpasses previous models. These advances require an extensive development and verification test program that employs test specimens as large as full-scale articles. In the case of fatigue testing, each test presents a unique task of balancing technical requirements with available test equipment. The magnitude of the task is usually proportional to specimen size. The purpose of this paper is to describe the procedure by which the cyclic test spectra were developed for the airframe fatigue tests of the Boeing Model 757 and 767 jet transports.

The primary objective of full-scale airframe fatigue tests is to locate areas that may exhibit early fatigue problems. The testing is accelerated relative to fleet usage so that corrective action can be made in a timely manner. Additional objectives of the test are to help develop and verify inspection and maintenance procedures and to provide test data for analytical service life predictions. The 757 and 767 tests were not designed to demonstrate "safe-life" limits for structure certified as damage tolerant and were not considered an alternative to the inspections required to maintain a damage tolerant design.

The flight loaded primary structure of the two new models was represented by five separate

[1] Structures Technology staff, Boeing Commercial Airplane Company, Seattle, WA 98124.

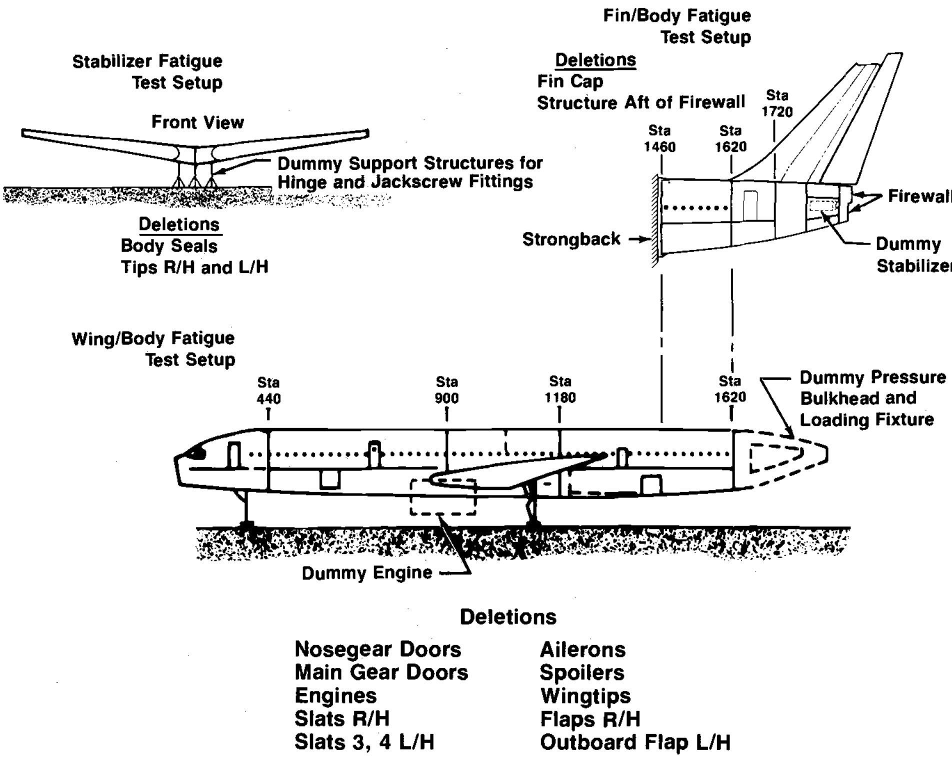

FIG. 1—*757 fatigue test articles.*

test articles: 757 horizontal stabilizer fin/aftbody and wing/body (Fig. 1), and 767 horizontal stabilizer and wing/body/fin (Fig. 2). Division of the structure in this manner provided the best match between test articles and facilities and reduced the time required to complete testing. These considerations were especially important because both models were developed concurrently.

Philosophy

Development of the subject test spectra was based on the concept of applying loads as realistically as possible while conforming to time and economic constraints. The frequency and magnitude of loads were defined by previously recorded incremental load spectra when possible and were sequenced into several flight types to meet observed statistical criteria. It is generally accepted that this approach, which minimizes reliance on damage model assumptions, gives more representative test results.

A single base mission, representing a typical combination of payload and range, was used to generate the multiple test flight types. Thus, the test flight types were composed of a variable number of incremental loads superimposed on a single 1-g or steady-state load profile. While this approach does not simulate a variety of payload and range 1-g load combinations, the sequence of stresses generated are assumed to be representative, as a given cyclic peak or valley can be arrived at with various combinations of 1-g and incremental loads. In addition, the distribution of extreme loads is derived to meet statistical criteria

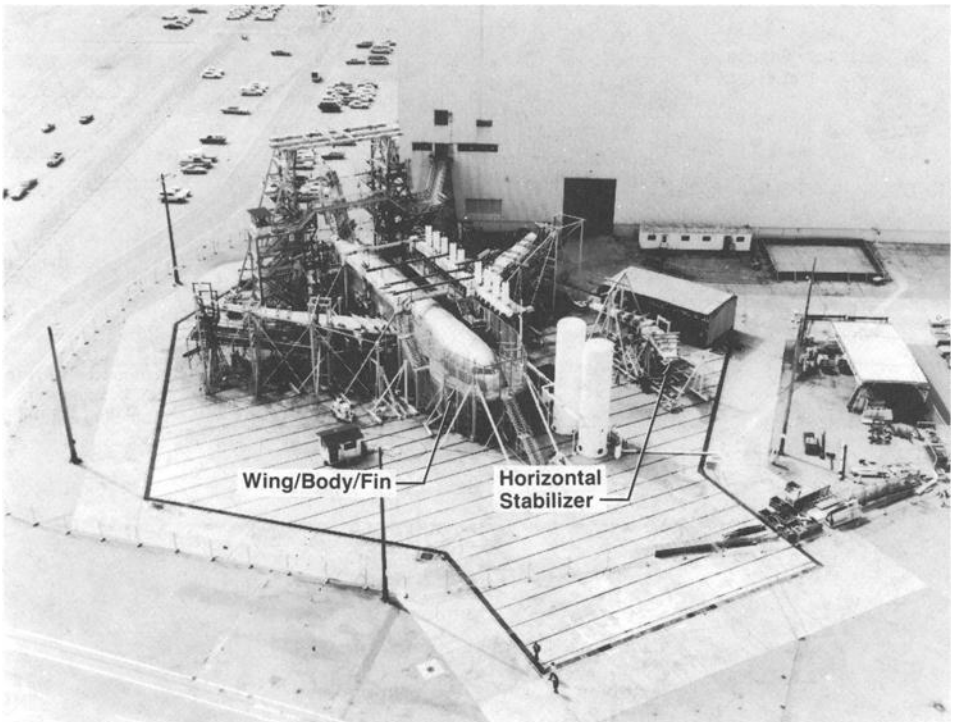

FIG. 2—*767 major fatigue test articles.*

that were established by measurements made in service with a typical variation of payload and range. This distribution of extreme loads was presumed to be a key factor in damage accumulation rates.

Selection of the number of test flight types and the associated number of load levels in each flight segment was made as a compromise between test representativeness and cost and schedule impact. As the number of flight types increased, the analysis required to continuously maintain equilibrium of the test article increased along with the effort required to program the load system controller and to verify that the intended spectrum of loads was being applied. The Transport Wing Standard Spectrum (TWIST) [*1*], whose statistical distribution criteria were loosely followed in the development of the present spectrum, is composed of ten flight types with ten load levels in a single flight segment representing climb, cruise, and descent gust loads. Previous large-scale tests at Boeing have employed eight flight types with eight load levels in each of three flight segments.

The 757 and 767 test spectra included five flight types and five load levels (referred to as 5 by 5) in each of nine segments. This choice provided the best balance between available resources and technical requirements. Supporting crack growth tests discussed later in this paper showed that this simplified spectrum is essentially equivalent to a much more complex spectrum with ten load levels per flight segment, 5000 unique flight types, and approximately twice as many average cycles per flight.

The 5 by 5 full-scale test spectrum is shown in terms of the stress response of a body crown detail for the 767 in Fig. 3. The full-scale tests of the 757 and 767 were broken up

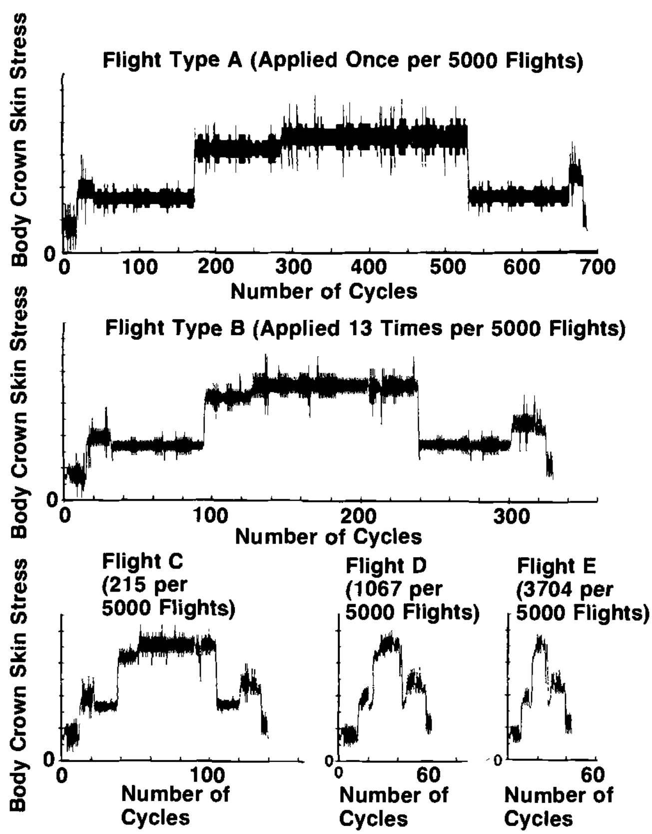

FIG. 3—*767 full-scale airframe fatigue test spectra.*

into a number of different test articles; however, the load sequences were made as similar as possible to facilitate comparisons from one article to the next.

Governing Parameters

The following maximum values for the average test flight time were established to meet schedule considerations. No maximum value was established for the 767 horizontal stabilizer test because the test was started approximately six months prior to the other tests and the test would naturally run quicker than the wing/body/fin test as fewer cycles were applied and the deflections were much smaller.

Test Article	Maximum Average Test Flight Time, min
757 horizontal stabilizer	1.7
757 fin/aftbody	2.6
757 wing/body	4.0
767 wing/body/fin	4.0

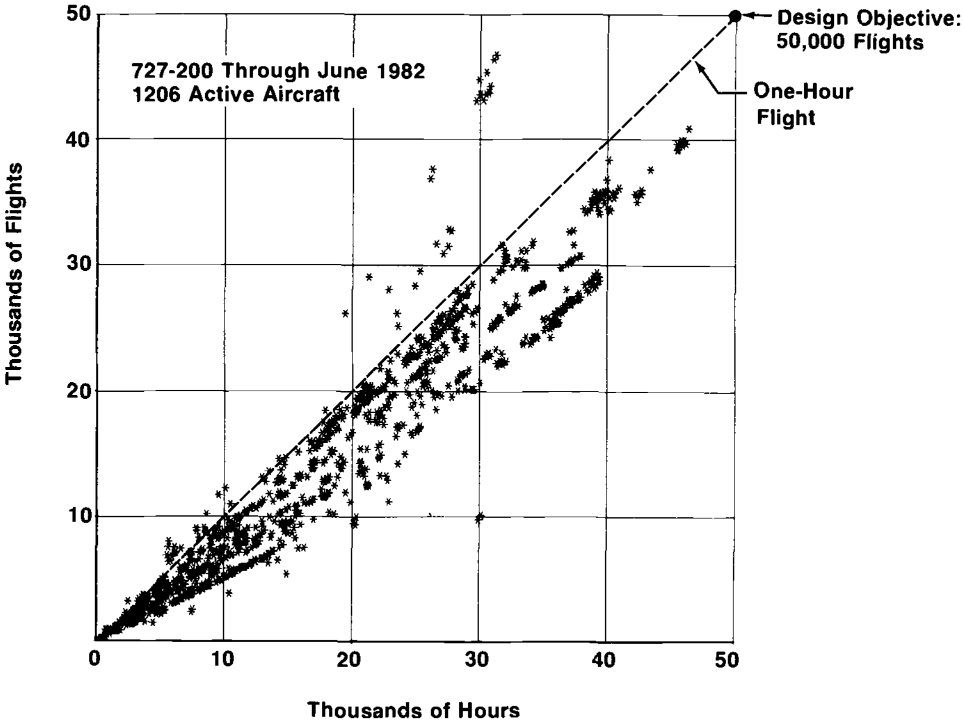

FIG. 4—*727-200 usage summary.*

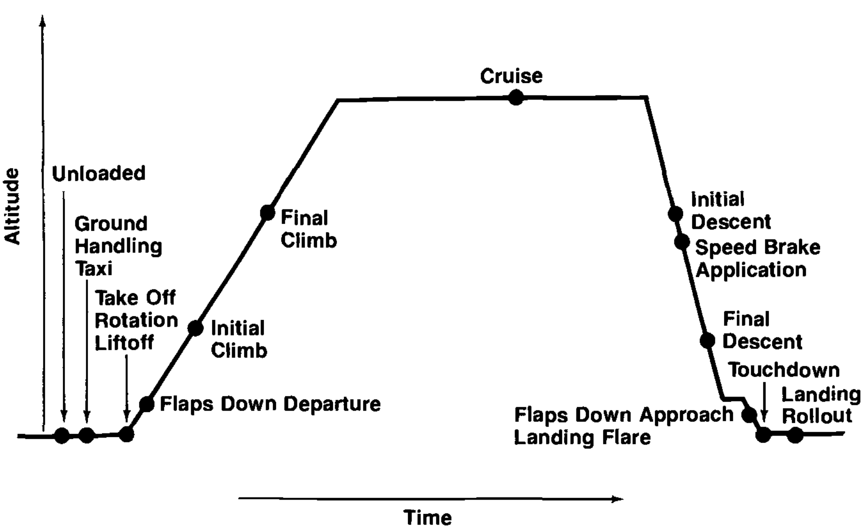

FIG. 5—*Typical flight segmentation.*

TABLE 1—*Operating conditions—757-200 1-h mission.*

Condition	Altitude, 1000 ft[a]	Distance, nmi	Speed, keas	Flaps, deg	Thrust, kips/engine	Gross Weight, kips
Unloaded	0	0	0	0	0	145
Ground handling	0	0	...	0	...	185
Liftoff	0	0	131	20	30.2	185
Flaps down departure	1	0	176	20	25.0	184
Initial climb	3	8	279	0	21.0	184
Final climb	15	59	276	0	16.0	183
Cruise	30	223	288	0		
			($M = 0.8$)		6.6	179
Initial descent	15	68	341	0	7.3	176
Final descent	3	10	250	0	4.9	176
Flap down approach	1	0	162	30	19.1	176
Yaw maneuver	1	0	162	30	19.1	176
Flare	0	0	125	30	0	176
Touchdown	0	0	125	30	0	176
Landing rollout	0	0	87	30	−12.5	176

NOTES:
Flight distance, nmi = 368.0
Flight length, h = 1.0
Life goal, flights = 50 000
Operating empty weight, kips = 134.9
Fuel reserve, kips = 11.9
Payload, kips = 29.4
[a] 1 ft = 0.3048 m.

TABLE 2—*Operating conditions—767-200 1-h mission.*

Condition	Altitude, 1000 ft[a]	Distance, nmi	Speed, keas	Flaps, deg	Thrust, kips/engine	Gross Weight, kips
Unloaded	0	0	0	0	0	191
Ground handling	0	0	...	0	...	246
Liftoff	0	0	131	20	42.7	246
Flaps down departure	1	0	185	20	32.2	245
Initial climb	3	7.8	250	0	26.4	244
Final climb	15	66.0	294	0	21.6	241
Cruise	30	249.1	296	0	8.8	237
Initial descent	15	60.2	354	0	9.5	234
Final descent	3	7.1	250	0	9.9	234
Flap down approach	1	0	162	36	12.7	234
Yaw maneuver	1	0	162	36	12.7	234
Flare	0	0	122	36	1.0	234
Touchdown	0	0	122	36	1.0	234
Landing rollout	0	0	91	36	−17.0	234

NOTES:
Flight distance, nmi = 390.2
Flight length, h = 1.0
Life goal, flights = 50 000
Operating empty weight, kips = 177.3
Fuel reserve, kips = 13.9
Payload, kips = 42.4
[a] 1 ft = 0.3048 m.

TABLE 3—*Operational condition application.*

	Test Article			
Condition	Horiz Stab	Fin Body	Wing Body	Wing Body Fin
Unloaded	...	X	X	X
Turn tow	...	...	X	X
Straight tow	...	...	X	X
Ground turn	...	...	X	X
Braked roll	...	X	X	X
Engine runup	...	...	X	X
Taxi-out	X	X	X	X
Rotation	X	X	...	X
Liftoff	X	X	X	X
Flaps down departure	X	X	X	X
Initial climb	X	X	X	X
Final climb	X	X	X	X
Cruise maneuver	X	X	X	X
Cruise gust	X	X	X	X
Descent spoiler	X	X	X	X
Initial descent	X	X	X	X
Final descent	X	X	X	X
Flaps down approach	X	X	X	X
Yaw maneuver	X	X	...	X
Flare	X	X	X	X
Main gear impact	X	X	X	X
Drift landing	...	...	X	X
Nose gear impact	...	...	X	X
Empennage buffet	X	X	...	X
Taxi-in	X	X	X	X

Average test flight time was estimated based on the travel of the limiting hydraulic load actuator: the most outboard wing or horizontal stabilizer actuator for vertical loadings, and the highest fin actuator for lateral loadings. The test laboratories specified a maximum actuator velocity and a minimum dwell time for each control point. A control point was either the end point of a cycle, that is, a peak or valley, or an intermediate load if it was required for proper load phasing. As a minimum, two control points were required to define a cycle and a maximum of eight control points were used to define vertical/lateral cycles in these spectra.

The systems used to control fuselage internal pressure were capable of controlling two pressure conditions; ambient and cruise pressure. The pressure ramps between these points were fixed in terms of application time from one flight to the next, however, the placement of the ramps in the five flight types could be varied to simulate the desired pressurization schedule. The time required to recycle the pressure system was accounted for by establishing minimum times between flight phases that were used in place of the hydraulic actuator application time limits, if the actuator times were less. A minimum of 2.5 min per flight was established for the 767 wing/body/fin test. A minimum depressurization time of 10 s and minimum pressurization times of 15 and 25 s were scheduled for the 757 wing/body and 757 fin/aftbody tests, respectively. The impact of these requirements was most significant on the 757 fin/aftbody test where cycling was halted temporarily during some flights to allow the pressure system to pressurize or depressurize.

TABLE 4—*Operational condition representation.*

Condition	Cyclic Representation
Unloaded	steady-state load
Turn tow	one cycle of same magnitude per flight
Straight tow	one cycle of same magnitude per flight
Ground turn	two cycles of same magnitude per flight
Braked roll	one cycle of same magnitude per flight
Engine runup	steady-state load
Taxi-out	5 by 5 spectrum
Rotation	steady-state load
Liftoff	steady-state load
Flaps down departure	5 by 5 spectrum
Initial climb	5 by 5 spectrum
Final climb	5 by 5 spectrum
Cruise maneuver	5 by 5 spectrum
Cruise gust	5 by 5 spectrum
Descent spoiler	one cycle of same magnitude per flight
Initial descent	5 by 5 spectrum
Final descent	5 by 5 spectrum
Flaps down approach	5 by 5 spectrum
Yaw maneuver	15 cycles of same magnitude per flight
Flare	steady-state load
Main gear impact	two cycles of same magnitude per flight
Drift landing	one cycle of same magnitude per flight
Nose gear impact	two cycles of same magnitude per flight
Empennage buffet	nine cycles of same magnitude per flight
Taxi-in	5 by 5 spectrum

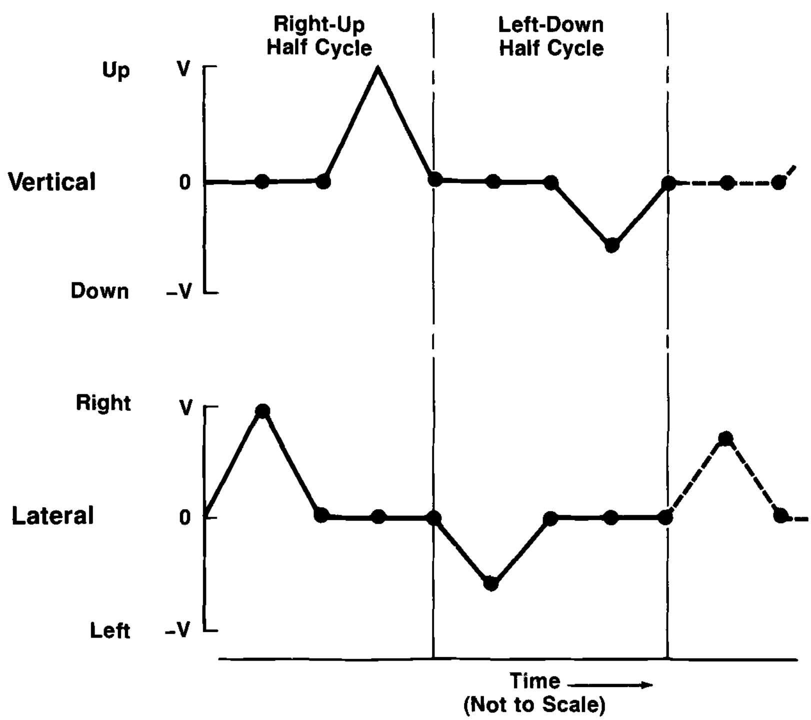

FIG. 6—*Vertical/lateral gust phasing.*

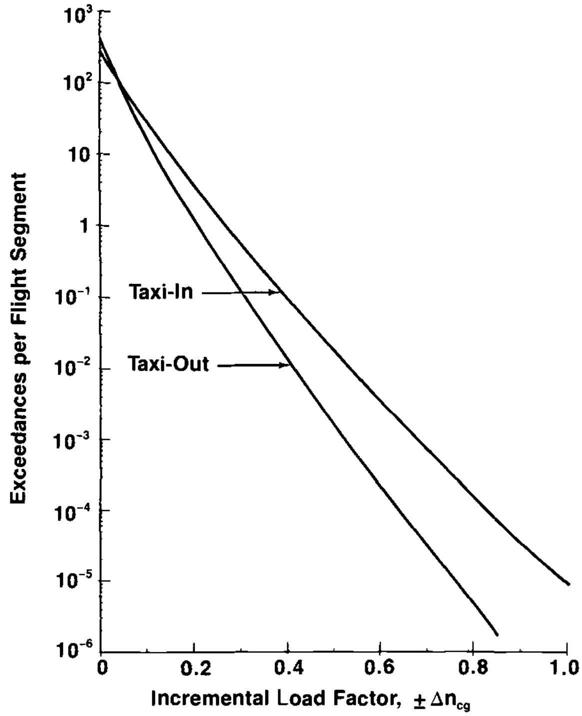

FIG. 7—*Runway roughness analytical spectrum.*

The final test system constraint concerned storage of the test spectrum in the computers that controlled the five tests. The 767 wing/body test setup was the most restrictive and was therefore used to optimize the five spectra. Optimization of the test spectra to fit within this limitation is discussed later.

Base Mission Selection

Boeing jet transports are designed to achieve a minimum of 20 years of service life without cracking causing an undue economic burden. Design life goals are based on the most critical combination of flight length and number of flights [2] to provide operational flexibility.

The service utilization of both the 757 and 767 was expected to be similar to the 727-200, and review of its usage is given in Fig. 4. This data shows that the average flight length for most aircraft falls between 0.75 and 1.5 h with the median slightly greater than 1 h. A 1-h flight length was selected as the base mission for the 757 and 767 test spectra. This was a conservative choice for most structure because shorter flights allow a greater number of ground-air-ground cycles to be accumulated in 20 years.

The 1-h flight length was divided into flight segments as shown in Fig. 5. The resulting segmented missions for the two aircraft are shown in Tables 1 and 2. Note that the segment distances and resulting total flight distances are slightly different although the segment altitudes and total flight duration are the same.

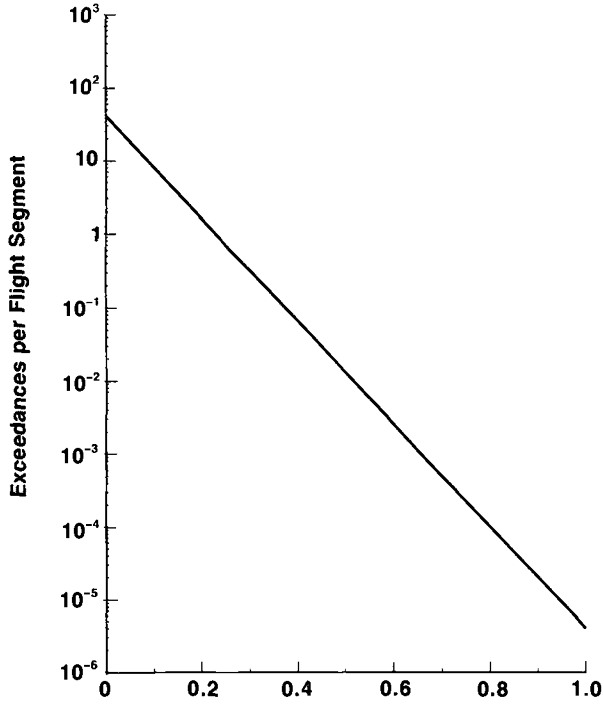

FIG. 8—*Flight maneuver analytical spectrum.*

Operational Condition Representation

Division of the 757 and 767 structure into separate test articles resulted in test time savings in part because many of the operational conditions defined in Fig. 5 did not cause significant loading on a given test article and therefore could be eliminated for that test. Examples of this are the ground handling conditions for the horizontal stabilizer tests and empennage buffet loads on the 757 wing/body test. Operational conditions that were represented on each test article are shown in Table 3.

Variability of the test load magnitudes from flight to flight was based on expected variation in service and damage imposed on the structure. Loads for conditions such as "straight tow" and "engine runup" are fairly consistent and were applied in the tests with the same magnitude in every flight. Other conditions that were applied as constant magnitude loads are variable in service but this did not have a significant effect on the damage accumulation rates of the structure. Operational conditions that exhibit significant load variability in service and cause significant damage such as maneuvers and gusts were applied with 5 by 5 spectra. The cyclic representation of the operational conditions is summarized in Table 4.

Gust loads were simulated both vertically and laterally on all but the horizontal stabilizer tests. The gusts were applied in the order: right, up, left, down (Fig. 6). The vertical and lateral loads that made up a half-cycle pair, right-up and left-down, represented the same magnitude gust, however, adjacent half cycles did not always represent the same magnitude.

Maneuver and taxi loads were applied so that positive and negative incremental accel-

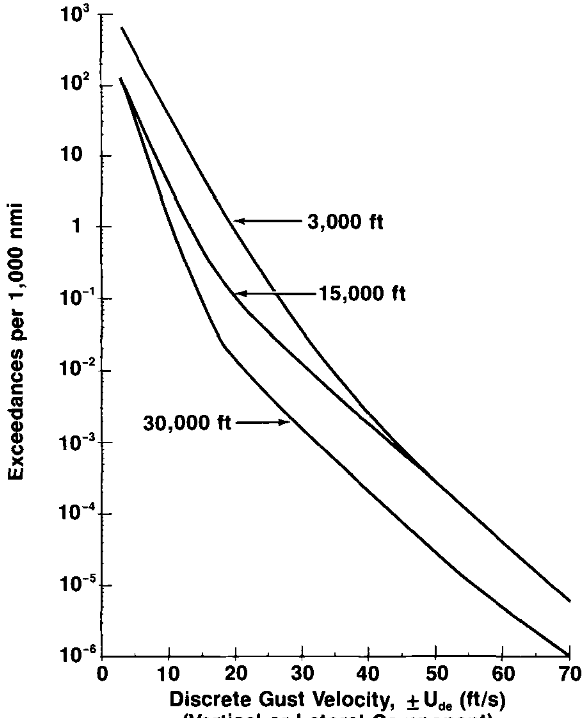

FIG. 9—*Gust analytical spectra.*

erations alternated. As for the gust loads, adjacent half cycle pairs often were of different magnitudes.

Alternating load peaks for certain cyclic conditions were separated by applications of the 1-*g* or condition reference load. This practice ensured that the full range of the load cycles was applied for structure that responded with alternating stresses of the same sign for both positive and negative (or left and right, etc.) alternating conditions. An example of this is the nose landing gear drag load component that has the same direction for both left and right turns.

Load Spectra Representation

Exceedance data for the five load level flight segments were drawn from early NACA/NASA reports (Figs. 7 through 9 and Refs *3* through *5*). These load spectra have been in use at Boeing for more than 15 years, forming an analytical standard used for design and service evaluation.

Recently recorded data from a number of sources (Refs *6* through *12*) have been compared with the Boeing standard spectra (Figs. 10 and 11). The Boeing standard spectra represent more incremental load activity than any of the more recently recorded spectra, perhaps due in large part to improved pilot techniques and advances in weather radar. These comparisons verify that a conservative representation of the load environment was applied to the test articles.

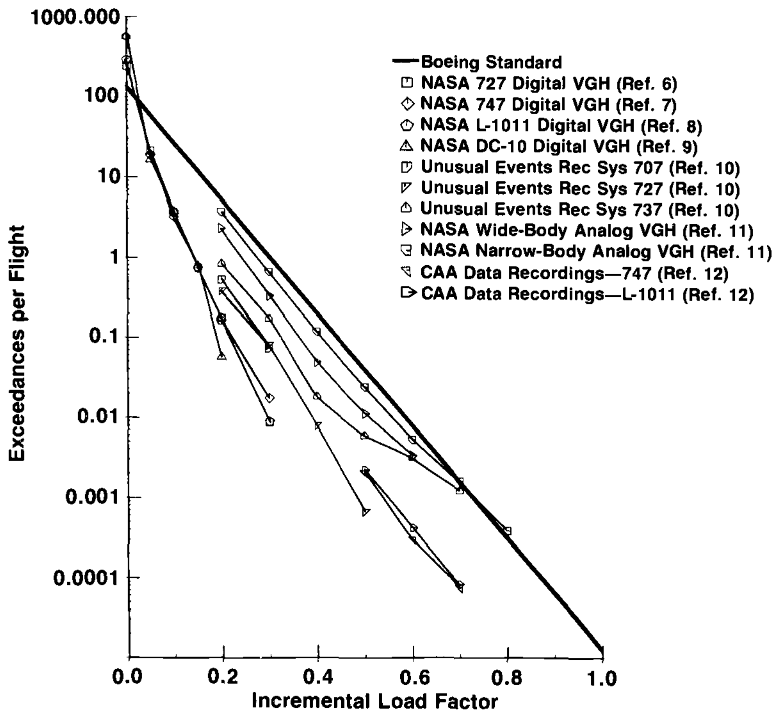

FIG. 10—*Comparison of recorded flight maneuver spectra.*

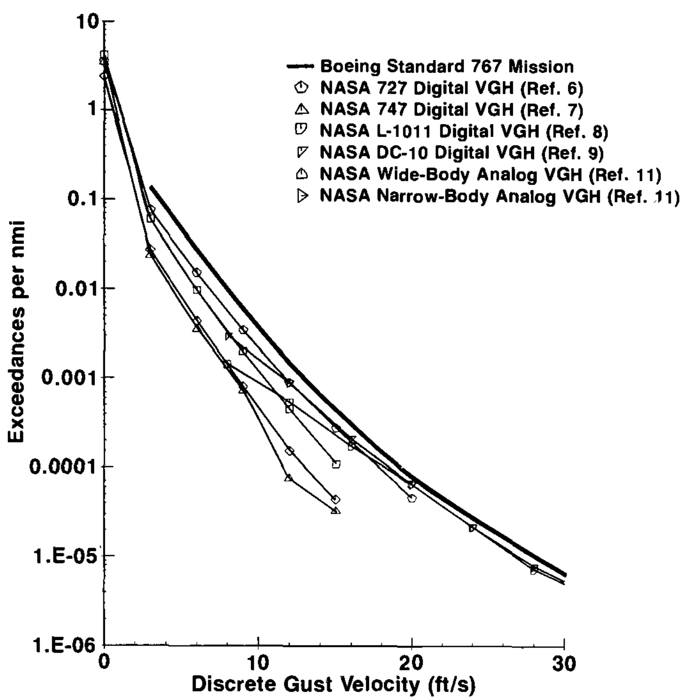

FIG. 11—*Comparison of recorded gust spectra for all altitudes combined.*

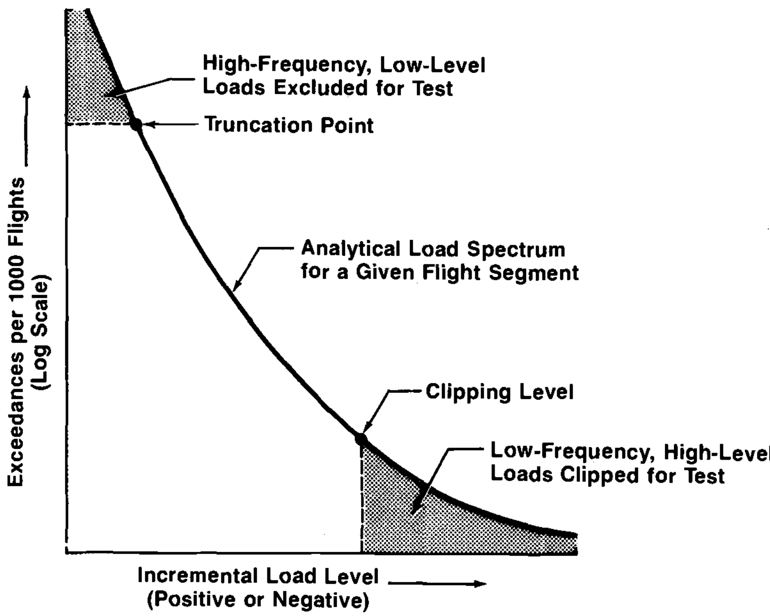

FIG. 12—*Truncation and clipping of analytical load spectra.*

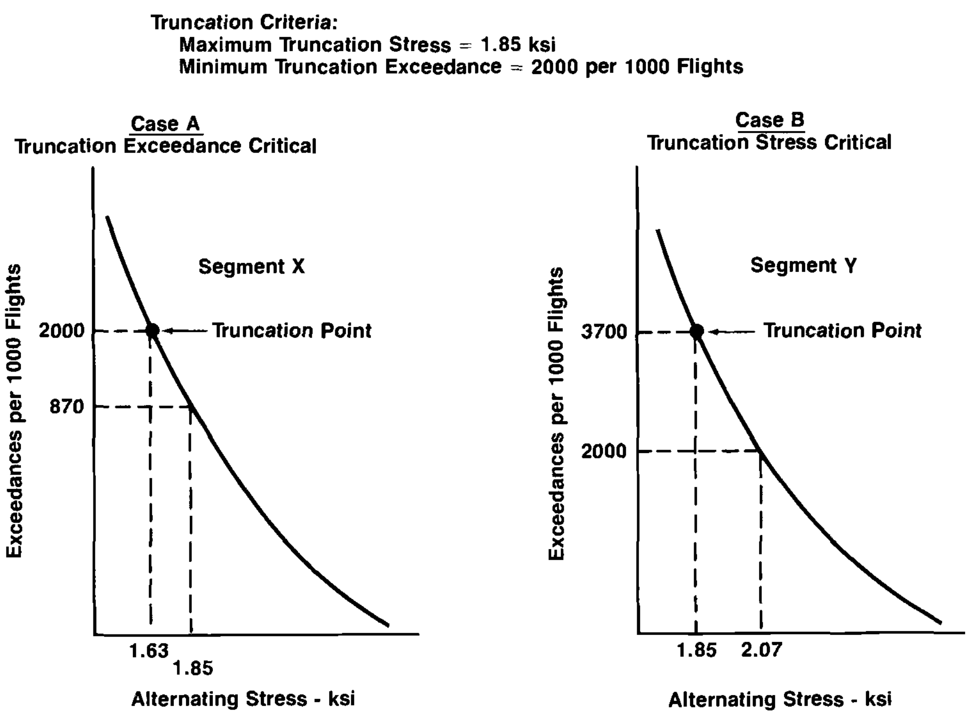

FIG. 13—*Truncation level determination example.*

The analytical load spectra are a statistical representation of load activity experienced during airline operations and have been extrapolated to include incremental loads as small as zero and as infrequent as once in 20 lifetimes. These spectra were modified for test use by truncating low loads to reduce test time and by clipping infrequent high loads to avoid unrealistic results due to crack growth retardation effects (Fig. 12).

The high-load portion of each of the analytical spectra was clipped at the load equaled or exceeded ten times per lifetime. This choice was based on criteria expressed in Ref *1* and results in a load that can be expected to be experienced several times by the majority of the fleet. Consequently, the most infrequent load occurs once per 5000 flights (1/10 of the life goal of 50 000 flights) so the test load spectrum is a repetition of 20 essentially identical blocks of 5000 flights to complete two lifetimes of loading. (Note that the location of the least frequent flight was varied for reasons discussed later.)

The average number of cycles per flight and thus the average test time per flight is a function of the low-load truncation level of the test spectrum. The truncation level was selected to meet the average test time requirements that ensured completion of 10 years of simulated flights prior to revenue service.

A study was conducted to select the lowest truncation level possible while conforming to the limits on average test flight times. This time was estimated by considering structural deflections and test load system performance. From this study, the truncation level was set at an alternating stress of at most 1.85 ksi for the most highly stressed wing details. If this criterion resulted in fewer than an average of two cycles per flight segment, the truncation stress was lowered to maintain this average (Fig. 13).

Clipping and truncation levels determined from these criteria are shown in Table 5 for the 757 and resulted in an average of 52 cycles per flight for the 757 wing/body test when all of the conditions of Table 3 were included. A test program to determine the effect of the truncation criteria and other test spectra variables will be discussed later. However, results of tests reported in Ref *13* gave an indication that the selected truncation criteria would have a small effect on the test life of the structure. In these tests, a change in the smallest alternating load from 22.2 to 37.5% of the flight mean stress had a small effect on

TABLE 5—*757 truncation and clipping levels.*

Flight Segment	Governing Detail[a]	Unit Stress Response, ksi	Truncation Load	Truncation Alternating Stress, ksi	Clipping Load	Clipping Alternating Stress, ksi	Average Cycles per Flight
Taxi-out	WU	2.95	0.157 Δg[b]	0.46	0.607 Δg	1.79	3.57
Flaps down departure	WL	11.22	0.151 Δg	1.69	0.759 Δg	8.52	3.68
Initial climb	WL	0.23	5.33 ft/s[c]	1.23	31.2 ft/s	7.18	2.00
Final climb	WL	0.25	5.53 ft/s	1.38	36.7 ft/s	9.18	2.00
Cruise maneuver	WL	11.56	0.151 Δg	1.75	0.759 Δg	8.77	3.68
Cruise gust	WL	0.30	5.61 ft/s	1.68	32.9 ft/s	9.87	4.74
Initial descent	WL	0.32	5.83 ft/s	1.87	37.5 ft/s	12.00	2.00
Final descent	WL	0.21	5.88 ft/s	1.23	32.0 ft/s	6.72	2.00
Flaps down approach	WL	12.17	0.151 Δg	1.84	0.759 Δg	9.24	3.68
Taxi-in	WU	2.59	0.214 Δg[b]	0.55	0.785 Δg	2.03	2.79

[a] WU = wing upper surface and WL = wing lower surface.
[b] Excludes damage matching factors, see Fig. 24.
[c] Ft/s = 0.3048 m/s.

the lives of notch and joint specimens. The smallest alternating load in the 757 and 767 spectra is less than 17.5% of the cruise mean stress for all of the five load level flight phases based on the greatest stress responses of wing lower surface details sampled.

Test Flight Type Definition

The test spectra were composed of a repetition of five different flight types. The cyclic makeup and relative frequency of the test flights was determined using methods similar to those used for the standardized spectrum TWIST [*1*]. The key requirements are:

1. A log-normal extreme value distribution of the highest loads per flight.
2. Similarity of the shapes of the gust spectra for the different flight types.

These two requirements were applied to the segment that had the highest loading per flight for most of the structure tested, which was the cruise gust segment of the subject spectra. A 5 by 5 matrix was formed (see Fig. 14) in which the rows represent different segment types and the columns represent different load levels. The load levels, number of each load level in each segment type, and the relative number of each segment type were adjusted iteratively until both distribution criteria were met. Throughout this process, the summation of the individual segment exceedance curves times their relative frequency was kept equal to the standard analysis spectra.

The final load matrix for the 767 cruise gust segment is shown in Fig. 15. The extreme

Segment Type / Number of Segments in a 5000 Flight Block	Initial Climb Gust				
	Number of Peaks/Valleys at Five Amplitude Levels [1]				
	(±30.2 ft/s) I	(±24.2 ft/s) II	(±14.9 ft/s) III	(±9.14 ft/s) IV	(±5.60 ft/s) V
A [2]	[3]	[4]	[4]	[4]	[4]
B [2]		[3]	[4]	[4]	[4]
C [2]			[3]	[4]	[4]
D [2]	No Cyclic Loads Allocated in This Region			[3]	[4]
E [2]					[3]

[1] One "cycle" consists of one positive (peak) and one negative (valley) load increment. Peaks and valleys of the same magnitude are not always paired. A value of N in the matrix above indicates N peaks and N valleys at the given incremental load level.

[2] The sum of these numbers is equal to the number of flights per block.

[3] Location of extreme loads for the various segment types. One or more occurrences of a peak and valley of the given magnitudes *must* be allocated in each of these locations.

[4] Values in these locations are chosen to meet gust or maneuver load distribution criteria.

FIG. 14—*Load matrix definition.*

Flight Type / Number of Flights in a 5000 Flight Block	Cruise Gust: Number of Peaks/Valleys at Five Amplitude Levels (±32.9 ft/s) I	(±26.4 ft/s) II	(±16.5 ft/s) III	(±10.4 ft/s) IV	(±6.64 ft/s) V	Number of Cycles in One Flight
A 1	1	3	6	56	61	127
B 13		1	2	32	40	75
C 215			1	12	23	36
D 1067				3	4	7
E 3704	4.74 Cycles per Flight Average				2	2
Number of Cycles in a 5000 Flight Block	1	16	247	6253	17202	

FIG. 15—*Cruise gust alternating load allocation.*

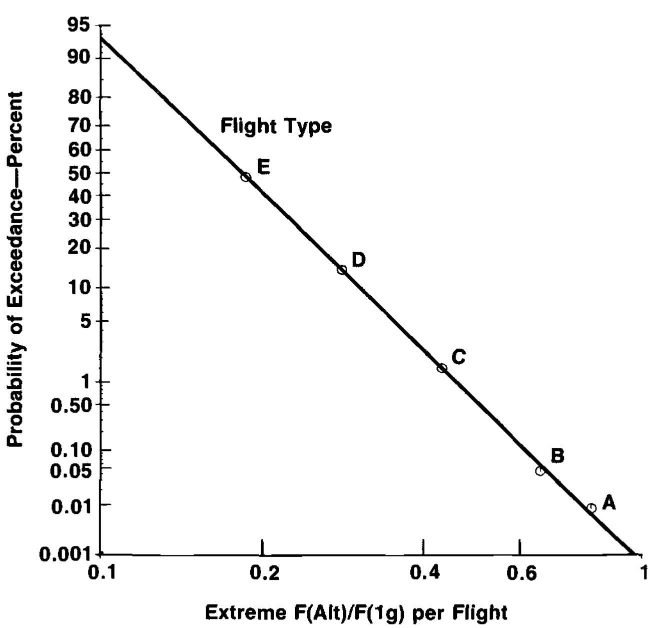

FIG. 16—*757 extreme load distribution.*

value distribution was determined from the highest loads of each flight that ranged from a maximum incremental gust per flight of 2.07 m/s (6.82 ft/s) occurring 3704 times per 5000 flight block in Flight Type E to a maximum per flight of 10.2 m/s (33.5 ft/s) occurring once per 5000 flights in Flight Type A. The extreme value distribution is plotted on log-normal probability paper in Fig. 16 after converting incremental gust velocity to the ratio of alternating to 1-g stress for a critical wing lower surface detail. The straight line drawn through the points for the five flight types demonstrates a log-normal distribution with a standard deviation of 0.19.

Exceedance curves for the individual segment types were made as similar as possible by developing a family of curves with a common value of N_o, the exceedance at an incremental load level of zero. Plotting these curves for the cruise gust segment, Fig. 17, reveals that some approximations had to be made due to the limited number of flight types and load levels. Summing these five curves times their relative frequency allows comparison with the analytical spectrum, Fig. 18.

Distribution of loads for the remaining four gust segments was made in a similar manner, except that the relative frequencies of the five segment severities were already determined (Fig. 19). Plots of these segments' exceedance curves by segment type and a comparison of the sum of their spectra versus the analytical spectra are given in Figs. 20 and 21. Division of the gust loads into segments with different 1-g load levels departs from the method of

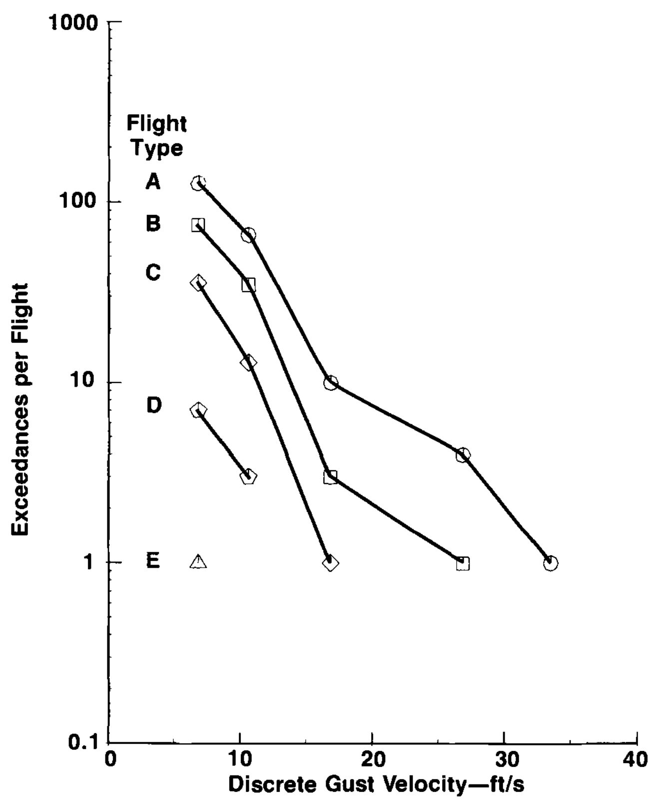

FIG. 17—*Cruise gust spectra by flight type.*

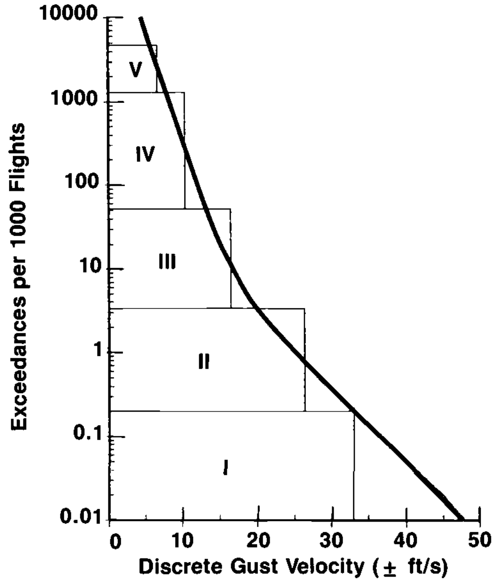

FIG. 18—*Cruise gust test versus analysis spectra.*

TWIST, where only one flight 1-*g* load level is used. This departure was necessary on a large-scale, multichannel test, to accurately represent service loading.

Maneuver loads were distributed among the various segment types of the five multilevel maneuver segments such that the total number of cycles per flight was approximately the same for each type. Equal apportionment in this sense refers to orders of magnitude rather than absolute values. The number of cycles per segment for the five severity levels were within an order of magnitude for the maneuver segments versus up to two orders of magnitude for the gust segments (see Figs. 19 and 22). This assumption on the distribution of maneuver loads, while not supported by operational data, is believed to be consistent with airline operations where a similar number of maneuvers are used for departure and approach from one flight to the next with some load level variation due to weather avoidance, air traffic considerations, etc.

Summations of the exceedance curves for the five multilevel maneuver segments are compared with the analytical spectra in Fig. 23. Examination of the curves for taxi-in and taxi-out reveals that the load level selection criteria were modified for these segments. Analyses of nacelle and landing gear support structure showed that the taxi segments contribute up to half of the damage for these details compared to less than 5% for most of the structure. The truncation levels for the taxi test spectra were selected as previously discussed, which gave approximately 50% of the damage of the analytical spectra. Damage matching factors plotted in Fig. 24 were then applied to the alternating loads to give the same fatigue damage as the analytical spectra. The damage matching factors vary linearly as a function of incremental load from 1.0 for the largest load level to 1.25 for the lowest load level. This approach was considered to be the best compromise between minimizing test flight time and realistically representing the analytical load spectra.

At this point, the cyclic content of the five test flight types had been completely determined. Each flight type was composed of a series of segments in the order shown in Fig. 5. For segments with multiple load levels, like segment severities were used in a given flight type

Flight Type / Number of Flights in a 5000 Flight Block	Initial Climb Gust — Number of Peaks/Valleys at Five Amplitude Levels: (±31.2 ft/s) I	(±25.1 ft/s) II	(±15.7 ft/s) III	(±9.86 ft/s) IV	(±6.30 ft/s) V	Number of Cycles in One Flight
A 1	1	10	61	57	2	131
B 13		3	19	37	3	62
C 215			1	11	3	15
D 1067				1	1	2
E 3704	2 00 Cycles per Flight Average				1	1
Number of Cycles in a 5000 Flight Block	1	49	523	3970	5457	

Flight Type / Number of Flights in a 5000 Flight Block	Final Climb Gust — Number of Peaks/Valleys at Five Amplitude Levels: (±36.7 ft/s) I	(±29.2 ft/s) II	(±17.2 ft/s) III	(±10.2 ft/s) IV	(±6.71 ft/s) V	Number of Cycles in One Flight
A 1	1	6	40	56	9	112
B 13		1	8	15	7	31
C 215			1	7	4	12
D 1067				1	2	3
E 3704	2.00 Cycles per Flight Average				1	1
Number of Cycles in a 5000 Flight Block	1	19	359	2823	6798	

Flight Type / Number of Flights in a 5000 Flight Block	Initial Descent Gust — Number of Peaks/Valleys at Five Amplitude Levels 1: (±37.5 ft/s) I	(±29.9 ft/s) II	(±17.7 ft/s) III	(±10.6 ft/s) IV	(±7.00 ft/s) V	Number of Cycles in One Flight
A 1	1	6	40	56	9	112
B 13		1	8	15	7	31
C 215			1	7	4	12
D 1067				1	2	3
E 3704	2.00 Cycles per Flight Average				1	1
Number of Cycles in a 5000 Flight Block	1	19	359	2823	6798	

Flight Type / Number of Flights in a 5000 Flight Block	Final Descent Gust — Number of Peaks/Valleys at Five Amplitude Levels 1: (±32.0 ft/s) I	(±25.8 ft/s) II	(±16.3 ft/s) III	(±10.4 ft/s) IV	(±6.85 ft/s) V	Number of Cycles in One Flight
A 1	1	10	61	57	2	131
B 13		3	19	37	3	62
C 215			1	11	3	15
D 1067				1	1	2
E 3704	2.00 Cycles per Flight Average				1	1
Number of Cycles in a 5000 Flight Block	1	49	523	3970	5457	

FIG. 19—*Alternating load allocation for remaining gust segments.*

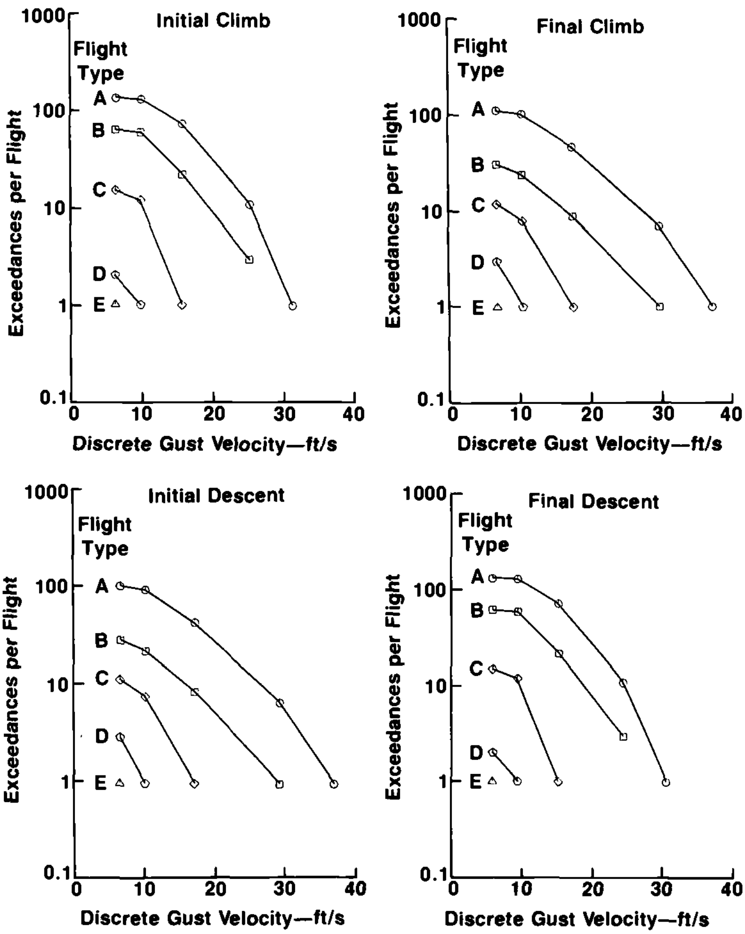

FIG. 20—*Gust spectra by flight type for remaining gust segments.*

(that is, B severity taxi-out, B severity flaps down departure, etc., were grouped into the Test Flight Type B).

Load/Flight Sequence Generation

The sequence of loads that made up the repeating block of 5000 flights was defined in two levels. First, one sequence of loads was developed for each of the five test flight types and then the sequence of these flight types was constructed. Ideally, the load sequence would have been generated by randomly selecting alternate peaks and valleys from each of the segment load matrices in succession. However, concessions were made to allow the test spectra to be applied with the test equipment available.

A computerized test control system consisting of three separate computers that could communicate with each other was used to control up to 84 independent load systems in a closed-loop type operation and also record data on a 1000 channel data acquisition system (Fig. 25). The hard disk drive used to store the load sequence, however, did not have the

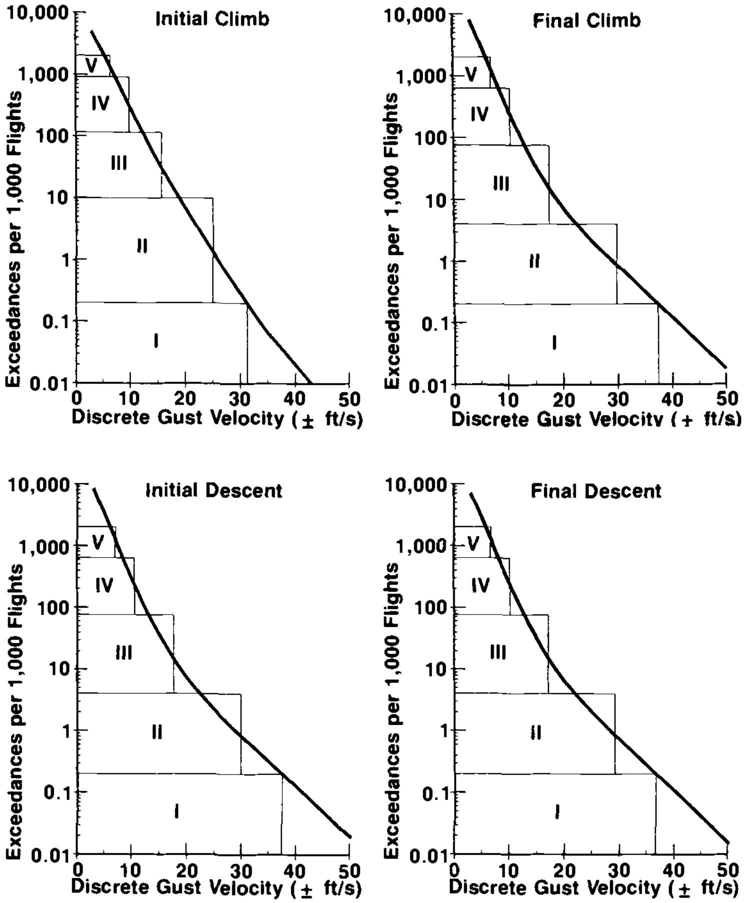

FIG. 21—*Test versus analysis spectra for remaining gust spectra.*

capacity to store a completely randomized sequence for the 5000 flight block. (Note that the block consisted of approximately 1.4 million end levels for as many as 84 independent load systems). Therefore, load sequence compression by grouping cycles of the same magnitude or multiple disks would be required. Cycle grouping was undesirable because of uncertain effects on damage accumulation rates and multiple disks were undesirable because of the lengthy procedure required to change disks.

A combination of the preceding options was used to meet test time requirements and still allow a high degree of randomization. It was decided to use the least amount of cycle grouping required to store Flight Type A on one disk and the remaining four flight types on one other disk. This decision minimized grouping of cycles and confined disk changes to once every 5000 flights, the frequency of application of Flight Type A. Cycle grouping tables were defined for each flight segment in a trial and error fashion to satisfy the storage limitations. The resulting cycle grouping tables for the cruise maneuver and cruise gust segments are shown in Fig. 26. Examination of these tables reveals that the cycle grouping is confined to the lower load levels for a given flight type. The extreme loads in each segment of each flight type were left as peak and valley half cycles. These measures were taken to

Flight Type / Number of Flights in a 5,000 Flight Block	Taxi-Out Maneuver: Number of Peaks/Valleys at Five Amplitude Levels ($\pm 0.607\ \Delta g$) I	($\pm 0.550\ \Delta g$) II	($\pm 0.442\ \Delta g$) III	($\pm 0.350\ \Delta g$) IV	($\pm 0.253\ \Delta g$) V	Number of Cycles in One Flight
A 1	1	1	0	0	1	3
B 13		2	0	0	1	3
C 215			1	3	0	4
D 1,067				1	1	2
E 3,704	3.57 Cycles per Flight Average				4	4
Number of Cycles in a 5,000 Flight Block	1	27	215	1,712	15,897	

Flight Type / Number of Flights in a 5,000 Flight Block	Taxi-In Maneuver: Number of Peaks/Valleys at Five Amplitude Levels ($\pm 0.785\Delta g$) I	($\pm 0.712\ \Delta g$) II	($\pm 0.576\ \Delta g$) III	($\pm 0.458\ \Delta g$) IV	($\pm 0.338\ \Delta g$) V	Number of Cycles in One Flight
A 1	1	1	0	0	1	3
B 13		2	0	0	1	3
C 215			1	2	0	3
D 1,067				1	1	2
E 3,704	2.79 Cycles per Flight Average				3	3
Number of Cycles in a 5,000 Flight Block	1	27	215	1,497	12,193	

Flight Type / Number of Flights in a 5,000 Flight Block	Flaps Down Departure Maneuver, Cruise Maneuver, Flaps down Approach Maneuver: Number of Peaks/Valleys at Five Amplitude Levels ($\pm 0.759\ \Delta g$) I	($\pm 0.656\ \Delta g$) II	($\pm 0.453\ \Delta g$) III	($\pm 0.297\ \Delta g$) IV	($\pm 0.196\ \Delta g$) V	Number of Cycles in One Flight
A 1	1	1	1	1	16	20
B 13		2	1	1	11	15
C 215			3	2	3	8
D 1,067				3	2	5
E 3,704	3.68 Cycles per Flight Average				3	3
Number of Cycles in a 5,000 Flight Block	1	27	659	3,645	14,050	

FIG. 22—*Load matrices for maneuver segments.*

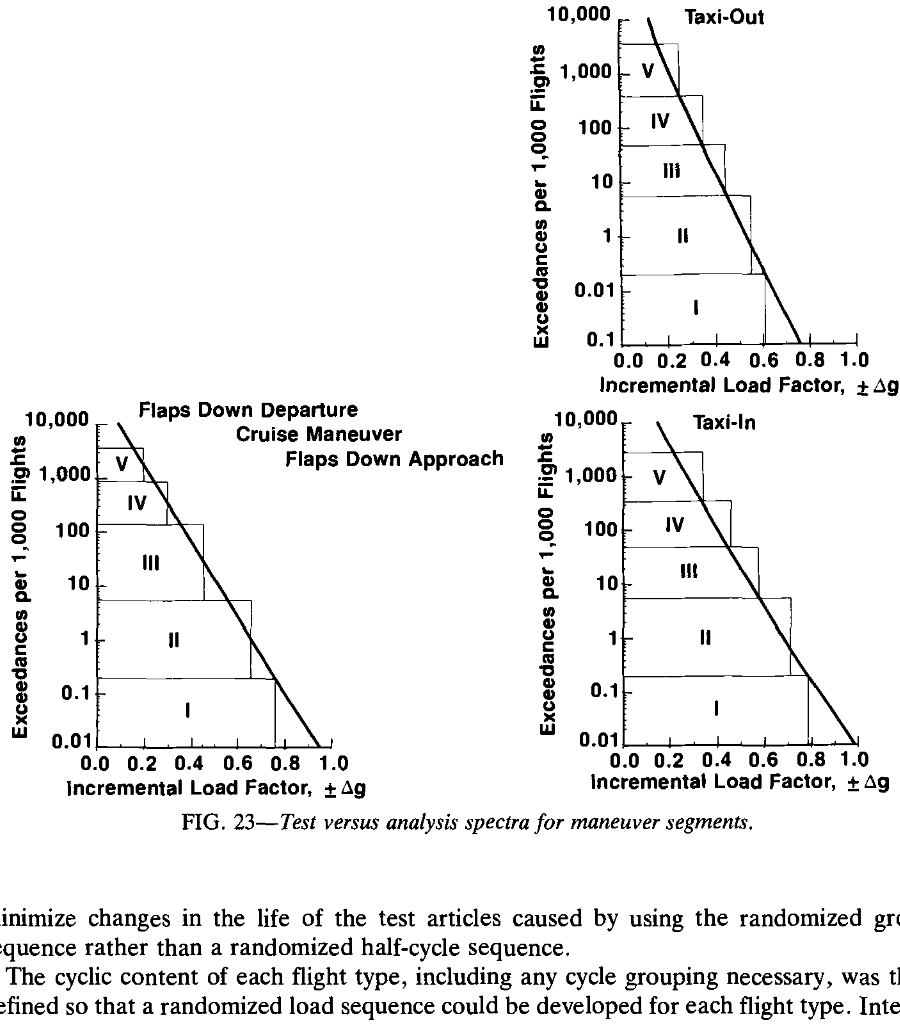

FIG. 23—*Test versus analysis spectra for maneuver segments.*

minimize changes in the life of the test articles caused by using the randomized group sequence rather than a randomized half-cycle sequence.

The cyclic content of each flight type, including any cycle grouping necessary, was then defined so that a randomized load sequence could be developed for each flight type. Integer load condition identifiers were assigned to each of the 195 unique cyclic end levels of the discrete and spectrum loads previously described. These integers were then loaded into tables for each flight type in numbers according to the cycle grouping tables for each segment. Randomization of the load sequence was then performed by random selection without replacement of load groups such that each load peak was followed by a valley. All of the loads for a given flight segment were selected before proceding to the next segment and each segment began and ended with its 1-*g* load level. The degree of randomization achieved is evident in the stress sequences of the body crown detail shown in Fig. 3.

Definition of the sequence of loads for the 5000 flight block was completed by determining the sequence of the five test flight types. A quasi-uniform distribution was selected where applications of a given flight type were approximately evenly spaced. This distribution allowed the most efficient storage of the flight type sequence on the computer, and preliminary crack growth tests showed a small difference in crack growth rates between uniform and randomized flight type sequences.

An unforeseen benefit of the uniform flight type distribution was easily discernable marker

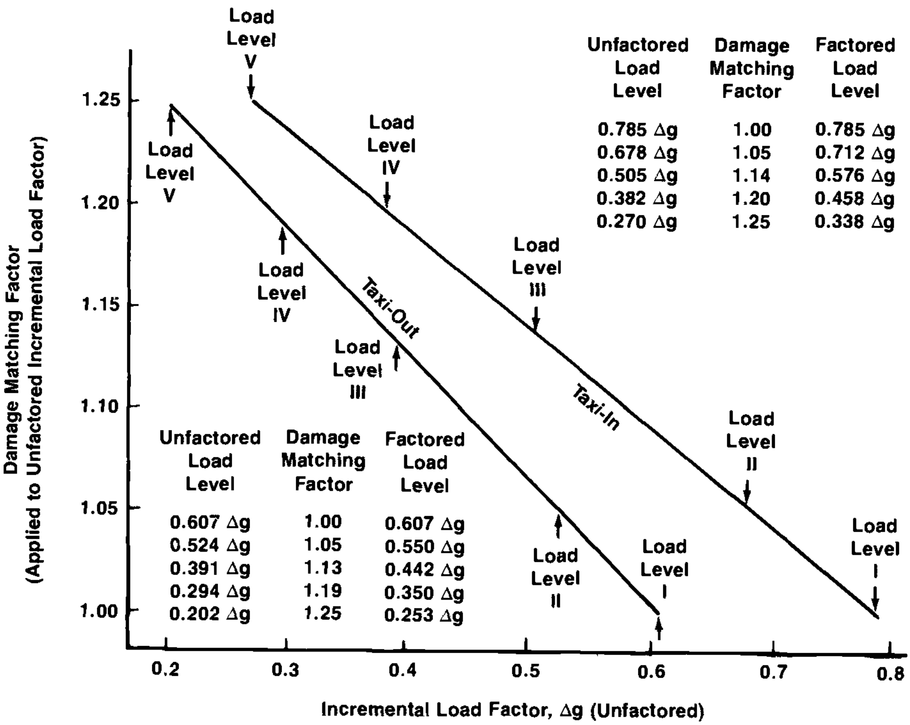

FIG. 24—*Taxi-out and taxi-in damage matching factors.*

bands on crack fracture faces (Fig. 27). Regularly spaced dark bands on the fracture surface produced by the less frequent flight types were clearly visible at moderate crack lengths and could be examined with a transmission electron microscope to within a few hundred flights of the crack origin in some cases. Based on these observations, the location of Flight Type A, which occurs once in each repeating block of 5000 flights, was varied to enable determination of the absolute number of flights at crack initiation and the phasing between interacting cracks.

Supporting Tests

A series of supporting crack growth tests were conducted to determine the impact of the compromises made in developing the full-scale test spectra [*14*]. A much more complex spectrum was developed in an attempt to recreate an actual service load history as closely as possible. This spectrum was developed in a similar manner to the full-scale spectrum with the following exceptions:

1. truncation load levels set at approximately two thirds of those used for the full-scale spectrum (this resulted in about twice as many cycles per flight on average or 5 million cycles per lifetime),
2. ten alternating load levels per flight segment instead of five,
3. no cycle grouping (all random selection of half cycles with new sequences for each flight type), and

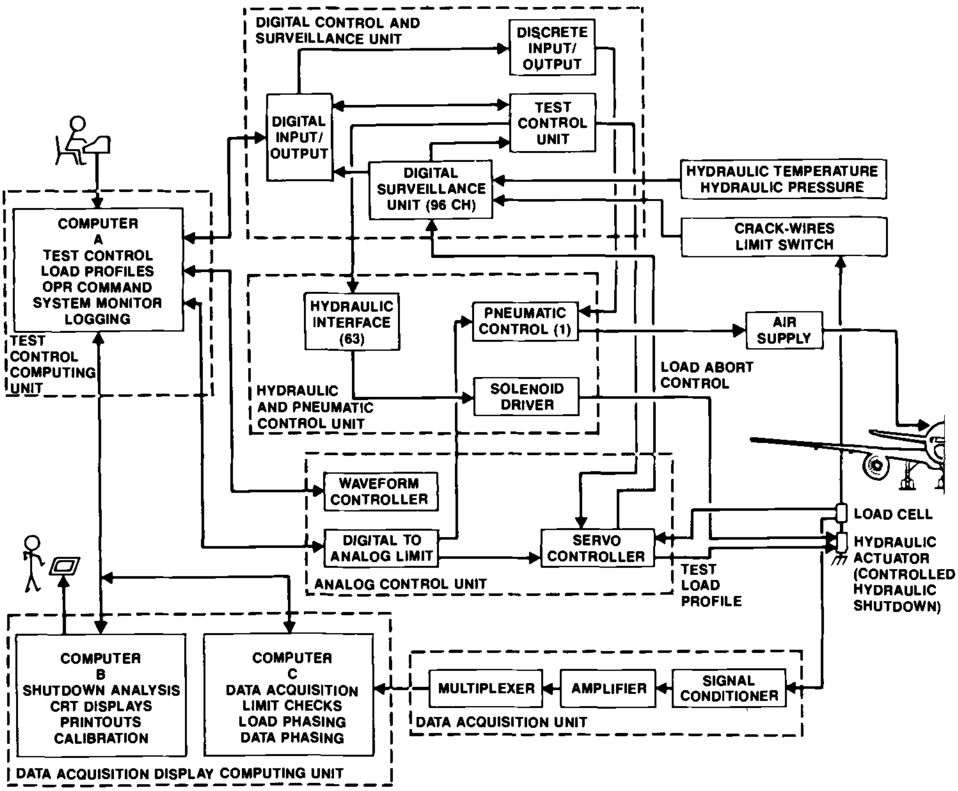

FIG. 25—757 major fatigue test system block diagram.

4. random selection of the sequence of segment severities (this resulted in 5000 different test flight types. (Nine flight segments with 10 different severity levels for each segment results in 10^9 different flight types possible).

Single-channel representations of both test spectra were applied to 0.609 m (24-in.) wide center cracked panels using stress responses for a variety of wing and fuselage details. The results of these tests, summarized in Fig. 28, confirmed that the full-scale test spectrum developed gave a good representation of expected service usage.

Conclusions

The development program for modern aircraft places large demands on available technology and physical resources to conduct the necessary supporting tests. The responsible engineer must in each case plan a test that satisfies all practical requirements. The test spectra work described was an example of the task of developing representative cyclic loading for major airframe fatigue tests.

By developing the spectra as a series of operational conditions and not specific loads, comprehensive test spectra for five separate airframe tests were easily developed concurrently. The structure was permitted to accumulate damage, initiate and grow cracks at realistic rates with minimal reliance on the derivation of equivalent loads based on damage

Flight Type / Number of Flights in a 5000 Flight Block	Cruise Maneuver — Number of Cycles/Groups at Five Amplitude Levels: I	II	III	IV	V
A 1	1 2 x 1/2	1 2 x 1/2	1 2 x 1/2	1 2 x 1/2	16 16 x 1
B 13		2 4 x 1/2	1 2 x 1/2	1 2 x 1/2	11 11 x 1
C 215			3 6 x 1/2	2 4 x 1/2	3 3 x 1
D 1067				3 6 x 1/2	2 4 x 1/2
E 3704					3 6 x 1/2

Flight Type / Number of Flights in a 5000 Flight Block	Cruise Gust — Number of Cycles/Groups at Five Amplitude Levels: I	II	III	IV	V
A 1	1 2 x 1/2	3 6 x 1/2	6 6 x 1/2	56 1 x 2 +18 x 3	61 19 x 3 + 1 x 4
B 13		1 2 x 1/2	2 4 x 1/2	32 4 x 6 + 1 x 8	40 1 x 5 + 5 x 7
C 215			1 2 x 1/2	12 12 x 1	23 23 x 1
D 1067				3 6 x 1/2	4 8 x 1/2
E 3704					2 4 x 1/2

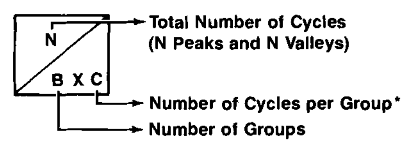

*1/2 Denotes Positive and Negative Peaks Are Applied Independently

FIG. 26—*757 test spectrum cycle grouping.*

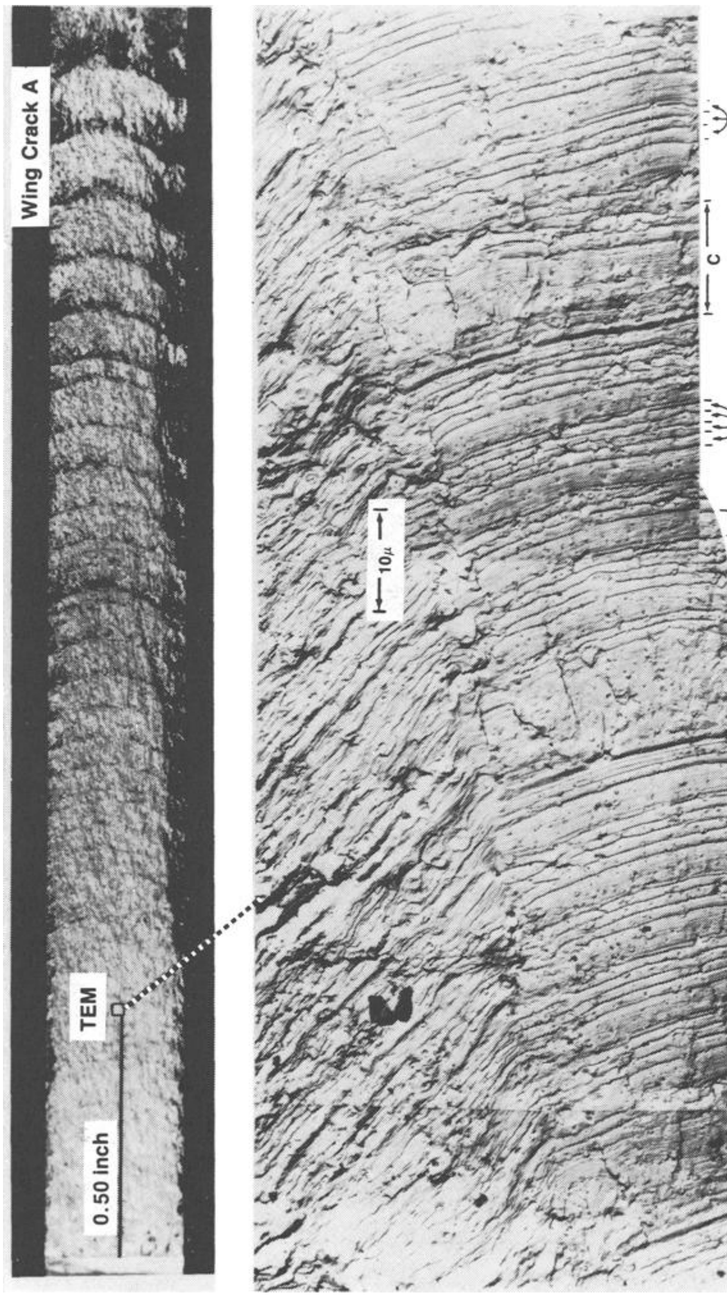

FIG. 27—*Photomicrographs from a center-cracked panel.*

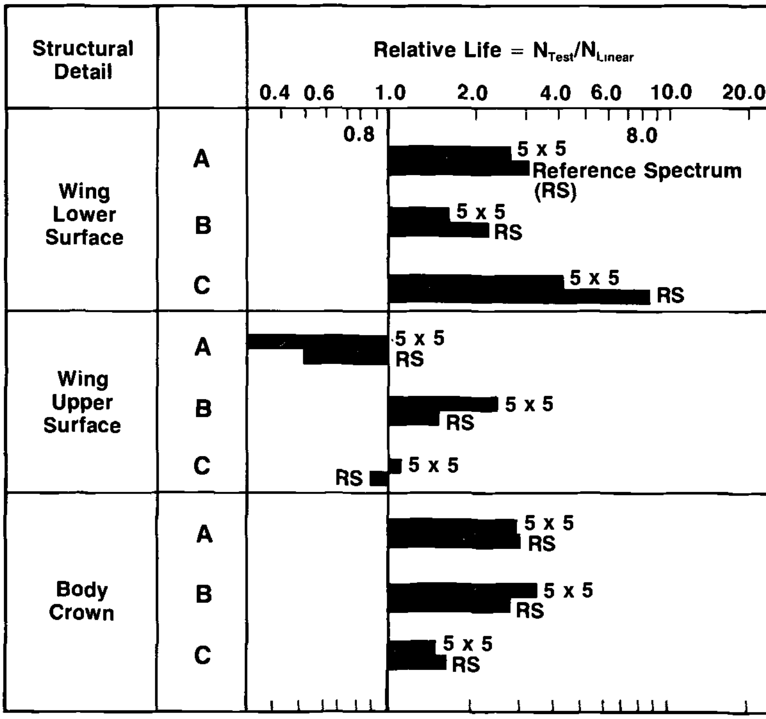

FIG. 28—*Test demonstrated crack growth lives of full-scale (5 by 5) and reference spectrum.*

model assumptions. The operational condition spectra and the supporting computer software were also sufficiently versatile to rapidly support development of more than 100 single-channel test spectra for damage accumulation/crack growth research and materials/processes evaluation programs.

The "spectrum marking" technique developed avoided application of additional cycles that have an unknown effect on test results and proved to be very useful in fractographic

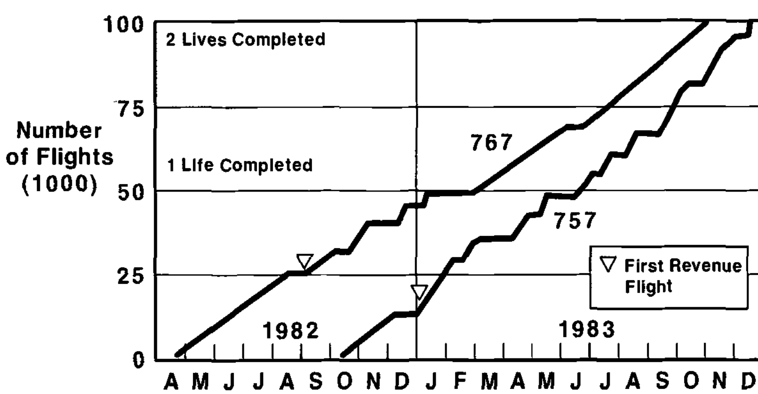

FIG. 29—*757/767 major fatigue test progress.*

reviews of test failures. This was particularly true when examining parts where cracks completely traversed structural details or where the fracture face was marred by corrosion products or closure effects.

The test spectra were relatively economical to apply and compared favorably with much more complex reference spectra in laboratory tests. All airframe tests were completed within the required time frame (Fig. 29) and were highly successful.

Acknowledgments

The authors are indebted to several members of Boeing Structures Technology staff whose contributions made this presentation possible. The paper preparation was greatly enhanced by the support of Dr. U. G. Goranson. Word processing assistance by L. Lofink was also appreciated.

References

[*1*] de Jonge, J. B., et al., "Standardized Load Sequence for Flight Simulation Tests on Transport Aircraft Wing Structures," Laboratorium for Betriebsfestigkeit, Darmstadt, German Federal Republic and National Lucht-en Ruimtevaartlaboratorium, Amsterdam, The Netherlands, LBF-BERICHT FB-106, NLR TR 73029 U, March 1973.

[*2*] Goranson et al., "Long-Life Damage Tolerant Jet Transport Structures," *Design of Fatigue and Fracture Resistant Structures, ASTM STP 761,* P. R. Abelkis and C. M. Hudson, Eds., American Society for Testing and Materials, Philadelphia, 1982, pp. 47–87.

[*3*] Hunter, P. A., "Summary of Center-of-Gravity Accelerations Experienced by Commercial Transport Airplanes in Landing Impact and Ground Operations," NASA TN D-6124, National Aeronautics and Space Administration, Washington, DC, April 1971.

[*4*] Hunter, P. A., "An Analysis of VGH Data from One Type of Four-Engine Transport Airplane During Commercial Operations," NASA TN D-4330, National Aeronautics and Space Administration, Washington, DC, Feb. 1968.

[*5*] Press, H. and Steiner, R., "An Approach to the Problem of Estimating Severe and Repeated Gust Loads for Missile Operations," NACA TN 4332, National Advisory Committee on Aeronautics, Washington, DC, Sept. 1958.

[*6*] Crabill, N. L., "NASA Digital VGH Program B-727 Final Report, National Aeronautics and Space Administration, Washington, DC, 6 May 1982.

[*7*] Crabill, N. L., "NASA Digital VGH Program B-747 Final Report," National Aeronautics and Space Administration, Washington, DC, 6 May 1982.

[*8*] Crabill, N. L., "NASA Digital VGH Program L-1011 Final Report," National Aeronautics and Space Administration, Washington, DC, 6 May 1982.

[*9*] Crabill, N. L., "NASA Digital VGH Program DC-10-30 Final Report," National Aeronautics and Space Administration, Washington, DC, 3 Sept. 1982.

[*10*] Clay et al., "Airline Operational Data from Unusual Events Recording System in 707, 727 and 737 Aircraft," FAA-RD-71-69, Federal Aviation Administration, Sept. 1971.

[*11*] Zalovcik et al., "Comparison of VGH Data from Wide-Body and Narrow-Body Long-Haul Turbine Powered Transports," National Aeronautics and Space Administration, Washington, DC, NASA TN D-8481, July 1977.

[*12*] "Observed Normal Acceleration Spectra on L-1011, 747 and 1-11 Aircraft," CAA-AD White Note 220, Issue 1, Civil Aviation Authority, U.K., June 1981.

[*13*] Schutz, D. and Lowak, H., "The Application of the Standardized Test Program for the Fatigue Life Estimation of Fighter Wing Components Part IV," *Proceedings,* Eighth ICAF Symposium, International Committee on Aeronautics Fatigue, June 1975.

[*14*] Goranson, U. G. and Rogers, J. T., "Elements of Damage Tolerance Verification," 12th ICAF Symposium, Toulouse, France, International Committee on Aeronautics Fatigue, 25–31 May 1983.

Günter E. Breitkopf[1]

Basic Approach in the Development of TURBISTAN, a Loading Standard for Fighter Aircraft Engine Disks

REFERENCE: Breitkopf, G. E., "**Basic Approach in the Development of TURBISTAN, a Loading Standard for Fighter Aircraft Engine Disks,**" *Development of Fatigue Loading Spectra, ASTM STP 1006,* J. M. Potter and R. T. Watanabe, Eds., American Society for Testing and Materials, Philadelphia, 1989, pp. 65–78.

ABSTRACT: The development of TURBISTAN was a joint effort by CEAT (Centre d'Essais Aeronautique de Toulouse, France); IABG (Industrieanlagen-Betriebsgesellschaft); LBF (Fraunhofer-Institut für Betriebsfestigkeit, West Germany); MTU (MTU Motoren- und Turbinen-Union München GmbH, West Germany); NLR (Nationaal Lucht- en Ruimtevaartlaboratorium, The Netherlands); RAE (Royal Aircraft Establishment, Great Britain); Rolls-Royce (Great Britain) and SNECMA (Société Nationale d'Etude et de Construction de Moteurs d'Aviation, France); RWTH (Rheinisch-Westfälische Technische Hochschule Aachen, West Germany); and University of Utah (United States) to derive a loading standard for fighter aircraft engine disk usage.

The sequence was designed to contain the characteristics that are determinants of cyclic fatigue in the form, frequency, and application typical of actual operations. It represents a unique standard for low cycle fatigue (LCF) and crack growth experiments, and enables quantitative insights to be gained into the sequencing effect at moderate experimental effort.

The subject of the paper is the basic approach used in the development process. The paper also adds a few application notes.

KEY WORDS: fatigue (materials), testing, aircraft, mission analysis, turbines, component reliability, cumulative damage, load spectrum

Rapid advances in aircraft jet engine construction towards higher thrust/weight ratios necessitate progressive development of methods to ensure the durability of highly-stressed fracture critical rotor components. These components are being designed in the fatigue range. At the present state of the art, their allowable usage is expressed in number of design missions or in flying hours, where these flying hours are based on a design mission. The design mission is generally selected to reflect the intended engine usage from the cyclic component load perspective.

The stress analysis accordingly involves the task of determining low cycle fatigue (LCF) damage, crack propagation, and conceivably creep at the critical areas for a certain succession of stress cycles of distinct mean stresses, ranges, and dwells. The LCF damage is historically predicted with the aid of constant-amplitude tests. The total damage from a design mission is then determined by breaking the mission down into individual subcycles, determining the amount of damage the subcycle has contributed to the results of the constant-amplitude tests, and accumulating the subcycle damage inputs to arrive at the total damage. In current design practice, accumulation often follows the simple linear Miner's rule.

[1] Manager, Material Data and Application, Motoren- und Turbinen-Union München GmbH, 8000 München 50, West Germany.

At the present state of material utilization and accuracy achieved in the identification of component temperatures and stresses, this approach is adequate only as long as the input of nonlinear load sequence effects to LCF damage and crack propagation remains modest. If these effects cannot be ignored, a considerable amount of specimen and component testing is needed to quantify their impact: for the foreseeable future, computer models designed for the nonlinear accumulation of damage fractions will still need experimental verification for specific applications. Test series involving groups of constant-amplitude block loading tests or certain load sequences consume a large amount of time. Investigations into load sequence effects, therefore, should be launched early in the game at the time the material is being optimized and the general data base generated, that is, before the design mission, the rotor structure with critical areas, and the temperatures and load levels are available for a certain application.

These tests would benefit from a standard load sequence that, from the cyclic material fatigue and crack propagation perspective, reflects the typical characteristics of actual load sequences in critical components during engine usage, and that contains these characteristics in their proper arrangement and weighting. This load sequence will quickly show whether a detailed study into the load sequence effect is indeed warranted. A few tests will then be sufficient to produce quantitative evidence for consideration in the initial stage of rotor design. It will also ultimately permit verification of computational assumptions to account for load sequence effects and adaptation of computational models to suit the problem.

A component's load sequence is governed significantly by the component's thermal environment. At low temperatures, like those prevailing in a low-pressure compressor, the stresses are mainly those induced by centrifugal force. At elevated temperatures, as in the high-pressure compressor and turbine, high stationary and, mainly, transient temperature differences occur in the components; the associated thermal stresses are superimposed on the centrifugal force-induced stresses to produce a very complex total stress profile in the critical areas. The two cases are compared for a flight cycle in Fig. 1.

The load profiles exhibit distinct characteristics and require individual investigation. The present study deals with the low component temperature application, which is the simpler throughout and also permits dwells to be neglected. For this application, a load sequence has been proposed that has previously been described in some detail by Mom et al.[2] The present paper describes the general approach taken to arrive at a typical load sequence.

Requirements for a Standard Load Sequence

The standard load sequence should contain the characteristics that determine LCF damage and crack propagation in rotor components. Although a rough notion of what a typical load sequence is should quickly come to mind, its exact shape is by no means a foregone conclusion, except for some obvious characteristics, such as the zero-max cycle per flight mission. Accordingly, an attempt must be made to identify and quantify related characteristics (for example, subcycle mean stress and stress range, dwell time) in actual load sequences, and to distill them into typical characteristics suitable for forming a standard sequence. This must be attempted, although some characteristics of flight load sequences have no typical patterns that can be clearly assigned a given value.

[2] Mom, A. J. A., Evans, W. J., and ten Have, A. A., "TURBISTAN, a Standard Load Sequence for Aircraft Engine Discs," *Damage Tolerance Concepts for Critical Engine Components*, AGARD-CP-393, Advisory Group for Aerospace Research and Development, San Antonio, 1985, pp. 20-1 to 20-10.

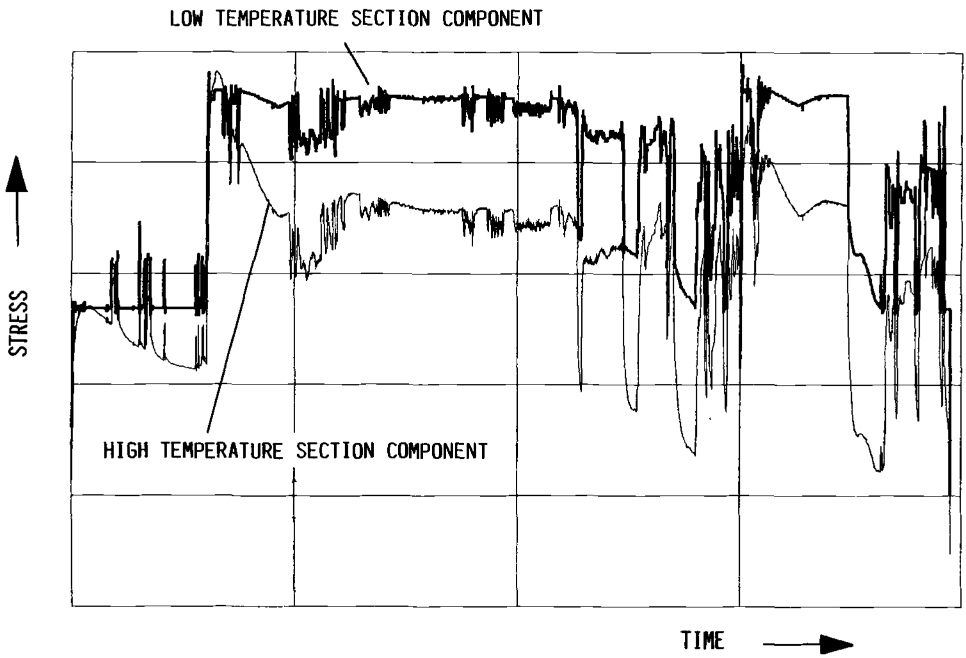

FIG. 1—*Flight cycle.*

Difficult as it may be to derive typical characteristics, there is no other conceivable option. Insights into load sequence effects are still rudimentary and confused by a plurality of interactive influences. Controlled substitution of worst-case characteristics for hard-to-define typical characteristics is therefore not possible, since the ability to define realistic worst cases is lacking.

Characteristics and Elements of In-Flight Load Sequences

For simplicity, the analysis is based on linear elastic stresses. They represent load histories reasonably, but are independent of the concrete stress/strain performance of individual critical areas.

A workable approach, and the one selected here, to explore in-flight stress cycles for common characteristics consists of breaking the general flight structure down into blocks as was done by Breitkopf and Speer.[3] For clarity, this breakdown is shown in Fig. 2.

In this manner, a flight is broken down into an initial block (ground handling and take-off), a center block (execution of the actual mission objective), and a final block (landing and parking). These major blocks are further subdivided into events that display common characteristics or can be described by the following characteristics.

[3] Breitkopf, G. E. and Speer, T. M., "In-Flight Evaluation of Life Consumption of Critical Rotor Components Subjected to High Transient Thermal Stress," *Engine Cyclic Durability by Analysis and Testing,* AGARD-CP-368, Advisory Group for Aerospace Research and Development, Lisse, 1984, pp. 1-1 to 1-15.

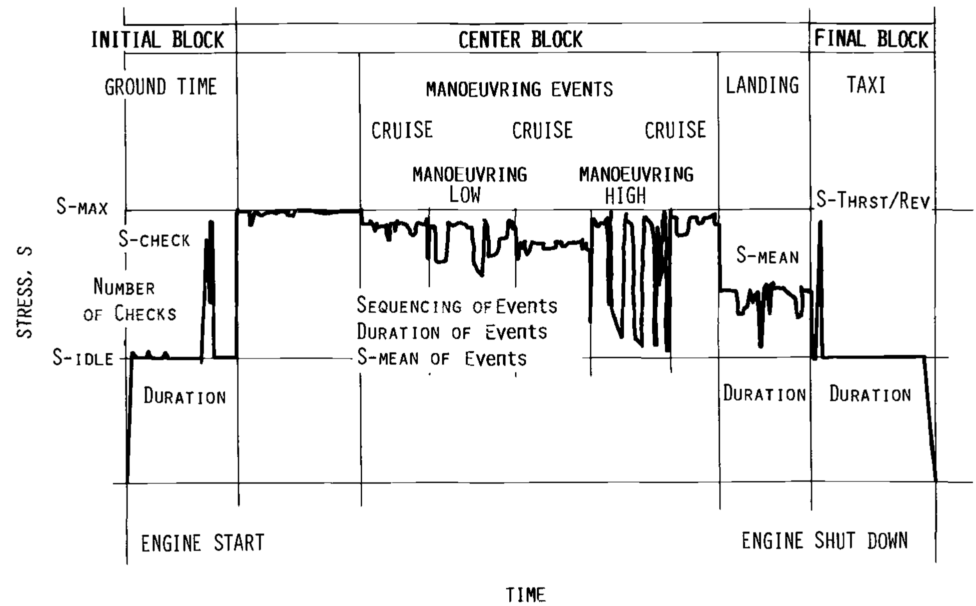

FIG. 2—*General flight cycle structure.*

Initial Block

The events of the initial block are:

1. Engine start, which brings the stress to an S-idle level associated with engine idle speed (the engine idle rpm depends entirely on the engine type).
2. A certain span of time for ground handling and taxiing to the take-off strip (in the process, a number of minor over-idle speed/stress peaks occur; these are random in nature).
3. Engine checks involving speed/stress peaks (the number of checks and the associated stress excursions S-check depend on the engine type).
4. Take-off with speed/stress rising to maximum S-max (the value is largely dependent on the engine type).

Center Block

A succession of various events characterized by speed/stress variations that by number and magnitude are random in nature. These variations reflect the flight maneuvers executed in performing the flight mission. The events are composed of sections within which the mean stress of the variations is considered constant. The respective mean stress is likewise random in nature.

The center block events can be grouped into three types:

1. Cruise, with relatively minor variations (amplitudes <4% of maximum stress) around the mean value.
2. Low (intensity) maneuvering, with medium-size variations (amplitudes essentially <10% of maximum stress).

3. High (intensity maneuvering with predominantly large variations (amplitudes >10% of maximum stress).

The sequence and length of the various events is random.

Final Block

The events of the final block include:

1. Landing, a random-length event characterized by constant, relatively low mean stress *S*-mean and random speed/stress variations, caused by flight maneuvers during approach.
2. Thrust reversal, associated with a commensurate speed/stress peak *S*-thrust reversal. Whether thrust reversal is used, and how much of it, depends to some extent on the engine/aircraft.
3. Taxi, to the parking location at idle speed with minor speed/stress peaks (number and magnitude of peaks, as well as the duration of taxi, are considered random).
4. Engine shutdown, with stress dropping to zero.

The events on this list can be picked by number, type, and sequence of event to map any flight cycle.

Definition of Typical Load Sequence

To construct a representative sequence, the event-related operational flight or engine variables must first be identified, together with their quantitative relationships. The parameters influencing engine operation have been compiled in Table 1, with distinctions being made between parameters that are most related to the engine/aircraft type, and those that are not. In Table 2 the relevant parameters have been related to event characteristics.

For event-related characteristics that are not related to the aircraft/engine, there is a plausible approach to defining typical patterns of these events. The load sequence impressed on a rotor through the usage period of an engine inherently contains these characteristics. Their frequency distribution can be determined by observations on a representative pool of aircraft/engines and flights. It would be appropriate, therefore, to construct a typical load

TABLE 1—*Parameters of influence for engine operation* (N = *engine speed*).

	DETERMINISTIC PARAMETERS DEPENDENT ON ENGINE/AIRCRAFT TYPE
1.1	Engine/performance, aircraft/performance
1.2	*N*-idle
1.3	*N*-max
1.4	Engine ground handling procedures (flight manual)
	RANDOM PARAMETERS CORRELATED WITH ENGINE/AIRCRAFT TYPE
1.5	Engine settings (governor, etc.), clearances, etc.
	INFLUENCE PARAMETERS INDEPENDENT OF ENGINE/AIRCRAFT TYPE
2.1	Position of engine on aircraft (right/left hand)
2.2	Local environment of air base, operational environment
2.3	Type of mission
2.4	Position of aircraft in flying unit
2.5	Experience, skill level, and aggressiveness of air crew

TABLE 2—*Correlation of event characteristics with relevant influence parameters.*

Event Characteristics	Parameters[a] of influence for engine operation: Dependent on Engine/Aircraft Type	Independent of Engine/Aircraft Type
Ground Time		
Duration	1.4	2.1 2.2 2.5
S-idle	1.2	
Cyclic content	1.1	2.5
Number of checks	1.4	
S-max checks	1.4	
Departure		
Duration	1.1	2.2 2.3
S-max	1.3 1.5	
Maneuvering		
Event sequencing	1.1	2.2 2.3 2.5
Duration of events	1.1	2.2 2.3 2.5
S-mean of events	1.1	2.3
Cyclic content of events	1.1	2.3 2.4 2.5
Landing		
Duration	1.1	2.2 2.3 2.5
S-mean	1.1	2.2 2.3 2.5
Cyclic content	1.1	2.3 2.4 2.5
Thrust reversal yes/no	1.1	2.2 2.3 2.4 2.5
S-max thrust reversal	1.1 1.5	2.2 2.5
Taxi		
Duration	1.4	2.1 2.2
S-idle	1.2	
Cyclic content	1.1	2.5

[a] For parameter notation, see Table 1.

sequence that would reflect these characteristics and their associated parameters by type and magnitude from the frequency distribution observed in the pool.

For parameters that depend on, or are closely correlated with the aircraft/engine type, however, it does not necessarily make sense to adopt the observed pattern of frequency distribution, because in the usage for a certain engine, or for a certain rotor, accumulation of usage will not inherently produce the frequency distribution that was determined independently of the aircraft/engine combination.

The main parameter in the group of parameters dependent on or related to engine/aircraft type (1.1 to 1.5 in Table 1) is the maximum speed, N-max, that governs the peak stress, S-max. It is considered an arbitrary parameter that lets a user of the load sequence adapt experimental conditions to the material, temperature, etc., involved. For this purpose, the sequence is represented in an S-max normalized form.

For the other characteristics governed by the engine/aircraft type, no modeling solution is apparent that would satisfy all cases. These characteristics are:

1. stress associated with idle rpm (S-idle),
2. number of engine checks, and
3. maximum stress for each check (S-check).

The aircraft/engine type pool underlying the quantitative flight cycle analysis is described in Table 3. It embraces single and twin-engined aircraft plus single, two, and three-pool

TABLE 3—*Numbers of engine/aircraft of indicated type in the TURBISTAN pool.*

	Number of engines on Aircraft	
Number of Engine Spools	1	2
1	1	...
2	...	3
3	...	1

engine configurations. In this pool, S-idle runs in the 40 to 70% S-max range. The number of engine checks runs between zero and three, and S-check ranges between 50% and maximum stress of the entire cycle S-max.

In the absence of arguments for other solutions, and in view of the minimal impact these characteristics have on total damage, the observed frequency distribution (that is, the data from the pool) is also used for modeling these characteristics.

For characteristics that depend only partially on influencing parameters, which are not correlated with engine/aircraft type (2.1 to 2.5 in Table 1), their dependence likewise necessitates this approach.

This roughly establishes the procedure for patterning a typical sequence:

1. Establish the total length of sequence, that is, the number of flights included.
2. Model flight by flight on the pattern on Fig. 2. In the process, the events are formed by random processing based on the frequency distribution identified in the pool investigated.

The cyclic content of random elements, such as cruise, etc., is formed by superimposing variations on S-mean of the event. For modeling these variations, cycles are drawn at random from matrices containing the observed variations for each type of event as found in the total pool of flights.

Modeling the Center Block Structure

A special problem is imposed by the structure of the center block, in which the flight mission type plays an important part. From the flight mission point of view, four general types of flight must be recognized:

1. air combat,
2. transition/training,
3. ground attack, and
4. navigation.

The center block structure contains the cruise, low maneuvering, and high maneuvering events. This structure is deemed a random variable analogous to the approach just described. However, the variable is of the vector type with the vector elements "number of events," "sequence of events," "length of each event," and "S-mean for each event." If we have, say, five events (mean figure for the flights investigated), three length levels, and seven levels for S-mean (S-max corresponding to ten levels), we get a high, nine-digit number of sequencing options. So, the multi-dimensional frequency distribution of that variable can not be obtained from an analysis of the comparatively low number of flights from the mission pool.

The alternative, which is a derivation of standard values of the vector from an analysis of in-flight specifics, is prevented by the large number of influencing parameters, the majority of which are again largely random in nature and puzzling in their correlations.

A third option would be to adopt the observed cases, that is, the center block structure of the flights contained in the pool. Since the underlying flights were considered representative for each of the four flight types, the occurrence of the observed frequency patterns is highly probable. It appears that a plausible solution is to adopt them directly.

Solution to Typical Mission Mix Problem

The mission mix imposed on an engine is regarded as a sequence parameter that is only partly correlated with the aircraft/engine type. A weighting of the flight types in the sequence according to an observed, general frequency, at first appears to be unsatisfactory in view of the significant influence of the sequencing on engine life. This prompted an investigation into the relative dependence of the center block structure on the type of mission, aimed at ascertaining if the center block structure of the four types of mission differ significantly from one another. For a clear statement to be made, a value that describes the structure in all its characteristics was developed.

This value was developed on the basis of the characteristics summarized in Table 4, where these characteristics are defined and standardized into a numerical value to be allocated to each mission. Consequently, it was possible first to eliminate those characteristics that were interrelated.

One way of determining the required characteristic value lies in the formation of a weighted average of the remaining characteristics. This was used where the weights were determined by a First Principal Component Analysis that is familiar from pattern recognition, see Kendall and Stuart[4].

In this type of analysis, the weights are chosen so that the samples differ as widely as possible with respect to the numerical values of the linear combination, Z_i, that describes them.

With the characteristic value

$$Z_i = \sum_{j=1}^{M} w_j \cdot x_{i,j}$$

where

w_j = the weight of the characteristic j;
j = 1, 2, 3, . . . M;
$x_{i,j}$ = characteristic j of the ith sample; and
i = 1, 2, 3, . . . N.

The weights, w_j, are to be determined such that the function

$$F = \sum_{i>j}^{N} (Z_i - Z_j)^2$$

[4] Kendall, M. G. and Stuart, A., *The Advanced Theory of Statistics,* Hafner, New York, 1966.

TABLE 4—*Characteristics to describe center block structure.*

No.	Characteristic	Notation	Quantities for Normalization of Characteristic	Notation	Definition of Normalized Characteristic
1	Number of direct transitions from CRUISE to MANEUVERING HIGH blocks or vice versa	NUG	total number of blocks within the center block structure of the flight in question	NBL	$NUGN = \frac{NUG}{NBL} \cdot 100\%$
2	Length of CRUISE blocks	LBL3	total length of center block structure of the flight in question	LCBS	$LBL3N = \frac{LBL3}{LCBS} \cdot 100\%$
3	Length of MANEUVERING LOW blocks	LBL4[a]			$LBL4N = \frac{LBL4}{LCBS} \cdot 100\%$
4	Length of MANEUVERING HIGH blocks	LBL5[b]			$LBL5N = \frac{LBL5}{LCBS} \cdot 100\%$
5	Number of CRUISE blocks	NBL3[c]	total length of center block structure of the flight in question.	LCBS	$NBL3N = \frac{NBL3}{LCBS} \cdot \frac{1}{NBMAX} \cdot 100\%$
6	Number of MANEUVERING LOW blocks	NBL4	maximum value of "number of blocks within the center block structure/total length of center block structure" in any of the flights in the pool.	NBMAX	$NBL4N = \frac{NBL4}{LCBS} \cdot \frac{1}{NBMAX} \cdot 100\%$
7	Number of MANEUVERING HIGH blocks	NBL5			$NBL5N = \frac{NBL5}{LCBS} \cdot \frac{1}{NBMAX} \cdot 100\%$

[a] Correlated to Characteristic No. 1 and No. 5.
[b] Correlated to Characteristic No. 2.
[c] Correlated to Characteristic No. 6 and No. 7.

will be a maximum, where the secondary condition

$$\sum_{j=1}^{M} w_j^2 = 1$$

must be fulfilled. (See Footnote 4 for the solution.)

In the present case, the sample consists of the four types of flight represented each by a linear combination, Z_i, in which the $x_{i,j}$ values are taken as mean values $x_{i,j}$ from all flights of the same type

$$\bar{x}_{i,j} = \frac{1}{L} \sum_{k=1}^{L} x_{i,j,k}$$

where $x_{i,j,k}$ = the characteristic value j of the kth flight of the ith type, and $k = 1, 2, 3, \ldots L$, with

$x_{i,1,k}$ = NUGN,
$x_{i,2,k}$ = LBL3N,
$x_{i,3,k}$ = NBL4N, and
$x_{i,4,k}$ = NBL5N.

The numerical values for the individual flights of the pool are summarized in Table 5. The characteristic values, $\bar{x}_{i,j}$, and the weights, w_j, resulting from the Principal Component Analysis, are summarized in Table 6. This enables the desired characteristic value for the four types of flight to be formed.

Further information about the differences between the flight types can be derived from the cumulative distribution of the characteristic totals (Fig. 3). From this, the distributions for "air combat," "transition/training," and "ground attack" are relatively close to one another, whereas "navigation" stands out. The relative weighting of the first three flight types is given little significance, while the total fraction of navigation is assumed at 15% and accordingly considered in the sequence. The sequencing of missions, again, is random.

Description of TURBISTAN Load Sequence, Application Problems

The typical TURBISTAN load sequence is defined as follows: 100 flights of 7726 cycles. Figure 4 shows Flight 1 of the sequence (ground attack) as a function of time. At a load variation rate of 0.5 s for $0/S$-max, the equivalent test duration is 22.2 min for the performance of a sequence.

The load sequence as just described represents a unique standard for LCF and crack growth experiments. To reduce test durations, it appears helpful to derive an abridged sequence from the full sequence where the number of minor cycles has been reduced. An abridged sequence, moreover, is necessary to the investigation of the damage input of minor cycles to the total damage.

No standard exists that can satisfy all aspects of the issue of reducing the full sequence. It is therefore left to the discretion of the user to reduce the sequence to suit the task at hand. One such reduction is based on the damage parameter of Smith et al.[5] On this basis,

[5] Smith, K. N., Watson, P., and Topper, T. H. "A Stress-Strain Function for the Fatigue of Materials," *Journal of Materials*, Vol. 5, No. 4, 1970, pp. 767–778.

TABLE 5—*The* $x_{i,j,k}$ *numerical values of characteristics to describe center block structure.*

Type of Flight	Flight No.	NUGN, $x_{i,1,k}$ (%)	LBL3N, $x_{i,2,k}$ (%)	NBL4N, $x_{i,3,k}$ (%)	NBL5N, $x_{i,4,k}$ (%)
Air combat	k = 1	0	0	0	26
(i = 1)	2	20	55	43	14
	3	67	7	0	48
	4	33	81	15	30
	5	11	7	61	61
	6	63	41	24	71
	7	50	42	14	43
Transition/training	k = 1	0	0	20	20
(i = 2)	2	50	19	14	42
	3	0	16	39	0
	4	0	0	0	34
	5	50	2	0	60
Ground attack	k = 1	25	50	16	16
(i = 3)	2	33	28	45	61
	3	29	47	40	60
	4	29	30	39	59
	5	0	0	0	8
	6	0	0	27	36
	7	0	0	59	59
	8	0	39	27	13
	9	57	9	16	63
Navigation	k = 1	57	41	11	34
(i = 4)	2	20	21	29	37
	3	0	100	0	0
	4	50	32	49	97
	5	75	90	0	17
	6	25	18	24	12
	7	30	29	19	26
	8	0	82	0	0
	9	13	25	48	36
	10	0	54	8	0

cycles of damage levels <10 and <30% were eliminated. The shortened versions are called MINITURBS. The result is shown in Fig. 4.

Figure 5 shows the range spectra, that is, the number of half-cycles versus range size, on the basis of a rainflow analysis for the complete TURBISTAN sequence and the shortened versions.

When reducing the full sequence, the time effect may have to be considered especially for comparative investigations. The TURBISTAN sequence can be applied as a representative load sequence only for rotor regions with low temperatures. In these regions, time effects (creep) are generally of secondary importance. However, there are exceptions, such as titanium alloys, which exhibit dwell effects even at low temperatures. In such cases, the associated time effects must be kept in mind when small cycles are omitted. Since the small cycles are to be found essentially with high mean stress levels, the omission of small cycles in the test signifies *de facto* reduction of times at high stress levels.

TABLE 6—*Mean characteristic values of characteristics weighting factors from principal components analyses characteristic totals of flight types.*

Type of Flight	Mean Characteristic Values, $\bar{x}_{i,j}$ (%) $j = 1$	$j = 2$	$j = 3$	$j = 4$	Characteristic Total, Z_i
Air combat (i = 1)	37	33	23	41	23.4
Transition/training (i = 2)	29	7	14	32	0.40
Ground attack (i = 3)	22	23	27	37	11.2
Navigation (i = 4)	31	49	16	20	42.1
Weighting, w_j	0.12	0.95	−0.016	−0.288	...

Summary and Prospects

The standard load sequence under study appears to maximally reflect typical engine rotor conditions at low temperatures. This was achieved by qualitative and quantitative analysis of a considerable number of representative load cycles selected from actual flight missions. In the process, a set of events and characteristics was developed in keeping with the basic structure of flight cycles to describe such load cycles. For a number of these characteristics, values were developed that can be considered typical. For some of these characteristics, however, this was ruled out altogether, but respective solutions were found that appear appropriate and plausible. From these events then, flight cycles were formed and linked together into a total sequence.

For components under major thermal stresses, such as high-pressure compressor and turbine disks, a comparable sequence, called HOT TURBISTAN, will be needed that also reflects in-flight dwells. A sequence of this description is currently under development.

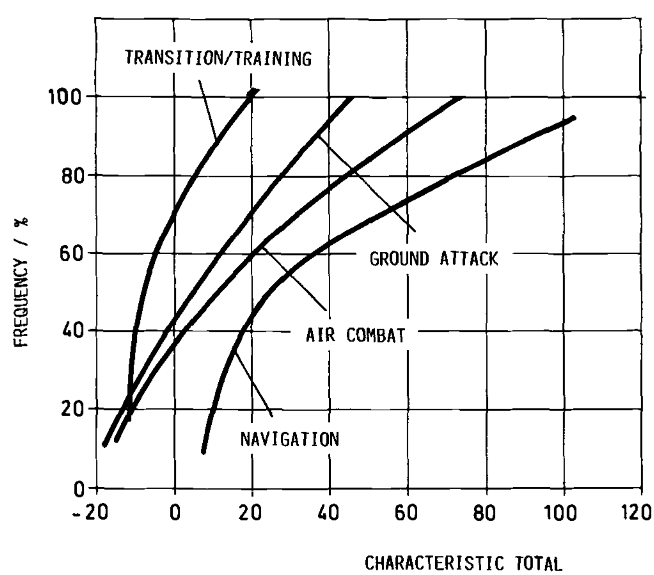

FIG. 3—*Cumulative distribution of characteristic totals,* Z_i.

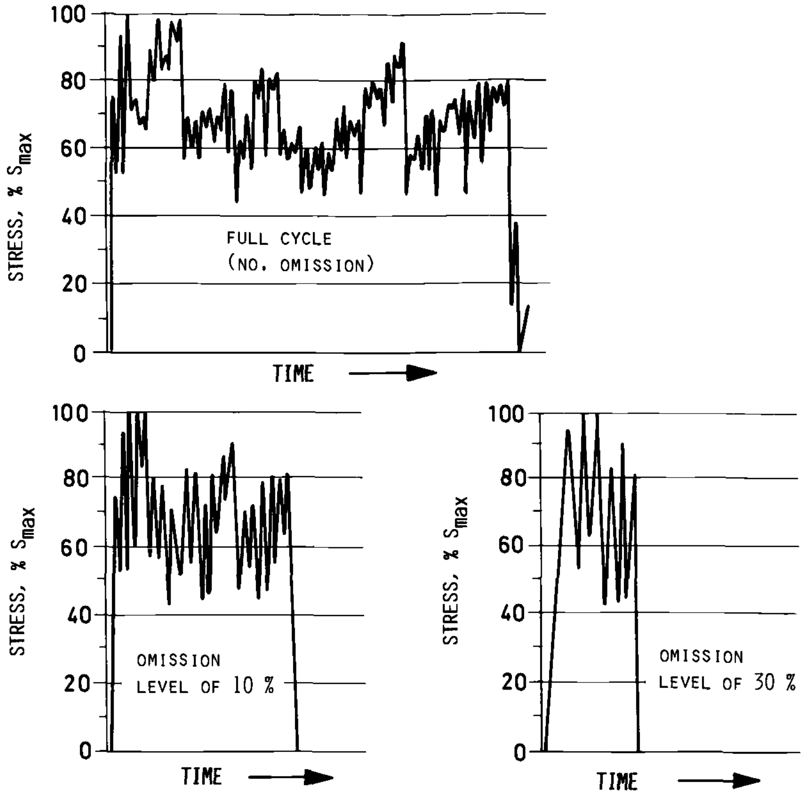

FIG. 4—*TURBISTAN Flight Type No. 1 (ground attack).*

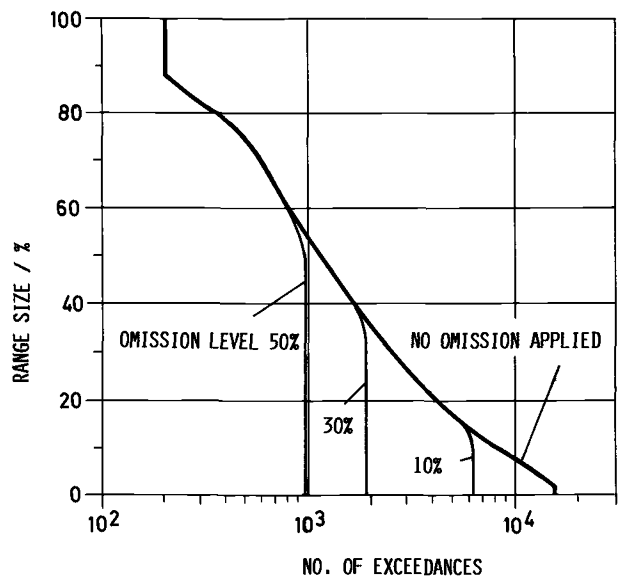

FIG. 5—*TURBISTAN range spectra.*

While the basic approach is the same, the dwells and thermal stresses prevailing in flight operations will have to be mapped accordingly.

Acknowledgment

The author wishes to thank Dr. H. T. Schmitt for performing the Principal Components Calculations.

Anthony G. Denyer[1]

Automated Procedure for Creating Flight-by-Flight Spectra

REFERENCE: Denyer, A. G., "**Automated Procedure for Creating Flight-by-Flight Spectra,**" *Development of Fatigue Loading Spectra, ASTM STP 1006,* J. M. Potter and R. T. Watanabe, Eds., American Society for Testing and Materials, Philadelphia, 1989, pp. 79–98.

ABSTRACT: This paper presents a functional description of a versatile computer program developed to provide rapid response to spectrum generation requirements. The program, when supplied with flight profiles and the distribution of those profiles during the aircraft lifetime, will create a randomly sequenced flight-by-flight spectrum in terms of load factors, loads, or stress at a specific structural location.

The heart of the program is a data base containing the frequency definition of load factor occurrences representing the gust and maneuver load cycles for various flight segments. This paper discusses the establishment of the data base from data published in MIL-A-87221 and the FALSTAFF reports, from analytically derived load factor data and from flight load records from specific aircraft. The various forms of load factor data acceptable to the program, namely, exceedance curves, range/mean tables, and the FALSTAFF methodology, are discussed as to advantages and disadvantages.

The program will accept multiple flight profiles each with multiple flight segments defined by segment title, segment time, and selected significant flight parameters such as gross weight, Mach number, altitude, and aircraft geometry. For each profile, the procedure creates a series of individual flight load factor spectra each of which differs from all others in load sequence and magnitude while maintaining the sequence of the flight segments. The spectra include the infrequent high loads randomly selected from within the statistics of the data base. Load-factor spectra to stress spectra conversion is briefly discussed in terms of the program capability.

The output spectrum is a series of flights representing a defined period of usage with the flights representing the various profiles randomly sequenced within the supplied distribution statistics. The spectrum form is suitable for direct input to fatigue or crack growth programs or can be output to tape for submittal to a fatigue testing machine.

KEY WORDS: load spectra, fatigue loads, load sequence, fatigue (materials), testing

Current aircraft procurement specifications include durability and damage tolerance requirements. The analytic methodology and the structural testing procedures used to verify the adequacy of the design require detailed load spectra that represent the projected utilization of the aircraft. In addition, the effect of utilization variations that occur during the service lifetime of the aircraft must be ascertained. Historically, spectra have been time consuming to generate or have been simplified to be gross approximations of the representative spectra. The program described herein was written to provide rapid response to a request for spectra to support preliminary design analysis, detail design analysis, structural testing, and service-life trade studies.

Structural damage accumulation, as computed by fatigue and crack growth programs, is a function of the magnitude, frequency, and sequence of the applied load cycles. Load cycles

[1] Senior engineering specialist, Rockwell International, Los Angeles, CA 90009.

on the structure are caused by the sequenced events defined by the flight profile from take off through the flight to landing and include the effect of airplane configuration changes during the flight. In addition, the aircraft is subjected to atmospheric gusts and pilot-induced maneuvers while in flight and to taxi and ground handling maneuvers while on the ground.

The program will generate a randomly sequenced flight-by-flight spectrum in terms of load factors, loads or stress at specific structural locations when provided with flight profiles, and the distribution of those profiles during the aircraft lifetime. An overview of the spectrum generation procedure is shown in the block diagram of Fig. 1. The heart of the program is a data base containing the load cycle occurrences representing the gust and maneuver conditions for various flight segments. Individual data bases are established for each aircraft type; bomber, transport, fighter, and trainer. The data bases are typically in the form of load factors or gust velocity and as such produce spectra in those terms. Stress transfer functions, unique to specific structural locations on a given aircraft, must be supplied by the user if a stress spectrum is required. If the airframe structural stresses are computed using a finite-element internal loads program, the results of that program (element forces and stresses and nodal forces) may be stored on the spectrum program data base for automatic recovery and use when generating stress spectra.

Data Base of Cyclic Loads

The loading parameter of the cyclic load data can be defined in several forms.

a. Load factor at the aircraft center of gravity is the most universal form of defining the load magnitude and has the advantage of allowing the data collected from one aircraft to be used or adapted to represent another aircraft. Military specification MIL-A-87221 [1] provides load-factor maneuver data for various flight segments for each class of aircraft, namely, fighter, trainer, bomber, and transport. Load-factor data due to gusts may be derived analytically using a power spectral density (PSD) approach per

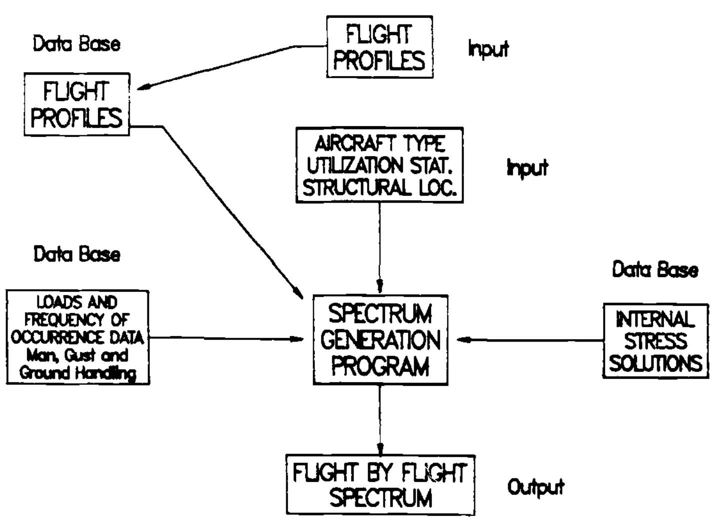

FIG. 1—*Spectrum generation program overview.*

TABLE 1—*Load cycle data base.*

Flight Segment	Load Cycle ID	Load Type	Aircraft Type: Fighter	Bomber	Transport	Trainer
Ground	1	taxi				[1]
	2	ground handling	[1]	[1]	[1]	
						load
Approach and pattern	3	maneuver				factor
Climb	4		load	load	load	...
Cruise	5		factor	factor	factor	
Descent	6					
Loiter	7			...	...	
Air-ground	8					
Air-air	9					
Special weapon	10					
Refuel	11		...			...
Training	12					[1]
Formation	13					load
Instrument and Navigation	14					factor
Administration and Test	15			...		
Terr. following	16		...	[a]	...	...
			[1]		[1]	[1]
Landing	17	landing	sink speed	sink speed	sink speed	sink speed
0 to 150 m	18	gust	...	[1]	...	...
0 to 1500 m	19				[3]	
1500 to 3000 m	20			load	gust	
3000 to 5000 m	21			factor	velocity	
5000 to 8000 m	22					
>8000 m	23					

[a] Based on data developed in the flight loads simulator.

Ref *1*. Additional data may be obtained from Loads/Environment Spectra Survey (L/ESS) programs undertaken on aircraft equipped with recording accelerometers as described in Ref *2*.

b. Gust velocity is frequently used for defining gust data in publications such as NACA TN 4332 [*3*] and the Royal Aeronautical Society Reference Data [*4*].
c. Sink speed is used to define landing loads in Ref *1*.
d. Loads or stresses at specific structural locations are not usually available unless a loads/environmental spectra survey is undertaken on a specific aircraft equipped with a recording device linked to strain gages or other load measuring sensors. Analytic techniques may be used to generate cyclic data in terms of load or stress. The FALSTAFF report [*5*] provides nondimensional loads on a fighter wing.

This program can, on demand, access the data base for trainer, fighter, bomber, or transport. The flight segments included in each data base are shown in Table 1 together with the form of the loads and the source of the data. Program editing capability allows the data bases to be expanded or modified as more or better data becomes available. If the in-service loads have been recorded for a specific aircraft, a data base can be established as described in Ref *2*.

TABLE 2—*Example of exceedance data. Bomber cruise data* [1]; *data represents 1000 flight hours.*

Positive Maneuver, *Nz*	Cumulative Occurrences in 1000 h	Negative Maneuver, *Nz*	Cumulative Occurrences in 1000 h
2.6	0.2	0.2	0.3
2.4	0.4	0.4	3.0
2.2	0.7	0.6	30.0
2.0	2.0	0.8	1000.0
1.8	6.0		
1.6	35.0		
1.4	300.0		
1.2	3500.0		

Form of Data Storage

The program accepts three common formats of compiled load cycle data.

Exceedance Data or Cummulative Occurrence Data

These data consist of a series of maximum and minimum load values and the number of times those loads are equaled or exceeded in a given time as shown in Table 2. This is the most common form of load cycle data; it is that used in Ref *1* and is that produced from PSD analysis of gust data. Load-factor data collected from L/ESS programs by means of counting accelerometers can be assembled in this form as can data from known time history traces. The advantage of this form of data is that it uses minimal storage capacity and data from various sources can be combined provided the mean loads (typically 1.0 *g*) are the same. Interpolation or extrapolation will provide load magnitudes occurring at any given frequency or provide the frequency of occurrence of any load magnitude. The disadvantage of exceedance data is that the range of individual cycles and the sequence of those cycles are undefined.

Mean/Range Data

An example of mean range data is shown in Table 3. The number of cycles in any cell is the number of cycles that occur in the given time period where the mean and load range is

TABLE 2*a*—*Discrete cycles from exceedance data. Composite spectrum,*[a] *2.0-h segment.*

Maximum Load Factor	Minimum Load Factor	Cycles per Flight
2.04	0.10	0.01
1.70	0.58	0.1
1.46	0.74	1.0
1.33	0.78	1.0
1.28	0.80	1.0
1.26	0.82	1.0
1.24	0.83	1.0
1.22	0.84	1.0
1.21	0.85	1.0

[a] Based on Table 2 data.

TABLE 2*b*—*Discrete cycles from exceedance data. Random spectrum, 2.0-h segment.*

Array 1 Cycles Occurring Every Flight[a]			Array 2 Cycles in 1000 Flights that Occur Less than Once per Flight[a]		
Maximum Load Factor	Minimum Load Factor	Cycles per Flight	Maximum Load Factor	Minimum Load Factor	Cycles per 1000 Flights
1.33	0.78	1.0	2.35	0.12	1
1.28	0.80	1.0	2.20	0.20	1
1.26	0.82	1.0	2.10	0.28	1
1.24	0.83	1.0	2.04	0.34	1
1.22	0.84	1.0	1.98	0.37	1
1.21	0.85	1.0	1.95	0.40	1
			1.92	0.41	1
			1.89	0.43	1
			1.87	0.44	1
			1.85	0.47	1
			1.79	0.52	10
			1.72	0.57	10
			1.68	0.60	10
			1.66	0.62	10
			1.64	0.64	10
			1.62	0.65	10
			1.60	0.66	10
			1.58	0.67	10
			1.57	0.68	10
			1.52	0.71	100
			1.48	0.73	100
			1.44	0.75	100
			1.42	0.76	100
			1.40	0.77	100
			1.39	0.78	100
			1.38	0.78	100
			1.37	0.79	100
			1.36	0.80	100

[a] Based on Table 2 data.

TABLE 2*c*—*Load factor spectrum for one segment of a composite spectrum, 2.0-h segment.*[a]

One Cycle Blocking			Blocked to Reduce Spectrum Length		
Maximum Load Factor	Minimum Load Factor	Cycles per Flight	Maximum Load Factor	Minimum Load Factor	Cycles per 1000 Flights
2.04	0.10	0.01	2.04	0.10	0.01
1.70	0.58	0.1	1.70	0.58	0.1
1.46	0.74	1.0	1.46	0.74	1.0
1.33	0.78	1.0	1.33	0.78	1.0
1.28	0.80	1.0	1.27	0.81	2.0
1.26	0.82	1.0	1.23	0.83	3.0
1.24	0.83	1.0			
1.22	0.84	1.0			
1.21	0.85	1.0			

TABLE 2*d*—*Load factor spectrum for one segment of one random flight, 2.0-h segment.*[a]

High/Low Sequence			Random Sequence		
Maximum Load Factor	Minimum Load Factor	Cycles per Flight	Maximum Load Factor	Minimum Load Factor	Cycles per 1000 Flights
1.68[b]	0.76[b]	1.0	1.28	0.80	1.0
1.33	0.78	1.0	1.21	0.83	1.0
1.28	0.80	1.0	1.68[b]	0.78	1.0
1.26	0.82	1.0	1.22	0.82	1.0
1.24	0.83	1.0	1.24	0.84	1.0
1.22	0.84	1.0	1.26	0.76[b]	1.0
1.21	0.85	1.0	1.33	0.85	1.0

[a] Based on Table 2 data.
[b] Load levels selected at random from infrequent high load Array 2.

defined. The advantage of this form of cyclic load definition is that both the load range and the mean load is explicitly defined for each cycle. The disadvantages are that the sequence of the discrete load cycles is unknown and that the two-dimensional character of the array makes interpolation or extrapolation of the data difficult.

Range/mean tables can only be compiled from recorded time history records and require the supplied load sequence to be converted to equivalent cycles using a range pair or rain flow cycle counting technique before storing the data in the appropriate cell. Range/mean data can be converted to exceedance data format, with the loss of individual cycle definition, in order to estimate the frequency of occurrence of any load level.

From/To Tables

An example of a From/To or Min Max table is shown in Table 4. This is the load cycle format used in the FALSTAFF program [5]. The number shown in each cell is the number of half cycles or excursions of load between the assigned From value and the To value in the given time period. The advantage of this form of compiling the cyclic loads is that each load excursion is explicitly defined and the sequence is automatically defined by matching each From load with the preceding To load and using only valid excursions.

TABLE 3—*Example of range/mean data. Data represents 1000 flight hours.*

Range of Load Factor for Cycles	Mean Load Factor for Cycles				
	1.2	1.1	1.0	0.9	0.8
2.0	...	...	1	...	...
1.8	...	...	15	...	...
1.6	...	1	40	...	...
1.4	1	7	100	1	...
1.2	15	30	350	7	...
1.0	90	120	1 000	20	1
0.8	260	520	2 300	210	30
0.6	580	1030	6 500	720	230
0.4	920	1820	10 000	1060	560

TABLE 3*a*—*Data for Arrays 1 and 2.*

Range of Load Factor for Cycles	Mean Load Factor for Cycles				
	1.2	1.1	1.0	0.9	0.8
ARRAY 1—LOAD CYCLES OCCURRING EVERY FLIGHT IN 2-H FLIGHT SEGMENT.[a] DATA REPRESENTS ONE FLIGHT.					
1.2	...	...	...	...	...
1.0	...	...	2	...	...
0.8	...	1	4	...	...
0.6	1	2	13	1	...
0.4	1	3	20	2	1
ARRAY 2—LOAD CYCLES OCCURRING LESS THAN ONCE PER FLIGHT FOR 2-H FLIGHT SEGMENT.[a] DATA REPRESENTS 100 FLIGHTS. MINIMUM FREQUENCY CONSIDERED ONE PER 100 FLIGHTS.					
2.0	...	...	...	...	...
1.8	...	...	3	...	...
1.6	...	...	8	...	...
1.4	...	1	20	...	...
1.2	3	6	70	1	...
1.0	18	24	0	4	...
0.8	52	4	60	42	6
0.6	16	6	0	44	46
0.4	84	64	0	12	12

NOTE—Average number of cycles per flight 606/100 = 6.06.
[a] Based on Table 3 data.

TABLE 3*b*—*Load factor spectrum for one segment; 2-h flight segment, composite spectrum, high/low sequence.*

	Load Factors			
Range	Mean	Maximum	Minimum	Cycles per Flight
1.6	1.0	1.8	0.2	0.01
1.2	1.1	1.7	0.5	0.01
1.2	1.0	1.6	0.4	1.00
1.0	1.0	1.5	0.5	2.00
1.0	0.9	1.4	0.4	0.01
0.8	1.2	1.6	0.8	1.00
0.8	1.1	1.5	0.7	0.01
0.8	1.1	1.5	0.7	1.00
0.8	1.0	1.4	0.6	5.00
0.8	0.8	1.2	0.4	0.01
0.6	1.2	1.5	0.9	1.00
0.6	1.1	1.4	0.8	0.01
0.6	1.1	1.4	0.8	2.00
0.6	1.0	1.3	0.7	13.00
0.6	0.9	1.2	0.6	1.00
0.6	0.8	1.1	0.5	1.00
0.4	1.2	1.4	1.0	2.00
0.4	1.1	1.3	0.9	4.00
0.4	1.0	1.2	0.8	20.00
0.4	0.9	1.1	0.7	2.00
0.4	0.8	1.0	0.6	1.00

TABLE 3c—*Load factor spectrum for one segment; 2-h flight segment, a sample of a random spectrum.*

	Load Factors			
Range	Mean	Maximum	Minimum	Cycles per Flight
0.4	1.1	1.3	0.9	1.00[a]
0.6	1.0	1.3	0.7	13.00
0.4	1.1	1.3	0.9	3.00
0.4	1.2	1.4	1.0	1.00
1.2	1.0	1.6	0.4	2.00[a]
0.8	1.1	1.5	0.7	1.00
0.6	1.1	1.4	0.8	2.00
1.0	1.0	1.5	0.5	2.00
1.2	1.2	1.8	0.6	1.00[a]
0.4	1.0	1.2	0.8	20.00
0.6	0.9	1.2	0.6	1.00
0.6	0.8	1.1	0.5	1.00[a]
0.6	1.2	1.5	0.9	1.00
0.8	1.0	1.4	0.6	4.00
0.4	0.9	1.1	0.7	2.00
0.8	1.0	1.4	0.6	1.00[a]
0.4	0.8	1.0	0.6	1.00

[a] Selected from infrequent loads Array 2.

The disadvantage is that the data cannot be extrapolated to estimate the frequency of individual load excursions outside the data range in the data base. Further, the data cannot be interpolated to define the frequency of a given load cycle. From/To tables can only be compiled from recorded time history records storing each load excursion in the appropriate cell. From/To data may be converted to exceedance data format, with loss of individual cycle definition and sequence, in order to estimate the frequency of occurrence of any load level.

Flight Profiles

A sample flight profile for a transport aircraft is given in Table 5. Typically, it defines a specific mission in terms of mission segments in appropriate sequence, the mission segment times and the primary flight parameters such as gross weight, Mach number, altitude, airspeed, center of gravity position, engine thrust, and airplane configuration. Both the

TABLE 4—*Example of From/To data. Data represents 1000 flight hours.*

TO Load Factor for Cycles	FROM Load Factor for Cycles					
	2.0	1.6	1.2	0.8	0.4	0.0
2.0	0	8	15	38	10	0
1.6	15	0	155	550	330	15
1.2	25	60	0	2553	525	80
0.8	28	840	2500	0	205	25
0.4	3	148	500	424	0	0
0.0	0	10	73	33	5	0

TABLE 4a—*Spectrum selections. Data represents 100 flights or 200 flight hours.*[a]

TO Load Factor for Cycles	FROM Load Factor for Cycles					
	2.0	1.6	1.2	0.8	0.4	0.0
2.0	0	2	3	8	2	0
1.6	3	0	31	110	66	3
1.2	5	12	0	511	105	16
0.8	6	168	500	0	41	5
0.4	1	30	100	85	0	0
0.0	0	2	15	7	1	0

NOTE—Number of flights to be generated = 50 (input via mission distribution Table 6).
Maximum load defined as load occurring once per 100 flights.
Number of flights necessary in From/To table is 100 (maximum of 100 and 50).
Segment length = 2.0 h (input via flight profile Table 5).
Number of flight hours necessary in From/To table is 2.0 · 100 = 200.
Factor to be applied to each cell = 200/1000 = 0.2.
Number of excursions per flight = 1834/100 = 18 (nine excursions with increasing load and nine with decreasing load).
[a] Based on Table 4 data.

airplane configuration values, which relate to the wing, flap, slat, and speed brake position, and the mission parameters represent the average conditions for each flight segment. Although the program is written to allow inclusion of 12 specified parameters, the minimum requirement of altitude is necessary to define the gust loads for each flight segment defined by segment title and segment time. The additional flight parameters may be required to support load cycle data selection or if the load factor to stress conversion procedure warrants.

TABLE 4b—*Load factor spectrum for one segment of one random flight, 2.0-h segment.*

Selections from Table 4a		Final Spectrum		
FROM Load Factor	TO Load Factor	Maximum Load Factor	Minimum Load Factor	Cycles per 1000 Flights
1.20	0.80	1.20	0.80	1.0
0.80	1.60	1.60	0.80	1.0
1.60	0.80	1.20	0.40	1.0
0.80	1.20	2.00	0.80	1.0
1.20	0.40	1.20	0.40	1.0
0.40	2.00	1.20	0.80	1.0
2.00	0.80	1.20	0.40	1.0
0.80	1.20	1.20	0.80	1.0
1.20	0.40	1.60	1.60	1.0
0.40	0.80			
0.80	1.20			
1.20	0.80			
0.80	1.20			
1.20	0.40			
0.40	0.80			
0.80	1.20			
1.20	0.80			
0.80	1.60			

TABLE 5—*Typical flight profile. Transport profile Number 2 (2.0-h flight with take off gross weight of 100 000 kg).*

Mission Segment	Segment Time, h	Gross Weight, kg	Altitude, m	Mach Number	Aircraft Geometry	
					Flap	Speed Brake
Ground	1 period	100 000	0	0	up	closed
Climb	0.25	95 000	5 000	0.6	up	closed
Cruise	1.40	85 000	10 000	0.7	up	closed
Descent	0.25	75 000	4 000	0.5	up	open
Approach	0.10	70 000	1 000	0.3	down	closed
Ground	1 period	65 000	0	0	down	open

This is discussed in the stress transfer section. Each flight profile necessary to define the utilization of the aircraft is stored on a random access file to be read by the program on demand. Additional data consists of the distribution of the profiles within the desired spectrum as shown in Table 6 and the definition of the lifetime requirements of the aircraft.

Load Factor Spectrum Generation

Basic Procedure

For the purposes of this paper, it is assumed that the load cycle data base is in load factor format. For each mission segment, the program automatically accesses the data base and selects the appropriate load cycle data as a function of the aircraft type, flight segment title, and the flight profile parameters. A typical selection algorithm, that for a transport aircraft, is shown in Table 7. For a bomber or transport aircraft, both gust and maneuver data are selected for each flight segment while for a trainer or fighter aircraft only maneuver data is considered. Although the algorithms are hard coded within the program, simple modifications to the selection subroutine for the appropriate class of aircraft will allow the inclusion of more data. The load cycle data is converted to discrete load steps defined by a maximum load factor, a minimum load factor, and the number of cycles. The number of steps and the number of cycles in each step is a function of the flight segment time, obtained from the flight profile, as compared to the time represented by the data base.

The program continues to the next mission segment until the flight is complete and then continues with the next flight until the requested number of flight spectra have been generated for that profile. After the spectra have been compiled for all mission profile types, complete individual flights are randomly ordered using a select and not replace procedure so as to provide a random sequence of mission types.

TABLE 6—*Typical distribution of flight profiles.*

Mission Number	Mission Title	Take Off Gross Weight, kg	Flight Length, h	Number of Missions
1	Transport Mission 1	100 000	1.5	25
2	Transport Mission 2	100 000	2.0	50
3	Transport Mission 3	120 000	3.0	24
4	Ferry Flight	100 000	1.0	1

NOTE—The generated spectrum that represents 100 flights will be repeated 100 times to represent the 10 000 mission, 21 050 flight hour life time requirement.

TABLE 7—*Load cycle data selection algorithm for transport.*

Flight Profile Data		Selected Load Cycle Data (refer to Table 1)				
Segment Title	Altitude, m	Taxi	Ground Handling	Landing	Maneuver	Gust
Ground climb	<1500	1	2		4	19
	1500 to 3000				4	20
	3000 to 5000				4	21
	5000 to 8000				4	22
	>8000				4	23
Cruise	<1500				5	19
	1500 to 3000				5	20
	3000 to 5000				5	21
	5000 to 8000				5	22
	>8000				5	23
Descent	<1500				5	19
	1500 to 3000				5	20
	3000 to 5000				5	21
	5000 to 8000				5	22
	>8000				5	23
Approach landing	<1500			15	3	19

Program Controls and Operations

The program allows the user to control some spectrum generation assumptions and to tailor the output to suit subsequent spectra requirements such as submittal to damage computation programs or application to test specimens. Among these are the number of flight spectra to be created for each profile, which defaults to one when generating composite spectra.

Highest Spectrum Loads

Control of the highest loads to be considered for inclusion within the spectrum is user defined as the loads that occur once in 1000 flights, once in 100 flights, or once in 10 flights. The choice is frequently a function of the number of missions in one lifetime of service utilization. The spectrum for a 10 000 flight aircraft will include loads that occur once every 1000 flights while loads that occur once every 100 flights may be the acceptable maximum loads for a 2000 flight aircraft. Loads that occur less frequently than the prescribed limit are removed from consideration when generating the spectrum.

Other controls and options are dependent upon the format of the data base.

1. *Exceedance Format Data Base*—The data for each flight segment is converted to represent a single flight by factoring the exceedance values by the ratio of the flight segment time to the data base time as shown in Fig. 2 that is based on the data in Table 2. Conversion of exceedance data into discrete load cycles is demonstrated in Fig. 1.

The user has control over the following options.

Spectra type—composite or random—Composite spectra will generate a single spectrum to represent each flight profile. Table 2*a* provides the discrete steps for a single 2-h segment of a composite spectrum using the exceedance data shown in Table 2 and Fig. 1. The infrequent high loads are included as those loads that occur once in 100 flights and once in 10 flights.

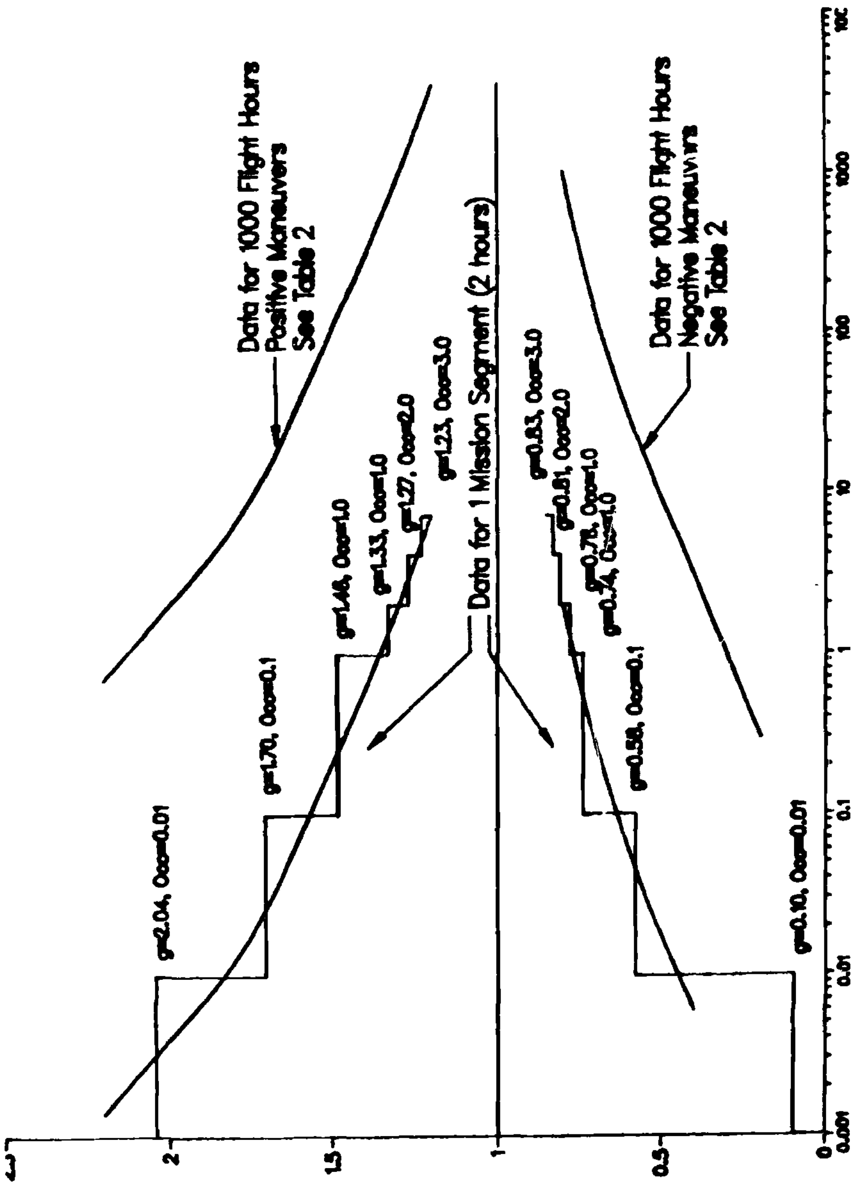

FIG. 2—*Typical exceedance data (bomber cruise data, Ref 1)*

Random spectra will generate the requested number of flight spectra to represent the profile. Each flight will differ from others in load magnitude and sequence. Array 1 in Table 2*b* shows the discrete cycles that occur, on average, in every flight. Array 2 in Table 2*b* provides 1000 load levels of both maximum and minimum load factors that occur more than once per 1000 flights and less than once per flight. The spectrum for the segment thus consists of all cycles that occur once or more per flight (Table 2*b*, Array 1) plus one cycle compiled by randomly selecting, and not replacing, one load level from each of the infrequent high load arrays (Table 2*b*, Array 2). Subsequent flights using the same exceedance data will select different loads to represent the infrequent high load condition.

Load sequence—high/low, low/high, or random—The load sequence option relates to the loads within each mission segment and will direct the pairing of loads from the maximum and minimum exceedance curves to form cycles as well as the sequence of those cycles. Cycles may be created by randomly pairing maximum and minimum loads that have equal number of cycles per flight using a select and not replace procedure. Alternatively, the cycles can be defined by pairing loads that have the same cumulative occurrences as shown in Fig. 1. The cycle sequence is selected by the required order of the maximum loads; high/low, low/high, or random. Sample load cycle sequences are shown in Table 2*d*.

Low-load truncation—Selection of a load range truncation level will result in the deletion of all spectrum steps where the load range is less than the truncation level. This will reduce the number of cycles in spectrum and thus the calendar time needed to conduct a fatigue test.

Block size control—When converting the exceedance data to discrete load steps as shown in Fig. 1, it is obviously possible to vary the number of spectrum steps. The smallest block size, that is, one cycle per step, will result in the closest proximity to the exceedance data and will allow the maximum possible degree of randomization in both pairing of peaks and valleys and in the sequencing of load steps. The problem is that the spectrum has the potential of being too long for use in available damage programs or fatigue test machines. The user has the option of selecting single-cycle blocking or of selecting the approximate load level drop between steps. Table 2*c* shows the comparison of single-cycle blocking and blocking for load range change of approximately 3% of the maximum load range (load factor = 2.23) defined by the load range occurring once per 1000 flights.

Load Factor Spectrum from Exceedance Data—An example of the final load factor spectrum for one flight segment is shown in Table 2*d* for both high/low and random sequences.

2. *Range/Mean Format Data Base*—The data for a flight segment, of which Table 3 is an example, is separated into two arrays as shown in Table 3*a*. In Array 1, which represents one flight, are all the cycles that occur once or more per flight. Array 2 contains all the cycles that occur less than once per flight for the number of flights defined by the highest load required. If the highest load, as in the example, is that occurring once in 100 flights, the array is for 100 flights. The average number of infrequent load cycles per flight in the example is 6.06. The spectrum is created in terms of maximum load (mean load + range/2), minimum load (mean load − range/2) and appropriate number of cycles.

The user has control over the following options.

Spectrum type—composite or random—Composite spectrum will generate a single spectrum to represent a single flight profile. The spectrum will include all the load cycles in Array 1. Twelve load cycles will be selected from Array 2 to represent the infrequent high loads. Six will be assigned a cycle value of 1.0 and six a cycle value of 0.01 as shown in Table 3*b*.

Random spectrum will generate the requested number of flight spectra to represent the profile. Each flight will differ from others in load magnitude and sequence. Each flight will include all load cycles from Array 1 plus six cycles selected at random from Array 2 using a select and not replace procedure. If Array 2 is cleared before the necessary number of flights have been created, it is refilled and used again. A single random spectrum for one flight segment is shown in Table 3*c*.

Cycle sequence—high/low, low/high, or random—The pairing of peaks and valleys is dictated by the data base. The cycle sequence, high/low, low/high, or random, is the sequence of the peak loads within each mission segment.

Low load truncation—Selection of a load range truncation level will result in the deletion of all spectrum steps where the load range is less than the truncation level so as to reduce the spectrum length for test purposes.

Block size control—When creating a spectrum from mean/range tables, a given step as defined by the range and mean load has a defined number of cycles. If the number of steps is increased such that each step is one cycle, the maximum possible degree of randomization of sequence may be achieved. The problem is that the spectrum has the potential of being too long for available damage programs or fatigue test machines. The user has the option of selecting one cycle blocking or of accepting the blocking as defined in the data base.

Load factor spectrum from range/mean data—An example of the final load factor spectrum for one flight segment is shown in Table 3*b* for high/low sequence and in Table 3*c* for a random sequence.

3. *From/To Format Data Base*—The number of necessary flights of From/To data is defined as the maximum of the number of missions to be created or the reciprocal of the frequency of the maximum load required. The number of cycles in each cell is computed as shown in Table 4*a* using the data in Table 4. The number of load excursions for each flight is computed from the total number of excursions in the array divided by the number of flights represented by the array. The spectrum is created by selecting, from Table 4*a* array, alternate load excursions from the two sections, separated by the null diagonal.

The starting location is selected as the cell with the maximum number of cycles thus defining the first load excursion by a From value and a To value. The second load excursion is found from a random selection of a legitimate To value where the From value is identical to the To value of the previous load excursion. The random procedure uses a select and not replace routine. If a required From value is not available in the array, the nearest From value is selected and the process continued until the necessary number of excursions per flight have been selected as shown in Table 4*b*.

The final spectrum is generated in terms of the maximum load, minimum load, and one cycle per step as shown in Table 4*b*.

The user has control over the following options.

Low load truncation—Selection of a load range truncation level will result in the deletion of all spectrum steps where the load range is less than the truncation level.

Block size control—When creating a spectrum from From/To tables, a given step, defined by the maximum and minimum load represents one cycle. The spectrum can be reduced in length by user request to search the spectrum for any cycles within the mission segment where the maximum and minimum loads are identical and to combine them into one step by summating the number of cycles. Such reduction will change the load sequence.

Load factor spectrum from From/To data—An example of the final load factor spectrum for one flight segment is shown in Table 4*b*.

Load Factor Spectrum

The final load factor spectrum is a sequential file of the number of flights requested in Table 6. Each flight is labeled with the flight profile title and a flight identification number within that flight profile type. The spectrum for each flight is a series of steps each of which is defined by the flight segment title, the type of load (gust, maneuver, taxi), the maximum load in the cycle, the minimum load in the cycle, and the number of cycles. A sample of a single flight is shown in Table 8.

Load Factor to Stress Transformation

The load factor to stress conversion assumes that the stress is linear with respect to load factor and takes the form

$$\text{stress} = a + b \cdot (Nz - 1)$$

where a is the stress due to a 1-g condition and b is the stress due to a 2-g condition minus the stress due to the 1-g condition.

The program provides two options for converting the load factor spectrum to a stress spectrum.

In the first option, the user provides one or more equations that in general relate the structural stress to the load factor and any of the mission parameters included in the flight profile. The equations may take a universal form applicable to any flight condition. In the simplest form, where stress solutions are known for only two conditions, the equations would be $a \cdot Nz$ for ground conditions and $b \cdot Nz$ for flight segments where a and b are the stresses for a unit Nz. If more stress solutions are available a "least squares regression" technique, as described in Ref *2*, may be used to generate complex equations such as

$$\text{ground segment stress} = a \cdot \text{weight} \cdot Nz$$

$$\text{flight segment stress} = 1/(1\text{-Mach}) \cdot (b + c \cdot \text{weight} + d \cdot \text{altitude}$$

$$+ e \cdot \text{weight} \cdot (Nzm - 1) + f \cdot \text{weight} \cdot (Nzg - 1))$$

where $a,b,c,d,e,$ and f are constants developed by least squares regression analysis; mission parameters of weight, Mach number, and altitude are provided in the mission profile; Nzm is the maneuver load factor; and Nzg is the gust load factor.

TABLE 8—*Transport profile Number 2, Flight 1 (2.0-h flight with take off gross weight of 100 000 kg).*

Step Number	Mission Segment	Load Type	Maximum Load		Minimum Load		Cycles per Flight
			Nz	Stress	*Nz*	Stress	
1	ground	taxi	1.23	−1.23	0.68	−0.68	1.000
2			1.29	−1.29	0.78	−0.78	1.000
3			1.25	−1.25	0.76	−0.76	1.000
4			1.27	−1.27	0.80	−0.80	1.000
5			1.32	−1.32	0.79	−0.79	1.000
6	climb	gust	1.17	8.69	0.76	7.05	1.000
7			1.59	10.38	0.80	7.21	1.000
8		maneuver	1.24	9.20	0.82	7.09	1.000
9		gust	1.24	8.95	0.88	7.41	1.000
10			1.46	10.28	0.72	6.97	1.000
11			1.20	8.79	0.83	7.31	1.000
12	cruise	gust	1.28	11.54	0.68	8.25	1.000
13			1.17	10.92	0.84	9.14	1.000
14			1.16	10.86	0.83	9.08	1.000
15		maneuver	1.27	11.91	0.89	9.24	1.000
16		gust	1.22	11.20	0.82	9.01	1.000
17			1.20	11.08	0.78	8.80	1.000
18			1.18	10.99	0.75	8.60	1.000
19			1.25	11.40	0.80	8.92	1.000
20	descent	maneuver	1.22	9.08	0.94	7.70	1.000
21			1.25	9.24	0.69	6.78	1.000
22			1.33	9.66	0.88	7.38	1.000
23		gust	1.25	9.00	0.83	7.32	1.000
24			1.17	8.68	0.75	7.00	1.000
25			1.19	8.75	0.81	7.25	1.000
26			1.21	8.85	0.79	7.15	1.000
27			1.35	9.40	0.77	6.83	1.000
28	approach	gust	1.15	9.73	0.85	8.27	1.000
29			1.22	10.03	0.76	7.86	1.000
30			1.16	9.76	0.84	8.24	1.000
31			1.19	9.89	0.78	7.97	1.000
32			1.40	10.86	0.91	8.45	1.000
33			1.28	10.30	0.83	8.20	1.000
34		maneuver	1.33	10.98	0.70	7.58	1.000
35		gust	1.24	10.14	0.82	8.16	1.000
36			1.17	9.80	0.80	8.05	1.000
37			1.18	9.84	0.81	8.11	1.000
38			1.20	9.95	0.72	7.70	1.000
39	ground	taxi	1.27	−1.27	0.78	−0.78	1.000
40			1.29	−1.29	0.76	−0.76	1.000
41			1.23	−1.23	0.79	−0.79	1.000
42			1.30	−1.30	0.80	−0.80	1.000
43			1.25	−1.25	0.77	−0.77	1.000

If stress solutions for the specific flight segment conditions of the flight profile are available, the equations would take the form

$$\text{ground stress} = a \cdot Nz$$

$$\text{climb stress} = b + d \cdot (Nzm - 1) + f \cdot (Nzg - 1)$$

$$\text{cruise stress} = c + e \cdot (Nzm - 1) + g \cdot (Nzg - 1), \text{ etc.}$$

where *a, b,* and *c* are stresses for 1-g conditions; *d* and *e* are stress for a Δg condition due to maneuver; *f* and *g* are stress for a Δg condition due to gust; *Nzm* is the maneuver load factor; and *Nzg* is the gust load factor.

The stress spectrum shown in Table 8 was compiled with the following equations

$$\text{ground stress} = 1.0 \cdot Nz$$

$$\text{climb stress} = 8.0 + 5.0 \cdot (Nzm - 1) + 4.0 \cdot (Nzg - 1)$$

$$\text{cruise stress} = 10.0 + 7.0 \cdot (Nzm - 1) + 5.0 \cdot (Nzg - 1)$$

$$\text{descent stress} = 8.0 + 5.0 \cdot (Nzm - 1) + 4.0 \cdot (Nzg - 1)$$

$$\text{approach stress} = 9.0 + 6.0 \cdot (Nzm - 1) + 4.5 \cdot (Nzg - 1)$$

The constants were computed using the applied loads applicable to the flight conditions defined in the flight profile (Table 5) and the NASTRAN program [*6*] to solve for the internal stresses.

The program will compile the supplied equations and compute the stress equivalent of each load factor in the spectrum.

The second option is used when the design is established and a large number of load condition solutions are available to represent flight and ground conditions. A typical list of such conditions, generated for a light utility transport is given in Table 9. Conditions of 1-g level flight, Δg; due to maneuver, and Δg due to gust are generated for each series of flight parameters and where the Δg conditions are created as the difference between the 2-g condition and the 1-g condition. The stress solutions are stored on the spectrum program loads data base.

If the structural stresses are computed with NASTRAN finite element program [*6*], the stresses on the NASTRAN output tape can be loaded directly to the spectrum program loads data base that, being a random access file, can be addressed by the internal loads model structural element number.

When using this option, the user selects the structural element number and provides an equation to convert the internal loads model defined stress to the true structural stress at the location being considered. The program automatically selects the conditions needed for each load factor using an algorithm, such as that in Table 10, based on the flight profile parameters. The program subroutine containing the condition selection algorithm must be exclusively compatible with the choice of load conditions for which the internal stresses are known. Therefore, the routine has been written to allow easy modifications as the internal loads data base changes. The algorithm in Table 10 was developed for the wing of a light utility transport after studying the stress solutions and performing least squares regression analysis in order to define the parameters to which the stress was most sensitive. The selection

TABLE 9—*List of load conditions for which internal loads are available.*

Condition Number	Load Type	Gross Weight, kg	Mach Number	Altitude, m	Airplane Condition
1	1-*g* inertia	8500			on gear
2	1-*g* inertia	6500			
3*a*	1 *g*	6500	0.4	1 500	flight
3*b*	Δ*g* maneuver	6500	0.4	1 500	
3*c*	Δ*g* gust	6500	0.4	1 500	
4*a*	1 *g*	6500	0.4	2 500	
4*b*	Δ*g* maneuver	6500	0.4	2 500	
4*c*	Δ*g* gust	6500	0.4	2 500	
5*a*	1 *g*	6500	0.45	3 000	
5*b*	Δ*g* maneuver	6500	0.45	3 000	
5*c*	Δ*g* gust	6500	0.45	3 000	
6*a*	1 *g*	6500	0.5	5 000	
6*b*	Δ*g* maneuver	6500	0.5	5 000	
6*c*	Δ*g* gust	6500	0.5	5 000	
7*a*	1 *g*	7500	0.5	4 000	
7*b*	Δ*g* maneuver	7500	0.5	4 000	
7*c*	Δ*g* gust	7500	0.5	4 000	
8*a*	1 *g*	7500	0.6	5 500	
8*b*	Δ*g* manuever	7500	0.6	5 500	
8*c*	Δ*g* gust	7500	0.6	5 500	
9*a*	1 *g*	7500	0.7	8 000	
9*b*	Δ*g* maneuver	7500	0.7	8 000	
9*c*	Δ*g* gust	7500	0.7	8 000	
10*a*	1 *g*	7500	0.8	10 000	
10*b*	Δ*g* maneuver	7500	0.8	10 000	
10*c*	Δ*g* gust	7500	0.8	10 000	
11*a*	1 *g*	8500	0.4	1 500	
11*b*	Δ*g* maneuver	8500	0.4	1 500	
11*c*	Δ*g* gust	8500	0.4	1 500	
12*a*	1 *g*	8500	0.4	2 500	
12*b*	Δ*g* maneuver	8500	0.4	2 500	
12*c*	Δ*g* gust	8500	0.4	2 500	
13*a*	1 *g*	8500	0.45	3 000	
13*b*	Δ*g* maneuver	8500	0.45	3 000	
13*c*	Δ*g* gust	8500	0.45	3 000	
14*a*	1 *g*	8500	0.5	5 000	
14*b*	Δ*g* maneuver	8500	0.5	5 000	
14*c*	Δ*g* gust	8500	0.5	5 000	
15*a*	1 *g*	7500	0.3	0	
15*b*	Δ*g* maneuver	7500	0.3	0	
15*c*	Δ*g* gust	7500	0.3	0	

of conditions and the accompanying algorithm will be unique to each aircraft and may be different for the various airframe components.

The establishment of the internal loads data base has the advantage of making stress spectra instantly available at any structural location.

Conclusion

The uniqueness of aircraft utilization requirements, coupled with a wide range of quality and quantity of input data, was the biggest obstacle in creating a universal spectrum generation program. The approach was to classify aircraft and provide data bases for each

TABLE 10—*Automatic load condition selection algorithm.*

GROUND CONDITIONS

Weight Range, kg	Condition
<7500	1
>7500	2

FLIGHT CONDITIONS

Mach Range	Altitude Range, m	Weight Range, kg	Condition Number
0 to 0.35	All	All	15x
0.35 to 0.55	0 to 2000	<7500	3x
		>7500	11x
	2000 to 2750	<7500	4x
		>7500	12x
	2750 to 3500	<7500	5x
		>7500	13x
	3500 to 4500	all	7x
	>4500	<7500	6x
		>7500	14x
0.55 to 0.65	all	all	8x
0.65 to 0.75	all	all	9x
>0.75	all	all	10x

NOTE—$x = a$ for 1-g condition, b for Δg maneuver condition, and c for Δg gust condition.

aircraft class. The data selection routines were written with the knowledge that modification will be necessary as the data bases expand with increasing availability of flight data. For the purpose of brevity, this paper discusses only symmetric loading as defined by load factor Nz. Assymmetric loads due lateral gusts, roll, and yaw maneuvers have been included by additions to the load cycle data base, development of appropriate load to stress transfer functions, and modification of the selection algorithms.

The advantage of this type of program is that the data base can be established from published data for initial spectrum development and easily modified and expanded as more rational data becomes available to represent a particular aircraft.

The system was successfully expanded to include load cycle data bases and accompanying selection routines for specific aircraft such as the B-1B bomber, the T-39 Utility Transport, and the Canadair CL600 Transport. The T-39 data base included flight loads records collected during the L/ESS program [2] in addition to analytic and military specification provided information. The internal loads data bases were also created for these aircraft allowing the program to generate spectra in support of design and verification analysis. The quality of the spectra generated is obviously a function of the completeness and relevancy of the data bases to the product under consideration but in general the program, using published data, is an ideal tool for trade studies of utilization variations or the evaluation of the effects of design stress level and materials.

References

[1] MIL-A-87221, Military Specification for Aircraft Structures, U.S. Air Force, 28 Feb. 1985.

[2] Denyer, A. G., "Generation of Fatigue Load Spectra from Recorded Flight Data," *Materials, Experimentation and Design in Fatigue,* Society of Environmental Engineers, UK, April 1981.

[3] NACA-TN-4332, "An Approach to the Problem of Estimating Severe and Repeated Gust Loads for Missile Operations," National Advisory Committee on Aeronautics, Washington, DC.
[4] ESDU-69023, Engineering Sciences Data, Royal Aeronautical Society, U.K., Sept. 1969.
[5] FALSTAFF, Description of a Fighter Aircraft STAndard For Fatigue Evaluation, LBF Laboratorium für Betriebsfestigkeit, Darmstadt, West Germany.
[6] NASA Report SP-221/03, NASA Structural Analysis Program (NASTRAN), National Aeronautics and Space Administration, Washington, DC, March 1976.

Leslie P. Pook[1] *and William D. Dover*[2]

Progress in the Development of a Wave Action Standard History (WASH) for Fatigue Testing Relevant to Tubular Structures in the North Sea

REFERENCE: Pook, L. P. and Dover, W. D., "**Progress in the Development of a Wave Action Standard History (WASH) for Fatigue Testing Relevant to Tubular Structures in the North Sea,**" *Development of Fatigue Loading Spectra, ASTM STP 1006,* J. M. Potter and R. T. Watanabe, Eds., American Society for Testing and Materials, Philadelphia, 1989, pp. 99–120.

ABSTRACT: Fixed tubular steel platforms were first installed in the North Sea in 1966. They are subjected to significant fatigue loads due to wave action, and consequently a large number of relevant fatigue tests have been carried out on representative tubular joints. In 1979, the Wave Action Standard History (WASH) Working Group was formed to develop standard load spectra for fatigue testing relevant to offshore structures. This paper reviews some of the work that has been carried out in support of the Working Group, but it is not an official Working Group document. It is concluded that construction of realistic load spectra representative of wave loading on tubular structures in the North Sea is feasible at the current state of the art. The basic steps needed for implementation of a tentative standard load spectrum are described.

KEY WORDS: fatigue testing, load spectra, offshore structures, welded joints, corrosion fatigue, wave loading, hydrodynamic theory, fatigue (materials), testing

Fixed tubular steel platforms were first installed in the North Sea in 1966. Offshore structures in the North Sea are subjected to significant fatigue loads due to wave action, and a large number of laboratory tests have been carried out to determine the fatigue behavior of tubular steel structures. Much research work on tubular welded joints has indicated that the conjoint action of service loading and a seawater environment must be taken into account in the fatigue assessment of offshore structures.

It is desirable that structural fatigue tests be carried out using standardized load spectra representative of service conditions. The first proposal for standardized load spectra representative of North Sea conditions was published in 1976 [*1*]. Since then, tests have been carried out using a variety of spectra, but there are as yet no generally agreed standards.

In 1979, increasing interest led to the formation of a European Working Group on Standardized Loading Sequences for Offshore Structures, now known [*2*] as the Wave Action Standard History (WASH) Working Group. In 1985, a report [*3*], based on the Working Group's deliberations, described a Common Load Sequence (COLOS), representative of North Sea conditions and gave a detailed description of its implementation. This is now in use for fatigue testing.

[1] Senior principal scientific officer, National Engineering Laboratory, East Kilbride, Glasgow, U.K.
[2] Shell professor of mechanical engineering, University College London, London WC 1, U.K.

The nature of offshore loading, and the complex interactions likely in a seawater environment, make the establishment of standard load spectra for offshore structures much more difficult than for say the aircraft industry. In the case of the latter, one has a common structural form and, especially for fighter aircraft, a loading environment controlled, and hence clearly defined, by operational requirements. Service loads, in these circumstances, can be measured at appropriate times and the characteristics of a standard loading spectrum determined. A well known example is FALSTAFF (Fighter Aircraft Loading STAndard For Fatigue [4]. By contrast, offshore oil exploration and production fixed and mobile platforms have a wide range of structural forms built up from common structural elements, in many cases tubular joints. In addition, the loading is mainly environmental, rather than man made, giving less predictable load sequences.

This paper reviews some of the work that has been carried out in support of the WASH Working Group, but it is not an official Working Group document. Details of the sources of strain gage and other data are given in an internal report [5] that has not yet been released for publication; various platforms are identified by code letters. These code letters are used to reference data sources in this paper.

The objectives of the present work were: to identify the major factors affecting wave loading of tubular members in the North Sea, to examine available service data in order to identify patterns of behavior, to present data in a form convenient for the construction of standard load spectra, to identify the major factors likely to influence the corrosion fatigue behavior of tubular welded joints, and to make practical suggestions for the construction of standard load spectra.

Wave Loading of Tubular Members

Sea-State Characterization

The primary parameter used in the characterization of sea state is the wave height, H, that is measured peak-to-trough. Over a period of time short enough (conventionally 20 min) for a sea state to be regarded as statistically stationary, the usual measurement of its severity is the significant wave height, $H_{1/3}$, that is the average height of the highest one-third portion of the waves. One of the ways in which wave height data can be usefully presented [2] is by means of a scatter diagram that gives the relative occurrence of sea states within specified small intervals of $H_{1/3}$ and wave period, T. Table 1 is an example [6] of a scatter diagram derived from data obtained by the *M V Famita*. The *M V Famita* is one of a number of ships that have been stationed in the North Sea to collect oceanographic data.

Such scatter diagrams were used by Holmes and Tickell [6,7] to calculate wave loadings on various diameter members immersed to various depths. They made two major simplifications in using the scatter diagrams. First, it was assumed that the waves were unidirectional; in practice, waves usually have a predominant direction. Second, the water surface elevation was assumed to be Gaussian and narrow band; this implies that wave heights follow the Rayleigh distribution. For a Rayleigh distribution, the exceedance, that is, the probability, $P(S/\sigma)$, that a positive going peak exceeds S/σ is given by [8]

$$P(S/\sigma) = \exp(-S^2/2\sigma^2) \tag{1}$$

where S is peak size ($= H/2$) and σ is the root mean square (rms) value of the whole process measured from the (usually zero) mean. For a narrow-band process, $H_{1/3}$ is very nearly equal to 4σ [2]. Differentiating, the probability density, $p(S/\sigma)$, is given by

$$p(S/\sigma) = S/\sigma \exp(-S^2/2\sigma^2) \tag{2}$$

TABLE 1—*Scatter diagram for* M V Famita *for full year.*

	Zero Crossing Wave Period, s[a]									
$H_{1/3}$, m	4.5	5.5	6.5	7.5	8.5	9.5	10.5	11.5	12.5	13.5
0.30	14	40	34	8	0	0	0	0	0	0
0.91	64	159	135	40	4	0	0	0	0	0
1.52	18	103	164	78	24	2	0	0	0	0
2.13	6	53	126	95	33	7	1	0	0	0
2.74	0	19	103	72	41	8	2	0	0	0
3.35	0	9	46	71	31	3	1	0	0	0
3.96	0	1	23	63	38	6	1	0	0	0
4.57	0	0	6	20	31	10	2	1	0	0
5.18	0	0	5	13	15	12	1	0	0	0
5.79	0	0	1	9	4	6	3	0	0	0
6.40	0	0	0	2	2	4	2	0	0	2
7.01	0	0	0	0	1	3	7	0	0	0
7.62	0	0	0	1	1	0	4	0	2	0
8.23	0	0	0	1	2	0	0	0	0	0
8.84	0	0	0	0	0	2	2	0	0	0
9.45	0	0	0	0	0	0	0	0	0	2

[a] Parts per 1924.

Long-term records show that the time history of $H_{1/3}$ has the appearance of a random process. Assume for the moment that all sea states are narrow band and their significant wave heights follow the (positive half) of a Gaussian distribution [2]

$$p(S/\sigma) = (2\pi)^{1/2} \exp(-S^2/2\sigma^2) \tag{3}$$

$$P(S/\sigma) = (2\pi)^{1/2} \int_{S/\sigma}^{\infty} \exp(-S^2/2\sigma^2)\, d(S/\sigma) \tag{4}$$

This integral does not have an elementary solution. It follows (Appendix I) that the sum of the peaks of all sea states follows the Laplace distribution

$$P(S/\sigma) = p(S/\sigma) = \exp(-S/\sigma) \tag{5}$$

where σ is interpreted as the long-term rms value.

Morison's Equation

In its original form [*9*], Morison's equation applies only to an isolated vertical member under the influence of unbroken waves. It gives the horizontal force, F, per unit length

$$F = \frac{C_m \rho \pi D^2}{4} \frac{\partial u}{\partial t} + \frac{C_d \rho D}{2} u^2 \tag{6}$$

where D is member diameter, ρ is water mass density, u is horizontal water particle velocity, $\partial u/\partial t$ is horizontal water particle acceleration, C_m is inertia (or mass) coefficient, and C_d is drag coefficient. The first term is the inertia term proportional to the accelerative force on the mass of water displaced by the member and hence to water particle velocity, and the second term is the drag term proportional to the square of the water particle velocity.

Entering values of $\partial u/\partial t$ and u obtained from linear wave theory [2], it follows that both terms vary cyclically about zero but are 90° out of phase. The two terms have to be summed throughout a cycle in order to find the force maxima needed for fatigue assessment [10].

Consider a stationary, Gaussian, narrow-band sea state. Then for the special case in which the drag term is negligibly small, Morison's equation is a linear transformation, the load distribution remains Gaussian and narrow band, and peak loads follow the Rayleigh distribution. More generally, Morison's equation is a nonlinear transformation, the load distribution is not Gaussian, it remains narrow band in the sense that individual cycles may be distinguished but these are not sinusoidal, and peak loads do not follow the Rayleigh distribution. For the special case in which the inertia term is negligible, peak loads follow the Laplace distribution (Appendix I).

Morison's equation may be applied to other than vertical members. It is usual to take components of horizontal velocities and accelerations perpendicular to the axis of the member, which simply introduces scaling factors into distributions. Nonvertical members are subjected to forces due to vertical velocities and accelerations, but these are relatively small.

Effect of Wave Period

Using linear wave theory, it may be seen [2,11] that the inertia term of Morison's equation includes a factor

$$B_m = \frac{1}{T^2} \frac{\cosh 2\pi (d + z)/L}{\sinh 2\pi d/L} \tag{7}$$

where d is still water depth, z is depth of immersion below still water level measured negatively downwards, L is wave length, and t is time, and the drag term a factor

$$B_d = \frac{1}{T^2} \left\{ \frac{\cosh 2\pi (d + z)/L}{\sinh 2\pi d/L} \right\}^2 \tag{8}$$

Since L is a function of T [2], the factors provide a measure of the influence of wave period on peak load. Figure 1 shows values of wave period factors. For zero depth of immersion, both factors are very nearly equal to $1/T^2$ for a wave period of up to about 12 s. Beyond this, they diverge and are greater than $1/T^2$. As the depth of immersion increases, these factors decrease reflecting the decreasing loading; the drag factor decreasing at a faster rate as the drag term in Morison's equation becomes relatively less important. Maxima appear, and at great depths the dependence on wave period will reverse, that is, the factors increase with wave period. For certain water depths within the wave period of interest (around 4 to 14 s, Table 1), B_m and B_d, and hence peak loads, are broadly independent of wave period.

Calculated Load Distributions

The peak load calculations carried out by Holmes and Tickell [6,7] used linear wave theory and Morison's equation in conjunction with sea-state scatter diagrams. The long-term distribution of peak loads was calculated as the sum of individual components from a scatter diagram using C_m as 2.0, C_d as 1.0, and d as 121.9 m. Calculations were carried out in Imperial units, these have been converted to SI units. Figure 2 shows a selection, listed in Table 2, of the calculated distributions. These were selected to demonstrate the effect of various parameters, and also for comparison later with measured peak stress distributions.

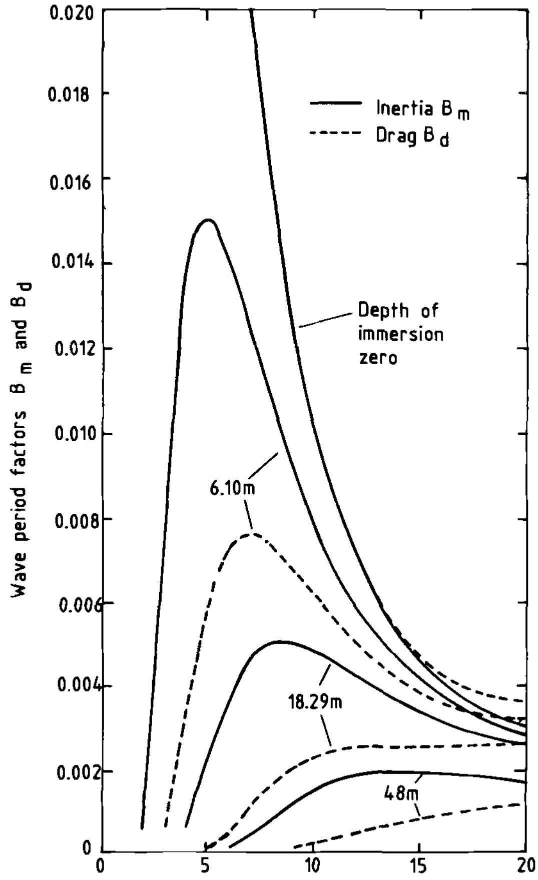

FIG. 1—*Effect of wave period.*

It is convenient to base discussion of calculated and measured distributions on the following idealized situation. Assume that sea states are narrow band, their rms values follow the Gaussian distribution, and wave period factors are independent of wave period; then it follows that wave heights will follow the Laplace distribution. If the drag term in Morison's equation is negligibly small (large-diameter members), then peak loads will also follow the Laplace distribution; whereas if the inertia term is negligibly small (small diameter members), they will follow the Weibull distribution, modulus 0.5.

Figure 2 shows for example that the exceedance curve for a 1.83-m-diameter member immersed 18.29 m, based on the winter six months, is very slightly S-shaped and could be represented by a Laplace distribution with the rms reduced by about 8%. The behavior appears to be close to the idealized situation with the inertia term dominant. Although the sea-state distribution for the winter six months is close to Gaussian and the member diameter fairly large, the relevant wave period factor, B_m (Fig. 1), cannot be said to be even approximately constant in the wave period range 4 to 14 s. It appears that deviations from ideal behavior have largely balanced out except that the slope of the exceedance curve has

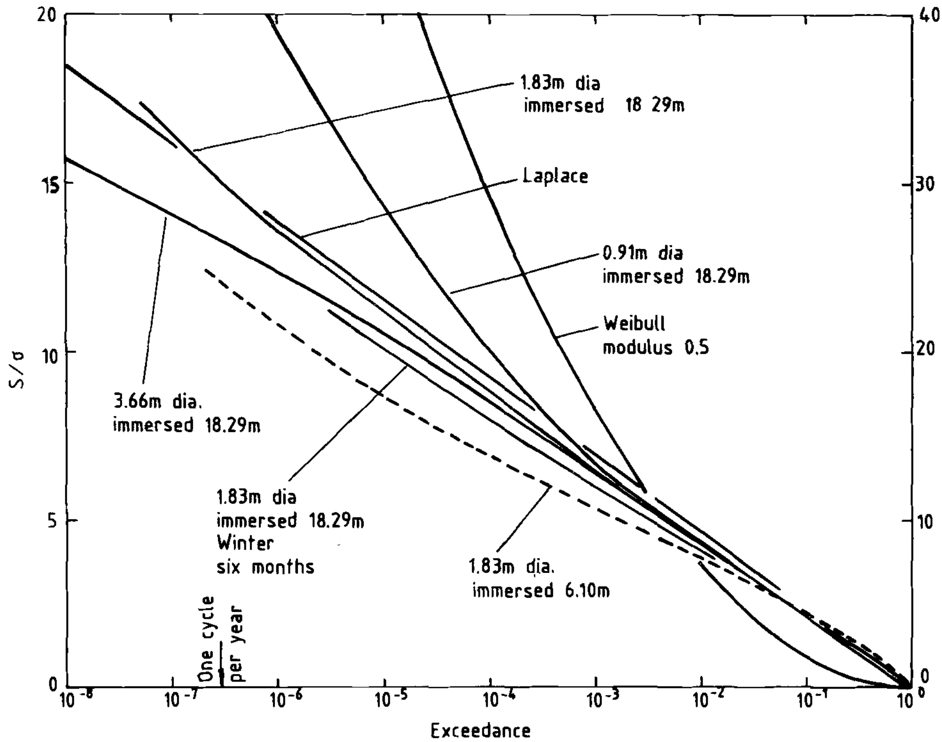

FIG. 2—*Calculated exceedances.*

changed. The curve for the full year is concave upwards due to deviation of the sea-state distribution from the Gaussian distribution (next section).

Compared with a 1.83-m-diameter member, the exceedance curve for a 3.66-m-diameter member immersed 18.29 m is distorted in a concave downwards direction.

The exceedance curve for a 0.91-m-diameter member immersed 18.29 m shows two distinct regions corresponding to inertia-dominated behavior at low values of S/σ and drag-dominated behavior at high values, with a sharply curved transition region. The member behavior follows both idealized situations but at different levels of S/σ.

The exceedance curve for a 1.83-m-diameter member immersed 6.10 m is significantly

TABLE 2—*Details of cases considered.*

Wave Data	Member Diameter, m	Depth of Immersion, m
M V Famita, winter six months. Average zero crossing wave frequency, 0.1439 Hz. 2.2 × 10^6 cycle/six months	1.83	18.29
M V Famita, modified for full year. Average zero crossing wave frequency, 0.1511 Hz. 4.77 × 10^6 cycle/year	0.91	18.29
	1.83	6.10
	1.83	18.29
	3.66	18.29

different from that for a member immersed 18.29 m, reflecting differences in wave period factors, that is, increase in B_d and decrease in B_m.

It may be concluded that load distributions approach one or the other of the two extreme idealized situations depending on the member diameter and level of S/σ. Also, sea-state data need to be examined to see how closely the Gaussian distribution is followed, and comparisons need to be made with measured load data.

Service Data

Sea-State Distribution

Long-term records (A)[3] show that sea state has the appearance of a random process. Sea-state data from four different sources were therefore examined (2) to see whether the distribution of $H_{1/3}$ was Gaussian, but the fit was not very satisfactory. A detailed examination of sea-state data for five years (G) showed that the distribution of $H_{1/3}$ was more accurately represented by the Gumbel distribution. In its simplest form, this is given by [*12*]

$$P(x) = 1 - \exp[-\exp(-x)] \tag{9}$$

where $P(x)$ is the exceedance of the variable x. For $x > 4$, $P(x) \approx \exp(-x)$, and for $x < -2$, $P(x) \approx 1$. The sea-state data are well fitted by the expression

$$P(H_{1/3}) = 1 - \exp\{-\exp[(1.9 - H_{1/3})/1.06]\} \tag{10}$$

where $P(H_{1/3})$ is the exceedance of $H_{1/3}$. The associated mean zero-crossing wave period, T_z, is given by

$$T_z = [8(H_{1/3} + 2.6)]^{1/2} \tag{11}$$

Table 3 shows a suggested approximation (G) of this sea-state data by 12 sea states. It is

TABLE 3—*Approximation of sea-state data.*

Sea-State Number	$H_{1/3}$,[a] m	Corresponding Range, m	Wave Period, T_z (s)	Fraction of Time, %
0	1.75	0.00 to 1.95	5.9	38.5
1	2.55	1.95 to 2.85	6.4	28.5
2	3.40	2.85 to 3.80	6.9	17.5
3	4.15	3.80 to 4.50	7.3	7.18
4	4.80	4.50 to 5.10	7.7	3.40
5	5.45	5.10 to 5.75	8.0	2.16
6	6.15	5.75 to 6.55	8.4	1.31
7	6.90	6.55 to 7.35	8.7	0.678
8	7.80	7.35 to 8.30	9.1	0.334
9	8.80	8.30 to 9.40	9.5	0.154
10	10.35	9.40 to 12.55	10.2	0.0797
11	13.60	12.55	11.5	0.0043

[a] The rms values of $H_{1/3}$ based on number of waves = 2.867 m.

[3] Letters in parentheses are codes used to identify data sources in Ref 5.

assumed that T_z is constant during each sea state. Sea State 11 is an extreme corresponding to only 1 h in 25 years.

It is recommended that a Gumbel distribution of sea states be used in the construction of standard load spectra, however, the assumption of a Gaussian distribution is adequate for examination of the general features of wave loading.

Sea-State Duration

The duration of a sea state is the time during which it remains statistically stationary. A proposed operational definition (G) of sea-state duration is "a time period during which $H_{1/3}$, computed over 18-min intervals, remains within 0.75 m of its overall average." (This definition allows the wave period to vary during a "statistically stationary" sea state.) Figure 3 shows observed (G) sea-state durations and numbers of observations for the data represented by Eqs 10 and 11. Relatively few low sea states were observed because of failure of the computational algorithm due to tidal effects on the reference level.

Clearly, realistic sea-state durations need to be incorporated in standard load spectra.

Effect of Resonances

For a stiff structure, neglecting yielding, stresses (and strains) are proportional to loads. However, this is not the case if structural resonances occur. Offshore structures are therefore designed [2] so that resonant frequencies, in particular the fundamental (sway) frequency,

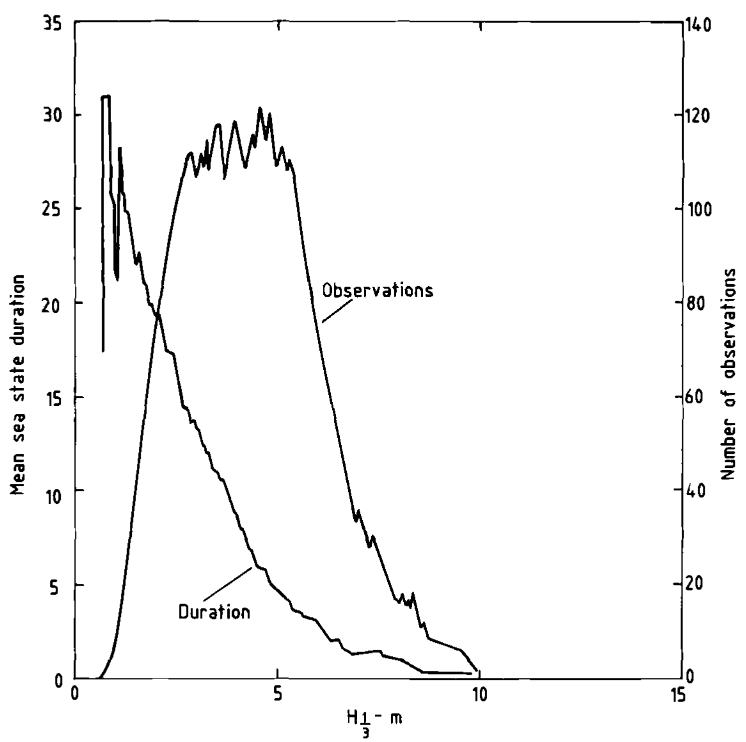

FIG. 3—*Observed sea-state durations.*

are significantly greater than the wave passing frequency. In practice, although sea states have a dominant frequency, they are not particularly narrow band so energy may be available to excite resonances. Structural resonances may also be excited at the third harmonic of the wave passing frequency through interference effects between different parts of the structure [*2*].

Power spectral density functions [*13*] provide information on the distribution of frequencies in a Gaussian random process. Bandwidth may be characterized by the spectral bandwidth, ϵ, that is a measure of the bandwidth of the spectral density and ranges from 0 (narrow band) to 1, and by the irregularity factor, I, that is the ratio of positive-going zero (mean) crossings to positive-going peaks. For a Gaussian process

$$\epsilon^2 + I^2 = 1 \tag{12}$$

A process is usually taken [*8*] as narrow band if $I \geq 0.99$ corresponding to $\epsilon \leq 0.14$. Spectral density function plots obtained from strain-gaged structures show a peak corresponding to the wave-passing frequency and subsidiary peaks at higher frequencies corresponding to any structural resonances. Figure 4*a* is an example (A). Figure 4*b* shows the corresponding spectral density function of the water surface elevation. Resonance is most often at the third harmonic of the wave-passing frequency (B). When resonance occurs, the bandwidth is substantially increased. If a process is not narrow band, individual cycles cannot be distinguished, and for fatigue purposes, it is usual to calculate equivalent cycles. The most commonly used procedure is the rainflow method [*10*].

A two-peaked spectral density function may be represented by Wirsching's equation [*14*]

$$S(f) = AH_{1/3}{}^{\phi} \frac{\exp\left[\dfrac{-1050}{(2\pi T_d f)^4}\right]}{T_D^4 (2\pi f)^5 \left\{\left[1 - \left(\dfrac{f}{f_n}\right)^2\right]^2 + \left[\dfrac{2\zeta f}{f_n}\right]^2\right\}} \tag{13}$$

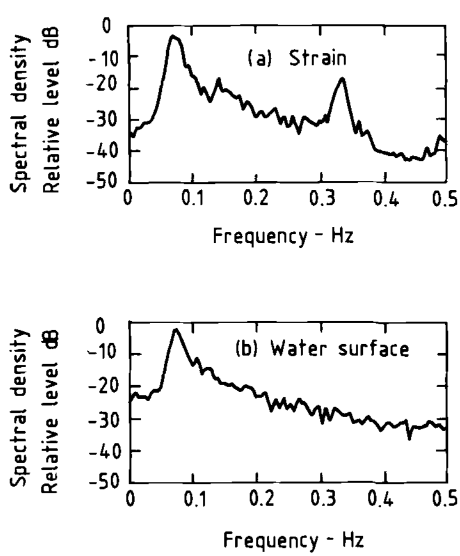

FIG. 4—*Measured spectral density functions.*

where $S(f)$ is the spectral density as a function of frequency, f; A and ϕ are scaling factors; T_D is the dominant wave period; f_n is the natural frequency of the structure; and ζ is the damping factor of the structure. The dominant wave frequency is close to, but not identical with, the reciprocal of the zero crossing wave period, but in calculations may be taken as numerically identical. Values that give realistic spectral density functions for the sea-state data given in Refs *14* and *15* are: $A = 5580$ (for $H_{1/3}$ in metres), $f_n = 0.286$, $\zeta = 0.02$, and $\phi = 3.25$.

Measured-load spectral density functions could be conveniently fitted using Wirsching's equation.

Measured Stress Distributions

Three sets of peak stress distribution data obtained from strain gages on North Sea structures were available for comparison with the calculated peak load distributions. In all cases, strain gages were mounted so as to measure loads going into nodes. The data are shown as exceedances in Fig. 5. All three data sets show the drop off at high values of S/σ (dashed lines) that is associated with finite sample size [*8*]. The following comments are confined to regions of the exceedance curves that do not appear to have been affected.

Mobile Rig (*D*)—This is a stiff structure moored on the Norwegian continental shelf, with strain gages on a 2-m-diameter member immersed about 9 m. There is a linear relationship between load and stress so time histories are essentially narrow band. Strain gage readings

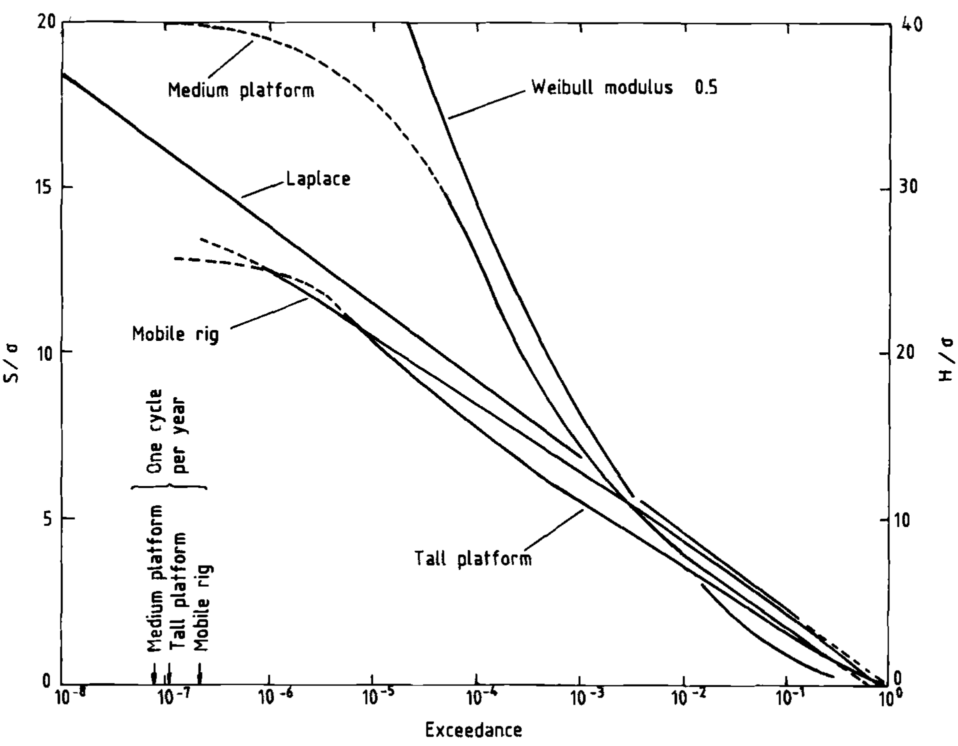

FIG. 5—*Measured exceedances.*

were taken over short periods and sea-state data used to transform these to a full year. The lowest sea state representing 1.05×10^6 cycles out of 4.68×10^6 cycles per year was omitted from the data supplied. The estimated full distribution is shown as a dashed line. The exceedance curve could well be represented by the Laplace distribution. The results are consistent with calculated results for 1.83-m-diameter members shown in Fig. 2.

Tall Platform (*A*)—This is a tall platform (181-m water depth) in the northern North Sea, with strain gages on a 2.1-m-diameter member immersed 48 m. Readings were taken over a period of 7½ months, and it was assumed that this was representative of a full year. Structural resonances were observed; the spectral bandwidth decreased as sea state increased. The total number of peaks per year was 8.76×10^6 compared with an expected number of 5.6×10^6 for the narrow-band case, so a lower bound for the irregularity factor is 0.64. Equivalent cycles were calculated using the rainflow method. A dashed line (low S/σ values) shows estimated narrow-band behavior. In the data used, rainflow cycles were given in terms of the rms of the rainflow count ranges, σ_{rf}. The conversion factor to S/σ is not available so values were plotted as if they were S/σ values. This is equivalent to assuming that $\sigma_{rf} = 2$; data in Ref *2* suggest that this is a reasonable approximation.

The estimated narrow-band exceedance curve is close to the calculated results for a 1.83-m-diameter member immersed 18.29 m, except that it is slightly more concave upwards. The inertia wave period factor, B_m, for a depth of immersion of 48 m (Fig. 1) has more emphasis at longer wave periods, which is the correct sense to account for the difference. The rainflow exceedance curve is distorted in a concave upwards direction at low levels. This is in accordance with theoretical predictions [*2*]. To a first approximation, neglecting resonances, stresses are proportional to wave height, *H*.

Medium Platform (*G*)—This is a medium platform (98-m water depth) in the central North Sea, with strain gages on 0.85-m-diameter members immersed 26.5 m. Intermittent readings were taken daily for several years and sea-state data used to transform these for a full year. Data from a particular gage were selected as representative of available data, partly because some information was available on individual sea states. Structural resonances were observed; the spectral bandwidth tended to decrease as sea state increased. The total number of peaks per year was 1.24×10^7, and the overall irregularity factor 0.61. Equivalent cycles were calculated using the rainflow method. A dashed line (low S/σ values) shows estimated narrow-band behavior. As for the Tall Platform, σ_{rf} was assumed to be 2σ. Irregularity factors for individual sea states are shown in Fig. 6; the spectral bandwidths shown were calculated using Eq 10. The irregularity factor decreases only slowly with increase in significant wave height.

The estimated narrow-band exceedance curve shows two regions that appear close to ideal behavior and are near to the Laplace distribution and Weibull modulus 0.5 distributions, respectively. The curve is broadly similar to the calculated results for a 0.91-m-diameter member immersed 18.29 m. Distortion of the rainflow exceedance curve is confined to very low levels. Exceedances were available for individual sea states and these suggest that loads are inertia dominated up to a significant wave height of 5 m and drag dominated above 7 m, with an intermediate transition region. To a first approximation stresses are proportional to $H^{1.6}$ if resonances are neglected.

Conclusion—Load distributions close to both idealized situations may be observed in measured stress distributions as well as in calculated load distributions.

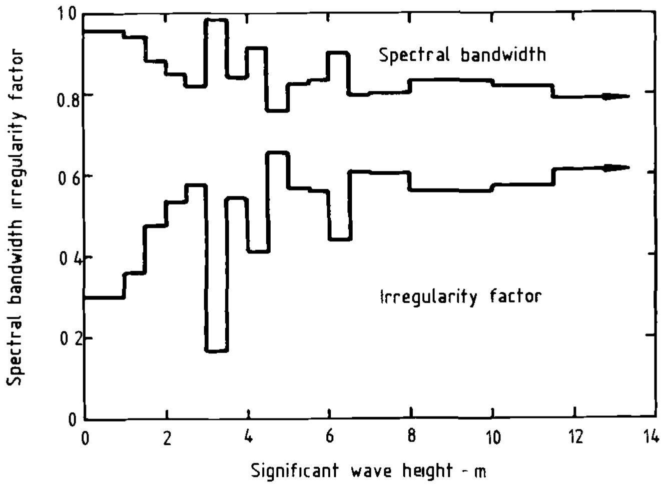

FIG. 6—*Spectral bandwidth and irregularity factor for Medium Platform.*

Discussion

It is clear that the main features of the statistical distribution of loads on tubular members can be predicted from oceanographic data using relatively simple hydrodynamic theory. In particular, relationships between wave loading and wave height, wave period, member diameter, and depth of immersion can be understood. The major factors influencing the stresses that occur in tubular members are the member diameter and depth of immersion, and whether or not structural resonance occurs. This apparent localization of effects is a useful simplification, but as there will usually be a number of similar diameter members used in the construction of a platform, it may be the result of integration of loads over a wider area.

There appears to be a consensus that standard load spectra should be based on a limited number of sea states representing the actual sea-state distribution, and that a year's data should be represented. There are significant differences between summer and winter conditions in the North Sea, so representation of less than a year's data would be unrealistic. Very severe storms that occur less frequently than once per year contribute very little fatigue damage and are therefore relevant to static strength rather than fatigue life assessments. In this context, "sea state" can mean either the water surface elevation or the resultant stresses in a structure. It also appears to be accepted that the spectral density function, and hence wave period, should be constant during a sea state.

Representative spectral density functions should be selected from service data and be fitted using Wirsching's equation. Transform techniques can be then used to produce equivalent time histories; a method in use at University College London is outlined in Appendix II.

Once the sea states have been decided upon, they have to be arranged in some order. Early practice [*13*] was to use a low-high-low sequence, but realistic randomization using a Markov Chain approach [*16*] seems preferable. A Markov transition matrix (G) corresponding to the data shown in Table 3 and Fig. 3 is given in Table 4. For example, if the current subblock is Sea State 5, the probability that the next subblock will be also Sea State 5 is 0.7143, and the probability that it will be Sea State 6 is 0.1385. The subblock length used in the construction of the matrix was 10 min. The use of this matrix for the construction of

TABLE 4—*Sea-state transition matrix.*

	To											
From	0	1	2	3	4	5	6	7	8	9	10	11
0	0.9970	0.0030	...	...	...	...	...	...	...	...	...	...
1	0.0075	0.9857	0.0068	...	...	...	...	...	...	...	...	...
2	...	0.0187	0.9697	0.0116	...	...	...	...	...	...	...	...
3	...	...	0.0345	0.9375	0.0280	...	...	...	...	...	...	...
4	...	...	...	0.0668	0.8571	0.0761	...	...	...	...	...	...
5	...	...	...	...	0.1472	0.7143	0.1385	...	...	...	...	...
6	...	...	...	...	...	0.2639	0.6000	0.1361	...	...	...	...
7	...	...	...	...	...	...	0.3056	0.5238	0.1706	...	...	...
8	...	...	...	...	...	...	...	0.3939	0.4737	0.1324	...	...
9	...	...	...	...	...	...	...	...	0.3244	0.4286	0.2470	...
10	...	...	...	...	...	...	...	...	...	0.5787	0.3939	0.0274
11	...	...	...	...	...	...	...	...	...	...	0.6250	0.3750

standard load spectra is appropriate since the distribution of sea states is correctly reproduced.

Corrosion Fatigue Behavior Relevant to Standard Load Spectra

Corrosion fatigue behavior has been studied using both fatigue life tests and fatigue crack growth tests. Fatigue life tests on simple specimens can provide understanding of the interaction between the environment and fatigue crack initiation. Fatigue life tests on simple welded joints yield information on the influence of the environment on crack initiation, early crack growth, and crack growth to failure. Some valuable information on these three phases can be obtained if detailed measurements are made of damage accumulation during tests on simple welded joints, but it is usually not possible to read this information across to the case of a tubular joint. Fatigue life tests on tubular joints, however, will provide the correct sequencing of these failure modes, but all fatigue life tests must be accelerated tests, either in terms of frequency or stress level. A 20-year test is just not possible. This has led to the conduct of both tubular joint tests and alternative tests based on precracked plate specimens. In these tests, the crack geometry and real-time damage can be simulated and this information can be utilized in predicting the service behavior of tubular joints.

Tests in Air

In-air fatigue studies, both fatigue life and crack growth, on structural steels show that steady-state damage accumulation conditions are quickly attained on commencing cyclic loading, and that stress and ΔK (stress intensity factor range) can be used to describe the damage. For both fatigue crack initiation and fatigue crack growth, there exists a level below which damage does not occur. These are the fatigue limit and fatigue crack growth threshold, respectively; but in both cases, the variation in stress is the primary variable. For some metals nonsteady-state (or transient) behavior can occur under variable amplitude test conditions. This phenomenon is known as load interaction and implies that the fatigue damage from the current cycle is influenced by previous cycles. The physical reason for this effect could well be connected with the variations in the crack-tip plastic zone size associated with varying stress amplitudes. Fortunately, in the case of offshore structural steels such as British Standard BS 4360 Grade 50D, the magnitude of this load interaction effect is small; and for clipping ratios (ratio of maximum to rms in load sequence) of around 4.0 or even more, it would seem to be negligible [13]. This reduces the possibility of transient phenomena, during in-air tests on these steels, to periods when the loading changes from one sea state to another. (A clipping ratio of 4.0 is a reasonable approximation for variable amplitude loading within an individual sea state, but the year-round clipping ratio could be much higher.)

Compared to alternating stress and ΔK, mean stress, effects for in-air fatigue crack growth tests are of secondary importance except when they cause crack closure (closure of a crack at above the minimum load in the fatigue cycle). Mean stress effects tend to be small for in-air fatigue crack growth tests on structural steels, and BS4360 50D is no exception.

Seawater Tests

The presence of a seawater environment introduces a major new factor in that fatigue damage becomes both time and cycle dependent. The time-dependent element can manifest itself through direct corrosive attack or through complex interactions with both environment and stress, such as stress corrosion. This change in the mode of damage accumulation increases the importance of mean stress, through both access (crack opening) and stress corrosion cracking, and test time.

Crack closure has the same significance for crack growth in seawater as in air, but there is the additional possibility that corrosion products can build up within the crack causing a change in the closure stress, local changes in electrolyte composition due to difficulties in refreshing the crack tip region, and changes in the corrosion process due to variations in deposits on the crack faces. The complexity of these chemical variations and the difficulties in attempting to model these processes makes it necessary to conduct some large-scale corrosion fatigue tests on tubular joints.

Stress corrosion cracking is usually considered in terms of the proximity of a material's threshold intensity factor for stress corrosion cracking, K_{Iscc}, to its plane strain fracture toughness, K_{Ic}. The conventional view is that either fatigue or stress corrosion cracking dominates at various levels of stress intensity factor, and that finally at high stresses, as K_{Ic} is approached, steady load cracking becomes important. This model has been slightly modified in recent years through the realization that K_{Iscc} may be much lower than previously thought in the presence of very low-level cyclic loading, known as ripple loading tests [17].

The effect of test time and test frequency is again complex mainly because the effect of environment on fatigue crack growth behavior is not influenced to the same degree by the environment at all values of ΔK. This means that in certain types of fatigue life test, the crack growth regime critically affected by the environment may occupy only a small part of the total crack growth process. This would lead in these cases to a very small influence of environment on test life and apparently no effect on fatigue life due to test time, frequency, etc. This conclusion is, of course, only valid for the particular test specimen geometry and mode of loading and, as with many other fatigue life results, is not general. From the results available so far from tubular joint tests, it would seem that test frequency cannot be accelerated [18].

One other problem that arises in corrosion fatigue tests is that steady-state crack growth rates are not attained rapidly after the commencement of cyclic loading [19]. During these transient periods, the stress intensity factor range does not uniquely define a fatigue crack growth rate. This transient behavior can occur with changing stress amplitude and with test interruption, and is particularly critical in the determination of the fatigue crack growth threshold where the stress intensity factor history may influence the measured threshold. Transient effects can cause variations in measured crack growth rates of as much as ten times, and are obviously an important consideration in the setting up of tests to measure steady-state behavior. Currently, no methodology exists for reintroducing transient effects into design calculations, and one would look instead to the effect being included in the test method in an appropriate way. One such method would be to include this feature in standard load spectra, that is, the transient behavior is included into the materials data rather than into analysis (analogous to the way that mean stress effects and local stress have been included in the fatigue life data for tubular joints). Such a route requires great care in the choice of standard load spectra.

Electrode potential is the primary variable controlling corrosion processes in offshore structures and it is used in offshore structures, through impressed current or sacrificial anodes, to give cathodic protection. This procedure leads to the steel structure becoming the cathode rather than the anode and the suppression of metal dissolution (corrosion). One effect of this change is the formation of calcareous deposits on the bare metal surface that can reduce access to the metal surface and assist in increasing the crack closure stress. The difficulty found in service of applying uniformly the optimum cathodic potential (-0.7 to -0.8 V) leads to the situation where some regions of an offshore structure may be overprotected by up to -1.1 V. This may lead to increased fatigue crack growth rates.

The enhancement of fatigue crack growth rates found in seawater tests, when compared to in-air tests, is considered to be due to hydrogen embrittlement even in the structural steels. This has led to studies of situations where sulfate-reducing bacteria are present. This work uses cultures of sulfate-reducing bacteria in anaerobic conditions that have indicated that crack growth rates can be as high as ten times the corresponding in-air rates and have confirmed the possibility of hydrogen embrittlement in structural steels [*20*].

Studies of the importance of environment in variable amplitude tests are not yet sufficiently advanced for the major contributing factors to be listed.

Discussion

It can be seen that the presence of a seawater environment changes the relatively simple response found in in-air tests to one where mean stress, frequency, cathodic protection level, crack size, temperature, and test time all become important factors. Some of these factors can be varied independently, but the presence of transient effects makes it imperative that load spectra be truly representative. This may mean both a close reproduction of all main features of service loading and the use of a range of load spectra during exploratory fatigue studies. This is felt to be advisable because it is not yet practical to incorporate all these factors into fracture mechanics design methodology, and one instead has to include some of these factors in the materials data (by testing under appropriate load spectra). It might be appropriate to consider a standard framework for producing a family of load spectra. From this could emerge a standard load spectrum, after further exploratory fatigue studies, but it would still allow the choice of slightly different load spectra for individual platforms or locations.

Omission of Low Loads

There appears to be a consensus that test frequency should not be increased to reduce testing time. The only practical alternatives are the omission of low loads, or the use of extrapolation procedures in design. Perhaps the most important unresolved issue in the development of standard load spectra for offshore structures is the extent to which low loads may be omitted. Low loads cause little fatigue damage and there are so many of them that their omission can significantly reduce testing time. They can be omitted either by omitting complete sea states or by omitting all loads below a certain level. The latter is difficult to implement unless sea states are narrow band. Another motive for omitting low loads is that they are at a small fraction of full scale on the load measuring system, and may be of the same order as noise levels in servo-hydraulic systems.

Fatigue damage due to different load levels may be estimated [*10*] by assuming linear accumulation of fatigue damage, that is, Miner's rule holds, and that fatigue damage is proportional to the *m*th power of the cyclic stress range (*m* is also the exponent in the Paris fatigue crack growth equation). A typical value of *m* for structural steels in air is 3. Damage density may be defined as $(S/\sigma)^m\, p(S/\sigma)$, where, if necessary, values are taken from a rainflow count. The area under the damage density curve is proportional to total fatigue damage, and individual points on the curve give the relative contribution of different level cycles. If the fatigue limit is taken into account, the lower end of the curve is truncated.

Figure 7 shows damage density curves, with *m* taken as 3, for the measured data, and for the Laplace and Weibull, modulus 0.5, distributions. As before, it was assumed for both the Tall Platform and the Medium Platform that $\sigma_{rf} = 2\sigma$. Values of S/σ of about 9, 12, and 20 correspond to one cycle per year for the Mobile Rig, Tall Platform, and Medium Platform data, respectively. In all cases there is very little damage at low levels. Data for the Mobile Rig are close to the Laplace distribution, and peaks above $S/\sigma = 5$ cause little fatigue damage. The curve for the Tall Platform is a scaled-up version, and peaks above $S/\sigma = 7$ cause little damage. The curve for the Medium Platform shows the influence of the small member diameter, and significant damage extends to very high levels. These results can only be taken as a rough guide since they are sensitive to the value of *m* [*15*] (increasing

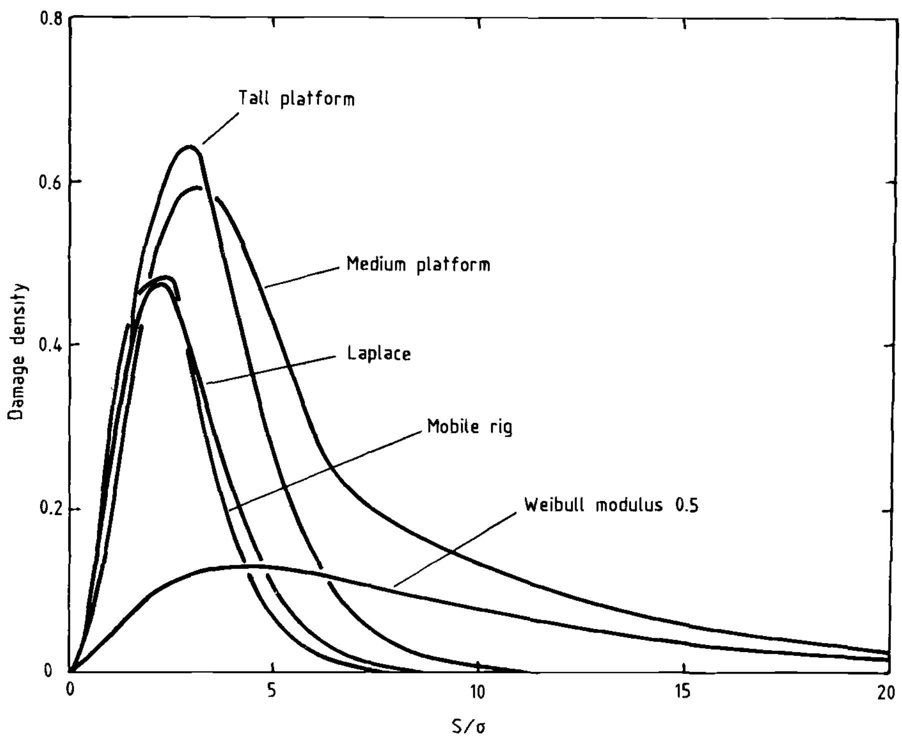

FIG. 7—*Damage density curves.*

m reduces the relative contribution of low loads), and corrosion effects are not taken into account.

Wirsching [14] suggested that Eq 13 should be used in conjunction with eleven sea states (of unknown source) in order to construct a standard load spectrum. Hartt [16], on the basis of calculations with m taken as 4.38, argued that Wirsching's three lowest sea states should be omitted as they occupied 89% of the life yet contributed little fatigue damage. However, recalculation [5] with $m = 3$ suggested that it was only possible to omit the two lowest sea states representing 68% of the life.

Recommendations

Although there are still some unresolved issues, construction of realistic load spectra representative of wave loading on tubular structures in the North Sea appears to be feasible at the current state of the art. The basic steps needed for implementation of a recommended tentative standard load spectrum are outlined below using a flexible framework.

Conditions to be Modeled

The standard load spectrum should be broadly representative of the Tall Platform data, with load assumed proportional to wave height. It should be pseudo-random and repeat exactly after one year. The overall level of the load spectrum and the mean load should be left as options for the user, as should the imposition of an overall load limit that may be needed to prevent premature specimen collapse [1,2].

Sea States

The individual sea states to be considered should be based on those shown in Table 3. The two lowest sea states and enough (about three fourths) of the next lowest should be omitted so as to retain 20% of the total time. Because of the decrease in wave period as sea state increases, the proportion of cycles retained will be somewhat less. The three highest sea states should be combined into a single sea state giving a total of eight levels. Exceedances, for the narrow-band case, with all sea states included and with the proposed combination and omissions are shown in Fig. 8. Also shown for comparison are the effects of omitting the highest sea state and the two lowest sea states.

Sea-state evolution should be modeled by means of a Markov Chain using a suitably modified version of the transition matrix shown in Table 4 with subblocks of 10-min duration. Sea-state durations obtained using this matrix are statistically equivalent (A) to the data shown in Fig. 3. Transition between sea states can be as a step change or possibly as a linear change from one sea state to another.

Frequency Content

The spectral density function should be constant within each sea state. A representative service spectral density function should be selected for each sea state and fitted using Wirsching's equation (Eq 11).[4] A platform resonant frequency (0.3 Hz) should be recommended, but selection of an appropriate value should be left as an option for the user.

[4] Analysis of spectral density functions at the National Engineering Laboratory has shown that Wirsching's equation may not be appropriate, but alternative approaches appear feasible.

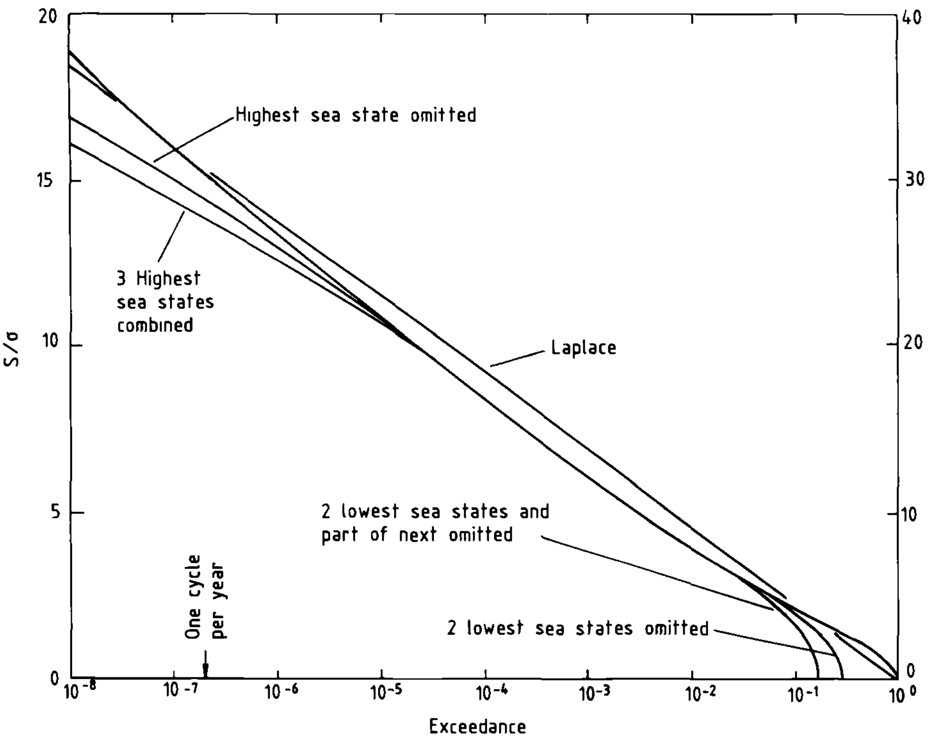

FIG. 8—*Exceedance of proposed standard load spectrum.*

Sea-State Load Sequences

Load sequences for individual sea states should be generated using a pseudo-random binary sequence based on a shift register (Appendix II). the generator should not be reset after each subblock. The clipping ratio for each sea state should be limited to 4.3.

Alternative Load Spectrum

Consideration should be given to the construction of a load spectrum broadly representative of the Medium Platform data. This could be achieved by raising each point on the Tall Platform load spectrum to the 1.6th power. Alternatively, the load distribution could be matched by adjusting sea-state levels using procedures described in Ref *13*.

Conclusion

Construction of realistic load spectra representative of wave loading on tubular structures in the North Sea is feasible at the current state of the art. The basic steps needed for implementation of a tentative standard load spectrum are described. In essence, this is a framework that could be used to formulate a particular standard load spectrum, but leaves open the option of incorporating alternative features, should this prove desirable, with relatively little additional work.

Acknowledgments

This paper contains British Crown copyright material that is published by permission of the Director, National Engineering Laboratory, UK Department of Trade and Industry. The work reported was partly supported by the Mechanical Engineering Committee of the UK Department of Trade and Industry. The work has benefited from discussions with other Wave Action Standard History Working Group members.

APPENDIX I

Two-Parameter Weibull Distribution

The positive half of the (two-parameter) Weibull distribution may be written in the form [*13*]

$$P\left(\frac{S}{\sigma}\right) = \exp\left[\frac{-b}{a}\left(\frac{S}{\sigma}\right)^{a}\right] \tag{14}$$

where a is the Weibull modulus or slope, and b is a function of a. Values of b are tabulated in Ref *13*. For a in the range 0.71 to 2.36 the expression

$$b = 1 - 0.076\,(a^2 - 3a + 2) \tag{15}$$

provides a satisfactory fit.

In this form, Eq 14 gives the distribution of the peaks of a sinusoidal process. Putting $a = 2, b = 1$ and $a = 1, b = 1$ gives as special cases the Rayleigh and Laplace distributions (Eqs 1 and 5).

A theorem due to Swanson [*21*] can be extended to show that the sum of the peaks of a sequence of Weibull distributions, modulus A, whose rms values follow the positive half of a Gaussian distribution, is a Weibull distribution, modulus A/2. In particular, summing Laplace distributions leads to a Weibull distribution, modulus 0.5, and as originally shown by Swanson, summing Rayleigh distributions leads to a Laplace distribution. Hence, for a Gaussian sea-state distribution, Morison's equation leads to peak loads that follow the Weibull distribution, modulus 0.5, if the drag term is dominant, and the Laplace distribution, if the inertia term is dominant.

APPENDIX II

Generation of Load Sequences

The generation of a sequence of load levels (in the time domain) can be conveniently accomplished using a pseudo-random binary sequence. The steps involved are:

A transfer function, $H(w)$, is determined so that the desired spectral density function, $\phi_x(w)$, can be obtained from a white noise source, $\phi_\epsilon(w)$, that is

$$\phi_x(w) = |H(w)|^2\phi_\epsilon(w) \tag{16}$$

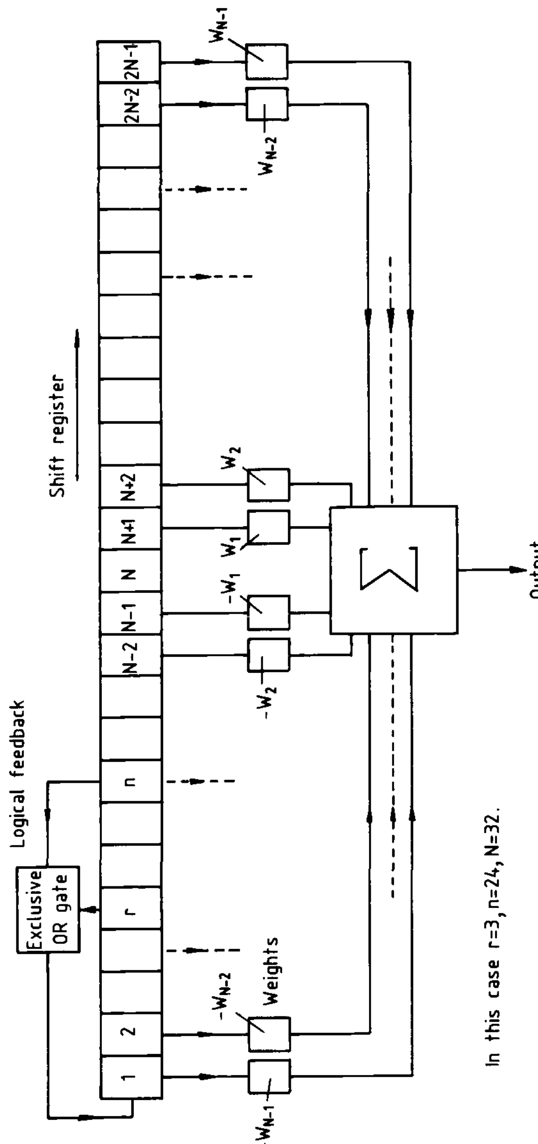

FIG. 9—*Schematic diagram of pseudo-random signal generation.*

A filter function, $h(\tau)$, the inverse Fourier transform of $H(w)$, can be evaluated and used to weight the white noise signal, $\phi_\epsilon(w)$. The function, $h(\tau)$, effectively amplifies all the desired frequencies so that unwanted frequencies remain but only as an insignificant part of the load sequence. The desired load sequence, $\eta(t)$, is given by

$$\eta(t) = \int_{-\infty}^{\infty} h(\tau)\epsilon(t - \tau)d\tau \tag{17}$$

The white noise source (uniform spectral density function) can be obtained by sampling a controlled semiconductor noise source and using the instantaneous value to switch the output signal to $+a$ or $-a$. However, a simpler more controlled software route is to use a discrete random number generator as the noise source. This is a digital circuit for producing a chain of numbers in a seemingly random order. These random numbers can be generated by a simple logical circuit using a "shift register," an adding device, and a clock.

Each stage of the shift register stores a digit, 0 or 1. At every pulse from the clock, all the digits are shifted one place to the right. The last digit is abandoned, the first is formed by adding (Modulo 2) the digits in the first and last stage. Using a shift register with m stages, the length of the chain can become $2^m - 1$ digits before a repeat and the pattern of every m adjacent digits is unique. The shift register with weighted output used at University College London is shown in Fig. 9.

References

[1] Pook, L. P., "Proposed Standard Histories for Fatigue Testing Relevant to Offshore Structures," NEL Report 624, National Engineering Laboratory, East Kilbride, Glasgow, U.K., Oct. 1976.

[2] Pook, L. P., "Some Factors Affecting Wave Loading of Tubular Members," NEL Report 712, National Engineering Laboratory East Kilbride, Glasgow, U.K., Sept. 1987.

[3] "The Common Load Sequence for Fatigue Evaluation of Offshore Structures," Report No. TF-1892, IABG, Ottobrunn, 1985.

[4] "FALSTAFF (Description of a Fighter Aircraft Loading Standard for Fatigue Evaluation)," Fraunhofer-Institut für Betriebsfestigkeit, Darmstadt, 1976.

[5] Dover, W. D. and Pook, L. P., "Standardised Load History for Offshore Structures," Final Report, University College London, June 1986.

[6] Holmes, P. and Tickell, R. G., "The Long Term Probability Distribution of Peak Wave Induced Loads on Structural Sections," Supplementary Report MCE/APR/75, University of Liverpool, April 1975.

[7] Holmes, P. and Tickell, R. G., "The Long Term Probability Distribution of Peak Wave Induced Loads on Structural Sections," Report MCE/NOV/74, University of Liverpool, Nov. 1974.

[8] Pook, L. P., *Journal*, Society of Environmental Engineers, Vol. 17-1, No. 76, March 1978, pp. 22–23, 25–28, 31–35.

[9] Morison, J. R., O'Brien, M. P., Johnson, W. F., and Schaaf, S. A., *Petroleum Transactions*, American Institute of Mining Metallurgical, and Petroleum Engineers, Vol. 189, 1950, pp. 149–154.

[10] Pook, L. P., *The Role of Crack Growth in Metal Fatigue*, Metals Society, London, 1983.

[11] Pook, L. P., "A Sensitivity Study of Wave Loading on Tubular Members," presented at the Welding Institute International Conference on Fatigue of Welded Constructions, Brighton, 7–9 April 1987.

[12] Gumbel, E. J., *Annals of Mathematical Statistics*, Vol. 12, No. 2, June 1941, pp. 163–190.

[13] Pook, L. P., "Approximation of Two-Parameter Weibull Distribution by Rayleigh Distributions for Fatigue Testing," NEL Report 694, National Engineering Laboratory, East Kilbride, Glasgow, U.K., Nov. 1984.

[14] Wirsching, P. H. and Light, M. C., *Journal*, Structural Division, American Society of Civil Engineers, Vol. 106, No. ST7, July 1980, pp. 1593–1607.

[15] Chaudhury, G. K. and Dover, W. D., *International Journal of Fatigue*, Vol. 7, No. 1, Jan. 1985, pp. 13–19.

[16] Hartt, W. H. and Linn, N. K., *International Journal of Fatigue*, Vol. 8, No. 2, April 1986, pp. 91–93.

[17] Crooker, T. W. and Hauser, J. A., "A Literature Review on the Influence of Small-Amplitude Cyclic Loading on Stress-Corrosion Cracking in Alloys," NRL Memorandum Report 5763, Naval Research Laboratory, Washington, DC, April 1986.

[18] Chaudhury, G. K., "Application of fracture mechanics to random load fatigue of tubular joints (in air and in sea-water)," Ph.D. thesis, University of London, 1986.

[19] Thorpe, T., Morgan, H. G., Rance, A., Silvester, D. R. V., and Scott, P. M. in *Proceedings*, Conference on Fatigue on Offshore Structures, Institution of Civil Engineers, London, 24–25 Jan. 1981, pp. 35–43.

[20] Cowling, M. J. and Appleton, R. J. in *Proceedings*, Conference on Fatigue and Crack Growth in Offshore Structures, Institution of Mechanical Engineers, London, 7–8 April 1986.

[21] Akaike, H. and Swanson, S. R. in *Proceedings*, Fifteenth Annual Technical Meeting of the Institute of Environmental Sciences, Anaheim, CA, 1969, pp. 66–77.

D. Allan Hull,[1] *Derek McCammond*,[1] *and David W. Hoeppner*[2]

Fatigue Crack Growth in a Rotating Disk Evaluated with the TURBISTAN Mission Spectra

REFERENCE: Hull, D. A., McCammond, D., and Hoeppner, D. W., **"Fatigue Crack Growth in a Rotating Disk Evaluated with the TURBISTAN Mission Spectra,"** *Development of Fatigue Loading Spectra, ASTM STP 1006,* J. M. Potter and R. T. Watanabe, Eds., American Society for Testing and Materials, Philadelphia, 1989, pp. 121–134.

ABSTRACT: Fatigue crack growth rates were generated from four rim cracks in a rotating disk that was evaluated with the TURBISTAN loading spectra. A fractographic investigation revealed the results of correlating variable-amplitude load cycles with fatigue crack striations and that constant-amplitude cycles had been successful in producing marker bands on the fracture surfaces.

An annular disk specimen was designed to study the propagation of through-the-thickness radial-edge fatigue cracks. TURBISTAN, which is a standard loading sequence developed for fighter aircraft disk usage, was employed because it provides a more realistic load sequence than the currently used zero-max-zero cycle. The MINITURB version for cold compressor disks was used in this study.

An approximate stress intensity solution for a radial-edge crack in a rotating annular disk was developed from two existing solutions by superposition. An aluminum 6061-T6 alloy was selected to provide a readable fracture surface because it striates well. The disk was pre-cracked on a load frame to introduce known discontinuities. It was then evaluated in a spin pit with MINITURB and constant-amplitude cycles. The constant-amplitude cycles were used to create marker bands on the fracture surface to aid a subsequent fractographic investigation. Periodic fluorescent penetrant inspection allowed fatigue crack growth to be tracked.

A scanning electron microscope was used to study crack fracture surfaces, correlate MINI-TURB cycles with fatigue striations, and identify marker bands. Plots of discontinuity length versus cycles and crack growth versus stress intensity are presented. The importance of coupling a realistic mission cycle with the spin pit evaluation of engine disk materials was emphasized.

KEY WORDS: fatigue crack propagation, rotating disk, spectrum loading, aluminum alloys, fractography, fatigue (materials), testing

Nomenclature

a	Crack length
a_c	Critical crack size
b	Disk outside radius
c	Disk inside radius
da/dN	Cyclic rate of crack growth
ΔK	Applied stress intensity factor range

[1] Graduate student and professor, respectively, Mechanical Engineering, University of Toronto, Toronto, Ontario, Canada.

[2] Chairman and professor, Mechanical and Industrial Engineering, University of Utah, Salt Lake City, UT 84112.

G	Function of disk geometry
H	Function of disk geometry
K_1^*	Radial edge crack stress intensity factor in a rotating solid disk
K_2^*	Pressurized radial-edge crack stress intensity factor in a solid disk
K_I	Radial-edge crack stress intensity factor in a rotating annular disk
K_{Ic}	Plane strain fracture toughness
ΔW	Normalized angular velocity range
N	Cycles
ρ	Density
ν	Poisson's ratio
ω	Angular rotation

Realistic mission loading sequences are required in the evaluation of gas turbine engines to ensure that the engine's design boundary conditions match its service usage. The structural integrity of the engine's rotating disks, in particular, are dependent on this condition being met. During a flight, an engine's disks will undergo major and minor load and temperature cycles as a result of changes in throttle settings. The effect of load and temperature magnitude, cycle reversals, and sequences on the disk's failure modes must be well characterized. Otherwise, the operating environment will invoke disk failure modes that were not considered during the design of the component. The nucleation and propagation of fatigue cracks to a critical size is a failure mode that can cause catastrophic loss of the engine, airframe, and personnel.

The research objective was to cycle a rotating disk with a realistic loading spectrum to obtain fatigue crack growth rate (FCGR) data and observe, with the aid of a scanning electron microscope (SEM), how the changing load magnitude had affected the local crack propagation.

A constant-amplitude idle-max power-idle cycle has been used in the past to evaluate disk components and materials in spin pits and uniaxial load frames. The detection of a 0.75-mm fatigue crack by a specified nondestructive inspection technique was defined as failure. A step toward providing loading conditions that are more representative of those found in service has been the development of TURBISTAN [*1*]. TURBISTAN is a standard loading sequence for fighter engine disk usage that has been created to identify the effect of heat treatment, forming and assembly operations, surface treatments, etc., on material properties. It will allow existing and potential disk materials to be ranked on a comparative basis.

A cold TURBISTAN mission consisting of 15 432 load reversals representing 100 flights was developed for the fan and early compressor stage disks where temperature changes on material properties were assumed to be small. An abbreviated form of the Cold TURBISTAN sequence called MINITURB was created to study the effect of eliminating minor load cycles on component life. MINITURB was constructed by filtering out minor cycles that were less than a specified percentage of the maximum speed range. MINITURB with a 50% filter, consisting of 1926 reversals was used as a rpm history in this study. Segments of MINITURB and Cold TURBISTAN are shown in Fig. 1.

Larsen and Annis [*2*] and Bucci et al. [*3*] have reported that overload and sequence effects caused crack retardation that made it difficult to correlate crack growth with specific load cycles. In addition, minor cycles with small values of ΔK did not always produce distinguishable fatigue crack striations. As a result, the simplified MINITURB sequence with a 50% filter was selected as the load spectrum. This selection represents a compromise between the realistic load variation embodied by the complete TURBISTAN sequence and the goal of correlating specific load cycles with fatigue crack striations.

Dainty [*4*] has shown that a block of constant-amplitude load cycles can be used to create

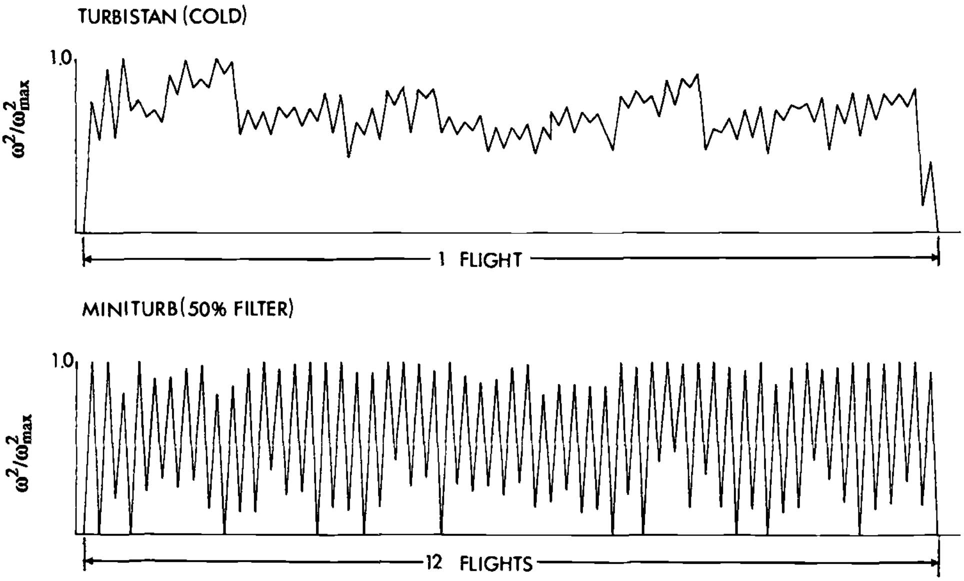

FIG. 1—*Segments of Cold TURBISTAN and MINITURB with a 50% filter.*

characteristic bands of fatigue striations or marker bands on the fracture surface. Periodically inserting constant-amplitude cycles between blocks of variable-amplitude cycles, brackets the latter's fatigue crack striations. Identification of these marker bands with a low power optical microscope or an SEM allows the fracture surface to be divided into segments that can be analyzed relative to a particular point in the load/time record. Consequently, marker bands were used in this study with the objective of facilitating the fractographic investigation of the fatigue crack fracture surface.

Experimental Aspects

Disk Design

An annular disk specimen was designed to allow through-the-thickness Mode I radial crack propagation to be studied. Fatigue cracks were introduced into the disk to allow immediate crack propagation tracking and to minimize their interaction. The problems of crack number, location, and the nondestructive inspection (NDIs) probability of detection associated with the nucleation of crack-like discontinuities were circumvented by this approach.

The material was assumed to be an isotropic homogeneous continuum that exhibited Hookean material response during loading. A constant section "thin disk" approximation allowed a plane biaxial state of stress to be assumed for a body in equilibrium. The variation of the radial and tangential stresses [*5*] across the disk are shown in Fig. 2. A stress intensity solution for a rotating annual disk with a through-the-thickness radial-edge crack was not found in the literature. However, following a method described by Cartwright and Rooke [*6*], an approximate solution was determined by superposition. The radial-edge crack stress intensity solution for a rotating solid disk, $K_1{}^*$, was combined with the solution for an internally pressurized disk crack, $K_2{}^*$ [*7*]. The pressure in the latter solution was taken to be the increase of the tangential stress by the introduction of the central hole. The hole

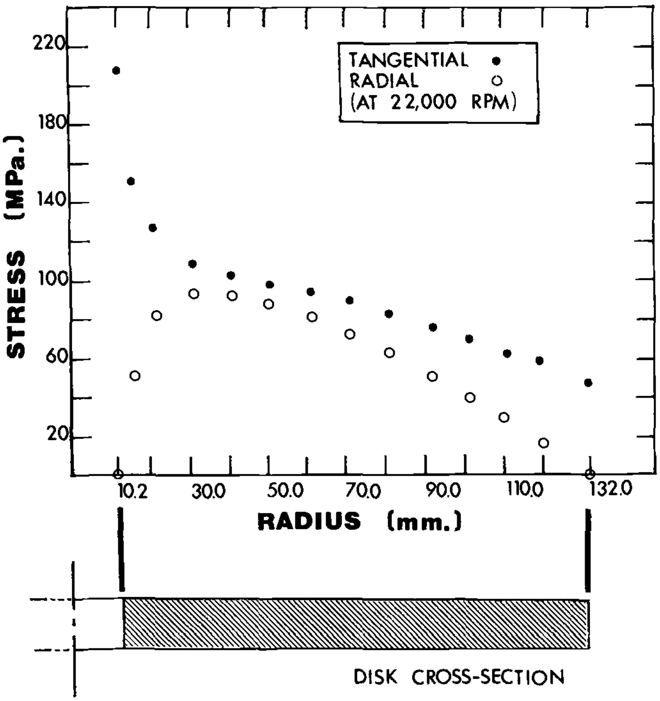

FIG. 2—*Rotating annular thin disk stress distribution.*

diameter was assumed to be less than 10% of the disk outside diameter to prevent crack/hole interaction. The complete solution is

$$K_I = K_1^* + K_2^* \tag{1}$$

$$K_I = \left[\frac{\rho\omega^2(3+\nu)}{8}\sqrt{\pi a}\, b^2\left(G - \frac{1+3\nu}{3+\nu}H\right)\right] + \left[\frac{\rho\omega^2(3+\nu)}{8}\sqrt{\pi a}\left(c^2 + \frac{c^2b^2}{(b-a/2)^2}\right)G\right] \tag{2}$$

$$K_I = \rho\omega^2\frac{(3+\nu)}{8}\sqrt{\pi a}\left[G\left(b^2 + c^2 + \frac{c^2b^2}{(b-a/2)^2}\right) - H\left(\frac{1+3\nu}{3+\nu}b^2\right)\right] \tag{3}$$

Where G and H are functions of disk geometry and are found in Ref 7. For the geometry studied, the second term in Eqs 1 and 2 contributed less than 4% to K_I suggesting that any inaccuracy in using K_2^* for modeling the annular disk will produce a substantially smaller error in K_I. The expressions for K_1^* and K_2^* are considered accurate to 1% [7].

Materials and Equipment

An aluminum 6061-T6 alloy (K_{IC} = 29.1 MPa$\sqrt{m}$ (T-L)) [8] was selected as the disk material with the objective of creating a readable fracture surface because this material striates well.

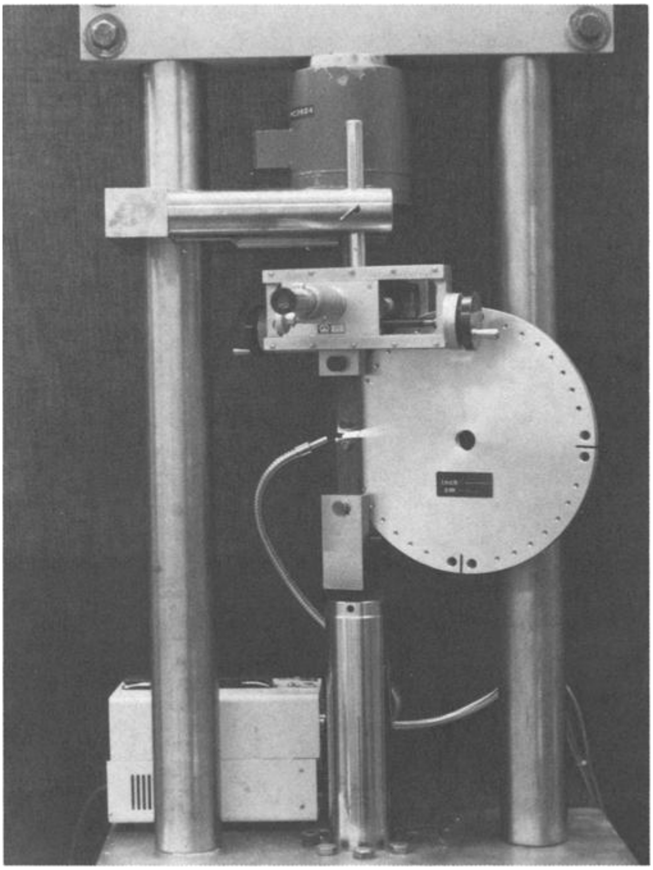

FIG. 3—*Pre-cracking the disk in a 50 kN load capacity load frame.*

The disk with an inside and outside radius of 10.2 and 132.0 mm, respectively, was machined from 12.7-mm-thick plate. Four equally spaced, straight-through, fatigue crack V-notches were placed at the disk's rim. Starter Notches 1 and 3 were oriented in the T-L direction.

Each of the four notches were pre-cracked on a 50 kN servo-hydraulic load frame (see Fig. 3). Two $\times 10$ traveling microscopes were used to measure the crack extension. In the figure, they are retracted to reveal the disk geometry. The four groups of seven holes allowed the disk to be dynamically balanced on two planes by the addition of balance weights.

A spin pit [9] was used to cycle the disk. An arbor was attached to the disk that mated with the spindle of a small air turbine. The air turbine with a safe maximum operating speed of 60 000 rpm spun the disk in an evacuated, below ground, reinforced chamber. A microcomputer was interfaced with the spin pit control hardware and specified the speed magnitudes of the MINITURB sequence.

Procedure

The ASTM Method for Constant-Load-Amplitude Fatigue Crack Growth Rates Above 10^{-8} m/cycle (E 647-86) was used as a guide to pre-crack the specimen. After crack extension from the V-notch occurred, the load was stepped down to decrease the crack tip plastic zone size. This action facilitated crack extension in the spin pit.

The disk was subjected to two types of load sequences in the spin pit. A marker block consisting of 1500 constant-amplitude cycles was inserted before every block of four repetitions of the MINITURB spectra. The maximum speed for both constant-amplitude and MINITURB blocks was 22 000 rpm and the constant-amplitude minimum speed was 11 000 rpm. A minimum speed of 900 rpm was substituted for the 0 rpm specified by MINITURB to prevent excessive vibrations at low rpm values. The tangential stress at 900 rpm is less than 0.2% of this stress at 22 000 rpm. Consequently, this change in the spectrum was assumed to have a negligible effect on the results. The constant-amplitude and average MINITURB R ratios were 0.25 and 0.10, respectively.

Fluorescent liquid penetrant inspection (FPI) of the disk was carried out in accordance with the ASTM Liquid Penetrant Inspection Method (E 165-80). Penetrant dwell times of 60 min instead of 7 min were used to improve the resolution of the fatigue crack tip's location. Fatigue crack indications were measured with a ×10 traveling microscope under ultraviolet light.

Evaluation of the specimen was halted after beginning the sixth MINITURB block because the disk was becoming dynamically unbalanced. After the final FPI, the fatigue cracks were sectioned from the disk. Heat tinting of the fracture surfaces was carried out at 427°C (800°F) for 1 h. A load frame was used to separate the crack faces to allow a final crack length measurement before the specimens were fractured. The fracture surfaces of Notches 3 and 4 were studied with a low-power metallographic microscope and an SEM.

Results and Discussion

Nondestructive Inspection

Figure 4 illustrates typical crack growth that occurred at Notch 3 between the beginning of the third and end of the fifth MINITURB block. The solid triangles in the figure mark

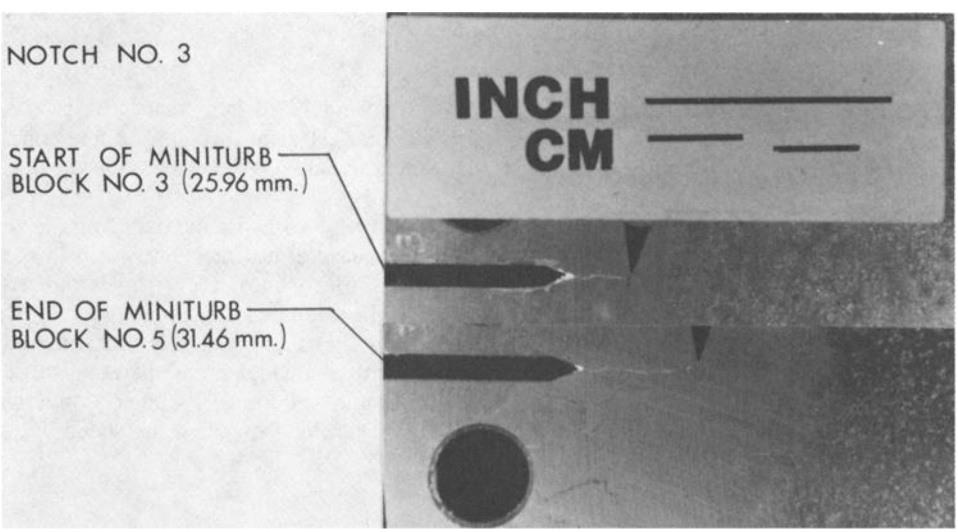

FIG. 4—*Tracking of Notch 3's spin pit crack propagation by FPI.*

the extent of the crack revealed by FPI. The measured lengths were 25.96 and 31.46 mm relative to the disk rim. At the conclusion of the spin pit evaluation, this crack had propagated 9.61 mm to a final average length of 32.7 mm.

The FPI crack length measurements versus load blocks are plotted in Fig. 5. Constant-amplitude load blocks are identified as C and MINITURB blocks are designated by M. Recognizing that the disk was in a state of plane stress, the 6061-T6 plane-strain fracture toughness value was used to determine a lower bound of 34.74 mm for the critical crack size. While the crack at Notch 4 had exceeded this limit, its increasing FCGR indicated that the plane stress critical crack size was being approached.

The ASTM E 647-86's secant method was used to calculate da/dN values that were plotted versus ΔK in Fig. 6. The figure shows the crack growth for the two sets of 24 data points. Comparisons between the constant-amplitude and MINITURB results should be done cautiously since they have been obtained from different load sequences and R ratios.

Fractography

The fractographic investigation concentrated on the fracture surface of Notch 3. Inspection of the surface in Fig. 7 revealed that the combination of constant-amplitude cycles and heat tinting had created some visible marker bands. Several of the more prominent bands are identified in the figure. Tunneling of the crack front shown by the marker bands' and final crack boundary shape was apparent. Twelve length measurements taken along the crack front established its through-the-thickness boundary variation at the 2C marker band and at final fracture. Superimposing the two crack front boundaries showed the crack front had

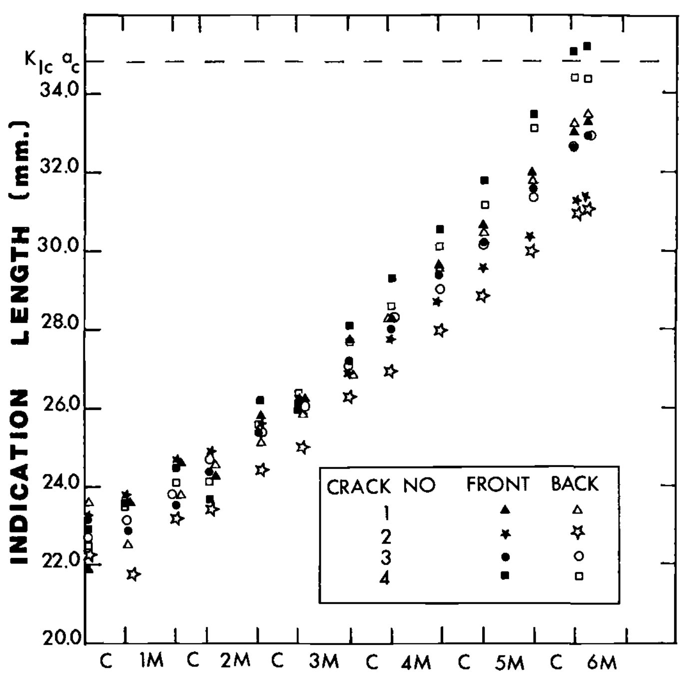

FIG. 5—*The FPI results of the spin pit fatigue crack propagation.*

remained approximately unchanged as it propagated. Analysis showed that the internal boundary was a maximum of 9% longer than surface FPI measurements had indicated.

Examination of the fracture surface with the SEM revealed that the pre-crack, constant amplitude, and MINITURB sequences had created distinguishable striation patterns. Figures 8 and 9 show some typical examples of these features. In all of the following photomicrographs, the magnification and scale are shown in the lower right corner and the general direction of crack propagation is given by the arrow in the top left corner. Crack propagation that occurred during pre-cracking in the load frame produced uniform, evenly spaced striations. In Fig. 8*a*, at a distance of 2.65 mm from the fatigue crack starter V-notch tip, the pre-crack striations had an average spacing of 0.5 μm. Figure 8*b* illustrates the regular appearance of the spin pit constant-amplitude striations. At a distance of 3.20 mm from the V-notch, these striations had an average spacing of 0.6 μm. In this figure, crack propagation appears to be occurring on two grains with the change in striation direction revealing the grain boundary. These striations, in comparison to the pre-crack striations in Fig. 8*a*, are more distinct.

Figure 8*c* depicts one of a series of secondary cracks propagating normal to the primary crack direction. They were noted at the crack front boundary between spin pit block sequences. In this figure, at a distance of 9.67 mm from the V-notch, MINITURB and constant-amplitude striations are in the background and foreground, respectively. Using the FPI results and allowing for crack front curvature, this block change occurred at the end of the 4M block. A higher magnification view of Fig. 8*c* in Fig. 8*d* reveals the MINITURB striation thickness variation in comparison to the constant-amplitude striations. In addition, material separation or secondary cracks between MINITURB striations are evident.

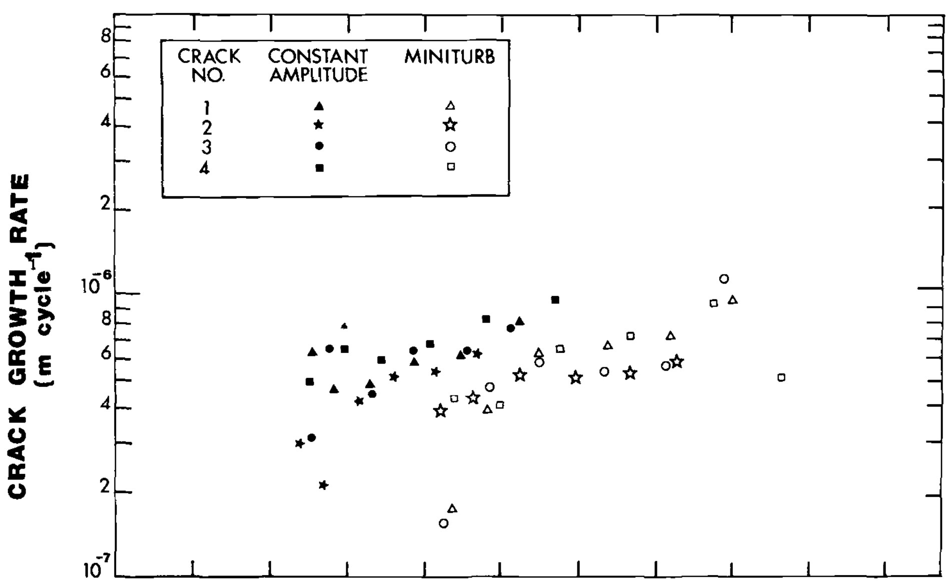

FIG. 6—*Constant-amplitude and MINITURB crack growth rates versus* ΔK.

FAST FRACTURE REGION (F)

SPIN PIT CRACK REGION (S)

PRE-CRACK REGION (P)

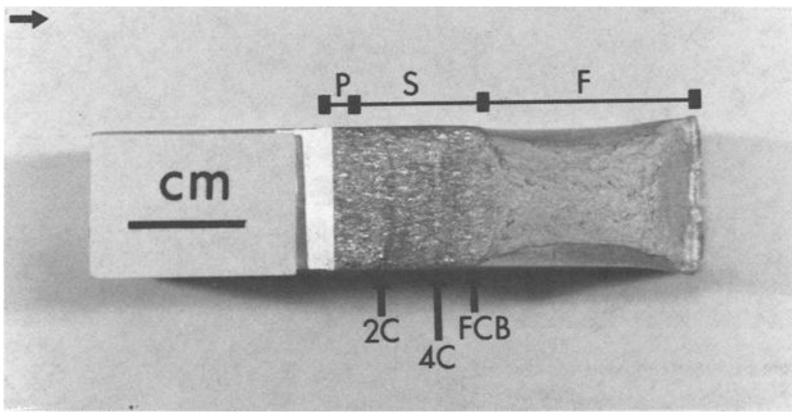

2C MARKER BAND (2C)

4C MARKER BAND (4C)

FINAL CRACK FRONT BOUNDARY (FCB)

FIG. 7—*Notch 3's marker bands on the fracture surface.*

A well-defined boundary between the 5M MINITURB and constant-amplitude striations was found 11.5 mm from the V-notch and is shown in Fig. 9. MINITURB's final series of cycles produced the striations in the upper portion of the fractograph. This surface was studied to determine to what degree the normalized square of the angular rotation range, $\Delta W = \Delta\omega^2/\omega_{max}^2$, could be correlated with MINITURB and constant-amplitude cycles. The ΔW range was chosen because it is a measurable physical parameter from which stress and stress intensity can be derived. Individual striation spacing measurements were made on 40 constant-amplitude and 90 MINITURB striations. Frequency histograms of ΔW and striation widths are presented in Fig. 10. In Fig. 10*a*, the constant-amplitude striation-spacing histogram revealed the variation in striation spacing associated with a single ΔW range at a specific fracture site. The sample mean and standard deviation were 5.79×10^{-7} m and $\pm 9.6 \times 10^{-8}$ m, respectively. The MINITURB and striation-spacing histograms both exhibited a skewed tendency, Fig. 10*b*. Inspection of the ΔW and striation-spacing histograms indicated the existence of modal values in the class intervals of 0.95 to 1.00 and 8.0 to 9.0×10^{-7} m, respectively. The MINITURB striation-spacing histogram was scaled relative to the ΔW histogram by using the constant-amplitude striation mean of 5.97×10^{-7} m and

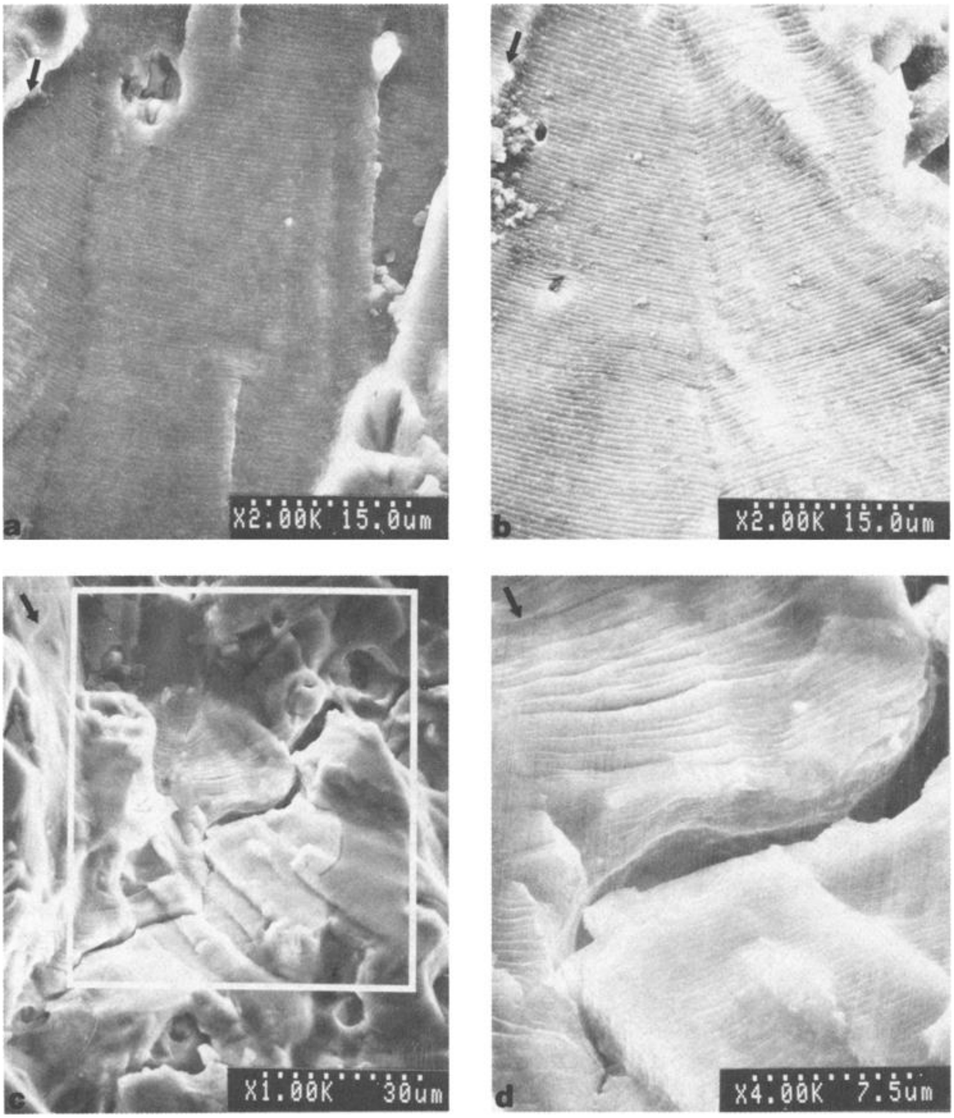

FIG. 8—*The SEM fracture surface striations,* (a) *pre-crack,* (b) *constant amplitude,* (c) *secondary crack at MINITURB/constant-amplitude boundary, and* (d) *higher magnification of* (c).

assuming that the peak values of the MINITURB ΔW and striation-spacing histograms coincided. The scaled striation spacing histogram is presented in Fig. 10c. This result suggests a relationship between ΔW and striation size at the local fracture site shown in Fig. 9.

The MINITURB sequence represents a known ordered series of events. Records showed the 5M block was composed of four MINITURB sequences and the first four cycles of a fifth MINITURB block before the constant-amplitude cycle began. The surface shown in

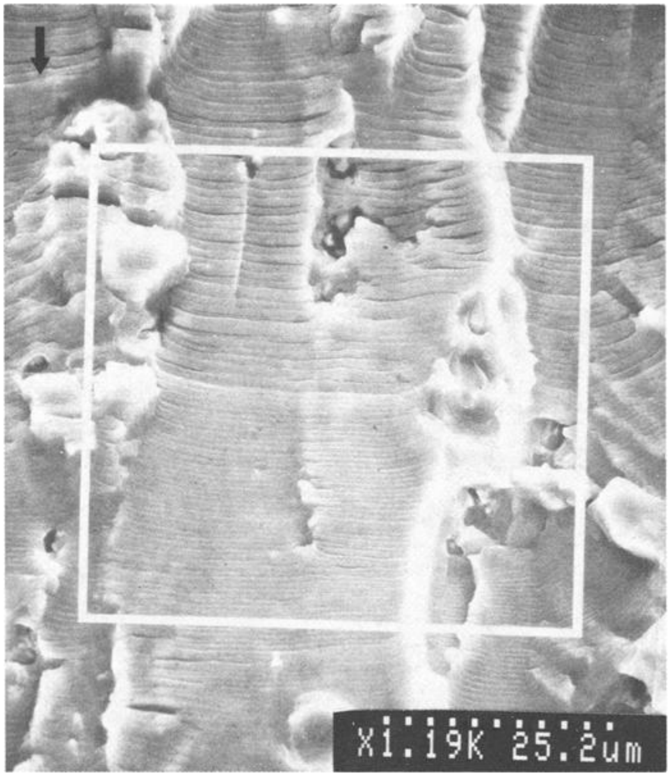

FIG. 9—*Clearly defined MINITURB and constant-amplitude striations.*

Fig. 9 has been reproduced in Fig. 11 at higher magnification. The end of the 5M MINITURB sequence is designated by the beginning of the constant-amplitude cycles at the left side of the fractograph. Moving right from this boundary, striations were numbered and measured. This produced an ordered series of striations spacing measurements that were compared to MINITURB cycles. Several iterations were necessary to identify striations that initially had been overlooked. The relationship between ΔW and striation spacing, in Fig. 11*c*, was used to determine the approximate size of a striation spacing that could be expected from a specific MINITURB cycle. In addition, Fig. 11*c* was used to investigate spacing measurements that subsequent study proved were composed of two striations. These actions allowed the MINITURB sequence to be paired with the striations on the fracture surface in Fig. 11. It is, however, important to note that the correlation of load cycles with striations is dependent on a subjective interpretation of the fracture surface. A comparison of the MINITURB and striation-spacing series for the last segment of the 5M block is shown in Fig. 12. This figure illustrates the coincidence of many of the peaks and valleys of the two histories. The degree of association between the paired values was evaluated by determining the correlation coefficient, r, that was 0.762. The expected r value for observations when there is no correlation is 0.302 at a 1% significance level [*10*]. Consequently, the MINITURB/striation spacing r-value indicates a reasonable degree of correlation between the MINITURB cycles and striation-spacing measurements.

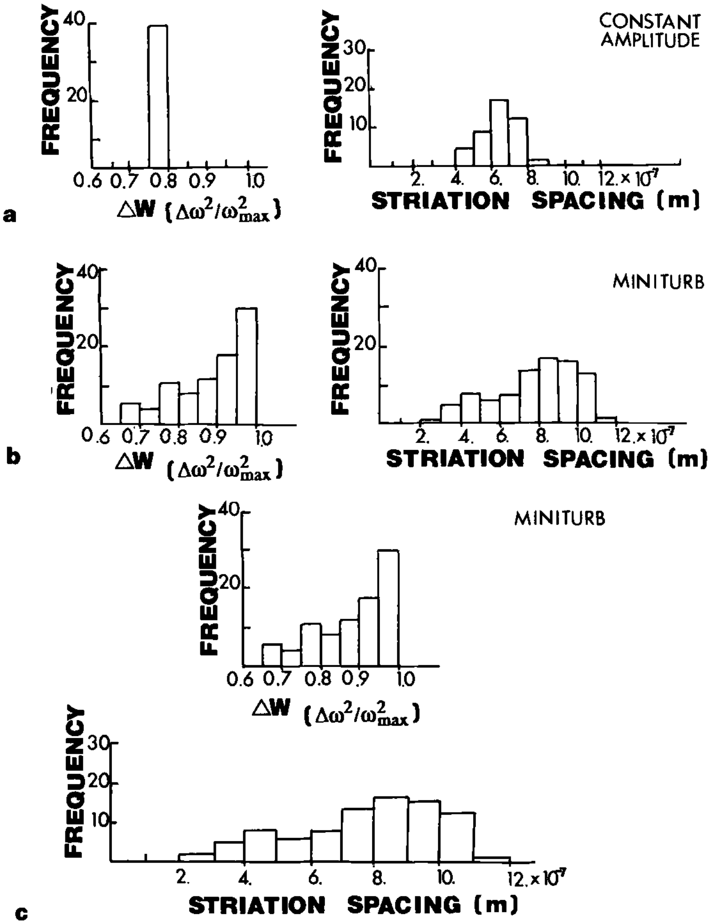

FIG. 10—*MINITURB and constant-amplitude* ΔW *and striation-spacing histograms,* (a) *constant amplitude,* (b) *MINITURB,* (c) *MINITURB* ΔW *and rescaled striation-spacing histogram.*

Concluding Remarks

The results of this study have illustrated how a uniaxial load frame may be used to introduce known discontinuities into a simple geometry disk. It has been shown that these cracks propagate during spin pit evaluation.

In this study, marker blocks have been used for several purposes. Consistent with other authors' results, they have bracketed the random variable-amplitude fatigue crack striations with a uniform characteristic striation pattern. Their presence on the fracture surface helped to identify the beginning and end of the MINITURB blocks. Analysis of the variation in striation spacing for constant-amplitude and MINITURB striation spacing allowed an empirical relationship to be established between MINITURB's ΔW and striation-spacing histograms. This relationship is highly dependent on the local material properties, fracture mechanisms, the materials' past load/time history, mode of crack extension, etc. and may vary at different fracture sites on the same specimen. However, it was a useful tool in

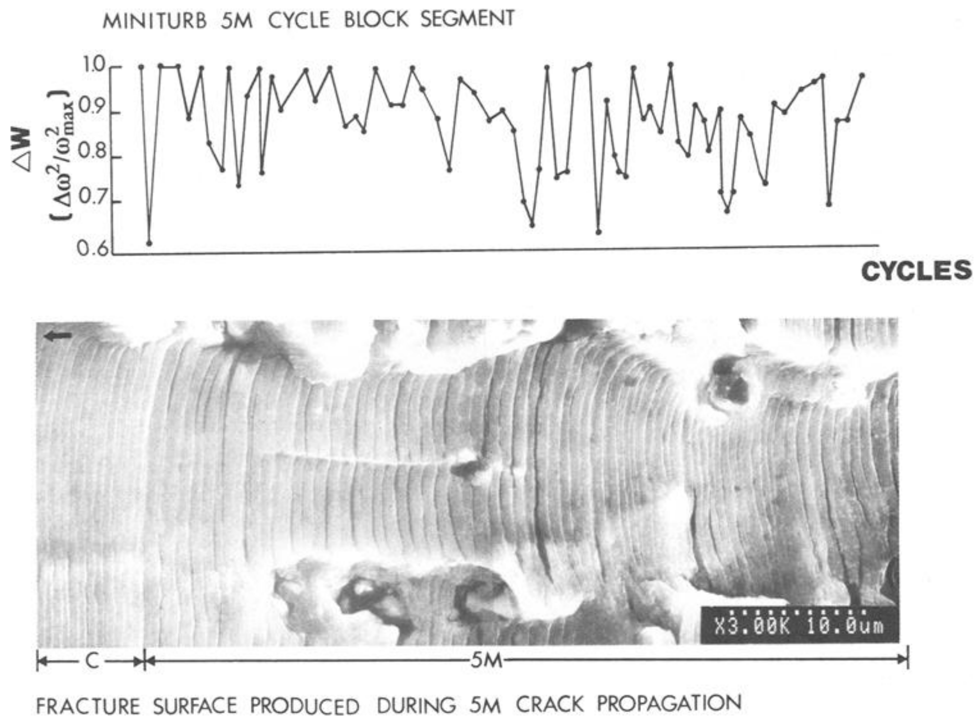

FIG. 11—*MINITURB cycles and the 5M fracture surface striations.*

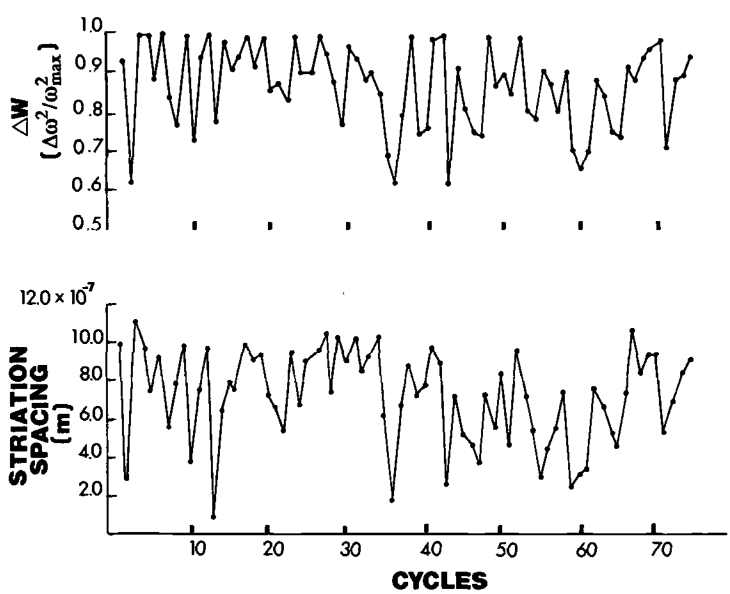

FIG. 12—*A comparison between 5M MINITURB cycle ranges and striation-spacing measurements.*

correlating fatigue striations with MINITURB cycles. The correlation of load cycles with striations is important because it establishes a link between the macroscopic load input and the microscopic material response. Each striation provides a permanent record of the increment crack extension.

The importance of using a realistic loading sequence to obtain fatigue crack growth in a rotating disk has been emphasized. The use of the relatively simple MINITURB sequence showed that it produced crack growth that differed from the constant-amplitude crack extension. The constant-amplitude cycles produced uniform striations with little local fracture surface deformation. MINITURB's fatigue crack regions frequently exhibited local tearing, discontinuous secondary cracks and fewer regions of well-defined striations. Clearly, MINITURB was more effective in revealing the material's possible crack extension mechanisms.

Acknowledgments

The interest and technical assistance provided by M. D. Raizenne and R. V. Dainty of the National Aeronautical Establishment at the National Research Council is deeply appreciated. Interaction with staff at Rolls Royce of Derby, England, has been of considerable help.

Financial assistance provided by the National Research Council of Canada is gratefully acknowledged.

References

[*1*] Mom, A. J. A., Evans, W. J., and ten Have, A. A., "TURBISTAN, A Standard Load Sequence for Aircraft Engine Discs," *Damage Tolerance Concepts for Critical Engine Components*, AGARD-C.P-393, Advisory Group for Aerospace Research and Development, pp. 20-1–20-11.

[*2*] Larsen, J. M. and Annis, C. G., Jr., in *Effect of Load Spectrum Variables on Fatigue Crack Initiation and Propagation, ASTM STP-714*, D. F. Bryan and J. M. Potter, Eds., American Society for Testing and Materials, Philadelphia, 1980, pp. 91–107.

[*3*] Bucci, R. J., Thakker, A. B., Sanders, T. H., Sawtell, R. R., and Staley, J. T. in *Effect of Load Spectrum Variables on Fatigue Crack Initiation and Propagation, ASTM STP 714*, D. F. Bryan and J. M. Potter, Eds., American Society for Testing and Materials, Philadelphia, 1980, pp. 41–78.

[*4*] Dainty, R. V. in *Fractography of Ceramics and Metal Failures, ASTM STP 827*, J. J. Mecholsky, Jr., and S. R. Powell, Jr., Eds., American Society for Testing and Materials, Philadelphia, 1984, pp. 285–308.

[*5*] Timoshenko, S. P. and Goodier, J. N., *Theory of Elasticity*, 3rd ed., McGraw-Hill, Toronto, 1970.

[*6*] Cartwright, D. J. and Rooke, D. P., *Engineering Fracture Mechanics*, 1974, pp. 563–571.

[*7*] Rooke, D. P. and Cartwright, D. J., *A Compendium of Stress Intensity Factors*, Her Majesty's Stationary Office, London, 1973.

[*8*] *Metals Handbook*, H. E. Boyer and T. L. Gall, Eds., American Society for Metals, Metals Park, OH, 1985, pp. 20–28.

[*9*] Hull, A., Dainty, R. V., Raizenne, M. D., and Hoeppner, D. W., *Canadian Aeronautics and Space Journal*, Vol. 32, No. 4, 1986, pp. 321–332.

[*10*] *Handbook of Tables for Probability and Statistics*, W. H. Beyer, Ed., Chemical Rubber Co., Cleveland, OH, 1974, p. 390.

Virginia M. Gallagher,[1] *Roger L. York,*[1] *and Henry O. Fuchs*[2]

Fatigue Spectra Development for Airborne Stores

REFERENCE: Gallagher, V. M., York, R. L., and Fuchs, H. O., **"Fatigue Spectra Development for Airborne Stores,"** *Development of Fatigue Loading Spectra, ASTM STP 1006,* J. M. Potter and R. T. Watanabe, Eds., American Society for Testing and Materials, Philadelphia, 1989, pp. 135–149.

ABSTRACT: Traditionally, airborne store design has been based on service life criteria similar to those used for aircraft development. Recent research has shown that an airborne store may be exposed to a unique loading environment and may therefore require a different approach. Moreover, flight loads data for aircraft and airborne stores are normally difficult and expensive to obtain, because resources are not available to fly a sufficient variety of combinations of aircraft, stores, and mission types. Finally, the increased life of many stores has made fatigue life an important consideration in design. These considerations led to development of an approach to building flight-load spectra for fatigue testing of externally mounted airborne stores (that is, fuel tanks, missiles, bombs, etc.) using time-history load data collected from U.S. Air Force and Navy training flights. The data are processed using a "racetrack" type data compaction algorithm to yield sequential peak/valley pair files, and then reorganized to build new mission profiles. Finally, the new mission profiles are weighted by expected frequency of occurrence and organized to reflect the expected service use over a period of time.

KEY WORDS: airborne stores, fatigue testing, flight loads, racetrack, testing, load spectrum, fatigue (materials)

Modern high-performance military aircraft carry different armament and peripheral flight equipment depending on their combat roles. These items, which include bombs, fuel tanks, missiles, and instrumentation pods, are normally carried as external stores (Fig. 1) [*1*]. The proliferation of modern airborne stores and their complexity of design plus the need to increase their service life has created the need for a clear set of guidelines for determination of their fatigue life.

Background

Aircraft fatigue has been studied for a number of years and the importance of several factors in fatigue testing has been recognized: the effect of load spectrum variation on crack growth in aircraft wings [*2*], the importance of realism in testing [*3*], and the value of a guide for load sequences [*4*]. However, the loads on an aircraft's stores can be quite different from the loads on the aircraft center of gravity–dynamic loads are magnified in a lever arm effect as the aircraft undergoes angular changes in flight, airflow patterns change as the shape of the wing varies, and modern fighter aircraft wings flex more than those of older

[1] Senior systems analyst and senior research engineer, respectively, SRI International, Menlo Park, CA 94025.
[2] Professor emeritus of Mechanical Engineering, Stanford University, Stanford, CA 94305.

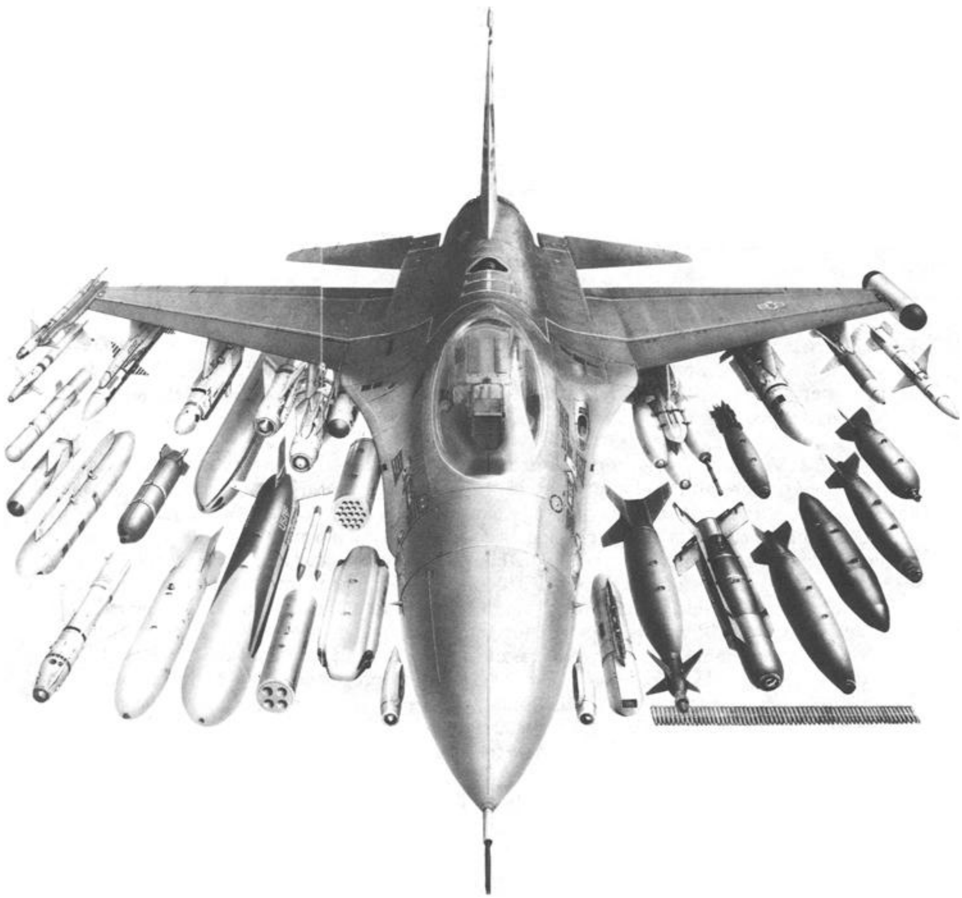

FIG. 1—*Modern fighter aircraft and stores* [1].

aircraft, thus creating new loading patterns. Finally, and possibly most important, is the fact that store mounting geometry with respect to the aircraft can vary by 180° as the store is moved from one wing to the other or from one side of a pylon to the other (see Fig. 2). Because of these factors, general aircraft fatigue methodology is not a sufficient approach for the fatigue evaluation and testing of airborne stores.

To aid in determining which factors were important to retain in the methodology, general damage-causing phenomena had to be considered. Shear stress ranges, with minor contribution by mean normal stress, are believed to be the most important factors in creating damage in the early stages of fatigue. Crack propagation depends on the tensile stress range. Loading sequence effects may be small or large, depending on the order of events and on the stress gradients, which are very steep at cracks, steep at notches, and moderate in smooth parts and specimens.

Sequence effects can be expected if the loading history shows infrequent, one-sided spikes, as, for instance, in the ground-air-ground cycle of aircraft usage. If a structure is exposed to few large-amplitude loads and many small-amplitude loads (such as those sustained by aircraft wings), the damage done by the small amplitudes could be significant depending on

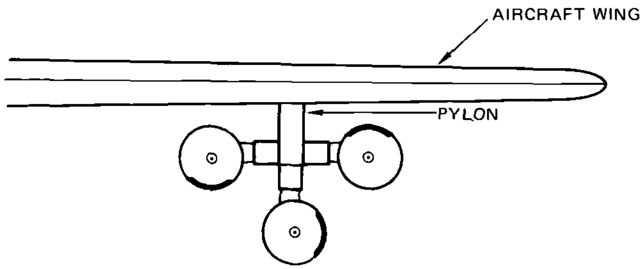

FIG. 2—*Possible store orientations.*

when they occur. Therefore, it was important that the methodology for developing flight-load spectra for fatigue testing of stores be capable of incorporating knowledge of the sequence of events.

Approach

Flight load data for aircraft and airborne stores have traditionally been difficult and expensive to obtain. Aircraft and stores have been instrumented and flown a limited number of times to measure and record flight load data; however, resources are not generally available to fly a variety of combinations of aircraft, stores, and mission types solely to collect data for a comprehensive flight load data base. Data from U.S. Navy and Air Force air combat training systems, which are readily available and reflect actual inflight loading conditions, offer a partial solution to the cost-prohibitive data acquisition problem. The methodology for development of stores loading spectra is thus characterized by realism and economy in data collection and therefore in the fatigue tests themselves. In addition, it is flexible enough to allow the development of new spectra when the service use of the store changes.

The methodology contains the tools and procedures to summarize and reduce the flight-load data base to a form suitable for storage and for input to fatigue tests. The procedure consists of six steps.

1. Identify (or develop) a definition of service life of the store including aircraft types and mission descriptions.
2. Collect appropriate loading data and store them in segments.
3. Develop software to condense time-history data.
4. Compact the data into normal acceleration (n_z) peak/valley (P/V) pair files.[3]
5. Organize the P/V pair files into missions as defined in Step 1.
6. Determine how the missions will be input to the test program.

Store Service Life

Since many stores are remaining in inventory for longer than was expected, they are exposed to a wide range of loading conditions (as aircraft change). Thus, stores may remain in inventory long enough so that fatigue may become a concern.

[3] Although n_z P/V is not necessarily the most critical parameter in store fatigue, it was used in this study because the fatigue test equipment available for this study was uniaxial. However, other parameters are retained in the data base.

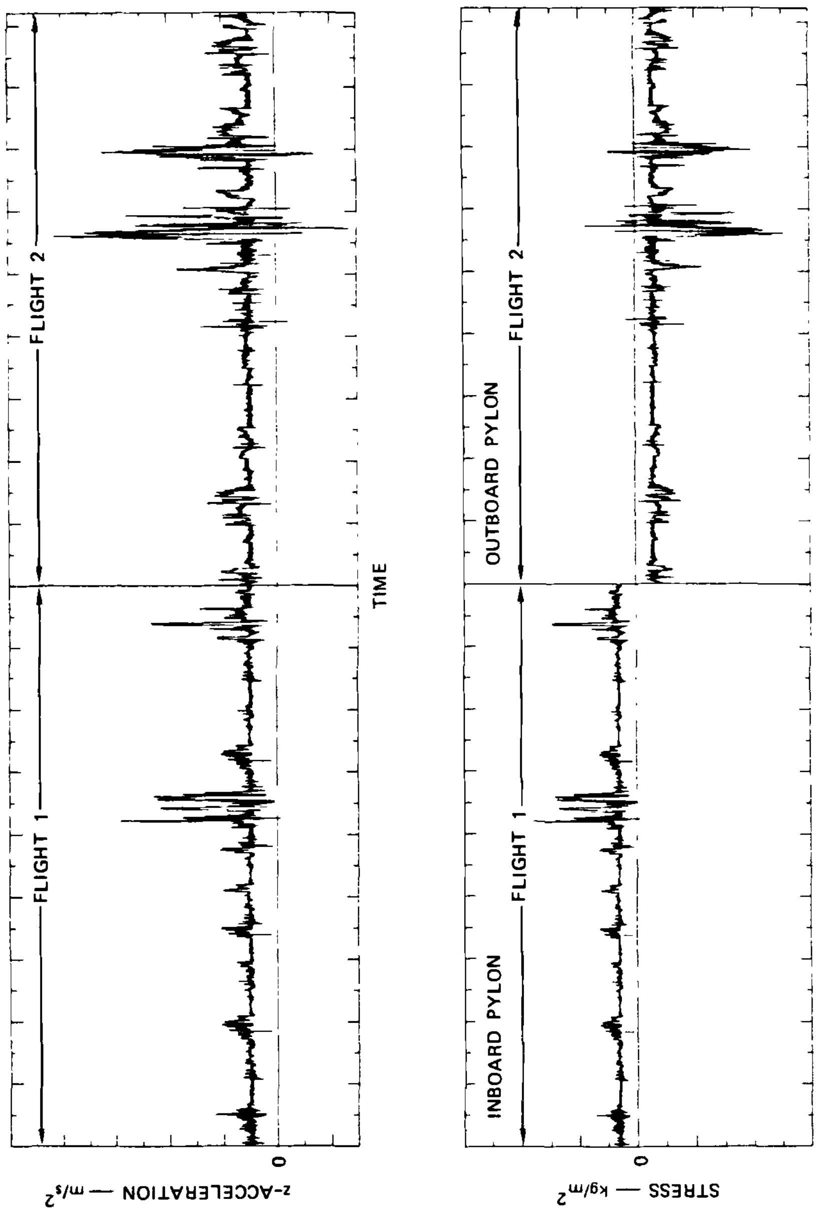

FIG. 3—*Aircraft load factors/store stresses:* (top) *typical aircraft load factor time history, and* (bottom) *typical store stress* (skin) *time history.*

The expected service life of the store must be defined before realistic fatigue spectra can be built. Service life definition should include information about the store and about all the aircraft on which the store will be carried. Typical store information includes the following.

1. What are the physical characteristics, for example, length, width, weight, moment of inertia, and center of gravity?
2. How many (average) flight hours per year does the store undergo?
3. Is the store downloaded after each flight?
4. How often is the store maintained/inspected?

Typical aircraft/store information includes the following.

1. On what aircraft types can the store be mounted?
2. What percent of yearly flight hours are on each aircraft?
3. What types of missions (including their duration and segments)[4] are performed by the aircraft?
4. Is there a sequence of missions?
5. What are the number, locations, and orientations of possible mounting points of the store?

Because the effects of being flown on a variety of aircraft and being mounted in a different location and orientation have not been measured in terms of fatigue life (but are expected to be significant), care must be taken to model as realistically as possible the movement of the store. If a store were mounted on the inboard side of a pylon for one flight, and the outboard side for the next (Fig. 2), the parts of the store that encountered tensile stresses on the first flight would encounter compressive on the second (and vice versa). Figure 3 shows two typical load factor time histories and the corresponding store stress (skin) time histories for a store on opposite mounting locations during two sample flights. This 180° roll greatly increases the overall range of the loads. For these reasons, it is important to model the irregularity of mounting.

To determine how much time-history data to collect for each aircraft/store combination, how to segment the data, and how to order them realistically for input to the fatigue test, information about expected flight hours per year must be defined and quantified. The first step is to calculate the percent of time per year that the store is flown on each aircraft type. Step two is to analyze each mission type for each aircraft and tabulate: (1) the percent of time the aircraft is involved in that mission type, (2) the duration of the mission, and (3) the breakdown of missions into segments and their corresponding duration. Table 1 is an example of the type of data to be collected for each of the aircraft that carry the store. Figure 4 is a graphic representation of a sample fighter aircraft flight profile. The numbers on the figure correspond to the mission segment numbers listed in Table 1. Other loads, such as gust and those caused by ejection of other stores, that do not occur on all flights should be identified. Finally, Step 3 describes potential store movement; that is, does the store stay with one aircraft type for a long period before it is flown on another, or does it move from one aircraft type to another sporadically?

[4] In this study, segment includes basic flight segments (take-off, climb, etc.), maneuvers (for example, jinking), and events (ejection of other stores).

TABLE 1—*Fighter aircraft mission segments.*

	Mission Type			
Mission Duration	CAP[a] (75)[e]	ACM[b] (15)[e]	Yo-Yo[c] (5)[e]	A/G[d] (5)[e]
Total mission, min	90 to 200	105 to 165	20	90 to 120
Mission, segments, min				
1. Taxi	5	5	5	5
2. Takeoff	0.1	0.1	0.1	0.1
3. Climb	3	3	3	3
4. Refuel	4	4	4	4
5. Commute	10 to 20	10 to 20	3	30 to 40
6. Loiter	30 to 70	20	2	...
7. Attack	...	...	...	5
8. Vector/intercept	20	40 to 80	...	...
9. Return to base	10 to 20	10 to 20	...	30 to 40
10. ACM	2 to 3	3 to 4	5	...
11. Descend	5 to 8	5 to 8	5 to 8	5
12. Land	0.1	0.1	0.1	0.1
13. Park	2	2	2	2

[a] CAP = combat air patrol.
[b] ACM = air combat maneuvering.
[c] Yo-Yo = shortened version of ACM.
[d] A/G = air-to-ground (takeoff, flight, landing).
[e] Percent of missions.

Data Base Development

Data from training flights flown by a number of aircraft types on Air Force and Navy ranges are measured by an instrumentation pod mounted at typical store locations on each aircraft and transmitted to a ground-based computer system where they are recorded at 0.1 to 0.4 s intervals. Time-history data from these flights for the following parameters are available for multivariable spectra development:

1. Flight load components (n_x, n_y, and n_z).
2. Attitude (roll, pitch, heading).
3. Angular rates (p, q, and r).
4. Angular accelerations ($\dot{p}$, $\dot{q}$, and $\dot{r}$).
5. Angles of attack and sideslip (α and β).
6. Altitude (h).
7. Mach number (Mn).

(Although a total of 16 parameters are available in segment files in the data base, only normal acceleration [n_z] is used in the procedure described here for the development of fatigue spectra. The rationale for this decision was that for this study only uniaxial test equipment was available. The importance of other parameters was recognized, but their use in this study was not addressed. The data base can be accessed to create spectra using the other loads.) Taxi, takeoff, and landing data are not recorded by the computer system and therefore are not available.

More than 60 missions involving eight aircraft were analyzed to develop the data base for the fatigue spectra methodology. Flight data for each aircraft in each mission were divided into segments, according to the segment types and the decision rules listed in Table 2. Data

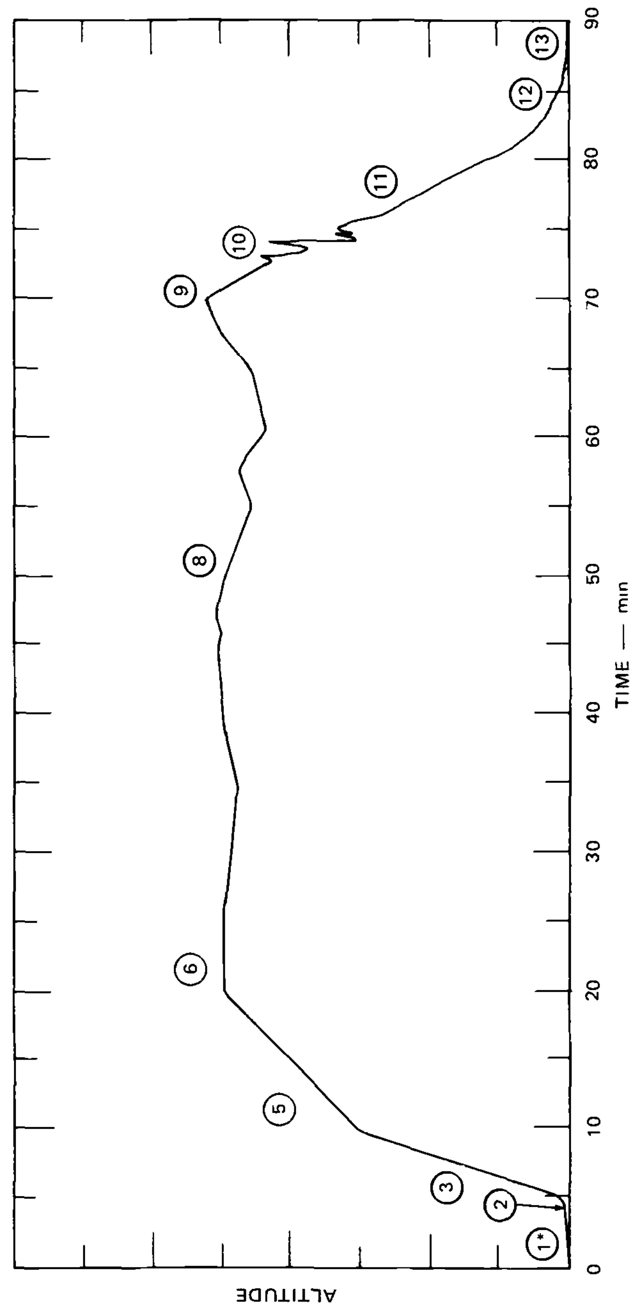

*Numbers refer to the mission segments listed in Table 1

FIG. 4—*Sample fighter aircraft flight profile.*

TABLE 2—*Mission segment definitions.*

Mission Segment	Definition: Speed, knots		Definition: Change in Altitude, m/min		Definition: Normal Acceleration, m/s^2	Preceding Segment	Succeeding Segment
Change of flight level (climb or descend)	between 100 and 200	and	300	and	20	take off cruise loiter engagement	cruise loiter
Cruise	200	and	300	and	20	change of flight level loiter engagement	change of flight level vector loiter
Loiter	between 100 and 200 change in speed <10%	and	600	and	20	cruise change of flight level engagement	cruise change of flight level vector
Vector to intercept ground or air target	Change in speed >10% in 3 min	or	between 600 and 1200	or	20	loiter cruise	engagement loiter cruise
Target engagement	change in speed >10%	or	1200	or	>20 m/s^2 for more than 3 s or change in acceleration >30 m/s^2 in 1 s	vector to intercept	cruise loiter change of flight level

TABLE 3—*Size of flight segment data base.*

Segment Type	Number of Files	Total Time, h
Air combat maneuvering (ACM)	510	21.9
ACM with buffet (ACMB)	92	6.6
Climb	181	5.1
Cruise	43	1.0
Descend	42	1.5
Loiter	146	5.2
Vector to intercept	293	8.1

for seven segment types were collected: climb, descend, loiter, cruise, vector to intercept, air combat maneuvering (ACM), and ACM with buffet (ACMB). Air-to-ground flight segments were not included because of lack of data at this time. When these data become available, the data base should be updated to include this information.

The time-history files created (one per segment) were set up starting with header records identifying the aircraft type, segment type, displacement of pod center of gravity from aircraft center of gravity, and labels for the columns of data. Time-history data were then listed sequentially at 0.1-s intervals for the previously listed parameters. The files varied in length from 20 s to more than 10 min. Aircraft type and segment type were encoded in the file name. Table 3 gives the number of files and approximate number of hours of data stored for each segment type for all the aircraft.

Not only are the recorded data at Air Force and Navy training ranges relatively inexpensive to collect and store, but they contain parameters measured at various store locations, which means they can be used directly in building spectra and need not be subjected to power spectral density and transfer functions. A set of comprehensive flight load files can be readily developed by choosing a variety of aircraft, mission types, and store locations.

Data Compaction and Spectra Development

The next step in the procedure is to reduce the amount of data to a manageable amount and to develop procedures for organizing it in a realistic manner. An important consideration in choosing the data compaction methodology for the spectra development procedures is the need to retain the sequence of events.

Load histories can be condensed in a number of different ways for use in fatigue testing. Three common algorithms that count peak/valley reversals are range-pair, rainflow, and racetrack. The results of applying each method to a time history are slightly different. The racetrack [5] method is the only one of the three that produces a condensed history in which significant peaks and valleys are retained in their original sequence. The racetrack method of peak/valley counting was chosen since it was important to retain the sequence of events. This method eliminates monotonically increasing or decreasing points between reversals, then identifies and saves "significant" reversals in the same order as they occurred in the original time history. Applying the racetrack algorithm to a history of load reversals to determine which ones are significant is a four-step process: (1) the original reversal points are plotted; (2) an equidistant pair of lines is drawn above and below the original reversals, which are separated by the racetrack width; (3) within the racetrack a curve is drawn with the minimum possible number of reversals (change in sign of the first derivative or slope); and (4) the original reversals located where the slope of the curve changed sign are listed sequentially. Figure 5 shows how the algorithm is applied and how the number of significant

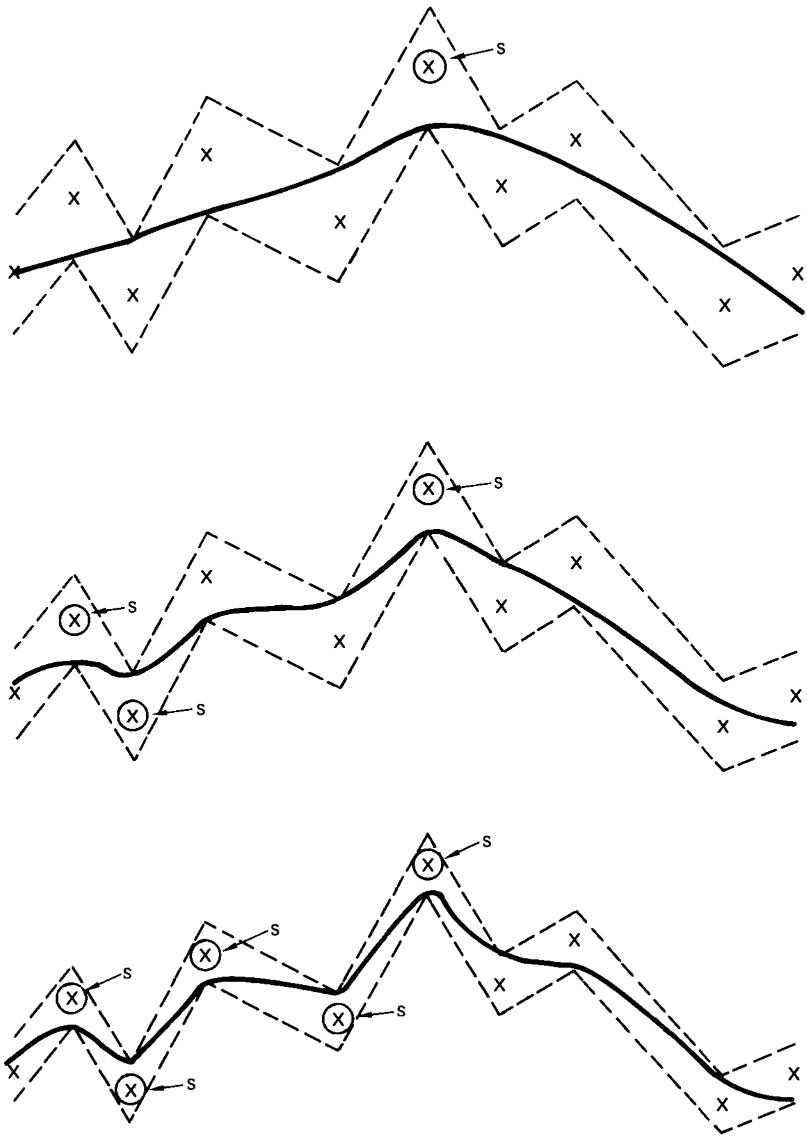

FIG. 5—*Significant reversals in racetrack algorithm:* (top) *width = eight units, one significant reversal;* (middle) *width = six units, three significant reversals, and* (bottom) *width = four units, five significant reversals.*

points varies, depending on the racetrack width. Implementation of the racetrack algorithm for spectra development in the methodology described here identifies peaks and valleys and yields outputs that include a peak/valley pairs file, a peak/valley pair occurrence matrix, and a peak/valley exceedance table. The peak/valley pair occurrence matrix is a Markovian matrix [6], which lists the number of times a peak of a specified level is transitioned to a specific valley level, and vice versa.

Time-history data were scanned to determine the maximum overall range (R) for guidance in determining the racetrack width (W); R was found to be about 120 m/s^2. The Markovian matrix output of this implementation of the racetrack algorithm is a 32 by 32 matrix, which implies that W should have a value of about $R/32$. The W was chosen to be 3 m/s^2, and when used seems to retain the character of the data. The number of points retained after racetrack processing for the samples processed ranged from less than 0.5% to over 25%, depending on the segment type. It was important to record the amount of flight time represented by each segment as it was processed. The time is needed to ensure that the proper proportion of data from each segment type is maintained in the reconstructed missions.

A set of missions was built from the peak/valley pair files. the files were concatenated in the order previously established in determining the store service life. At least one file was developed for each aircraft and mission type in which the store is used. If other flight loads (for example, takeoff and landing) were available, they were inserted in appropriate places.

Figure 6 is a plot of z-acceleration of the raw time-history data. Sixteen segment files were concatenated to form this sample mission profile. Figure 6 is a plot of the sample profile after racetrack processing. Visual comparison shows that the second plot has retained the major characteristics of the first. Approximately 25% of original time-history points in the ACMB segments and almost all reversals in those segments were retained, and an average of about 2% of the data was retained for the rest of the segments where many peaks and valleys were "insignificant." The width of the racetrack for this example was 3 m/s^2. Table 4 shows how much time was spent in each segment type in the sample mission shown in Fig. 6. It also gives the percent of the original time-history points remaining after racetrack processing and the number of reversals per minute for each segment type in the sample.

Following racetrack processing, the new mission profile files were grouped and weighted to reflect the expected service use of the store over a period of time. As an example, consider a store that is available to aircraft Types 1 and 2 and can be mounted on either. From the service use definition, it can be determined which mission types are flown and how often. From that information one can calculate the percent of time the store will be flown on a specific aircraft on a specific mission. Multiplying these percentages by the expected number of flights in a one-year interval yields the number of times each mission profile should be used in the fatigue test. If the store is transferred to a maintenance facility and then to a new location, its use for the next year might be limited to aircraft Types 1 and 3. By the same procedure just described, a new table of expected number of flights for each aircraft/mission may be calculated. This process can be continued until all likely deployments have been analyzed. Table 5 illustrates this procedure for a store that is expected to fly 200 missions each year. The service use blocks thus defined are used as inputs. Thus, referring

TABLE 4—*Amount of data compaction by segment type.*

Segment Type	Duration, min	Time in Segment, %	Original Points Remaining After Racetrack Process, %	Number of Reversals per Minute
ACM	2	4.4	9.7	58
ACMB	2.5	5.6	25.3	152
Climb	6.5	14.4	1.3	8
Cruise	12	26.7	4.4	26
Descend	2	4.4	2.0	12
Loiter	15	33.3	1.1	6.6
Vector	5	11.1	4.8	10.4

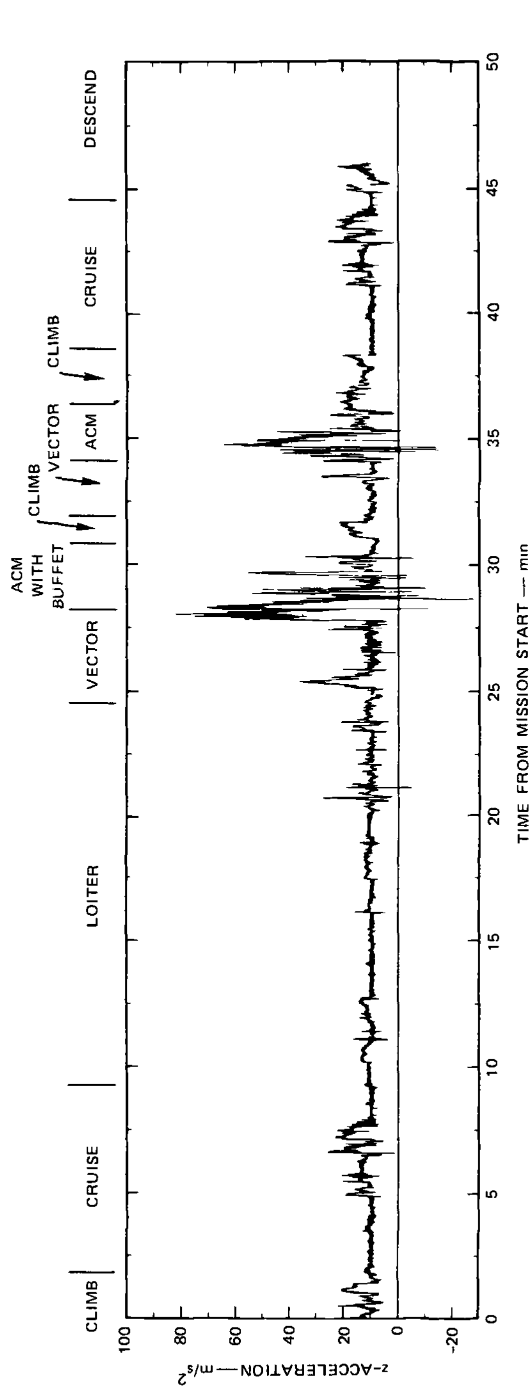
CLIMB
CRUISE
LOITER
VECTOR
ACM WITH BUFFET
CLIMB
VECTOR
ACM
CLIMB
CRUISE
DESCEND
z-ACCELERATION — m/s²
TIME FROM MISSION START — min

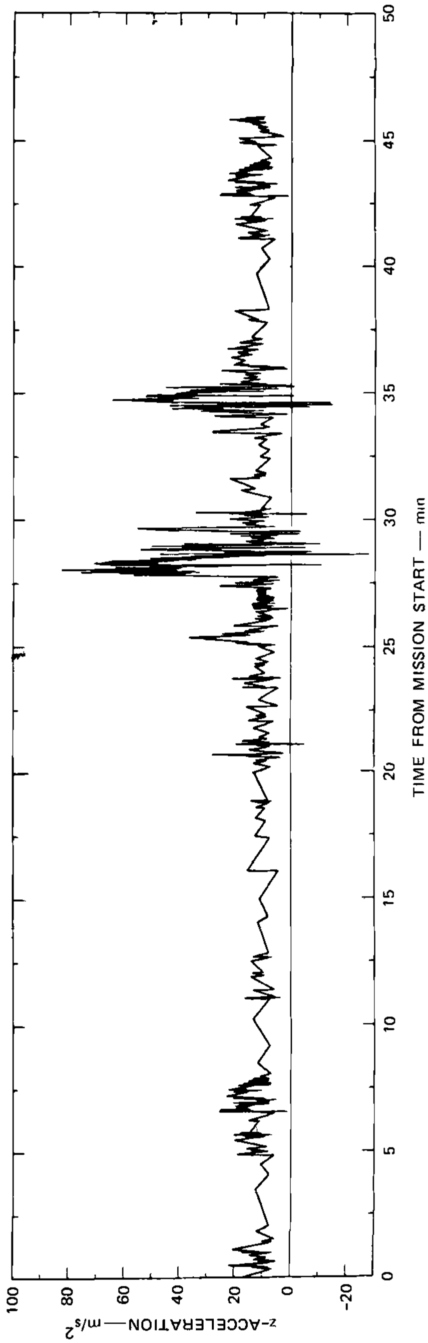

FIG. 6—*Sample fighter aircraft mission profile:* (top) *raw data, and* (bottom) *0.3-g racetrack processed.*

TABLE 5—*Possible aircraft/store use in one year.*

Service Use Blocks, %	Aircraft Type, % B	Mission Type, % C	Percent of Flights by Aircraft and Mission B × C	Number of Flights N × B × C
I (60)	1 (50)	A (50)	25	50
		B (25)	12.5	25
		C (25)	12.5	25
	2 (50)	D (50)	25	50
		C (50)	25	50
II (30)	1 (60)	A (50)	30	60
		B (25)	15	30
		C (25)	15	30
	3 (40)	F (60)	24	48
		G (40)	16	32
III (10)	2 (50)	D (50)	25	50
		E (50)	25	50
	3 (50)	F (60)	30	60
		G (40)	20	40

to Table 5, Block I is used 60% of the time, Block II, 30%, and Block III, 10%. Missions within each block or the blocks themselves can be used as input to a fatigue test either deterministically or randomly depending on the service life description and the test equipment available.

Outlook

This approach to fatigue spectra development for airborne stores is important because (1) the data are measured at store locations, (2) changes in the test spectra may be made easily as new data become available or as the service life changes, (3) the order of flight loads within a segment is maintained and the segments and missions are ordered in a realistic manner thus ensuring that possible sequence effects are retained, and (4) the test engineer can trade-off appropriate realism versus economy, as circumstances dictate. The trade-off is accomplished in the choice of the racetrack width—the narrower the racetrack, the more realistic the spectrum. For this investigation, a width of 3 m/s^2 was chosen, which is believed to be conservative. Future comparisons between service life and test life will show whether this width was too economical.

Summary

This study was an initial step in the development of a methodology using flight loads recorded from Navy and Air Force training flights to build fatigue spectra for testing of stores. Although a number of simplifications and generalizations were made, such as using only n_z in the procedure, both the data base and the software are flexible. The data base includes measurement of 16 parameters for each aircraft and segment type and has the capability to generate spectra based on both symmetrical and asymmetrical flight maneuvers. The data compaction software can reduce any of the parameters at a level specified by the process engineer and outputs results as peak/valley pairs, Markovian matrix, and an exceedance table.

References

[1] Gunston, B. and Spick, M., *Modern Air Combat,* Crescent Books, New York, 1983.
[2] Abelkis, P. R., "Effect of Transport Aircraft Loads Spectrum Variation on Crack Growth," Douglas Paper 6786, Douglas Aircraft Company, presented at ASTM Symposium on Effects of Load Spectrum Variables on Fatigue Crack Initiation and Propagation, San Francisco, CA, 21 May 1979.
[3] Wilkins, D. J., Wolff, R. V., Shinozuka, M., and Cox, E. F. in *Fatigue of Composite Materials, ASTM STP 569,* American Society for Testing and Materials, Philadelphia, 1975, pp. 307–322.
[4] Geissler, F. J., "Handbook of Guidelines for the Development of Design Usage and Environmental Sequences for USAF Aircraft," Air Force Weapons Avionics Laboratory, Report No. AFWAL-TR-80-3156, Wright-Patterson Air Force Base, OH, Feb. 1981.
[5] Fuchs, H. O., Nelson, D. V., Burke, M. A., and Toomay, T. L., *Fatigue Under Complex Loading,* Society of Automotive Engineers, 1977, pp. 145–162.
[6] Haibach, E., Fisher, R., Schutz, W., and Huek, M., *Fatigue Testing and Design,* Vol. 2, Society of Environmental Engineers, 1976, pp. 29.1–29.21.

N. E. Dowling[1] *and A. K. Khosrovaneh*[1]

Simplified Analysis of Helicopter Fatigue Loading Spectra

REFERENCE: Dowling, N. E. and Khosrovaneh, A. K., "**Simplified Analysis of Helicopter Fatigue Loading Spectra,**" *Development of Fatigue Loading Spectra, ASTM STP 1006,* J. M. Potter and R. T. Watanabe, Eds., American Society for Testing and Materials, Philadelphia, 1989, pp. 150–171.

ABSTRACT: In employing the Palmgren-Miner rule for irregular loading spectra applied to notched members, it is necessary to employ rain-flow or an equivalent cycle counting method, and also to consider the accelerated damage at low stress levels due to the presence of high-level cycles. Additional interactions between high and low stress levels, which are associated with local notch mean stress effects, also occur and can be specifically analyzed using the local strain approach. A simplified application of the local strain approach is described that results in upper and lower bounds on life being calculated. This is applied with reasonable success to the standard helicopter loading spectra Helix and Felix, and a much simplified version of Helix is proposed that consists of repetitions of a single typical flight.

KEY WORDS: fatigue (materials), stress, strain, cracking (fracturing), plastic deformation, cyclic loads, helicopters, loading spectra, notches, stress raisers, testing

Structural components that are sensitive to fatigue failure are commonly subjected to highly irregular load spectra, and they virtually always contain stress raisers that are the sites of fatigue crack initiation. If the components are small and highly stressed, the fatigue cracks that limit the life may be too small to reliably find nondestructively, and perhaps even so small that the theoretical limits of linear-elastic fracture mechanics are exceeded. In such cases, it is appropriate to use some variation of an *S-N* approach and the Palmgren-Miner rule [*1,2*].

However, the Palmgren-Miner (P-M) rule, which assumes linear accumulation of cycle ratios to unity, must be used with care in three areas. First, in recent years a concensus has been reached that rain-flow cycle counting [*3,4*] or an equivalent method is necessary to prevent major errors being made in handling the large cycles associated with shifts in mean level due to duty-cycle loading. For example, the ground-air-ground cycle in aircraft causes such a major cycle. Rain-flow cycle counting was proposed in Ref *3* and is described in the ASTM Practices for Cycle Counting in Fatigue Analysis (E 1049-85) [*4*].

Second, the presence of high stress levels in a load spectrum causes the lower levels to cause more fatigue damage than would be expected based on the P-M rule [*5–7*]. Figure 1 illustrates this effect for 2024-T4 aluminum with data from Ref *6*. In particular, the prior application of only a few cycles of plastic prestrain causes the strain-life curve to be lowered in the long-life region. This effect can be included in life predictions by simply basing life predictions on data for specimens that have been prestrained [*7,8*]. Such behavior even

[1] Professor and graduate research assistant, respectively, Engineering Science and Mechanics Department, Virginia Polytechnic Institute and State University, Blacksburg, VA 24061.

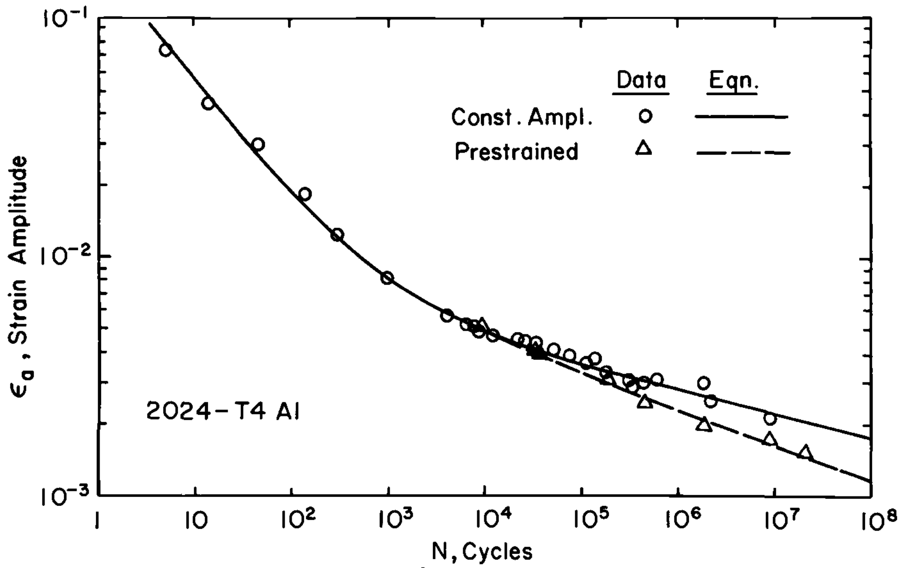

FIG. 1—*Strain versus life curves for 2024-T4 aluminum.*

causes cycles below the endurance limit to cause fatigue damage, so that endurance limits should be considered not to exist, or at least to be lowered considerably [*9–13*]. In steels that show a distinct endurance limit under constant-amplitude loading, fatigue test data obtained under periodic overstrain are necessary for successful use of the P-M rule.

And third and finally, plastic deformation locally at stress raisers during the high load levels causes the local mean stress during low load levels to depend on the prior loading in a complex manner. Local mean stresses of either sign may exist in the absence of mean applied loads [*14,15*], and the mean load and the local mean stress may even be opposite in sign. This situation may cause difficulty with attempts to account for mean stress effects unless a local strain approach [*16–19*] is employed. Such an approach specifically analyzes the local notch plasticity and mean stress effects as illustrated by Fig. 2.

To summarize, successful use of the P-M rule requires proper handling of cycle counting, overstrain effects, and local notch mean stress effects. Past failures to consider all of these complexities have resulted in erroneous conclusions that the P-M rule is not valid, and also in proposals for more complex rules. Here, the simple rule will be used, and the three complexities just described will be specifically included in life calculations.

In the remainder of this paper, the local strain approach will first be discussed, including a simplified version that results in upper and lower bounds on the predicted life. This approach, and especially the simplified version, will then be applied to the standard helicopter load spectra Helix and Felix. Based on this analysis, a simplified version of Helix will be proposed.

Local Strain Approach

For this approach, materials properties are obtained from unnotched axial test specimens as summarized in Ref *20*. A cyclic stress-strain curve is needed.

$$\epsilon_a = \sigma_a/E + (\sigma_a/A)^{1/s} \qquad (1)$$

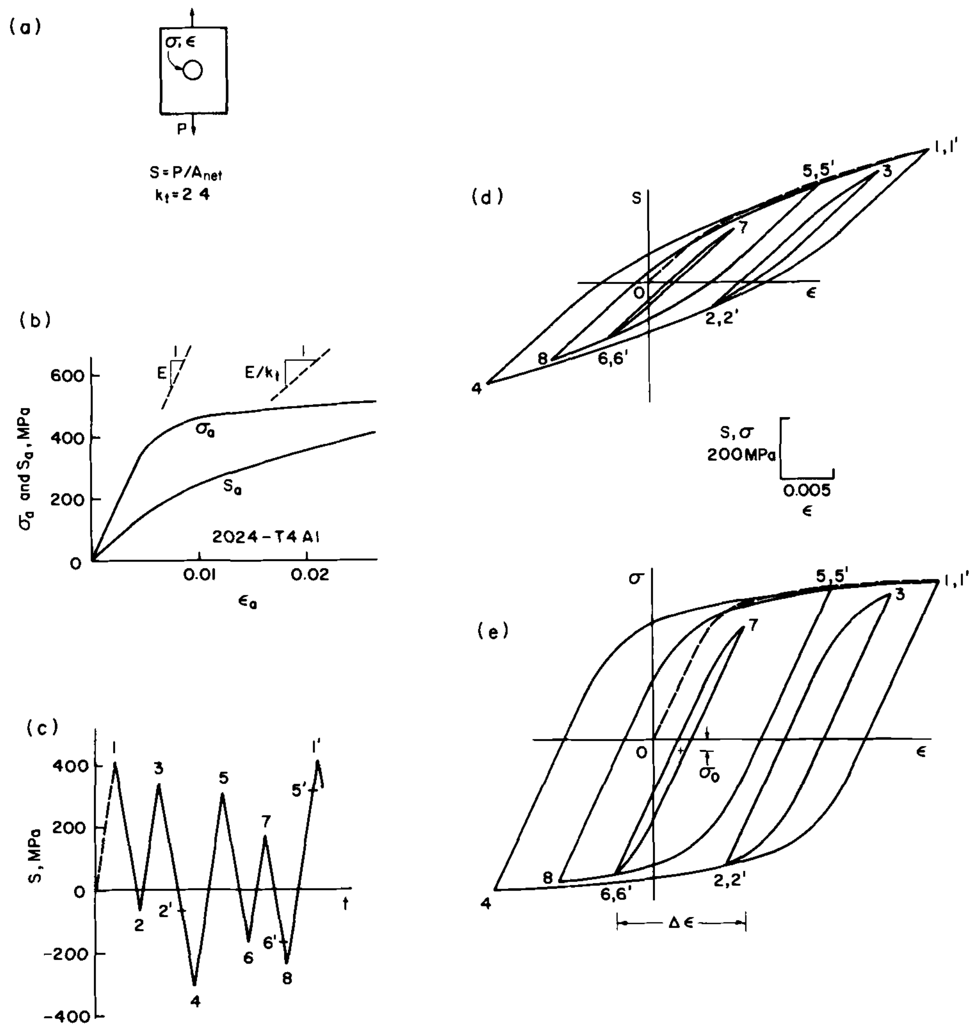

FIG. 2—*Illustration of local strain approach for an irregular load versus time history. Notched member* (a), *having cyclic stress-strain and load-strain curves as in* (b), *is subjected to load history* (c). *The resulting load-strain response is shown in* (d), *and the local notch stress-strain response in* (e).

where σ_a and ϵ_a amplitudes of stress and strain, respectively; E is the elastic modulus; and A and s are material constants. A strain versus life curve is also needed.

$$\epsilon_a = \frac{\sigma_f'}{E}(2N^*)^b + \epsilon_f'(2N^*)^c \tag{2}$$

where N^* is the life in cycles for zero mean stress, and σ_f', b, ϵ_f', and c are additional material constants. If the rule of Morrow [21] is used to account for mean stress effects, the final life, N, which includes this effect is given by [*19*]

$$N = N^*(1 - \sigma_o/\sigma_f')^{-1/b} \tag{3}$$

where σ_o is mean stress.

Life Predictions by the Local Strain Approach

Figure 2 illustrates the initial and most difficult step of a life calculation by this approach, namely, the estimation of the local notch stress-strain response. First, the cyclic stress-strain curve, as in Fig. 2*b*, is employed in an analysis of the notched member to obtain a curve relating nominal stress, S, and strain, ϵ, as also shown in Fig. 2*b*. An approximate analysis based on Neuber's rule is often used for this purpose. These curves are then used to estimate the local stress-strain response at the notch by following the load history while modeling the hysteresis looping behavior of the material. As a convenience, a repeating load history is assumed to start at the highest absolute value of load. (See Refs *16–19* for details of the procedure used.)

For the example of Fig. 2, the irregular load history of (*c*) results in load-strain and stress-strain responses as shown in (*d*) and (*e*). Note that there is a set of closed hysteresis loops, such as 2–3–2′, 6–7–6′, 5–8–5′, 2–3–2′, and 1–4–1′ for this example. Each such loop is identified as a cycle, and the cycles so defined are the same as would be obtained from applying rain-flow cycle counting to the load (S) versus time history.

Each cycle now has a known strain range, $\Delta\epsilon = 2\epsilon_a$, and mean stress, σ_o, as shown for Cycle 6–7–6′ in Fig. 2*e*. The life, N, corresponding to each combination of ϵ_a and σ_o can be then obtained from Eqs 2 and 3. The final step is then to apply the P-M rule. For a load history that is assumed to repeat until failure occurs, the rule takes the form

$$B \sum_{\substack{\text{per}\\ \text{block}}} \frac{n_i}{N_i} = 1 \tag{4}$$

where n_i is the number of occurrences per block of a cycle corresponding to life N_i, and B is the unknown number of blocks (repetitions) to failure.

Life Calculations Neglecting Mean Stress Effects

The local strain approach as just summarized requires a knowledge of the full sequence of loads. However, if mean stress effects can be neglected, a much simpler procedure without stress-strain modeling is possible. It is then necessary to know only the ranges, ΔS, of each cycle. This requires only the result of rain-flow cycle counting of the load (S) history, with no need to subsequently retain any other information. Figure 3 shows such a cycle counting of the load history of Fig. 2*c*. For this example, the only values needed are load ranges $\Delta S_{2\text{-}3}$, $\Delta S_{6\text{-}7}$, $\Delta S_{5\text{-}8}$, and $\Delta S_{1\text{-}4}$.

These values are then used with Neubers rule, which in its simplest form is

$$\sigma_a \epsilon_a = \frac{(k_t S_a)^2}{E} \tag{5}$$

where $S_a = \Delta S/2$, and k_t is the elastic stress concentration factor. Equations 1 and 5 can then be solved iteratively to obtain the ϵ_a corresponding to each ΔS. Equation 2 is then

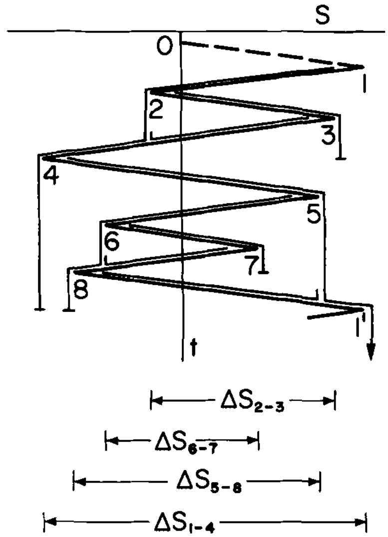

FIG. 3—*Rain-flow cycle counting result for the load history of Fig.* 2c.

solved for each N^*. These N^* values, which assume zero mean stress, are then used in place of N in Eq 4 to obtain the life estimate.

The first two columns of Table 1 give sufficient information to apply this procedure to the standard helicopter spectrum Helix [*22*].

Simplified Life Calculation for Upper/Lower Bounds on Mean Stress Effect

However, cycle counting of a load history readily yields not only ranges, ΔS, but also mean values, S_o. For example, in Fig. 2*c*, the S_o value for Cycle 2–3 is $(S_2 + S_3)/2$, and the others are similarly obtained. This information is generally presented in a matrix, such as that shown in Table 2 for Helix. It is possible to take advantage of the additional S_o information to place upper and lower bounds on the life as influenced by local notch mean stress.

The possibility of making such a bounded estimate has been known for some time. It is briefly described in a paper by Conle [*23*], and also previously implied by Socie et al. [*24*]. However, to our knowledge, no complete description exists in the literature, and so we provide it in this paper.

The procedure is illustrated in Fig. 4 for one of the cycles, specifically 6–7, of the example of Fig. 2. The guiding principle is that both load-strain Loop 6–7 in Fig. 2*d* and stress-strain Loop 6–7 in Fig. 2*e* must lie within the corresponding loop for the major (largest) cycle in the history, in this case Cycle 1–4. Since the load limits S_6 and S_7 are known, this places limits on the mean strain of Cycle 6–7. In particular, in Fig. 4*a*, load-strain Loop 6–7 could be so far to the right that it is attached at A, or so far to the left it is attached at B.

Similarly, consider the load versus stress response in Fig. 4*c*. Here, Loop 6–7 could be so low that it is attached at A, or so high that it is attached at *B*. Stress-strain loops having the corresponding attachment Points A and B are shown in Fig. 4*b*. Note that Loop A corresponds to the lower limit on stress and the upper limit on strain, and vice-versa for Loop B. The mean stresses of these loops, σ_{oA} and σ_{oB}, are the extreme possibilities.

Knowing these bounds on the mean stress for Cycle 6–7 allows bounds to be placed on the life, N, from Eq 3. The upper bound values on N are similarly obtained for all cycles in the history, and these are used with the P-M rule in the form of Eq 4 to obtain the upper bound on calculated life for the irregular load history. The lower bound N values are similarly used in Eq 4 to obtain the lower bound on the life. The details of the calculations needed to obtain the upper and lower bounds on mean stress are given in the Appendix.

Note that the upper and lower bounds on life are identical if there is no reversed plastic strain during the major cycle, that is, if the major loop such as 1–4 in Fig. 4 has degenerated to a straight line. Also, at high load levels, the cycles causing most of the fatigue damage may not have significant mean stresses due to their plastic strains being large. The bounds will then be close. Hence, the widest separation between the bounds is expected at intermediate load levels. But the degree of separation of the bounds will be greatest for histories where most of the damage is done by low-level cycles. If all of the damage is done by the major cycle, then the two bounds are again identical.

Analysis of Helix and Felix

Reference *22* gives fatigue life data for both Helix and Felix applied to plate-with-hole test specimens having an elastic stress concentration factor of $k_t = 2.5$. Data are given for

TABLE 1—*Cycles from rain-flow counting for Helix.*

Stress Range for S_{max} = 100 Units	Helix, Cycles per Flight, average[a]		Reconstruction, cycles per flight	
	Number	Cumulative	Number	Cumulative
120	1	1	1	1
116	0	1	0	1
112	0	1	0	1
108	0	1	0	1
104	0	1	0	1
100	0	1	0	1
96	0	1	0	1
92	0	1	0	1
88	1	2	2	3
84	0	2	10	13
80	7	9	20	33
76	3	12	0	33
72	42	54	80	113
68	2	56	50	163
64	74	130	120	283
60	16	146	280	563
56	8 344	8 490	8 030	8 593
52	26	8 516	190	8 783
48	3 252	11 768	2 730	11 513
44	3	11 771	1 810	13 323
40	3 425	15 196	100	13 423
36	2	15 198	1 510	14 933
32	0	15 198	40	14 973
28	2	15 200	130	15 103
24	0	15 200	50	15 153
20	1	15 201	50	15 203
16	0	15 201	0	15 203
12	2	15 203	0	15 203
8	5	15 208	0	15 203
4	21	15 229	0	15 203

[a] The values were obtained by dividing the cycles counted for all of Helix by 140, the number of flights.

TABLE 2—*Range-mean matrix for Helix from rain-flow cycle counting (cycles per flight, average).*[a]

	Mean									
Range	40	44	48	52	56	60	64	68	72	All
4	0	0	0	1	0	2	16	2	0	21
8	0	0	0	0	1	0	4	0	0	5
12	0	0	0	0	0	0	2	0	0	2
16	0	0	0	0	0	0	0	0	0	0
20	0	0	0	0	0	1	0	0	0	1
24	0	0	0	0	0	0	0	0	0	0
28	0	0	0	0	0	0	2	0	0	2
32	0	0	0	0	0	0	0	0	0	0
36	0	0	0	1	0	0	0	1	0	2
40	0	12	0	43	30	1 742	1 348	27	223	3 425
44	0	0	0	1	0	1	0	1	0	3
48	0	0	0	14	5	453	2 613	155	12	3 252
52	0	0	0	0	0	5	20	1	0	26
56	0	0	0	24	6	65	7 785	460	4	8 344
60	0	0	0	0	1	0	15	0	0	16
64	0	0	0	6	8	30	6	24	0	74
68	0	0	0	1	1	0	0	0	0	2
72	0	0	0	10	4	28	0	0	0	42
76	0	0	0	1	1	1	0	0	0	3
80	0	0	0	1	1	5	0	0	0	7
84	0	0	0	0	0	0	0	0	0	0
88	0	0	0	0	1	0	0	0	0	1
92	0	0	0	0	0	0	0	0	0	0
96	0	0	0	0	0	0	0	0	0	0
100	0	0	0	0	0	0	0	0	0	0
104	0	0	0	0	0	0	0	0	0	0
108	0	0	0	0	0	0	0	0	0	0
112	0	0	0	0	0	0	0	0	0	0
116	0	0	0	0	0	0	0	0	0	0
120	1	0	0	0	0	0	0	0	0	1
All	1	12	0	103	59	2 333	11 811	671	239	15 229

[a] The matrix entries were obtained from those for all of Helix by dividing each by 140, the number of flights. The range and mean values correspond to S_{max} = 100 units.

several levels of maximum nominal stress, S_{max}, for both 2024-T4 aluminum and titanium 6Al-4V. Corresponding local-strain-approach life calculations were made and are compared below with these data. However, these comparisons are preceeded by some general information on Helix and Felix.

General Description of Helix and Felix

Helix and Felix [22] are standard loading sequences for the main rotors of helicopters with articulated and semi-rigid rotors, respectively. Helix describes a load history for a 190.5-h (2 132 024 cycle) sequence of 140 helicopter flights, while Felix describes a load history for a 190.5-h (2 285 072 cycle) sequence of 140 helicopter flights. Each flight in the sequence represents one of either training, transport, antisubmarine warfare, or search and rescue. Each of these appears in three different lengths of 0.75, 2.25, and 3.75 h. There are twelve unique flights in either Helix or Felix, which are applied in a specified sequence and number of repetitions to obtain the total of 140 flights. Figure 5 shows the load versus time history for portions of a transport flight in Helix.

Helix is composed of 24 unique maneuvers, and Felix of 22 maneuvers, which are repeated in various sequences and numbers of repetitions to compose the various flights. The maneuvers, such as take-off, forward flight at various load levels, turns, etc. each consists of a constant mean level and a relatively small number of cycles. These cycles occur at one or more stress amplitudes, with the number of cycles being between 1 and 40 for Helix, and between 2 and 74 for Felix.

The mean levels for the various maneuvers in Helix are relatively high, mostly ranging from 60 to 68% of the maximum nominal stress in the load spectrum, S_{max}. Felix has relatively lower mean levels, mostly between 36 and 48% of S_{max}. Helix reaches the 100% of S_{max} level at least once in each flight and returns to −20% at the end of each flight. Felix is similar but does not reach the full 100% of S_{max} level in all flights, and returns to −28% at the end of each flight.

Hence, Helix and Felix have a large ground-air-ground cycle and a large number of cycles at relatively high mean levels. In general, there are many repetitions of certain cycles or combinations of cycles that occur in the most frequently needed maneuvers. Refer to Tables 1 and 2 to examine Helix more closely. Helix and Felix are completely defined in Ref *22*.

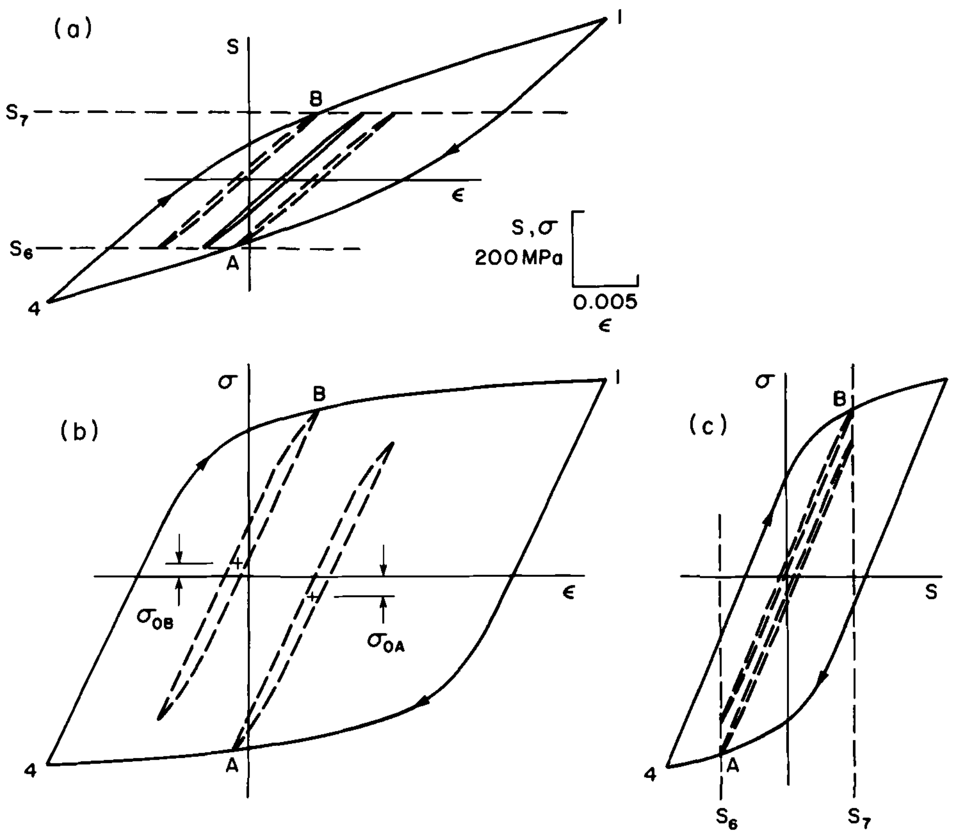

FIG. 4—*Illustration based on Fig. 2 of placing bounds on the mean stress of a subcycle when the sequence of the applied loads is not known. The mean stress for Cycle 6-7 must lie between the values of* σ_{oA} *and* σ_{oB}.

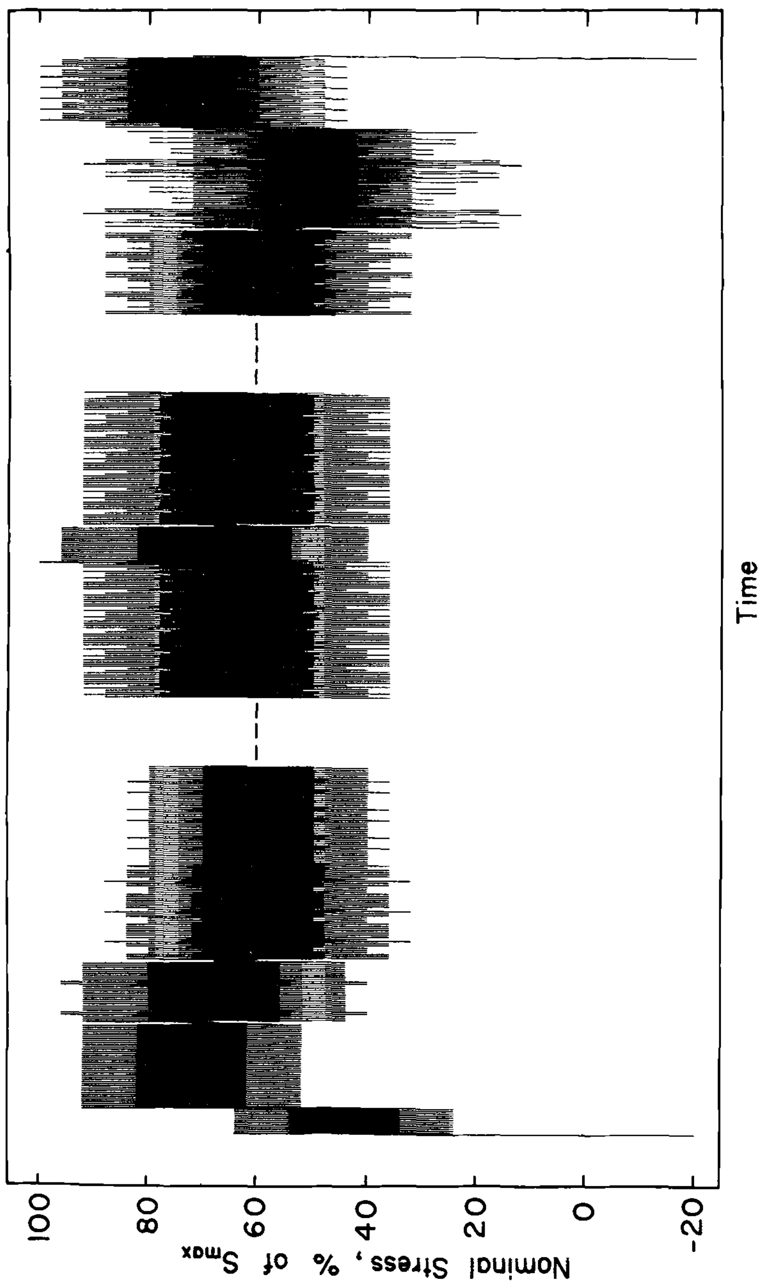

FIG. 5—*Example of the load-time history for portions of a transport flight in Helix.*

TABLE 3—*Constants for strain versus life curves.*

Symbol, units	2024-T4 Aluminum Constant Ampltiude	2024-T4 Aluminum Prestrained	Titanium 6Al-4V
E, GPa	73.1	73.1	113.8
A, MPa	738	738	1 327
s	0.080	0.080	0.0755
ϵ_f'	0.327	0.327	6.22
c	−0.645	−0.645	−1.01
σ_f', MPa	900	1 294	1 523
b	−0.102	−0.142	−0.0763

Detailed Local Strain Analysis of Helix

Unnotched axial specimen data for 2024-T4 aluminum from Ref *6* were fitted to Eqs 1 and 2. This was done for both ordinary constant-amplitude tests and for tests on previously prestrained specimens. The resulting constants are given in Table 3, and the ones for the strain-life curve yield the lines plotted in Fig. 1. For titanium 6Al-4V, only ordinary constant-amplitude data could be found, specifically in Ref *25*. Constants fitted to these data by A. Conle of Ford Motor Co. were used and are also given in Table 3.

Life calculations were made for the plate-with-hole specimens of 2024-T4 Al subjected to Helix using the full local strain approach as just summarized. A computer program developed by Wirsching (*26*) from an earlier program due to Brose [*27*] was employed. The program was used as received except for minor debugging. Some minor corrections were made for errors associated with the use of discrete strain levels in that program.

Figure 6 shows curves based on these life calculations, as well as the test data. Table 4 gives the calculated lives in the second column. Reasonable agreement is obtained between

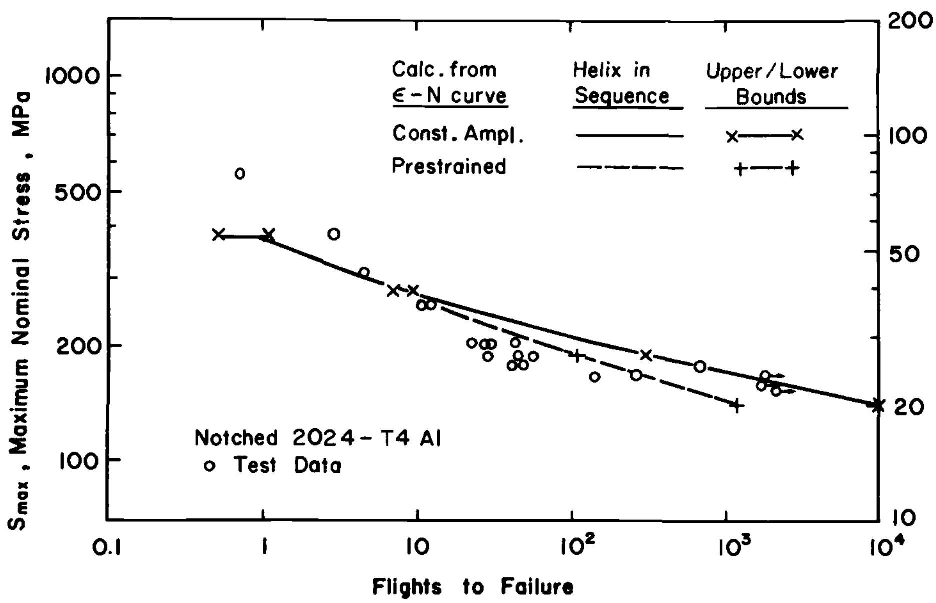

FIG. 6—*Analysis of Helix compared to test data for 2024-T4 aluminum, including both the full history in sequence and upper/lower bounds.*

TABLE 4—*Calculated flights to failure for Helix for notched specimens* (k_t = *2.5*).

S_{max}, MPa (net area)	Helix Full Analysis	Rain-Flow Matrix	
		Lower Bound	Upper Bound
	(*a*) 2024-T4 AL, CONSTANT-AMPLITUDE STRAIN-LIFE CURVE		
138	9 614	10 005	10 006
186	295	294	296
276	7.95	6.88	8.57
379	0.95	0.50	1.07
	(*b*) 2024-T4 AL, PRESTRAINED STRAIN-LIFE CURVE		
138	1 107	1 149	1 149
186	107.0	108.0	108.2
276	7.94	7.55	8.37
317	...	3.10	3.86
	(*c*) TITANIUM 6AL-4V		
317	...	26 193	26 213
358	...	4 415	4 433
407	...	857	876
455	...	221	240
517	...	46.9	62.8

data and analysis for the case of prestrained material properties. An exception is at the lowest stresses where these calculations are conservative. The calculations not including prestrain effects are generally nonconservative.

Upper/Lower Bound Analysis of Helix and Felix

The calculations just described for Helix applied to 2024-T4 aluminum notched specimens were then repeated using the simplified local strain analysis that places bounds on the life. First, rain-flow cycle counting was applied to each of the twelve unique flights of Helix. This yielded a range-mean matrix for each type of flight. These were then combined to obtain an overall prediction by considering the number of times each unique flight was repeated in Helix. However, there was no significant difference between the results of this procedure and results obtained from the simpler procedure of using one matrix derived from all of Helix.

Hence, the simpler procedure of using a single matrix was adopted, with the matrix used for Helix being the one of Table 2. (Note that the division by 140 in Table 2 is of no significance, causing only inconsequential roundoff errors compared to using the matrix for all of Helix.) The resulting bounds on life are given in the third and fourth columns of Table 4*a* and *b* and are shown in Fig. 6. Note that the bounds are very tight except at the higher stress levels, and that the lives from the full local strain analysis occur within these bounds where they are distinct. Where the bounds are tight, the agreement with the full analysis is within the accuracy permitted by various sources of minor error, such as roundoff errors, in the Wirsching program calculations.

Tables 4*c* and 5 give the results of additional life calculations made. Note that Helix is now analyzed for the titanium material also, and Felix is analyzed for both titanium and aluminum. Figures 7 through 9 compare these calculated lives with the test data. Reasonable agreement is obtained except for the combination of titanium and Felix. Note that materials data for prestrained titanium were not available, and these might give a better comparison.

TABLE 5—*Calculated flights to failure for Felix for notched specimens* (k_t = 2.5).

S_{max}, MPa (net area)	Rain-Flow Matrix	
	Lower Bound	Upper Bound
	(*a*) 2024-T4 AL, CONSTANT-AMPLITUDE STRAIN-LIFE CURVE	
186	5 597	5 634
276	227	364
	(*b*) 2024-T4 AL, PRESTRAINED STRAIN-LIFE CURVE	
186	1 285	1 291
276	100	132
379	10.0	27.3
	(*c*) TITANIUM 6AL-4V	
517	1 033	1 270
552	560	795
648	104	283

Peak/Valley Reconstruction of Helix

In the research program underway, it was desired to develop a version of Helix that was reconstructed from a concise description and that caused equivalent fatigue damage. Ideally, this would be done to have equivalent rain-flow cycles and equivalent local notch mean stresses. Conle [28] has investigated this possibility and found it to be possible, but difficult, to achieve.

However, a simpler strategy was suggested by the fact that Helix has a preponderance of cycles at a few levels. This can be seen from Tables 1 and 2. Furthermore, most of the

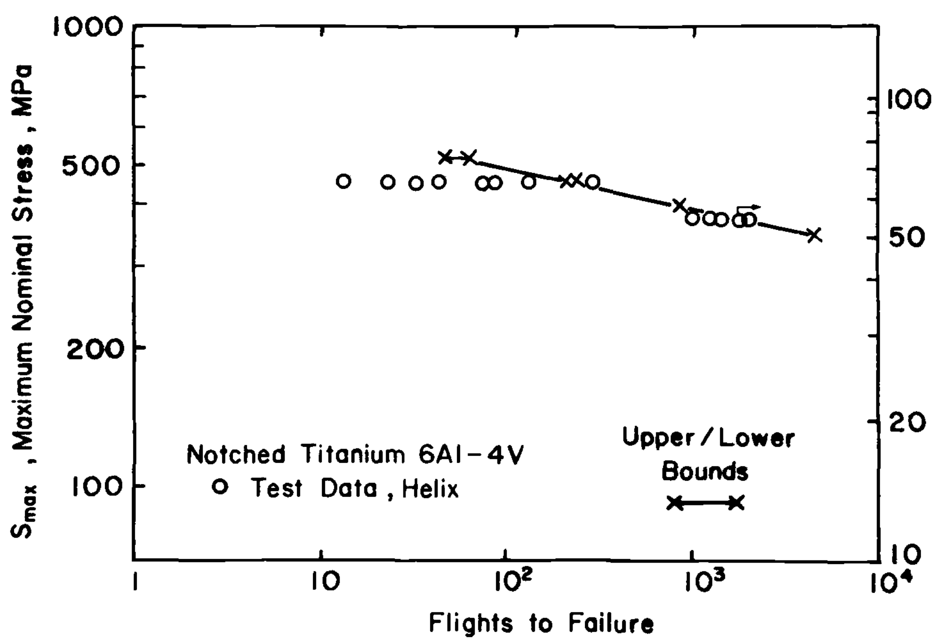

FIG. 7—*Analysis of Helix for titanium 6Al-4V. The line shown is the middle of the bounds.*

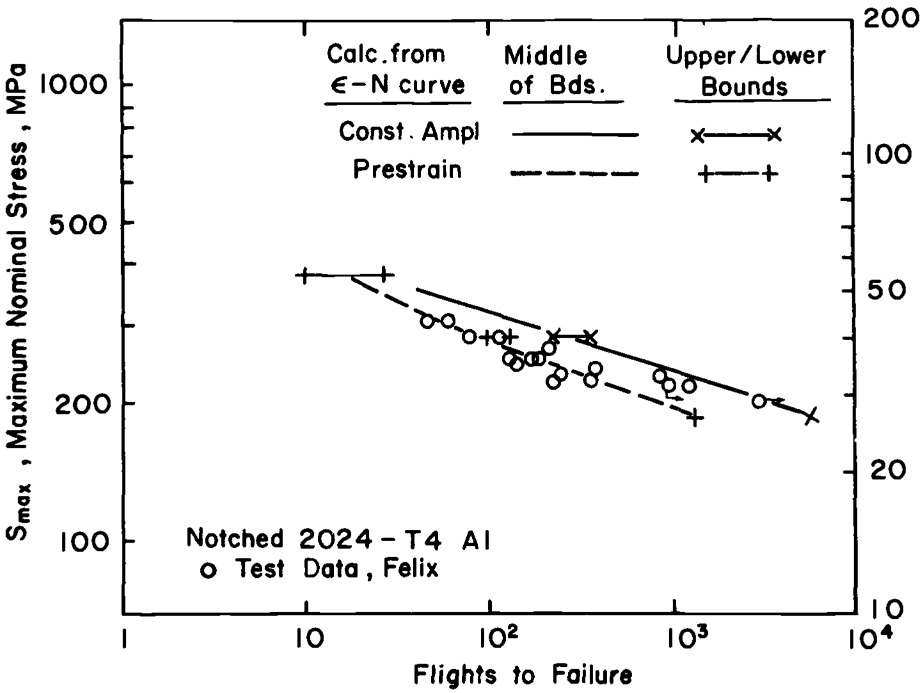

FIG. 8—*Analysis of Felix for 2024-T4 aluminum. The lines shown are middles of bounds.*

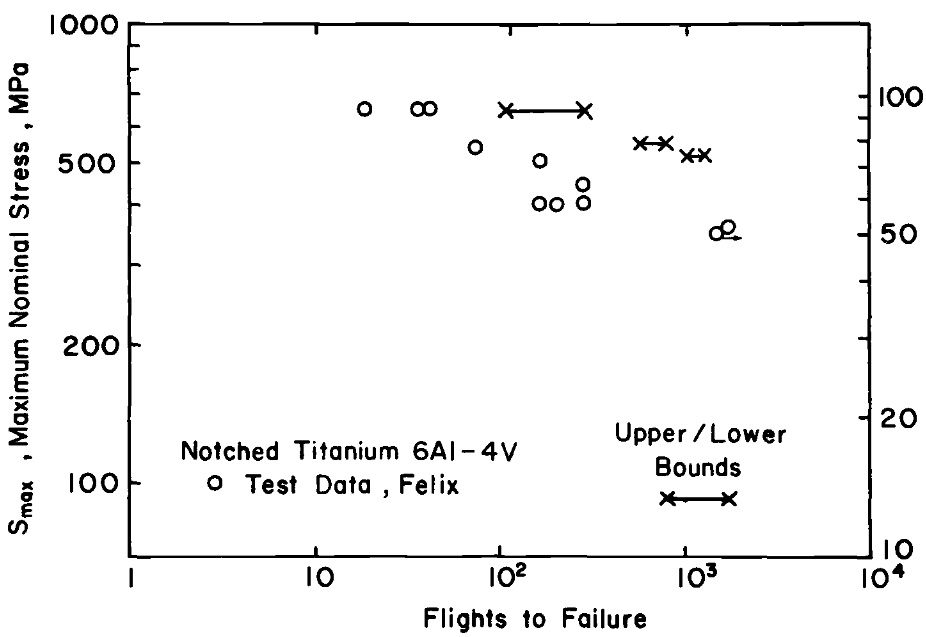

FIG. 9—*Analysis of Felix for titanium 6Al-4V.*

fatigue damage, as calculated by the local strain approach, tends to be concentrated at a single level. This is illustrated by Fig. 10 for one stress level for 2024-T4 Al. Note that the major ground-air-ground cycle does not itself cause significant fatigue damage. But it does affect the local mean stress of the lower level cycles, and it can increase the damage they do through the prestrain effect.

Hence, the most important features of a reconstructed Helix would be to have a similar major cycle and similar proportions of lower level cycles in each flight, especially at the most damaging levels. This was accomplished by a simple peak/valley reconstruction.

In particular, the highest peak and lowest valley were combined to form a cycle, and the second highest and second lowest, and so on, were similarly combined until all events were used. The result was then divided by 140, with some care to avoid nonconservatism in rounding off numbers, to obtain a single representative flight. The result is described in Table 6. Note that, except for three cycles at the beginning and a return to the −20% level at the end, the cycles are applied in a hi-lo-hi sequence that is repeated five times.

Such a peak/valley reconstruction is conservative with respect to rain-flow cycle counting in that some of the cycles will appear at higher values of range than in the original history. This is evident from the comparison of rain-flow counts in Table 1. The difference in the rain-flow cycle count for an original history compared to its peak/valley reconstruction can be significant. But in this case, the difference is small due to the preponderance of peaks and valleys of a single combination that causes most of the rain-flow cycles.

Upper/lower bound life calculations for the peak/valley reconstruction of Helix were made for both materials and are given in Table 7. Comparison with Table 4 indicates that the lives obtained are slightly shorter than those for Helix, specifically around 20% in life or less, so that the reconstructed Helix is slightly more damaging, as expected.

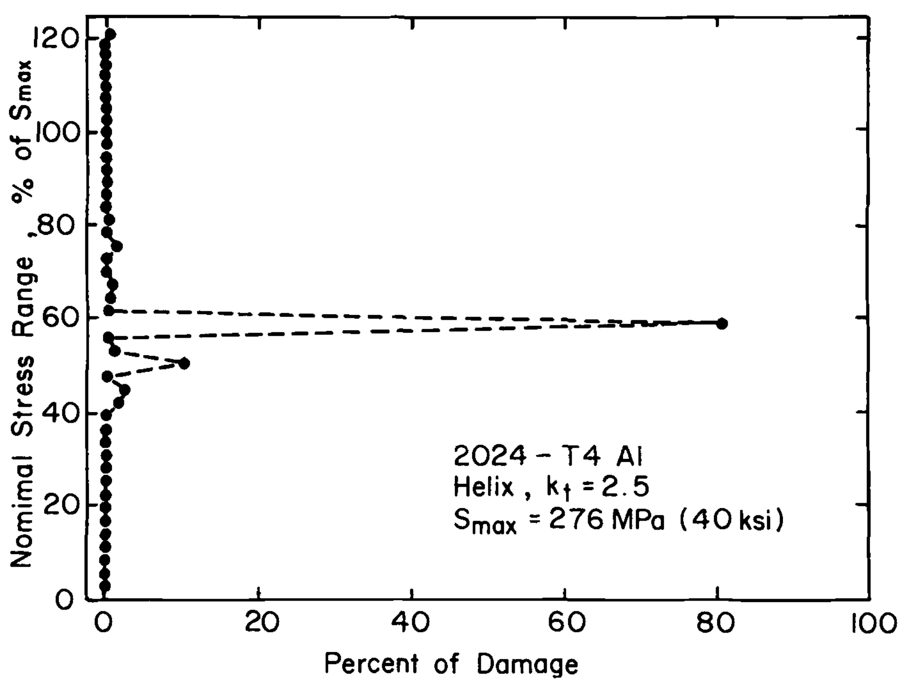

FIG. 10—*Distribution of fatigue damage with stress level for one case of Helix.*

TABLE 6—*Peak/valley reconstruction of Helix.*

(*a*) BLOCKS OF STRESS CYCLES

Block Number	Stresses for S_{max} = 100 units: Minimum	Stresses for S_{max} = 100 units: Maximum	Number of Repetitions	Comment
1	−20	100	1	do once at start of
2	−12	100	2	each flight
3	16	100	1	
4	20	100	2	
5	24	96	8	
6	28	96	5	
7	32	96	12	
8	36	96	28	
9	36	92	803	
10	40	92	19	repeat 10 times
11	40	88	273	(1 520 cycles each time)
12	40	84	181	
13	40	80	10	
14	44	80	151	
15	48	80	4	
16	52	80	13	
17	52	76	5	
18	52	72	5	
19	52	68	1	omit as trivial
20	56	68	0	(occurs 10 times)
21	60	68	1	
22	−20	...	1	return to level to start next flight

(*b*) SEQUENCE OF BLOCKS BY NUMBER FOR COMPLETE FLIGHT (15 203 CYCLES)

1	start flight
2	
3 thru 18, 18 thru 3	
3 thru 18, 18 thru 3	this is a hi-lo-hi
3 thru 18, 18 thru 3	sequence of blocks
3 thru 18, 18 thru 3	repeated 5 times
3 thru 18, 18 thru 3	
22	end flight

NOTE—If the flight as in (*b*) is repeated 140 times, this will approximate one repetition of all of Helix, and it will contain 2 128 420 cycles.

Discussion

The life calculations for Helix and Felix based on the local strain approach were more accurate than those in Ref *22*. This appears to be primarily due to the availability of materials data for prestrained specimens of the aluminum alloy. Mean stress effects are also handled in a more rigorous manner, and this may have been beneficial. Cycle counting was probably not a factor, as the rain-flow method appears to have been used in Ref *22* also.

It is noteworthy that prestrain effects could be included in life predictions by methods

TABLE 7—*Calculated flights to failure for peak/valley reconstruction of Helix.*

S_{max}, MPa (net area)	Peak/Valley Reconstruction	
	Lower Bound	Upper Bound
	(*a*) 2024-T4 Al, Constant Amplitude Strain-Life Curve	
138	8 562	8 563
	(*b*) 2024-T4 Al, Prestrained Strain-Life Curve	
138	1 057	1 057
276	7.12	7.90
317	2.95	3.66
	(*c*) Titanium 6Al-4V	
317	20 258	20 272
358	3 431	3 443
407	673	686
455	176	190
517	38.5	50.2

other than the local strain approach. It is simply necessary that the *S-N* data used, which could be for components or notched specimens, include this effect.

It is interesting to note in Figs. 6 and 8 that the data agree more closely with the prestrain calculations except at the lowest stress levels, where they approach the constant-amplitude calculations. This appears to be due to the fact that these stress levels are so low that even the major ground-air-ground cycle is approaching the endurance limit. Hence, an endurance limit is expected for spectrum loading, but only when the major cycle is sufficiently low. If the major cycle is above the endurance limit, then, as just discussed, the lower level cycles below it still cause fatigue damage.

Considering the upper/lower bound calculation method, note that the Helix and Felix spectra are typical of cases where the bounds would tend to be widely separated. This is due to most of the damage being done at a relatively low level within the spectrum. For many load spectra, such as those used extensively by the Society of Automotive Engineers in their SAE Vol. AE-6 fatigue studies [29], the bounds will be quite close due to most of the damage being done at levels near the highest in the spectrum. Wide separation of the bounds is not likely to very often be a difficulty with this approach.

The upper/lower bound approach has two very distinct advantages. First, a range-mean matrix from rain-flow cycle counting is the only information needed on the load spectrum. This represents a compact form of information that is much easier to store and handle than the full list of peaks and valleys. And second, the life calculations are simpler and more economical. For Helix, the reduction in computer run costs compared to full local-strain-approach calculations was about a factor of 50.

Conclusions and Recommendations

The following conclusions, stated in the form of recommendations, are reached based on the preceding analysis and discussion.

1. Where notched geometries and complex variable-amplitude load spectra occur, as for helicopter components, life calculations should employ rain-flow cycle counting and should consider sequence effects due to the local notch plasticity and mean stress behavior. Increased damage at the lower stress levels due to overstrain effects caused

by the higher stress levels should also be included. This is especially true for cycles below the endurance limit where some cycles in the load spectrum are above the endurance limit.

2. Upper/lower bound life calculations based on the local strain approach, as described herein, should be more widely used. This method has important advantages of simplicity and economy.
3. The single-flight simplified version of the helicopter spectrum Helix that is developed herein should be considered for use where the full spectrum is too cumbersome. Verification by mechanical testing is needed, and a similar simplified version of Felix can be very easily developed.

Acknowledgment

This work was supported by the U.S. Army Aviation Applied Technology Directorate, Fort Eustis, Virginia, as part of the Investigation of Fatigue Methodology program with the University of Dayton Research Institute (UDRI), Dayton, Ohio. Virginia Tech participated in this program as a subcontractor to UDRI.

APPENDIX

Details of Upper/Lower Bound Calculations

The detailed equations needed to accomplish the procedure described in the main part of this paper are given here. The example of cycle 6–7–6′ of Fig. 2 is further employed as an example with the aid of Fig. 4.

It is convenient to write Eqs 1 and 5 in general form without subscripts

$$\epsilon = \sigma/E + (\sigma/A)^{1/s} \tag{6}$$

$$\sigma\epsilon = \frac{(k_t S)^2}{E} \tag{7}$$

The values of the constants E, A, s, and k_t are of course unchanged.

Combining Eqs 6 and 7 gives a relationship involving only strain, ϵ, and nominal stress, S.

$$\epsilon = \left[\frac{k_t S}{E}\right]^2 \frac{1}{\epsilon} + \left[\frac{(k_t S)^2}{E\epsilon A}\right]^{1/s} \tag{8}$$

Considering Fig. 4, the goal is to determine the bounds on mean stress, such as σ_{oA} and σ_{oB}, and from these the bounds on life. Point 1 corresponds to the maximum load in the history, and Point 4 corresponds to the minimum load in the history. As a convenience, it is assumed that the largest absolute value of load is positive. If not, then what follows will need to be modified with appropriate sign changes. Note that the load history is known, which implies that S values are known for all calculations, so that the unknowns are the σ and ϵ values. These calculations take advantage of the fact that various loop curves in either Fig. 4*a* or *b* have the same shape, which is that of the corresponding curve from Fig. 2*b* expanded with a scale factor of two.

To obtain the unknowns for Point 1 let

$$S = S_1 \tag{9a}$$

$$\epsilon = \epsilon_1 \tag{9b}$$

$$\sigma = \sigma_1 \tag{9c}$$

Substitute Eq 9 into Eqs 6 and 8, and solve for ϵ_1 from Eq 8. Then using Eq 6, solve for σ_1. To analyze the range of major cycle 1–4–1′, let

$$S = \frac{\Delta S_{1\text{-}4}}{2} \tag{10a}$$

$$\epsilon = \frac{\Delta \epsilon_{1\text{-}4}}{2} \tag{10b}$$

$$\sigma = \frac{\Delta \sigma_{1\text{-}4}}{2} \tag{10c}$$

Using a parallel procedure to that just described, $\Delta\epsilon_{1\text{-}4}$ and $\Delta\sigma_{1\text{-}4}$ are obtained. Then the stress and strain at Point 4 are

$$\epsilon_4 = \epsilon_1 - \Delta\epsilon_{1\text{-}4} \tag{11a}$$

$$\sigma_4 = \sigma_1 - \Delta\sigma_{1\text{-}4} \tag{11b}$$

To analyze the range of minor cycles, such as 6–7, let

$$S = \frac{\Delta S_{6\text{-}7}}{2} \tag{12a}$$

$$\epsilon = \frac{\Delta \epsilon_{6\text{-}7}}{2} \tag{12b}$$

$$\sigma = \frac{\Delta \sigma_{6\text{-}7}}{2} \tag{12c}$$

Using the same procedure, $\Delta\epsilon_{6\text{-}7}$ and $\Delta\sigma_{6\text{-}7}$ are determined.

Once the stress and strain at Points 1 and 4 are obtained, the points of attachment of Loops A and B in Fig. 4 must be determined. In order to determine point of attachment of Loop A, let

$$S = \frac{S_1 - S_A}{2} \tag{13a}$$

$$\epsilon = \frac{\epsilon_1 - \epsilon_A}{2} \tag{13b}$$

$$\sigma = \frac{\sigma_1 - \sigma_A}{2} \tag{13c}$$

where $S_A = S_6$ in this case. Then substitute Eq 13 into Eqs 6 and 8 and obtain ϵ_A and σ_A. Then to find the point of attachment of Loop B, let

$$S = \frac{S_B - S_4}{2} \tag{14a}$$

$$\epsilon = \frac{\epsilon_B - \epsilon_4}{2} \tag{14b}$$

$$\sigma = \frac{\sigma_B - \sigma_4}{2} \tag{14c}$$

where $S_B = S_7$ in this case. Again substituting into Eqs 6 and 8, obtain ϵ_B and σ_B.

The bounds on mean stresses are then

$$\sigma_{oB} = \sigma_B - \frac{\Delta\sigma_{6\text{-}7}}{2} \tag{15a}$$

$$\sigma_{oA} = \sigma_A + \frac{\Delta\sigma_{6\text{-}7}}{2} \tag{15b}$$

Next, into Eq 2 substitute

$$\epsilon_a = \frac{\Delta\epsilon_{6\text{-}7}}{2} \tag{16}$$

and obtain N^*, the life for zero mean stress. Finally, substitute this N^* and σ_{oB} into Eq 3 to obtain the lower bound in life, N, for cycle 6–7–6′. Similarly, substitute N^* and σ_{oA} to get the upper bound on N.

Following a similar procedure for all cycles smaller than the major one then allows the P-M rule, Eq 4, to be employed once with all of the lower bound N values, and a second time with all of the upper bound N values, to obtain bounds on the calculated number of blocks (repetitions) to failure, B.

A computer program consistent with this was developed and used in the analysis of Helix and Felix.

References

[1] Palmgren, A., *Ball and Roller Bearing Engineering,* translated by G. Palmgren and B. Ruley, SKF Industries, Inc., Philadelphia, 1945, pp. 82–83.

[2] Miner, M. A., "Cumulative Damage in Fatigue," *Journal of Applied Mechanics,* American Society of Mechanical Engineers, Vol. 12, Sept. 1945, pp. A-159–164.

[3] Matsuishi, M. and Endo, T., "Fatigue of Metals Subjected to Varying Stress," presented to Japan Society of Mechanical Engineers, Fukuoka, Japan, March 1968; see also T. Endo et al., "Damage Evaluation of Metals for Random or Varying Loading," *Proceedings,* 1974 Symposium on Mechanical Behavior of Materials, Vol. 1, Society of Materials Science, Japan, 1974, pp. 371–380.

[4] *1986 Annual Book of ASTM Standards, Vol. 03.01,* American Society for Testing and Materials, Philadelphia, 1986, pp. 836–848.

[5] Manson, S. S., Freche, J. C., and Ensign, C. R., "Application of a Double Linear Damage Rule to Cumulative Fatigue," *Fatigue Crack Propagation, ASTM STP 415*, American Society for Testing and Materials, Philadelphia, 1966, pp. 384–412.
[6] Topper, T. H. and Sandor, B. I., "Effects of Mean Stress and Prestrain on Fatigue Damage Summation," *Effects of Environment and Complex Load History on Fatigue Life, ASTM STP 462*, American Society for Testing and Materials, Philadelphia, 1970, pp. 93–104.
[7] Watson, P. and Topper, T. H., "The Effects of Overstrains on the Fatigue Behavior of Five Steels," presented at the 1970 Fall Melting of the Metallurgical Society, American Institute of Mining, Metallurgical, and Petroleum Engineers, Cleveland, Oct. 1970.
[8] Dowling, N. E., "Fatigue Failure Predictions for Complicated Stress-Strain Histories," *Journal of Materials*, Vol. 7, No. 1, March 1972, pp. 71–87.
[9] Dowling, N. E., "Fatigue Life and Inelastic Strain Response Under Complex Histories for an Alloy Steel," *Journal of Testing and Evaluation*, Vol. 1, No. 4, July 1973, pp. 271–287.
[10] Kikukawa, M., Jono, M., and Song, J., "Cumulative Damage and Behavior of Plastic Strain Below Fatigue Limit," Third International Conference on Fracture, Munich, West Germany, April 1973.
[11] Koibuchi, K. and Kotani, S., "The Role of Cyclic Strain Behavior on Fatigue Damage under Varying Load," *Cyclic Stress-Strain Behavior—Analysis, Experimentation, and Failure Prediction, ASTM STP 519*, American Society for Testing and Materials, Philadelphia, 1973, pp. 229–245.
[12] Dowling, N. E., Brose, W. R., and Wilson, W. K., "Notched Member Fatigue Life Predictions by the Local Strain Approach," *Fatigue Under Complex Loading: Analyses and Experiments*, Vol. AE-6, Society of Automotive Engineers, Warrendale, PA, 1977, pp. 55–84.
[13] Heuler, P. "A Criterion for Omission of Variable Amplitude Loading Histories," *International Journal of Fatigue*, Vol. 8, No. 4, Oct. 1986, pp. 225–230.
[14] Morrow, J., Wetzel, R. M., and Topper, T. H., "Laboratory Simulation of Structural Fatigue Behavior," *Effects of Environment and Complex Load History on Fatigue Life, ASTM STP 462*, American Society for Testing and Materials, Philadelphia, 1970, pp. 74–91.
[15] Stadnick, S. J. and Morrow, J., "Techniques for Smooth Specimen Simulation of the Fatigue Behavior of Notched Members," *Testing for Prediction of Material Performance in Structures and Components, ASTM STP 515*, American Society for Testing and Materials, Philadelphia, 1972, pp. 229–252.
[16] Wetzel, R. M., "A Method of Fatigue Damage Analysis," Ph.D. thesis, Department of Civil Engineering, University of Waterloo, Ontario, Canada, 1971; see also Technical Report No. SR 71-107, Scientific Research Staff, Ford Motor Co., Dearborn, MI, Aug. 1971.
[17] Landgraf, R. W., Richards, F. D., and LaPointe, N. R., "Fatigue Life Predictions for a Notched Member Under Complex Load Histories," *Fatigue Under Complex Loading: Analyses and Experiments*, Vol. AE-6, Society of Automotive Engineers, Warrendale, PA, 1977, pp. 95–106.
[18] Socie, D. F., "Fatigue Life Prediction Using Local Stress-Strain Concepts," *Experimental Mechanics*, Society for Experimental Stress Analysis, Vol. 17, No. 2, Feb. 1977, pp. 50–56.
[19] Dowling, N. E., "Fatigue Failure Predictions for Complex Load Versus Time Histories," Section 7.4 of *Pressure Vessels and Piping: Design Technology—1982—A Decade of Progress*, S. Y. Zamrik and D. Dietrich, Eds., Book No. G00213, American Society of Mechanical Engineers, 1982; also in *Journal of Engineering Materials and Technology*, Vol. 105, July 1983, pp. 206–214, with Erratum, Oct. 1983, p. 321.
[20] Landgraf, R. W., "The Resistance of Metals to Cyclic Deformation," *Achievement of High Fatigue Resistance in Metals and Alloys, ASTM STP 467*, American Society for Testing and Materials, Philadelphia, 1970, pp. 3–36.
[21] Morrow, J., "Fatigue Properties of Metals," Section 3.2 of *Fatigue Design Handbook*, Society of Automotive Engineers, 1968; Section 3.2 is a summary of a paper presented at a meeting of Division 4 of the SAE Iron and Steel Technical Committee, 4 Nov. 1964.
[22] Edwards, P. R. and Darts, J., "Standardized Fatigue Loading Sequences for Helicopter Rotors (Helix and Felix), Parts 1 and 2," Reports Nos. TR84084 and TR84085, Royal Aircraft Establishment, Ministry of Defence, Farnborough, Hants, England (also ICAF Document No. 1442), 1984.
[23] Conle, A. and Landgraf, R. W., "Fatigue Analysis Program for Ground Vehicle Components," *Proceedings*, International Conference on Digital Techniques in Fatigue (SEECO '83), Society of Environmental Engineers, March 1983, London, pp. 1–28.
[24] Socie, D., Shifflet, G., and Berns, H., "A Field Recording System with Applications to Fatigue Analysis," *International Journal of Fatigue*, Vol. 1, No. 2, April 1979, pp. 103–111.
[25] Nachtigall, A. J., "Strain-Cycling Fatigue Behavior of Ten Structural Metals Tested in Liquid Helium (4K), in Liquid Nitrogen (78K), and in Ambient Air (300K)," NASA TN D-7532, National Aeronautics and Space Administration, Lewis Research Center, Cleveland, OH, 1974.

[26] Wirsching, P. H., "Computer Program for Local Strain Analysis—User Manual," Aerospace and Mechanical Engineering Dept., University of Arizona, Tuscon, AZ; report prepared under Grant 3-41-3 from NASA Lewis Research Center, Cleveland, OH, July 1982.
[27] Brose, W. R., "Fatigue Life Predictions for a Notched Plate with Analysis of Mean Stress and Overstrain Effects," Report No. 402, Department of Theoretical and Applied Mechanics, University of Illinois, Urbana, Sept. 1975; see also *Fatigue Under Complex Loading: Analyses and Experiments*, Vol. AE-6, Society of Automotive Engineers, Warrendale, PA, 1977, pp. 117–135.
[28] Conle, A. and Topper, T. H., "Fatigue Service Histories: Techniques for Data Collection and History Reconstruction," Paper No. 820093, Society of Automotive Engineers, 1983.
[29] *Fatigue Under Complex Loading: Analyses and Experiments*, R. M. Wetzel, Ed., Society of Automotive Engineers, Warrendale, PA, Vol. AE-6, 1977.

DISCUSSION

H. O. Fuchs[1] (*written discussion*)—The choice of helicopter spectra to demonstrate this refinement of rain-flow counting and notch strain analysis deserves plaudits and warnings. Plaudits because these spectra provide good tests of the method, as pointed out by the authors. Warnings because this analysis, although it agrees with tests on notched coupons, would not agree at all with tests on helicopter rotor parts. Such parts fail unless they are properly shot peened[2] and survive if properly peened.

Notch strain analysis predicts the formation of cracks in the notch roots but cannot predict whether the cracks will propagate or will be arrested. Helicopter rotor parts survive because compressive self stresses below the surface arrest or delay the growth of cracks. A simplified analysis of crack arrest can be done if the threshold stress intensity factor range is assumed to be zero tensile range. This eliminates the need to know crack depth and geometry factors. Only the profiles of load stress and of self stress need to be known. A crack growth analysis, which is much more complex, will be necessary only if many loads in the spectrum exceed the limit for crack arrest. Even then the simplified analysis of crack arrest provides a useful reference point.

Compared to the importance of self stress profiles in helicopter rotors, the effect of mean stresses on crack initiation can be neglected in a simplified analysis.

N. E. Dowling and A. K. Khosrovaneh (*authors' closure*)—Initial residual stresses from shot peening or other intentional or unintentional causes are indeed sometimes an important factor in determining fatigue life. Once local plastic deformation occurs at a stress raiser, the residual stress is altered, and the new value is insensitive to the initial value. As a consequence, the initial residual stress is important only where there are no high loads during service that cause local plastic deformation. Note that a critical feature of the local strain approach is that it predicts the residual stress changes, and the resulting effects on fatigue life, due to each loading event that causes local plastic deformation.

The local strain approach as described in the paper can be extended to include the effect of initial residual stress as follows: Let $S(t)$ be the actual time history of nominal stress, and let σ_{res} be the initial residual stress at a stress raiser, k_t. The effect of the residual stress will be included by replacing the actual nominal stress history with a fictitious one, $S'(t)$, where

$$S'(t) = S(t) + \sigma_{res}/k_t$$

[1] Mechanical Engineering Department, Stanford University, Stanford, CA 94305.

[2] "Fatigue Fracture of a Spindle for a Helicopter Blade because of Incomplete Shot Peening Prior to Plating," *Metals Handbook*, 8th ed., Vol. 10, *Failure Analysis and Prevention*, American Society for Metals, Metals Park, OH, 1975, pp. 115–117.

However, caution is needed in that net section yielding does not occur when $S'(t)$ exceeds the critical value; rather, this is controlled by the actual $S(t)$. The equivalent but more direct approach could also be employed of simply starting the stress-strain modeling at $\sigma = \sigma_{res}$ rather than at $\sigma = 0$.

Note that the local strain approach is intended only to predict the initiation of an easily detected crack of size on the order of 1 mm. Analysis of crack growth as affected by residual stresses would require a thoughtful application of linear-elastic fracture mechanics. The procedure outlined by the discusser and described in more detail in some of his publications seems to us to contain worrisome simplifying assumptions, and also to lack support outside the discusser's own publications.

Note that it is the intent of this paper to describe a methodology that has broad application, not only to helicopter components other than rotors, but also to components of other types of vehicles, machines, and structures. With this intent in mind, analysis of initial residual stress is viewed as a detail that can be added when needed, but not as a matter of overriding importance as implied by the discusser. Also, specifically concerning helicopter rotors, it is noteworthy that shot peening is a common practice, but not a universal one, and that its beneficial effect may or may not be permanent, depending on the service loading.

Paul S. Veers,[1] *Steven R. Winterstein,*[2] *Drew V. Nelson,*[3] *and C. Allin Cornell*[4]

Variable-Amplitude Load Models for Fatigue Damage and Crack Growth

REFERENCE: Veers, P. S., Winterstein, S. R., Nelson, D. V., and Cornell, C. A., "**Variable-Amplitude Load Models for Fatigue Damage and Crack Growth,**" *Development of Fatigue Loading Spectra, ASTM STP 1006,* J. M. Potter and R. T. Watanabe, Eds., American Society for Testing and Materials, Philadelphia, 1989, pp. 172–197.

ABSTRACT: Load models for fatigue analysis and testing are tailored to the level of complexity required for the application. Random variable models are developed and applied to analyses in which load sequence effects can be neglected. Conventional narrow-band load peak and range distributions are applied to crack initiation and growth. It is shown that narrow-band load models provide useful, conservative life estimates for general Gaussian loadings. Distributions of significant peaks and ranges for wide-band loadings are developed empirically through simulations with racetrack filtering. An efficient "sequential" simulation technique is introduced for continuous generation of both narrow- and wide-band random loads. Based on a simplified crack closure model, simulations of crack growth suggest that sequence effects are most influential when any or a combination of the following are present: larger ratios of crack opening stress to maximum applied stress, lower values of applied tensile mean stress, smaller values of yield stress and crack growth coefficient. When sequence effects are present, the regularity of the spacing between tensile overloads can be important. In particular, assumption of regularly spaced overloads can be nonconservative.

KEY WORDS: random loading, crack growth, fatigue (materials), load sequence effects, simulation, load models, wide-band loading, narrow-band loading, loading statistics, rainflow method, racetrack filtering, crack closure, bandwidth, testing

The rates at which engineering materials accumulate damage, either in the form of crack growth or the less quantifiable "damage" of crack initiation, are generally defined in terms of constant-amplitude loadings. However, service loads on most fatigue-susceptible structures are rarely of constant amplitude. Variable-amplitude loads can be described by an actual sequence of peaks and troughs or by a limited number of statistics that reflect, on average, various load characteristics. The statistical description may be both more efficient and more consistent with the extent of knowledge of the loading. Our purpose here is to find a minimally sufficient set of load statistics for various fatigue applications and to illustrate how they can be used to estimate life. Load models and analysis techniques are provided here (1) for analytical life estimates that ignore sequence effects, and (2) for numerical life

[1] Member of the technical staff, Applied Mechanics Div. 1524, Sandia National Laboratories, Albuquerque, NM 87185; and research assistant, Mechanical Engineering Department, Stanford University, Stanford, CA 94305.

[2] Acting assistant professor, Civil Engineering Department, Stanford University, Stanford, CA 94305.

[3] Associate professor, Mechanical Engineering Department, Stanford University, Stanford, CA 94305.

[4] Research professor, Civil Engineering Department, Stanford University, Stanford, CA 94305.

estimates that include sequence effects, based on a new load simulation method, which reflects the likelihood of various load sequences.

Background

The type of fatigue analysis that is chosen depends on the nature of the fatigue process; whether it is "crack initiation" or crack growth to failure. Crack initiation life estimates based on the Palmgren-Miner cumulative damage summation are still the most prevalent form of fatigue analysis. If localized plasticity in the material is minimal, damage accumulation is governed by the means and amplitudes of stress cycles, usually rainflow counted, and the sequence of load applications does not affect the calculations. Random load models for this type of analysis have been explored often [*1–4*]. Similar models are used here to obtain closed-form "sequenceless" crack growth results (that is, ignoring sequence effects). Extensions are also derived here to account for load bandwidth through racetrack filtering.

In linear elastic fracture mechanics, crack growth under nominally elastic stresses is predicted by the stress intensity factor range, ΔK, through the now well-established da/dN versus ΔK curves. The sequence of load applications has been shown to be quite important in certain cases [*5,6*]. This has been tied to the fact that the crack opening stress increases when a large tensile load is applied [*7*]. The crack growth is then governed by the range from crack opening stress to local maximum stress [*8–10*]. However, sequenceless crack growth analysis often produces nearly the same prediction as more complex models that explicitly include sequence-induced changes in crack opening stress [*11*]. Parametric crack growth simulations are used here to offer guidance as to when these simpler sequenceless predictions will be sufficiently accurate for practical purposes.

Low cycle fatigue, where there is considerable localized plasticity, has its own special traits. If the plasticity is nonuniform, states of residual stress are continually changing and the sequence of loading has a noticeable effect on the resulting fatigue damage. Such cases will not be studied in this paper.

Load Models

As just suggested, one common way to represent variable amplitude loads is to list the precise sequence of peaks and valleys in a sample block. This sample may be derived either from actual load measurements or from some load simulation technique. The sample block is used in both analysis and testing by repeating the block until failure. This method has the disadvantage that only a single sample of all possible load sequences is produced. In addition, an artificial sequence effect may be introduced by the periodic repetition of the largest loads in the sample block. The potential for errors in life prediction due to block structure is examined here.

Another way of specifying a random loading is through a "frequency of exceedance" diagram, which defines the number of times within a block that the load will exceed any given level. This is equivalent to describing the peaks of a loading as a random variable. Simple random variable models of various useful load parameters (peaks, ranges, mean stresses, etc.) are shown here. These models permit efficient sequenceless crack growth analysis by summing contributions from all cycles at a specified stress level, avoiding the need for cycle-by-cycle integration. Life predictions from this simple analysis technique are compared here with ASTM variable-amplitude test results [*11*].

These random variable models provide no information, however, on load sequences. To retain a complete description of both load peaks and ranges and the possible load sequences, the load must instead be described through a random process model [*4*]. However, the full specification of a random process load model is often unnecessary for fatigue analysis, which is most sensitive to the overall behavior of load peaks and troughs. Minimal load statistics are suggested here to describe this dynamic behavior. An efficient "sequential" load simulation method is also presented to preserve these important dynamic aspects, while avoiding the computational expense of conventional random process simulation. This method is used to simulate load sequence effects on crack growth and to study the adequacy and limitations of simpler, sequenceless predictions.

Crack Growth Model

For the purpose of these studies, crack growth is predicted with a simple model that reflects crack closure effects without the detailed stress analysis needed to determine the precise crack opening stress level. A brief description of the model is provided here; a more detailed description is given in Ref *12*.

When a tensile load is applied to a cracked body, the stress concentration at the crack tip produces a zone of plastic deformation with a radius that depends on the magnitude of the stress intensity factor, K, the yield stress of the material, S_y, and the plane strain constraint factor, γ ($\gamma = 1$ for plane stress and $\gamma = 3$ for plane strain). A "reset stress," S_r, is defined here as the stress necessary to produce a plastic zone that extends beyond the previous maximum extent of the crack tip plastic zone (similar to the Willenborg retardation model [*13*]). The crack opening stress is then assumed to be a fraction, q, of the reset stress, $S_{op} = qS_r$.

Based on this approximate crack opening stress, an effective stress range, S_{eff}, and stress intensity factor, ΔK_{eff}, can be defined for each cycle

$$\Delta K_{eff} = Y(a)\sqrt{\pi a}\,\Delta S_{eff} \tag{1a}$$

$$\Delta S_{eff} = \begin{cases} (S_{max} - qS_r) & S_{max} > qS_r,\ S_{min} < qS_r \\ (S_{max} - S_{min}) & S_{max} > qS_r,\ S_{min} \geq qS_r \\ 0 & S_{max} \leq qS_r \end{cases} \tag{1b}$$

in which S_{min} is the local minimum stress, a is crack length, and $Y(a)$ is a shape factor. The crack growth rate is assumed to depend on ΔK_{eff} in a way that is analogous to Paris' law

$$\frac{da}{dN} = C\Delta K_{eff}^{b} \tag{2}$$

No threshold effective stress intensity range is included.

The basic crack growth rate constants C_0 and b are estimated from constant-amplitude tests with $R = 0$ in which the relationship between crack growth rate and total stress intensity range, ΔK, is given by

$$\frac{da}{dN} = C_0\Delta K^{b} \tag{3}$$

The conversion from C_0 to C is

$$C = C_0(1 - q_0)^{-b} \tag{4}$$

where q_0 is the crack opening stress ratio at $R = 0$. The crack growth exponent, b, is unchanged.

Several studies have shown q to be a function of stress ratio, R, as well as maximum stress [*8,14,15*]. Here, for the sake of simplification, q is taken as a function of R alone [*12*]

$$q = q_0\left(1 - \frac{R}{R_0}\right) \tag{5}$$

in which R_0 is a constant that equals the (negative) stress ratio at which q becomes zero.

Values of q_0 for zero-to-maximum loading have been reported ranging from 0.2 [*16*] to 0.5 [*7*]. The value of q_0 can have a substantial influence on the estimated crack growth life, especially when a loading is nearly constant amplitude with occasional tensile overloads. But when the variations in load amplitude are less distinct, q_0 can be fixed at a midrange value of about 0.35, as a simplification that recognizes realistic uncertainties in knowledge of q_0 while preserving reasonable accuracy [*9,12*]. When the loading is irregular, R is taken to be the ratio of the lowest minimum to the highest maximum within a block. Therefore, q remains constant within the block [*10,17*].

Values of R_0 between -2 and -5 cover most of the reported dependence of q on R [*14,15,18*]. This dependence is minimal when $R_0 < -5$, which will minimize the effect on the model of crack growth acceleration due to compressive stresses. Different choices of R_0 have a minor effect on crack growth predictions except at relatively large negative stress ratios (R near R_0).

ASTM and SAE Test Series

To check the applicability of this model to analyze crack growth under irregular loading, predicted crack growth lives are compared with published test results for several irregular load histories.

Fighter aircraft loadings have been published by ASTM in Ref *11*, along with the resulting crack growth lives of 2219-T851 aluminum center-cracked tension specimens. The loads were not taken directly from measurements, but were derived from power spectral densities (PSDs) estimated from actual flight data [*19*]. The load histories were divided into three types: Air-to-Air (AA), Air-to-Ground (AG), and Instrumentation-and-Navigation (IN). From a combination of these three, a fourth type of loading, called Composite Fighter (CF), was generated. All of these loadings have a tensile mean with relatively frequent compressive loads of 15 to 25% of the maximum tensile load.

A Society of Automotive Engineers (SAE) sponsored test series [*20*] attempted to model a realistic situation for ground vehicles. The tests used keyhole notched plate specimens and monitored "crack initiation" and subsequent growth to fracture. Two types of steel were used: Manten and RQC-100. The portion of the test from crack initiation to failure is used here to test the ability of the proposed crack growth model to predict test results.

The SAE load histories are sample measurements taken from three different ground vehicle components. The SP history is a record of the load in a vehicle suspension component. This loading has a large compressive mean. The BR history, measured on a mounting bracket, is an almost classic narrow-band random vibration with near zero mean stress. The TR history is a torque measurement on the transmission of a front-end loader. Many of the tests in the SAE series included substantial plasticity extending well beyond the notch root. Since the proposed model is limited to linear elastic fracture mechanics, those tests were not considered here.

TABLE 1—*Material constants for the ASTM and SAE test series.*

Material	Specification	Yield Stress, ksi	b^a	C_0^a
Aluminum	2219-T851	50	3.64	8.4×10^{-10}
Steel	manten	48	3.43	8.6×10^{-11}
Steel	RQC-100	95	3.25	1.5×10^{-10}

[a] b, C_0 for crack growth rate in inches/cycle and stress intensity range in ksi$\sqrt{\text{in}}$.

Comparison of Predictions with Test Results

The only material properties required for the model are the crack growth rate constants, C_0 and b, and the monotonic yield stress, S_y. These are listed in Table 1 for the ASTM and SAE test series materials. The remaining parameters (γ, q_0, and R_0) are estimated for the ASTM test series from the crack tip plastic zone analysis of Newman [*21*]: $\gamma = 2.3$, $q_0 = 0.3$, and $R_0 = -3.5$. For the SAE test series, no estimates of these parameters were available so the midrange values are used: $\gamma = 2.0$, $q_0 = 0.35$, and $R_0 = -3.5$.

The predicted number of cycles to grow from initial to final crack lengths are plotted against the number of test cycles for the ASTM test series in Fig. 1. As shown in the figure, there is a tendency for the model to overestimate life at lower stress levels (corresponding to large numbers of cycles N_{test}). This is consistent with other predictions for these data and has been attributed [*22*] to insufficient $R = 0$ crack growth data at low stress intensity levels.

Predictions of the number of blocks of loading to failure for the SAE test series are shown in Fig. 2. This figure shows a great deal more scatter than the ASTM test series. The major source of variability can be found by comparing the scatter in prediction ratios (ratios of

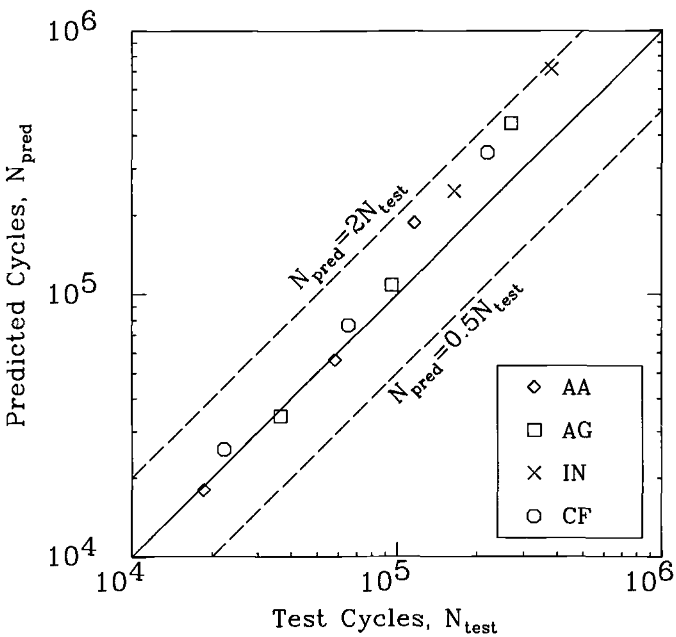

FIG. 1—*Predicted cycles to failure using the simplified crack closure model versus test cycles to failure for the ASTM test series.*

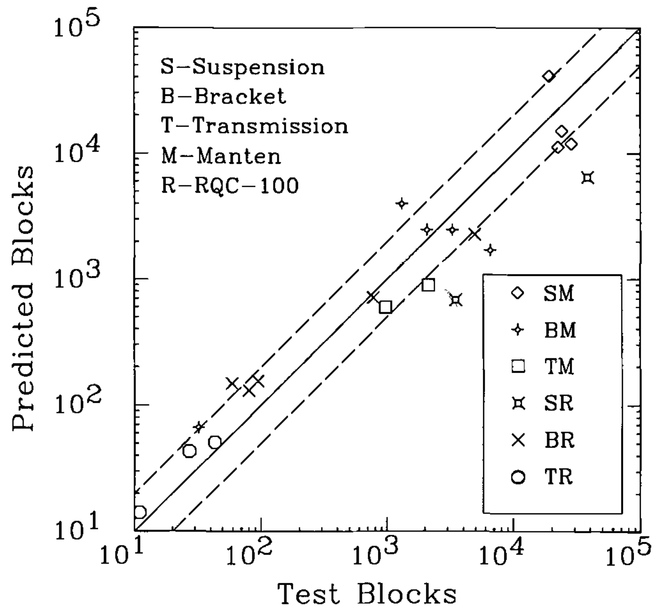

FIG. 2—*Predicted load blocks to failure using the simplified crack closure model versus test load blocks to failure for the SAE test series.*

predicted life to test life) within each load/material grouping to the prediction ratios of all the tests. The groupings with the most replicates are: four tests with the SP loading of Manten steel, five tests with the BR loading of Manten steel, and five tests with the BR loading of RQC-100. The coefficients of variation (standard deviation divided by the mean) of the prediction ratios for each of these three groups are 0.90, 0.76, and 0.53, respectively. The coefficient of variation (COV) of prediction ratios for the entire SAE test series is 0.76. This indicates that the variability from specimen to specimen within a grouping is the source of most of the scatter in Fig. 2.

Both test series define the load history by repeating a single block of sequential load peaks and valleys. A fatigue test is conducted by applying the load block in a continuous loop fashion until either the specimen fails or the test is suspended. The block structure gives well-defined minimum and maximum stress levels that repeat at time intervals equal to the block length. In an actual random loading, by contrast, the maximum and minimum stress levels in any given block of time will be random variables, as will the time between these local extremes.

Implications of Block Loading

The ASTM AA load history is an example of block loading. The tabulated AA block is composed of 1300 peak-valley pairs produced by the simulation method outlined in Ref *19*. One hundred more statistically equivalent blocks have been simulated here using the same procedure and input data. The highest peak in the tabulated AA block is 92.5% of design limit stress (DLS), while the highest peak in each of the 100 simulated blocks varies between 87% and 115% of DLS with a mean of 101% of DLS. Using the foregoing model, the crack growth life that would result if each of these blocks were used repeatedly is predicted. These are plotted in Fig. 3 versus the peak load in the block showing the correlation between peak

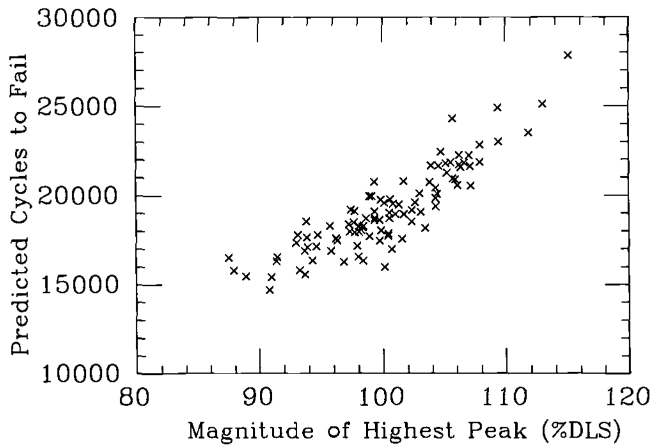

FIG. 3—*Predicted life versus highest peak in the simulated AA load block for repeated block loading.*

load and predicted life for block loading. The life estimates have a mean of 19 200 cycles and a COV of 0.13. Statistics of this peak load are available from random vibration theory [*4*]; however, they depend on the assumed block length.

If, instead of repeating one simulated block, the statistically equivalent AA loading is simulated continuously (and these crack growth simulations are repeated many times), the mean life is 20 400 cycles with a COV of just 0.03. This suggests that the artificial block structure is responsible for a four fold increase in the uncertainty (COV) of the life estimate. Simulations of the other ASTM load histories show similar results. These estimates neglect material variability, which can be much greater than load-induced variability (as can be seen from the previous section). However, it is especially important in testing that the loading be representative of the actual environment so that the resulting test lives do not contain an important and possibly nonconservative bias due solely to the block structure.

The benefit of block loading is to simplify the testing or analysis by specifying a finite and reproducible set of peaks and valleys. Alternatively, the load may be more simply characterized through a few select statistics, described later. We also include a sequential simulation technique to efficiently create a sequence of load peaks and valleys without block structure, for testing as well as analysis. Our prime focus is on modeling stationary Gaussian loads. Nonstationary and non-Gaussian aspects can be easily included, for example, by applying functional transformations to these models [*12,23,24*].

Narrow-Band Load Models and Sequenceless Fatigue Analysis

Loads from structural vibrations are often nearly sinusoidal, producing cycles with roughly constant mean, m_X, and slowly changing amplitude, A (Fig. 4*a*). Because such loads have significant contributions from only a narrow band of frequencies, they are often referred to as "narrow-band" loads. Narrow-band load models have the advantages of (1) simplicity, requiring only a single parameter: the load standard deviation, σ_X, and (2) conservatism, that is, narrow-band models tend to overpredict fatigue crack growth and damage accumulation (see discussion of bandwidth effects below). Simple analytical fatigue results are shown in this section and compared with test data for these narrow-band load models.

For narrow-band loads, the fraction of cycles with amplitudes between A and $A + dA$ is $p(A)dA$, in which $p(A)$ is the following probability density function (PDF)

$$p(A) = \frac{A}{\sigma_X^2} e^{-A^2/2\sigma_X^2} \quad (A \geq 0) \tag{6}$$

This is the well-known Rayleigh PDF model [1–4]. Corresponding peaks and troughs are assumed to occur at levels $S_{max} = m_X + A$ and $S_{min} = m_X - A$, producing a range $R = 2A$. Fatigue damage accumulation, whether related to peaks or ranges, may thus be related to cycle amplitude and Eq 6 used to calculate the average fatigue or crack growth under narrow-band loads.

Consider, for example, a Palmgren-Miner analysis in which a cycle with range R_i causes damage cR_i^b. The total damage in N cycles, D_N, can be calculated in one of two ways: (1) summing contributions cycle by cycle, so that $D_N = c\Sigma_i R_i^b$; or (2) summing average contributions to D_N from each possible amplitude level, A. In the latter case, in N cycles one expects $N \cdot p(A)dA$ amplitudes between A and $A + dA$ so that

$$D_N = \int_{A=0}^{\infty} c(2A)^b \,[N\,p(A)dA] = cN\,(2\sqrt{2}\sigma_X)^b\,(b/2)! \tag{7}$$

Thus, the average value of $c\Sigma_i R_i^b$ can be calculated from the random variable model (Eq 6) without the need for cycle-by-cycle summation. Actual D_N values will vary negligibly from this average in most high-cycle (large N) cases of practical interest. Equation 7 is a well-

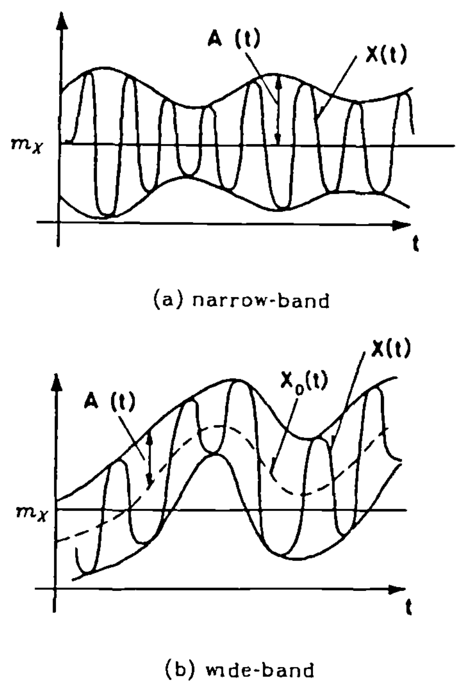

FIG. 4—*Schematic of (a) narrow-band and (b) wide-band loadings showing the range amplitude,* A, *and mean,* X_o (from Ref 4).

known result for fatigue under random loads, originally obtained by Miles [1]. If $b/2$ is not an integer, $(b/2)!$ can be evaluated through the widely tabulated Gamma function.

This random variable model can also be applied to crack growth, if sequence effects are neglected and the crack growth equation is a separable function of stress and crack size. For example, a sequenceless crack growth model is formed by defining the effective stress range as [9]

$$\Delta S_{\text{eff}} = \begin{cases} (1 - q_0)S_{\max} & S_{\min} < q_0 S_{\max};\ S_{\max} > 0 \\ S_{\max} - S_{\min} & S_{\min} > q_0 S_{\max};\ S_{\max} > 0 \\ 0 & S_{\max} < 0 \end{cases} \tag{8}$$

A crack growth equation such as Eq 2 can then be integrated, after separating stress and crack length terms

$$\int_{a_0}^{a_f} \frac{da}{C(Y(a)\sqrt{\pi a})^b} = \sum_{i=1}^{N} \Delta S_{\text{eff},i}^b \tag{9}$$

in which N is the number of cycles needed for crack growth from a_0 to a_f.

To apply the random variable model of Eq 6 to this sequenceless crack growth model, we write ΔS_{eff} as a function of amplitude and mean stress, $\Delta S_{\text{eff}}(A,m_X)$, replacing $S_{\max}$ and $S_{\min}$ in Eq 8 with $m_X \pm A$. The average value of the sum in Eq 9 is then calculated as in the Palmgren-Miner case

$$\int_{a_0}^{a_f} \frac{da}{C(Y(a)\sqrt{\pi a})^b} = N \int_{A=0}^{\infty} [\Delta S_{\text{eff}}(A,m_X)]^b\, p(A)\, dA \tag{10}$$

This result may be solved for (an average value of) N. While numerical integration is generally required, this integration is usually much faster than cycle-by-cycle crack growth calculation.

For loads with arbitrary bandwidths, the narrow-band model in Eq 6 remains useful when a rough (and generally conservative) estimate of life is required. For example, analytical life estimates using the Rayleigh PDF are shown in Fig. 5 for the ASTM test series (which are not narrow band). The narrow-band (Rayleigh) life estimates are conservative with respect to predictions using actual (tabulated) test loads. The difference, in this case, is less than a factor of two. Because they ignore retardation due to tensile peak stresses, these narrow-band, sequenceless life estimates are also conservative with respect to analytical predictions that include sequence effects (Fig. 1). Less conservative estimates may be formed from the methods described in the next section, which include a measure of load bandwidth.

Bandwidth Effects and Racetrack Filtering

As the load bandwidth increases, narrow-band models ignore two important effects: (1) the number of small-amplitude, high-frequency oscillations grows, so that actual peak and range values are less, on average, then the narrow-band model predicts; and (2) life estimation from constant-amplitude results requires identification of the larger amplitude, lower frequency, "global" or "overall" cycles formed by the multiple peaks and troughs that are most damaging [25]. The first effect leads to conservative errors in the narrow-band

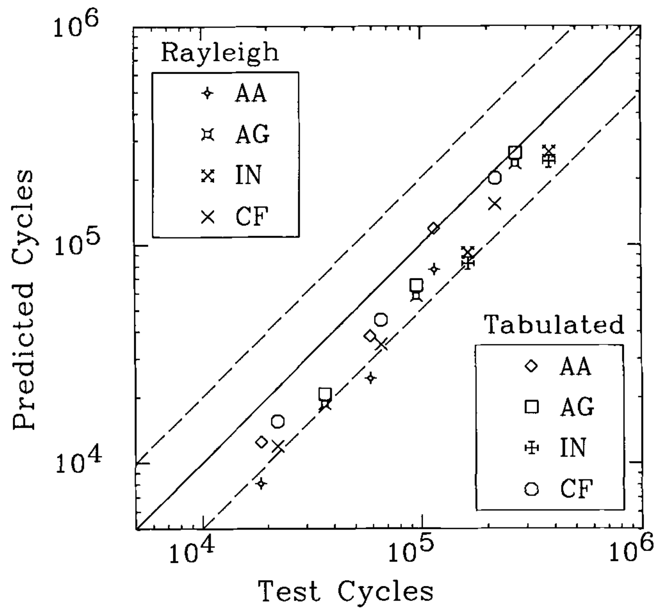

FIG. 5—*Predicted cycles versus test cycles using the tabulated ASTM load peaks and using the Rayleigh, narrow-band, approximation for load peaks (with the sequenceless crack growth model of Eq 8).*

model while the second effect introduces nonconservatism. Significantly, the first effect tends to dominate so that the narrow-band load model is generally conservative. Analytical results are shown here to correct for the first effect (deviations of the actual distribution of local peaks and ranges from the Rayleigh model). Empirical results account for the second effect (with global cycles identified by racetrack filtering).

Bandwidth Measures and Distributions of Local Mean and Amplitude

The dynamic behavior of the load is conveniently summarized by its power spectral density (PSD), $G(f)$, defined so that $G(f)\,df$ gives the contribution to load variance or "power", σ_X^2, due to frequency components between f and $f + df$. (For long load histories, $G(f)$ may be assumed proportional to the squared amplitude of the load history's Fourier transform.) Various useful measures of load bandwidth can be calculated as weighted averages of $G(f)$ [26]. For example, the spectral moments, $\lambda_n = \int_0^\infty f^n G(f)\,df$, can be combined to form the quantity

$$\alpha_n = \frac{\lambda_n}{\sqrt{\lambda_0 \lambda_{2n}}} \tag{11}$$

Various measures follow from different choices of n. In general, α_n is a unitless quantity varying between zero (wide-band limit) and unity (narrow-band limit). For relatively narrow bandwidths, the α_n values are roughly proportional: $\alpha_n \approx n\alpha_1 \approx n\alpha_2/2$. . . .

Fatigue studies typically rely on the "regularity" factor, α_2, because it represents the ratio f_0/f_p between the rate of mean-level upcrossings, $f_0 = \sqrt{\lambda_2/\lambda_0}$, and the rate of peaks, $f_p = \sqrt{\lambda_4/\lambda_2}$. This interpretation is useful in estimating α_2 from a (Gaussian) load history, that is, as the observed ratio of the number of upcrossings of the mean load level to the number of peaks. A more "regular" load, which is more nearly sinusoidal or narrow band, has fewer peaks per upcrossing of its mean. In the narrow-band limit, there is a one-to-one correspondence and $\alpha_2 = 1$. Alternatively, Eq 11 can be used to estimate α_2 (or other α_n values) if $G(f)$ is known or estimated from data. Lesser values of n are useful in reducing sensitivity of α_n to high-frequency load behavior that does not significantly affect fatigue.

The value of α_2 can be used [4] to estimate the distributions of the mean, X_0, and amplitude, A, of a load cycle (Fig. 4*b*). Their joint PDF is taken as $p(A,X_0) = p(A)p(X_0)$, in which the individual PDFs of $p(A)$ and $p(X_0)$ are

$$p(A) = \frac{A}{(\alpha_2\sigma_X)^2} \exp\left[-\frac{A^2}{2(\alpha_2\sigma_X)^2}\right] \quad (A \geq 0) \tag{12}$$

$$p(X_0) = \frac{1}{\sqrt{2\pi(1-\alpha_2^2)}\sigma_X} \exp\left[-\frac{1}{2}\left(\frac{X_0 - m_X}{\sqrt{1-\alpha_2^2}\sigma_X}\right)^2\right] \tag{13}$$

In the narrow-band limit as α_2 approaches unity, $p(A)$ reduces to the conventional Rayleigh model (Eq 6) and X_0 becomes fixed at the mean level m_X. If fatigue damage or crack growth is related to the peak, $S_{max} = X_0 + A$, and trough, $S_{min} = X_0 - A$, of each local cycle, Eqs 12 and 13 can be used to form sequenceless life predictions by simple integrations analogous to Eqs 7 and 10

$$\int_{a_0}^{a_f} \frac{da}{C(Y(a)\sqrt{\pi a})^b} = N \int_{A=0}^{\infty} \int_{X_0=-\infty}^{\infty} [\Delta S_{eff}\,(A,X_0)]^b\, p(A)p(X_0)\, dA\, dX_0 \tag{14}$$

As the load bandwidth increases, numerous small-amplitude cycles can obscure the more important, slower load cycles. If these overall cycles are neglected, fatigue damage can be significantly underestimated [25]. Thus, the distributions of (all) peaks and valleys in Eqs 12 and 13 may not always be directly applicable to fatigue analysis. Both small excursions and overall cycles can be identified through rainflow counting, but statistics of rainflow counted ranges may be difficult to predict analytically. Also, rainflow counting does not preserve the sequence of the load peaks. Racetrack filtering [27,28] provides an alternative by removing small-amplitude ranges from the time series without disturbing fatigue damaging characteristics, for example, the sequence, mean, or range of the significant load excursions. The distribution of racetrack filtered ranges, and hence fatigue damage rates, is estimated here.

Load Statistics after Racetrack Filtering

Racetrack filtering was created to condense load histories for analysis or testing. To visualize the method, suppose that a load history, as shown by the lower set of peaks and valleys in Fig. 6, is converted into a "racetrack" by offsetting its profile by a selected "track width" or threshold level, R_{th}. Imagine that a race car driver wishes to traverse the course from west to east making as few turns as possible involving a change in direction from northerly to southerly, or vice versa. The resulting path is the dashed line in Fig. 6. Peaks and valleys on the original segment of loading, corresponding to locations where such turns are made, are identified by letters. For the value of R_{th} used in Fig. 6, a condensed segment

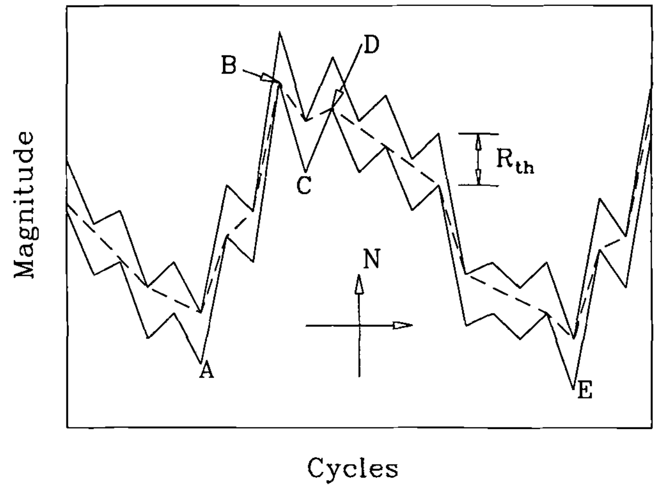

FIG. 6—*Schematic of racetrack filtering of a segment of loading.*

of loading is created by a line from Valley A to Peak B to Valley C to Peak D to Valley E. Smaller load fluctuations are "filtered" out. Peaks and valleys that were separated by smaller ranges in the original loading become adjacent, creating larger local ranges such as the one from D to E. If a sufficiently high R_{th} is used, the relatively few local ranges remaining after racetrack filtering converge to the largest overall ranges defined by rainflow counting and will produce nearly equivalent damage in many, but not all, cases [*27*]. Because it preserves the sequence of important loads, racetrack filtering can be followed by an analysis that either includes sequence effects or not.

Because racetrack filtering makes the load less irregular, the post-filtered regularity, $\hat{\alpha}_2$, is greater than the original regularity, α_2 (the circumflex (^) is used here to denote post-filtered parameters). Significantly, Eqs 12 and 13 can give useful models of the post-filtered stress cycles, if used with the modified regularity $\hat{\alpha}_2$. This is illustrated in Fig. 7. Figure 7*a* shows the cumulative distribution function (CDF) of tabulated peaks for the ASTM AA, AG, and IN load cases, which have been filtered [*11*] at R_{th} levels of $0.61\sigma_X$, $0.67\sigma_X$, and $1.33\sigma_X$, respectively. The figure shows these distributions of peaks to be well represented by theoretical results (Eqs 12 and 13) based on the $\hat{\alpha}_2$ rather than α_2. Figure 7*b* shows similar agreement between predicted and tabulated distributions of load *ranges* in these cases. The analytical predictions here use a Rayleigh distribution model for all load ranges, that is, $R \approx 2A$ has PDF estimated from Eq 12 with σ_X replaced by $2\sigma_X$. This Rayleigh model is then truncated below the threshold level, R_{th}, to reflect post-filtered ranges. These analytical approximations become conservative as the filtering level increases.

To apply these results in practice, it is useful to estimate $\hat{\alpha}_2$ directly from original load statistics. This avoids the need to actually filter each new load case that arises. To establish such $\hat{\alpha}_2$ estimates, simulated loads with various spectral shapes (Fig. 8 with all combinations of parameters in Table 2) have been racetrack filtered. This provides results for nearly 400 different spectral shapes with a broad range of bandwidths.

One may anticipate that the original load regularity α_2 could be used to reliably estimate $\hat{\alpha}_2$. However, rather poor correlation between α_2 and $\hat{\alpha}_2$ was found from the simulation study (Fig. 3.8 of [*12*]). The parameter, α_1 (Eq 11 with $n = 1$), of the original load was found to better predict $\hat{\alpha}_2$. This reflects that α_1 is less sensitive than α_2 to high-frequency, low-amplitude

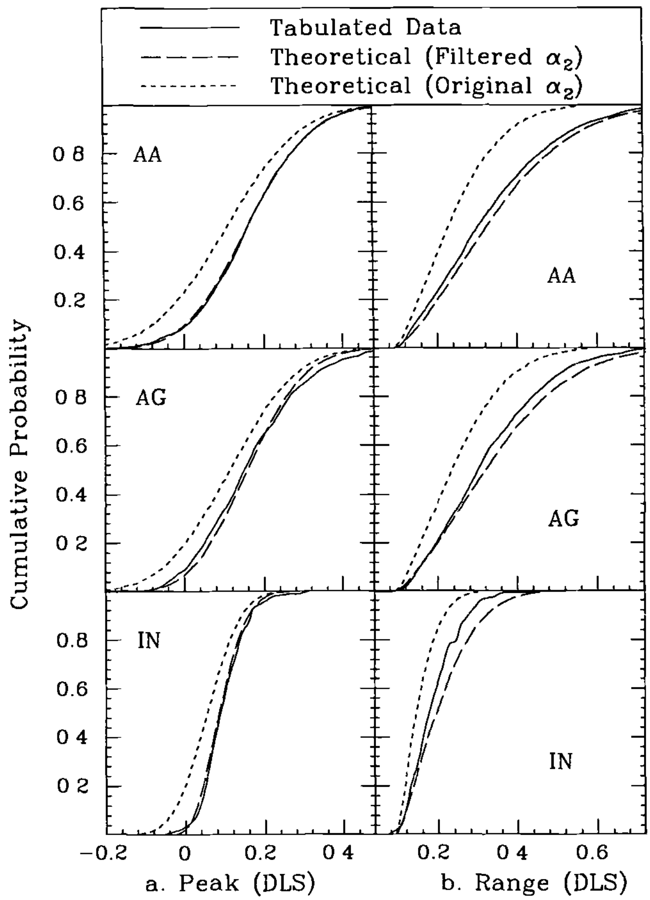

FIG. 7—*Comparison of actual CDFs to the theoretical results for (a) peaks and (b) ranges with and without adjusting α_2 for racetrack filtering.*

contributions that racetrack filtering removes. Correlation is also enhanced by introducing "irregularity" factors, z_n, related to α_n as follows

$$z_n = \frac{\sqrt{1 - \alpha_n^2}}{\alpha_n} \quad n = 1,2, \ldots \tag{15}$$

As opposed to α_n, z_n is a more direct bandwidth measure, steadily increasing with bandwidth from $z_n = 0$ for perfectly narrow-band loads.

Figure 9 shows the relationship between pre- and post-filtered irregularities, $z_1 = \sqrt{1 - \alpha_1^2}/\alpha_1$ and $\hat{z}_2 = \sqrt{1 - \hat{\alpha}_2^2}/\hat{\alpha}_2$, for various thresholds. Also shown is a linear fit between z_1 and $\hat{z}_2$

$$\hat{z}_2 = Mz_1 + B \tag{16a}$$

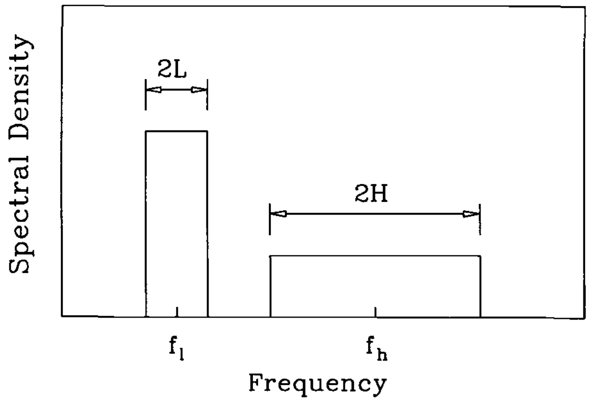

FIG. 8—*Spectral densities used in the simulations with racetrack filtering, showing the parameters that define the spectral shape* (L, H, f_l, f_y). V_l *and* V_h *are the areas of the respective boxes.*

in which

$$M = 1.7 - 0.8 \left(\frac{R_{th}}{\sigma_X}\right) \tag{16b}$$

$$B = 0.18 \left(\frac{R_{th}}{\sigma_X}\right)^2 - 0.36 \left(\frac{R_{th}}{\sigma_X}\right) \tag{16c}$$

There is low correlation between z_1 and $\hat{z}_2$ when $R_{th} \geq 1.5\sigma_X$, but for such high thresholds the filtered processes are essentially narrow-band ($\hat{z}_2 < 0.4$, $\hat{\alpha}_2 > 0.93$) regardless of the original regularity.

Finally, to completely account for the effects of racetrack filtering, we must also estimate the post-filtered rate of peaks (and of ranges), $\hat{f}_p$. Figure 10 shows the average reduction in the rate of peaks, $\hat{f}_p/f_p$, due to filtering at various thresholds, R_{th}, for initially narrow-band ($z_1 < 0.2$), moderately wide-band ($z_1 \approx 0.5$), and very wide-band ($z_1 > 0.9$) loads. One

TABLE 2—*Values of the dimensionless parameters used to define the spectral shapes for the simulations with racetrack filtering.*

V_h/V_l	f_h/f_l	L/f_l	H/f_h
0.25	1.0	0.25	0.25
0.5	2.0	0.5	0.5
1.0	3.0	0.75	0.75
2.0	4.0	1.0	1.0
4.0	5.0	...	...

NOTES—
V_h = variance of the high-frequency box in Fig. 8.
V_l = variance of the low-frequency box in Fig. 8.
f_h = center frequency of the high-frequency box.
f_l = center frequency of the low-frequency box.
H = width of the high-frequency box.
L = width of the low-frequency box.

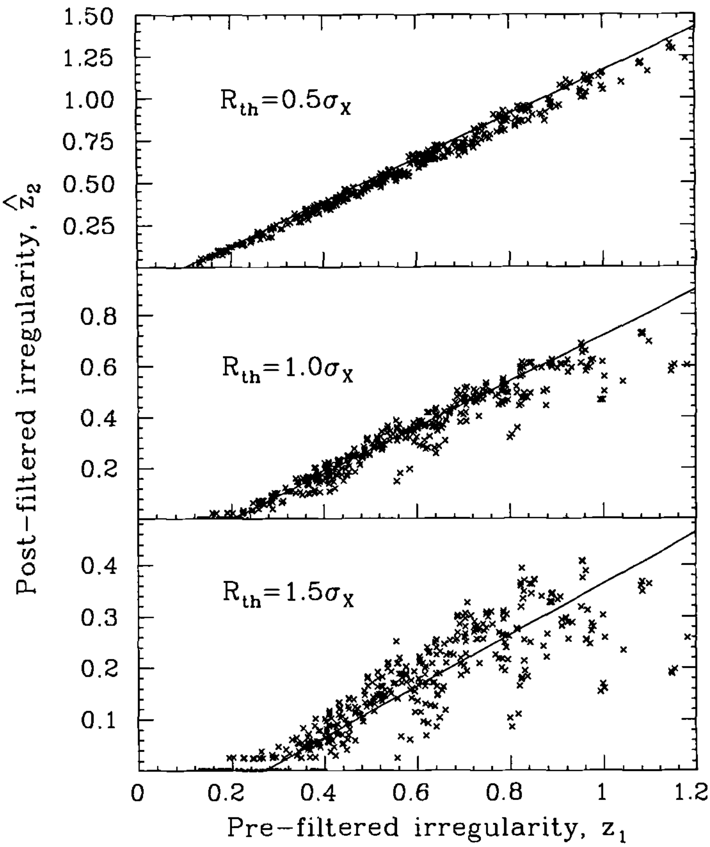

FIG. 9—*Irregularity measures before and after racetrack filtering at three threshold levels.*

standard deviation error bars are shown on the simulation results. The following empirical relationship is shown to be fairly accurate

$$\frac{\hat{f}_p}{f_p} = \exp\left[-\frac{1}{2}\left(\frac{R_{th}}{2\sigma_X}\right)^2\right] - \frac{3z_1^2}{5z_1+1}\left(1 - \exp\left[-\frac{3R_{th}}{\sigma_X}\right]\right) \tag{17}$$

In summary, sequenceless estimates of crack growth or fatigue life due to wide-band Gaussian loading can be obtained as follows:

1. Calculate α_1 (Eq 11) and f_p from moments (λ_n) of the load spectral density.
2. Calculate z_1 from α_1 (Eq 15).
3. Estimate $\hat{z}_2$ from z_1 and R_{th} (Eq 16).
4. Calculate the post-filtered regularity from $\hat{z}_2$: $\hat{\alpha}_2 = 1/\sqrt{1 + \hat{z}_2^2}$ (Eq 15).
5. Estimate the post-filtered peak rate, $\hat{f}_p$, from z_1 and R_{th} (Eq 17).

6*a*. For a fatigue damage calculation, the mean damage D_N after N cycles is estimated by substituting Eqs 12 and 13 with $\hat{\alpha}_2$ into Eq 7 (or an equivalent form if mean stress fluctuations are significant). The number of cycles to "failure" (or crack initiation perhaps) can be estimated by setting $D_N = 1$ and solving for N.

6*b*. For a crack growth calculation, substitute Eqs 12 and 13 with $\hat{\alpha}_2$ into Eq 14 and solve for N.

7. From the number of (racetrack) cycles to "failure", N, the actual failure time can be estimated as $N/\hat{f}_p$.

Three associated questions are answered here. (*a*) How accurately does this analytical racetrack model predict fatigue damage? (*b*) What optimum filtering threshold, R_{th}, should be adopted to best preserve fatigue damaging characteristics (for example, as identified through the well-established rainflow counting method)? (*c*) How do these sequenceless crack growth estimates compare with those that include sequence effects (as in Eq 1)?

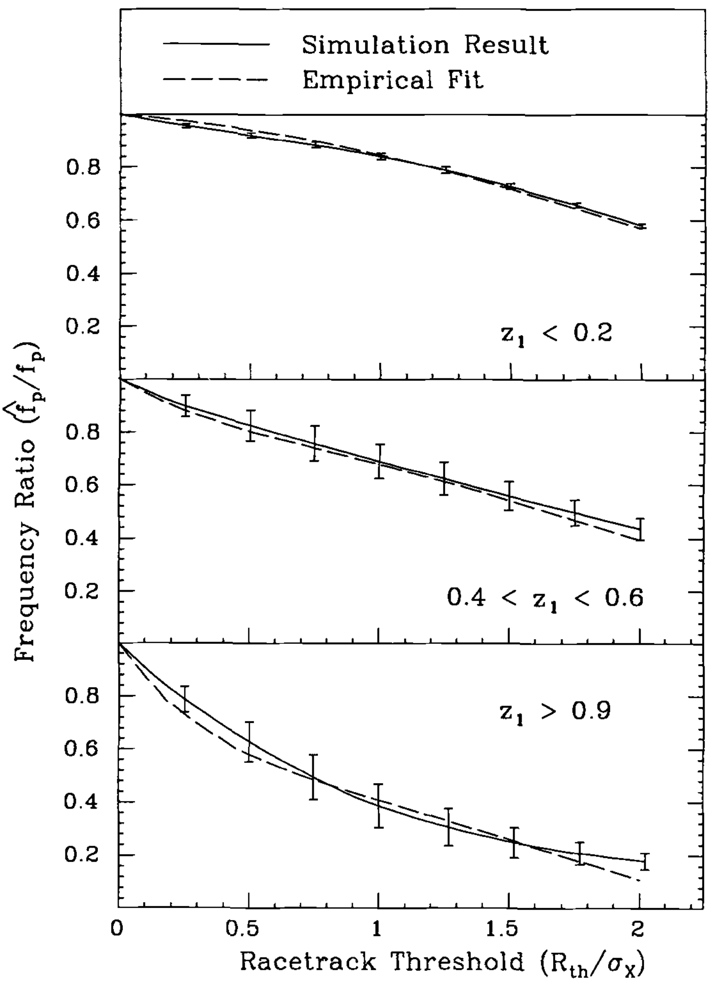

FIG. 10—*Reduction in frequency of peaks as a function of racetrack filtering threshold for narrow-band* (top), *moderately wide-band* (middle), *and very wide-band* (bottom) *loadings.*

Comparison of Predicted and Simulated Racetrack Damage

Figure 11 compares the predicted and simulated effects of racetrack filtering on fatigue "damage." Simulated damage, D, has been calculated from Palmgren-Miner summation of local racetrack-filtered ranges, R_i (neglecting mean stress effects)

$$D = \sum_{i=1}^{N} R_i^b \tag{18}$$

Exponent values $b = 2$, 4, and 8 were used. The figure shows the normalized damage, D/D_{norm}, in which D_{norm} is the damage caused by a narrow-band process with the same standard deviation and mean crossing frequency (Eq 7). Thus, D/D_{norm} is a damage correction factor that accounts for load bandwidth. For racetrack filtering, this correction factor is generally less than 1; similar behavior is shown for rainflow counted damage [3].

Figure 11 shows normalized damage results for narrow-band, moderately wide-band, and

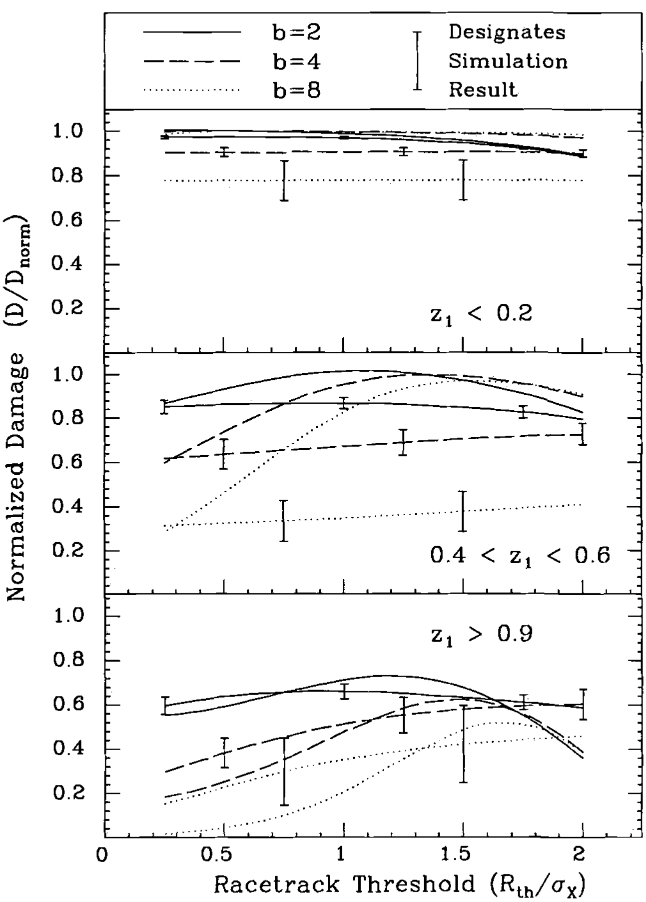

FIG. 11—*Normalized damage due to local ranges after racetrack filtering from simulations (with error bars) and from empirical adjustments to analytical parameters (without error bars).*

very wide-band loadings. As in Fig. 10, the curves with error bars display simulation results, both averages and ± 1 standard deviation bounds. The curves *without* error bars are analytical predictions found from Steps 1 through 6*a* in the preceding section (in Step 6*a*, N is set equal to $\hat{f}_p T$ and D_N is calculated). These analytical predictions are conservative over most useful combinations of bandwidth and threshold (suggested threshold values for various b are given subsequently). Differences are due mainly to the conservative nature of the truncated Rayleigh model for racetrack filtered ranges (Fig. 7*b*). Also, the empirical estimates of the post-filtered statistics begin to deteriorate as R_{th} approaches $2\sigma_X$. Note that, unlike these damage calculations, fatigue crack growth is often based on tensile ranges or peaks, which are generally better predicted by the analytical models given here (Fig. 7*a* versus Fig. 7*b*).

Racetrack Threshold Selection and Comparison with Rainflow Counting

To use racetrack filtering, it is important to select the threshold, R_{th}, so that the damaging potential of the loading is accurately reflected. In Fig. 11, narrow-band results are insensitive to R_{th} because filtering the already regular load only removes small amplitude ranges; it does not join small ranges into larger ranges. In fact, damage decreases when $b = 2$ because the low exponent makes small ranges relatively more important. In the wide-band case, as R_{th} increases there is more concatenation of local ranges, resulting in increased damage despite the reduction in the total number of ranges.

One way to assess the effect of varying R_{th} in racetrack filtering is to compare resulting damage estimates with those produced by rainflow counting. Figure 12 shows the ratios of damage based on racetrack filtered ranges to rainflow counted ranges from the simulations. For narrow-band loadings ($z_t < 0.2$) there is little difference, even for large b. As in Fig. 11, racetrack damage increases with R_{th} for wider load bandwidths, due to the increased concatenation of local ranges. When b equals two or four, as in fatigue crack growth, racetrack-filtered ranges can account for over 80% of the damage that rainflow counting identifies if the appropriate threshold is used. When $b \geq 8$, as in high-cycle crack initiation, the thresholds investigated here will only produce local ranges about half as damaging as rainflow counting suggests, when the loading is even moderately wide-band.

To conservatively estimate damage or crack growth from a wide-band loading, the analytical predictions of racetrack results (Steps 1 to 7) should use $R_{th} \approx 1.0\sigma_X$ when $b = 2$ and $R_{th} \approx 1.5\sigma_X$ when $b = 4$. These analytical estimates should be used with caution for wide-band loadings when $b > 4$ both because errors in the distributions are magnified and because local ranges can underestimate damage by a factor of about two (which still may be acceptable in view of other uncertainties in estimating life).

Sequential Simulation of Random Loadings

The foregoing random variable models provide useful analytical fatigue predictions when load sequence effects are negligible. To include these sequence effects, crack growth may be estimated cycle-by-cycle from a simulated (correlated) sequence of load peaks and troughs. To adopt conventional simulation techniques for these purposes, the load must first be simulated many times per cycle (at regular intervals), and the peaks and troughs then identified by interpolation. A more efficient "sequential" simulation method, which estimates the sequence of load peaks and troughs directly, is outlined briefly here. A more detailed explanation is given in Refs *12* and *29*.

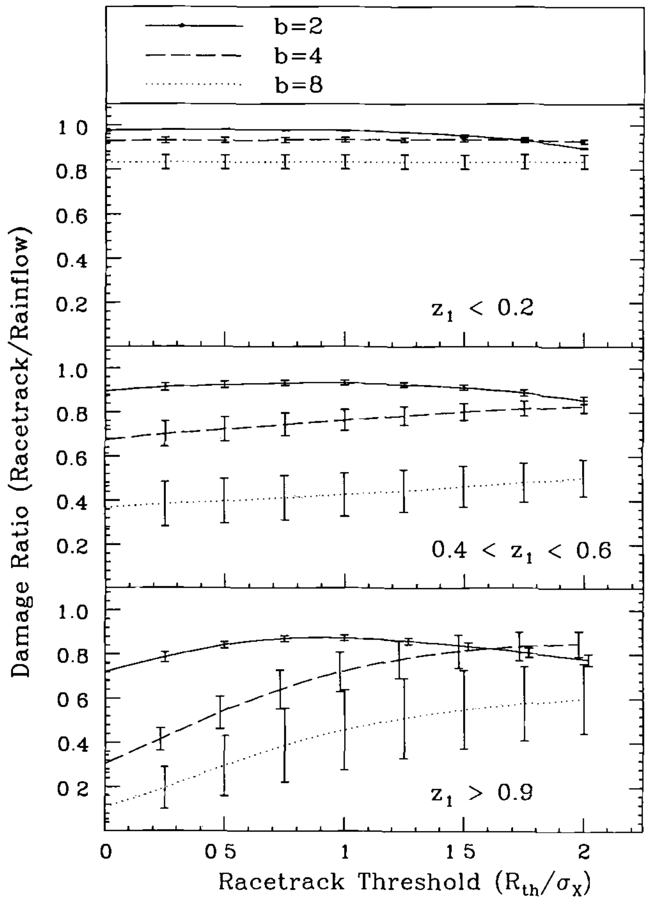

FIG. 12—*Ratio of damage due to local ranges after racetrack filtering to damage due to rainflow counted ranges.*

A correlated sequence of Gaussian random variables, U_n, (a Gauss-Markov process) can be generated from uncorrelated unit-variance Gaussian random variables, ξ_n, by

$$U_{n+1} = U_n e^{-2\Delta t/\theta_X} + \xi_n \, \sigma_X \, (1 - e^{-4\Delta t/\theta_X})^{1/2} \tag{19}$$

in which Δt is the time step between simulated values and θ_X is the length of time over which the process is significantly correlated, which can be calculated from either the spectral density, $G(f)$, or the normalized covariance, $\rho(\tau)$, of the load process

$$\theta_X = \frac{G(0)}{2\sigma_X^2} = \int_{-\infty}^{\infty} \rho(\tau)\, d\tau \tag{20}$$

Several Gauss-Markov processes, each simulated as in Eq 19, can be combined to directly simulate peaks and troughs of both narrow- and wide-band loads. In the narrow-band case, values of the load amplitude process ($A(t)$ in Fig. 4a) can be generated from two such

Gauss-Markov sequences, U_n and V_n, through the relationship

$$A_n = (U_n^2 + V_n^2)^{1/2} \tag{21}$$

(The underlying values of U_n and V_n are somewhat analogous to components of a phase plane diagram, and A to its amplitude.) If the load is a narrow-band Gaussian process with standard deviation σ_X, consistent levels of amplitude correlation are ensured by generating U_n and V_n from Eq 19 with $\theta_X = 2\theta_E$, in which θ_E is the correlation time of load peaks ("energy fluctuation scale" [*26*])

$$\theta_E = \frac{1}{\sigma_X^4}\int_0^\infty G^2(f)df = 2\int_{-\infty}^\infty \rho^2(\tau)d\tau \tag{22}$$

Taking Δt as half the period of load cycles, successive amplitude values from Eq 21 can be alternately added and subtracted from the mean, m_X, to simulate peaks and valleys.

Wide-band load processes can be simulated in a similar sequential fashion. Three such Gauss-Markov sequences (Eq 19) are generally required: one to simulate the mean cycle level ($X_0(t)$ in Fig. 4*b*), and two to simulate the cycle amplitude, $A(t)$, as before. In Eq 19, σ_X should now be replaced by $\sqrt{1 - \hat{\alpha}_2^2}\sigma_X$ to simulate X_0 values, and by $\hat{\alpha}_2\sigma_X$ to form both U_n and V_n values that comprise the amplitude in Eq 21. These amplitude values are again added and subtracted from the mean, X_0, to obtain peaks and troughs. (It has been found sufficient in numerical studies to simulate X_0 values only once per cycle, taking Δt as the total cycle period.)

Comparison of Crack Growth Calculations With and Without Sequence Effects

To investigate when it is necessary to include the complexity of sequence effects in crack growth analysis, random loadings are simulated and used to estimate crack growth life with and without sequence effects, using Eqs 1 and 8, respectively. In the sequence effect model of Eq 1, the reset stress and crack opening stress ($S_{op} = qS_r$) are updated every cycle. The stress ratio and q (Eq 5) are updated at an arbitrary interval of every one thousand cycles.

This simulation study was conducted by varying a few selected load and modeling parameters about two baseline cases: the ASTM AA and SAE BR loading histories and test specimens. The baseline parameters are listed in Table 3. All loadings have been generated with the preceding sequential simulation technique. (Simulation results are plotted in Figs. 13 through 16. The figure label "Ratio" shows ratios of sequenceless predictions to those that included sequence effects. The solid lines are for variations about the ASTM base case and the dashed lines are for variations about the SAE base case.)

TABLE 3—*Baseline case parameters for the sequence effect simulations.*

Parameter	q_0	m_X/σ_X	C_0	b	$S_y/(m_X + 3\sigma_X)$
ASTM	0.30	2.3	8.4×10^{-10}	3.64	1.45
SAE	0.35	0.0	1.5×10^{-10}	3.25	4.96
Parameter	R_{th}/σ_X	$\hat{\alpha}_2$	a_0	a_f	γ
ASTM	0.6	0.8	0.1in	1.0in	0.23
SAE	1.0	1.0	0.35W	0.7W	0.20

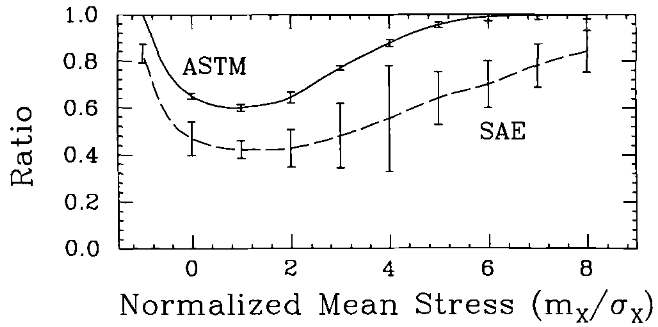

FIG. 13—*Ratio of crack growth life predictions without sequence effects to predictions with sequence effects versus normalized mean stress.*

The loading parameters that were varied include the normalized mean stress m_X/σ_X, the regularity $\hat{\alpha}_2$, and the racetrack threshold R_{th}. Of these, only the mean stress had a significant impact on the prediction ratio just described (Fig. 13). The maximum difference (minimum ratio) occurs at mean stresses between zero and three times the standard deviation. Very high mean stresses keep the crack from closing so the effective stress range is unaffected by crack closure. Sequence effects are likely to be minimal when the mean stress is greater than about $3\sigma_X(1 + q_0)/(1 - q_0)$. This is consistent with a reported lack of sequence effects in high tensile mean stress tests [*30*]. At negative mean stresses, acceleration and retardation effects begin to balance, resulting in a reduction in the difference between the two prediction methods.

Figures 14 through 16 show the effects of varying the material parameters q_0, C_0, and S_y (the yield stress is normalized by $m_X + 3\sigma_X$, a crude estimate of maximum applied stress). Sequence effects become more important as C_0 and S_y decrease and as q_0 increases. The greatest influence, independent of all other parameters, appears to be due to the crack opening stress ratio, q_0. Variations in the plane strain constraint factor, γ, did not change the results significantly although there was a small increase in sequence effects as γ decreased. The SAE base case shows more sensitivity to sequence effects than the ASTM case. The parameter with the largest difference between the SAE and ASTM base cases is the crack growth rate coefficient, C_0.

All of the preceding results point to a common effect. The greater the number of cycles required to grow the crack through the crack tip plastic zone, the greater the influence of

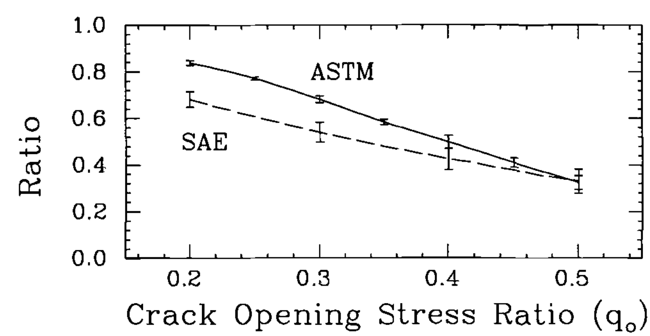

FIG. 14—*Ratio of crack growth life predictions without sequence effects to predictions with sequence effects versus crack opening stress ratio.*

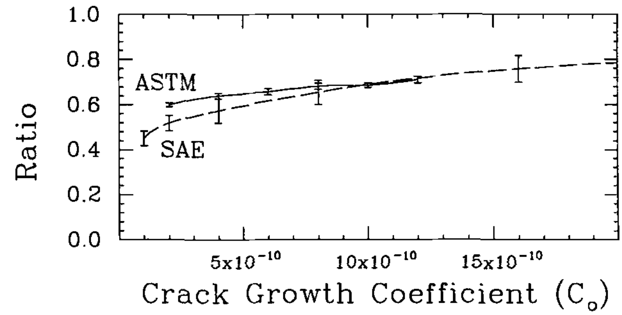

FIG. 15—*Ratio of crack growth life predictions without sequence effects to predictions with sequence effects versus crack growth rate coefficient.*

sequence effects. The magnitude of the difference between predictions with and without sequence effects depends on load and material parameters that determine the duration of the effect of an overload, which is governed by the size of the crack tip yield zone and the rate of crack growth through it.

Distinct Overloads

The foregoing simulations represent a general class of loadings where the maximum stresses are caused by the same source as the rest of the cyclic loading. If the overloads are caused by some other source or are due to brief periods of increased load intensity, their magnitude may be much greater than the cycles responsible for most of the crack growth. This case of exogenous overloads is the one that has been used most often in laboratory tests to demonstrate sequence effects in crack growth.

As an example of the way that variations in the spacing of overloads affect crack growth life, consider a loading that is constant amplitude between a minimum of zero and a maximum of S with tensile overloads equal to S_{ol}. (This is the simplest and most often investigated situation in which retardation effects are evident.) Also, for simplicity, assume that the reset stress, S_r remains equal to S_{ol} until one of the background stress peaks extends the crack tip plastic zone, at which time the reset stress drops to S. This revision of the crack growth model retains the qualitative retardation effect and helps to visualize the state of the crack opening stress because there are now only two possible states: high crack opening stress

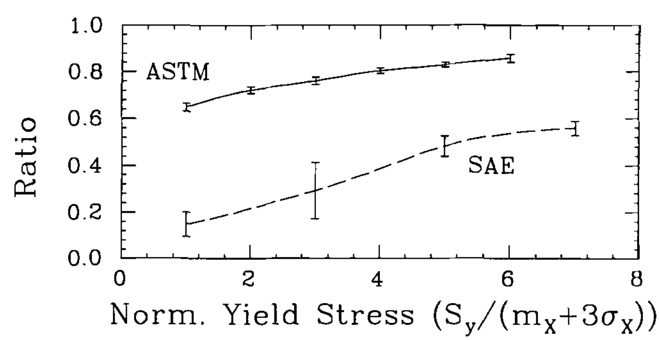

FIG. 16—*Ratio of crack growth life predictions without sequence effects to predictions with sequence effects versus normalized yield stress.*

following an overload, and low crack opening stress after the crack has grown through the overload affected zone. This simplified model is not, however, recommended for quantitative life estimates.

If both the number of cycles between overloads and overload magnitudes are constant, there is no variation in the *predicted* number of cycles to failure. If, however, the time between overloads is random, the number of cycles to failure becomes random as well.

Figure 17 shows the mean and COV of the predicted crack growth life, normalized by the predicted life without any overloads, as a function of the average number of cycles between overloads. Simulations were done for a few values of COV of overload interarrival cycles. Evenly spaced overloads have an interarrival COV value of zero. As the COV increases, the number of cycles between overloads can vary increasingly from the mean. A COV value of unity is consistent with overloads equally likely to occur at any time (the Poisson model of "memoryless" random arrivals unaffected by times of previous overloads). The COV values in excess of unity suggest that the overloads may " cluster"; for example, several closely spaced overloads followed by a large number of cycles without an overload.

The average increase in life due to overloads is reduced as the interarrival COV, and hence the clustering, increases. Even spacing between overloads allows each to have maximum effect, while irregularly spaced overloads allow more gaps between periods of retarded growth. It takes much more frequent overloads, on average, to achieve a state of constant retardation when overloads cluster.

In addition, the COV of the time to failure increases as the number of interarrival cycles becomes more irregular. In general, it is not the mean that is of interest but rather some percentile confidence level that is important. The combination of decreased mean and

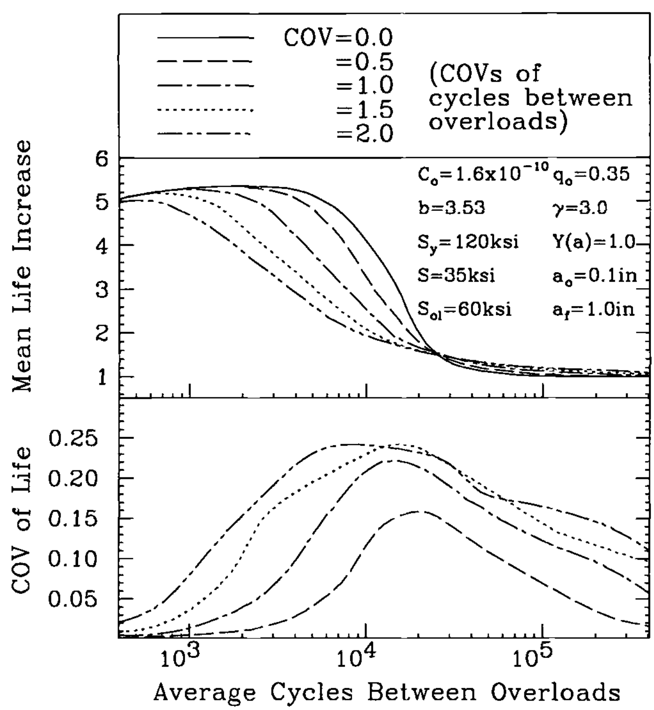

FIG. 17—*Mean and coefficient of variation (COV) of the predicted increase in crack growth life (ratio of life with retardation to life without retardation) due to tensile overloads.*

increased COV makes the likelihood of a significantly lower crack growth life much greater. Assuming a constant number of cycles between overloads is almost always nonconservative.

If a random loading has such distinct overloads, the distribution of load peaks (relative number of overloads to background loads) is insufficient information to accurately estimate crack growth life. The dynamics of the overload arrivals must also be modeled when sequences matter.

Summary

Various load models and analysis techniques have been developed for fatigue life estimation. As a practical guide to the fatigue analyst or designer, these are summarized here in order of increasing detail and complexity.

Analysis Neglecting Sequence Effects

The conventional narrow-band Gaussian load model is particularly simple and useful, and serves as the basic building block for more complex loadings. In this model, load cycles have Rayleigh distribution of amplitudes (Eq 6), which require only the load mean (m_X) and standard deviation (σ_X) as descriptive statistics. For loads with arbitrary bandwidths, this model remains useful when a rough (and generally conservative) life estimate is sought for either crack initiation or growth. Life estimates that ignore sequence effects require only a single integral (Eq 10) over cycle amplitude, avoiding the need for cycle-by-cycle analysis. For the ASTM test series, these estimates were found to under-predict sequenceless life estimates based on the actual tabulated loadings, but by less than a factor of two (Fig. 5).

A more refined wide-band Gaussian load model has been developed here from load bandwidth measures (for example, α_n from Eq 11). The distributions of mean and amplitude in each load cycle, $p(X_0)$ and $p(A)$, are conveniently estimated from the regularity factor α_2 (Eqs 12 and 13). These distributions define the local peak and trough (or equivalently, the mean and amplitude) of each cycle. To account for the effects of racetrack filtering, the post-filtered regularity $\hat{\alpha}_2$ has been estimated from the bandwidth parameter α_1 of the original load (Eqs 15 and 16, Fig. 9). The frequency of peaks, $\hat{f}_p$, has also been adjusted to account for racetrack filtering effects (Eq 17, Fig. 10). Sequenceless life predictions can then be formed as in the narrow-band case (see Steps 1 to 7). The distributions of racetrack filtered peaks and ranges from Eqs 12 and 13 agree well with similarly filtered ASTM loadings (Fig. 7). The distribution of local ranges after racetrack filtering are shown to account for over 80% of the damage identified by rainflow counting when the exponent, b, is less than or equal to 4 (Fig. 12).

Analysis Including Sequence Effects

If load sequence effects are to be retained in the analysis, an efficient algorithm is shown (Eqs 19 and 21) to sequentially simulate a series of load peaks and valleys. When based on the parameters $\hat{\alpha}_2$ and $\hat{f}_p$, peaks and valleys of the racetrack filtered process can be directly simulated. The additional statistics required for the simulation are: θ_E for narrow-band loading (Eq 22), and θ_E and θ_X for wide-band loading (Eq 20 and 22). This method permits continuous simulation of loads of arbitrary bandwidths for analysis and testing, avoiding the increased variability and possible bias in life estimates based on repetitions of an identical load "block" (which may not be representative). Table 4 summarizes the necessary Gaussian load model statistics for various fatigue applications.

TABLE 4—*Minimally sufficient statistics for Gaussian load models.*

Narrow-Band	Wide-Band
NEGLECTING SEQUENCE EFFECTS	
Mean; m_X	Mean; m_X
Standard deviation; σ_X	Standard deviation; σ_X
Frequency of cycles: $f_0 \approx f_p$	Frequency of peaks; $\hat{f}_p$ (Eq 17)
	Post-filtered regularity; $\hat{\alpha}_2$ (Eqs 15 and 16)
INCLUDING SEQUENCE EFFECTS (Load simulation requires all of the above plus the following.)	
Envelope correlation; θ_E (Eq 22)	Envelope correlation; θ_E (Eq 22)
	Cycle mean correlation; θ_X (Eq 20)
DISTINCT OVERLOADS (The following statistics of the overloads must be modeled in addition to describing the background loading.)	
The size of the overloads	
The mean time between overloads	
The COV of the time between overloads	

When Must Sequence Effects Be Included?

It is found that including sequence effects often produces comparatively small differences in life predictions (for example, less than a factor of two) when, as in random vibration, the highest load peaks come from the same process as the other peaks. From parametric simulation studies using two different base cases, three dominant sources of larger differences emerge:

1. mean stress less than about $3\sigma_X(1 + q_0)/(1 - q_0)$, where σ_X is the load standard deviation (Fig. 13);
2. crack opening stress ratio, q_0, between roughly 0.35 and 0.50, the upper half of its usual range (Fig. 14); and
3. yield stress, S_y, and crack growth coefficient, C_0, both sufficiently small that the crack does not grow quickly through the crack tip plastic zone (Figs. 15 and 16).

The simulation results showed minimal effect on the ratio of life predictions with and without sequence effects due to γ, R_{th}, and α_2.

Sequence effects have been repeatedly demonstrated for exogenous tensile overloads. Because of the sequence effect, a load model that includes only overload magnitude and frequency of occurrence is insufficient for crack growth estimation. The regularity of the spacing between the overloads must also be included. The assumption of regularly spaced overloads can be nonconservative (Fig. 17).

References

[1] Miles, J. W., "On Statistical Fatigue Under Random Loading," *Journal of Aeronautical Sciences*, Vol. 21, 1954, pp. 753–762.
[2] Yang, J. N., *Journal of the Engineering Mechanics Division*, Vol. 100, No. EM3, American Society of Civil Engineers, June 1974, pp. 469–475.
[3] Wirsching, P. H. and Light, M. C., *Journal of the Structural Division*, Vol. 106, No. ST7, American Society of Civil Engineers, July 1980, pp. 1593–1607.
[4] Madsen, H. O., Krenk, S., and Lind, N. C., *Methods of Structural Safety*, Prentice-Hall, NJ, 1986, pp. 252–284.

[5] Schijve, J., *Engineering Fracture Mechanics,* Vol. 5, 1973, pp. 269–280.
[6] Trebules, V. W., Roberts, R., and Hertzberg, R. W. in *Progress in Flaw Growth and Fracture Toughness Testing, ASTM STP 536,* American Society for Testing and Materials, Philadelphia, 1972, pp. 115–146.
[7] Elber, W. in *Damage Tolerance in Aircraft Structures, ASTM STP 486,* American Society for Testing and Materials, Philadelphia, 1971, pp. 230–242.
[8] Socie, D. F., *Engineering Fracture Mechanics,* Vol. 9, 1977, pp. 849–865.
[9] Nelson, D. V. and Fuchs, H. O. in *Fatigue Crack Growth under Spectrum Loads, ASTM STP 595,* American Society for Testing and Materials, Philadelphia, 1977, pp. 267–291.
[10] Jono, M., Song, J., and Kikukawa, M., "Fatigue Crack Growth and Crack Closure of Structural Materials under Random Loadings," *Advances in Fracture Research ICF-6,* Vol. 3, Pergamon Press, Oxford, 1984, pp. 1735–1742.
[11] *Methods and Models for Predicting Fatigue Crack Growth Under Random Loading, ASTM STP 748,* J. B. Chang and C. M. Hudson, Eds., American Society for Testing and Materials, Philadelphia, 1981.
[12] Veers, P. S., "Fatigue Crack Growth due to Random Loading," Ph.D. thesis, Stanford University, Aug. 1987.
[13] Willenborg, J., Engle, R. M., and Wood, H. A., "A Crack Growth Retardation Model Using an Effective Stress Concept," TM-71-1-FBR, Wright Patterson Air Force Base, OH, 1971.
[14] Newman, J. C., Jr., in *Design of Fatigue and Fracture Resistant Structures, ASTM STP 761,* Abelkis and Hudson, Eds., American Society for Testing and Materials, Philadelphia, 1982, pp. 255–277.
[15] Schijve, J., *Engineering Fracture Mechanics,* Vol. 14, 1981, pp. 461–465.
[16] Jono, M., Song, J., and Sugeta, A., "Prediction of Crack Growth and Crack Closure Under Non-Stationary Random Loading," *Proceedings,* Fourth International Conference on Structural Safety and Reliability (ICOSSAR), Kobe, Japan, May 1985, pp. 1246–1274.
[17] Elber, W. in *Fatigue Crack Growth under Spectrum Loads, ASTM STP 595,* American Society for Testing and Materials, Philadelphia, 1976, pp. 236–250.
[18] de Koning, A. U., "A Simple Crack Closure Model for Prediction of Fatigue Crack Growth Rates under Variable Amplitude Loading," NLR MP 80006, National Aerospace Laboratory, Amsterdam, 1980.
[19] Dill, H. D. and Saff, C. R., "Effect of Fighter Attack Spectrum on Crack Growth," AFFDL-TR-76-112, McDonnell Douglas Aircraft Co., March 1977.
[20] *Fatigue Under Complex Loading: Analysis and Experiments,* R. M. Wetzel, Ed., SAE Advances in Engineering, Society of Automotive Engineers, Vol. 6, 1977.
[21] Newman, J. C., Jr., in *Methods and Models for Predicting Fatigue Crack Growth Under Random Loading, ASTM STP 748,* J. B. Chang and C. M. Hudson, Eds., American Society for Testing and Materials, Philadelphia, 1981, pp. 53–84.
[22] Chang, J. B. in *Methods and Models for Predicting Fatigue Crack Growth Under Random Loading, ASTM STP 748,* J. B. Chang and C. M. Hudson, Eds., American Society for Testing and Materials, Philadelphia, 1981, pp. 3–40.
[23] Winterstein, S. R., *Journal of Engineering Mechanics,* Vol. 111, No. 10, American Society of Civil Engineers, Oct. 1985, pp. 1291–1295.
[24] Winterstein, S. R., "Moment-based Hermite Models of Random Vibration," Technical Report No. 219, Series R, Dept. of Structural Engineering, Technical University of Denmark, 1987.
[25] Socie, D. F. and Kurath, P. in *Fracture Mechanics: Fourteenth Symposium—Volume II: Testing and Applications, ASTM STP 791,* J. C. Lewis and G. Sines, Eds., American Society for Testing and Materials, Philadelphia, 1983, pp. II–19 to II–32.
[26] Winterstein, S. R., and Cornell, C. A., *Journal of Engineering Mechanics,* American Society of Civil Engineers, Vol. 111, No. 2, Feb. 1985, pp. 125–142.
[27] Fuchs, H. O., Nelson, D. V., Burke, M. A., and Toomay, T. L., "Shortcuts in Cumulative Damage Analysis," *Fatigue under Complex Loading: Analyses and Experiments, Advances in Engineering,* Vol. 6, R. M. Wetzel, Ed., Society of Automotive Engineers, 1977, pp. 145–162.
[28] Nelson, D. V. and Fuchs, H. O., "Predictions of Cumulative Fatigue Damage Using Condensed Load Histories," *Fatigue under Complex Loading: Analyses and Experiments, Advances in Engineering,* Vol. 6, R. M. Wetzel, Ed., Society of Automotive Engineers, 1977, pp. 163–187.
[29] Winterstein, S. R., "Diffusion Models and the Energy Fluctuation Scale: A Unified Approach to Extremes and Fatigue," Technical Report No. 64, John A. Blume Earthquake Engineering Center, Stanford University, Nov. 1984, pp. 72–73, 96–99.
[30] Fleck, N. A. and Smith, R. A., *International Journal of Fatigue,* Vol. 6, No. 4, 1984, pp. 203–210.

F. Albrecht Conle,[1] Thomas R. Oxland,[2] Dana Wurtz,[2] and Timothy H. Topper[2]

Tracking Time in Service Histories for Multiaxis Fatigue Problems

REFERENCE: Conle, F. A., Oxland, T. R., Wurtz, D., and Topper, T. H., **"Tracking Time in Service Histories for Multiaxis Fatigue Problems,"** *Development of Fatigue Loading Spectra, ASTM STP 1006,* J. M. Potter and R. T. Watanabe, American Society for Testing and Materials, Philadelphia, 1989, pp. 198–210.

ABSTRACT: Techniques are presented for the acquisition, reduction, storage, and retrieval of time-sequenced, multi-channel, service load information. The relative merits of other methods are discussed and the advantages of time information demonstrated in a component analysis example.

KEY WORDS: testing, fatigue (materials), load histories, data acquisition, variable amplitude, metals, stress (materials), strain (materials)

In engineering design, the advent of computers has significantly changed many of the common tools used to design components: primarily in the areas of computer-aided design (CAD) (that is, drafting) and component stress analysis (that is, finite element analysis (FEA)). The disciplines that supply the inputs to the CAD and FEA procedures (Fig. 1) have not been automated extensively. Descriptions of the component load environment are the weakest feature of this iterative process. Reasons for the lack of load information can be attributed to:

(*a*) the expense of obtaining reliable loads data;
(*b*) the design critical load was not measured;
(*c*) the latest loads are not for the latest component revision;
(*d*) the load data are not in a format useful for the analysis desired;
(*e*) the load data have been lost or their existence is now known; and
(*f*) "test later" philosophy overshadows the "measure now" requirements.

Load acquisition exercises may or may not be a part of each design iteration. Generally, it is desirable to measure loads on each new prototype or production version. If no hardware exists, other forms of estimates are employed, for example impulse function response or loads from similar vehicles or models. Regardless of the source of load information, it is imperative that it be made available in a form that allows maximum flexibility and utility. Past work [*1*] and the present study suggest that previous storage formats, primarily histogram-type summaries, only retain a fraction of the information that could potentially be extracted from typical load history recordings. It is possible to minimize many of the problems

[1] Ford Scientific Research Laboratory, Dearborn, MI 48121.
[2] Department of Civil Engineering, University of Waterloo, Waterloo, Ontario, Canada N2L 361.

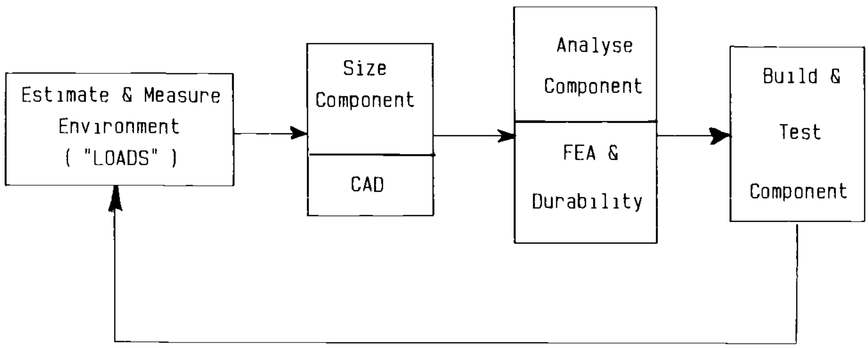

FIG. 1—*Features of component design.*

just listed by saving as much of the "raw" data as possible, that is, the longer one can practically delay the data reduction step in the load acquisition process, the greater the amount of useful information that can be extracted. This philosophy leads to the conclusion that one must save the time at which events occur. The retention of time as part of the data is the subject of this study.

Signal Descriptions and Data Reduction

Data acquisition of "load" signals is always a compromise between the objectives of maximizing the amount of signal saved, minimizing the storage requirements, and minimizing subsequent data processing computation time. The ultimate signal storage technique would be the complete record of sequenced digitized samples. In practical terms, this implies storing all samples at rates such as 1000 samples/channel/second. Most present, easily accessible, digital storage media make this "best possible" alternative impractical. In the ground vehicle industry, the number of channels of interest can, at times, approach 100, and a service history data acquisition session can often be of the order of 1 or 2 h; thus creating approximate storage requirements of 1000 million samples (about two Giga bytes). Modern random access disk storage could handle this volume, but not cheaply, and not for more than a few data acquisition exercises. The volume of data would also overload the processing capability of most laboratory-sized computer systems, if repetitive arithmetic operations need to be performed. These storage and processing considerations result in the necessity for establishing some form of data reduction criteria.

Various histogram summarization techniques have been applied in previous fatigue studies. In the automotive industry, level crossing or cumulative exceedance histograms have been used for many years, along with the more recent introduction of "rainflow" counted histograms and the Markov matrix-type techniques [*2–4*]. Unfortunately, all these techniques are single-channel summarizers, and although it is possible to extend the methods to create a cross-channel capability, in general, all time of occurrence information is lost. This makes the present histogram techniques useless for any data analysis requirements that involve multiple interrelated channels. It is the opinion of the authors that such cross-channel (or time-versus-load) information will be a basic requirement in the next generation of vehicle behavior studies, and also in newer fatigue analysis calculations that can account for multiaxial material behavior.

Past methods of preserving cross-channel synchronization of data have either used the technique of saving all samples (for short-time segments) or used simultaneous values at

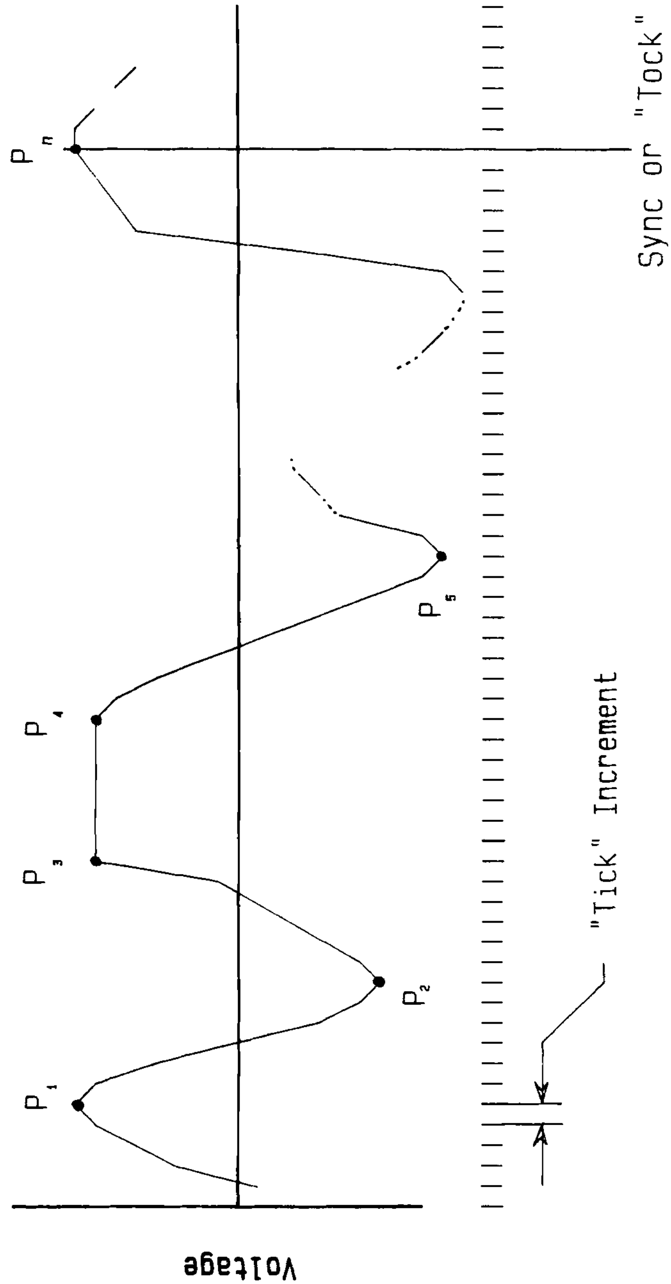

FIG. 2—*The selection of peak time values.*

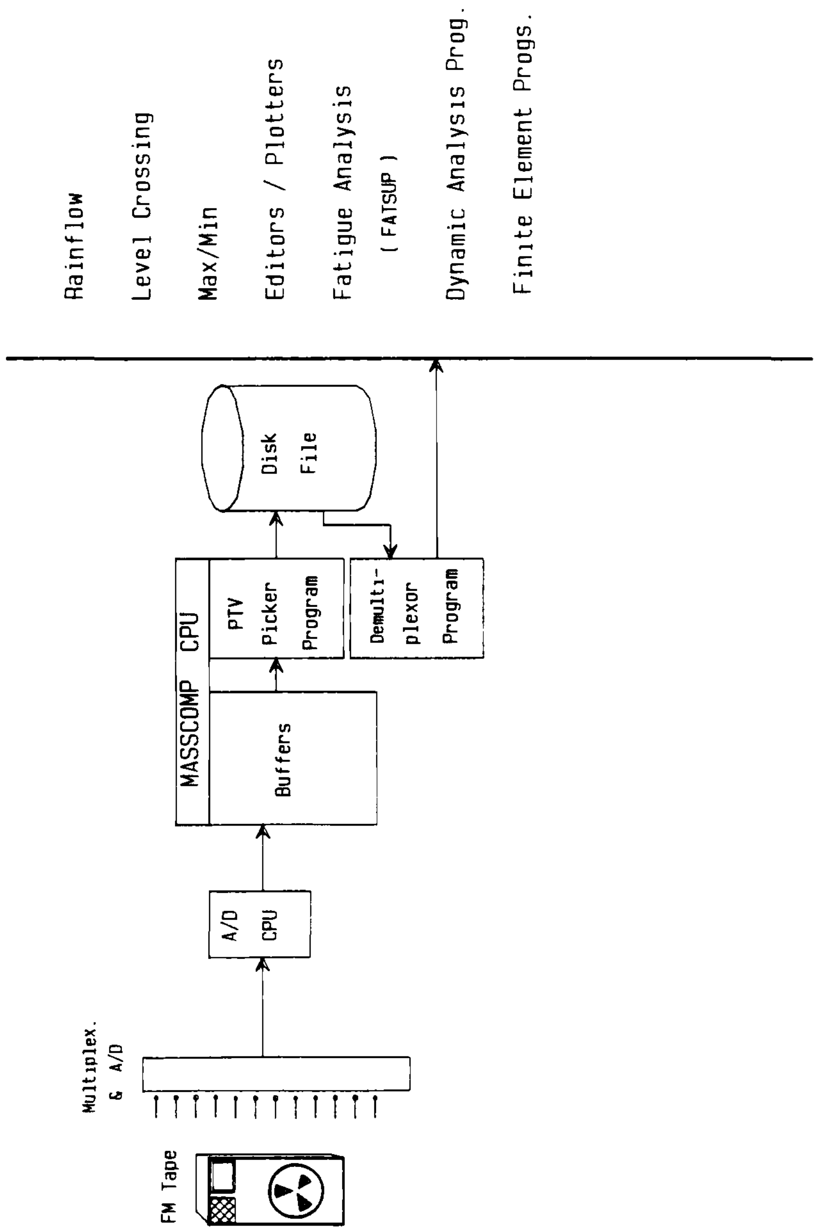

FIG. 3—Computer system used for data acquisition.

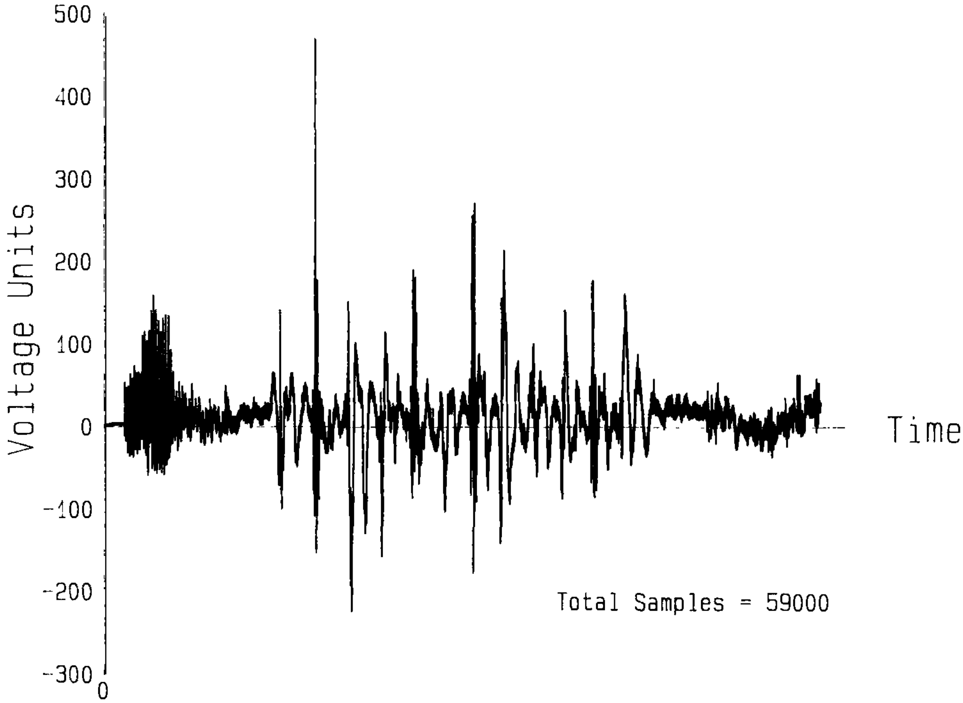

FIG. 4—*Original signal segment of a proving ground event.*

peaks; that is, whenever any channel has a peak or valley, save the simultaneous values of the other channels, irrespective of whether the other channels are at their peaks or not. This latter method was quite good at preserving the cross-channel information about the signals for a few channels, but lost the actual time-of-peak occurrence. It also tended to require excessive amounts of storage when a large number of channels were being sampled, each with signals of differing phase or frequencies. Given these and other constraints, it was decided here to characterize signals by saving the peak (or valley) values and the time at which each occurred (Fig. 2). The procedure consists of simply sorting through the sequential clocked samples, detecting the peaks (or valleys), and recording the sample number (where sample number is a measure of time, given a constant sample rate). Two criteria were added to the peak-picking algorithm, namely, a detector of flat spots, or constant voltage intervals (for example, the signal between P3 and P4), and a cross channel synchronization event or "tock" that corresponds to some selected number of clock "ticks."

The hardware and software interaction used to acquire the data is shown in Fig. 3. The first version of the peak-time-valley (PTV) picker measured the voltage with 5-bit resolution (approximately 32 divisions) and an 11-bit clock. Each voltage-time value could thus be stored in a 2-byte word. Although this arrangement provided the highest degree of data compression, it was found that the resolution was not sufficient in some applications. Resolution could be improved only with added file complexity. The compromise eventually adopted was to use a 16-bit voltage word accompanied by a 16-bit clock word. Figure 4 shows a complete, uncompressed trace of a 1-min proving ground signal sampled at 1000 Hz/channel. It was one of six channels acquired simultaneously on the computer system. The analogue to digital (A/D) converter's multiplexor was switched between channels at the rate of 100 kHz. A portion of one of the major events is shown in exploded view in Fig. 5*a*. Figure 5*b* and *c* depict the same time segment after PTV condensation using a 20 and 40-voltage unit window, respectively, to extract peaks. A visual comparison of traces such as Fig. 5*a,b,* and *c* indicate that the essential features are preserved in both cases and respective data file compressions of 15 and 7% of the original full six-channel histories were achieved.

Applications

There are numerous design environments where this data format is helpful. The present study concerns finite element or other elastic analysis based design situations that yield a transformation equation between some nominal force input and the stresses at some critical locations of "hot spots" (Fig. 6). Past methods of analysis in such situations usually assume some worst case load set, apply the loads to an FEA model, and compute the maximum hot spot stress. By assuming constant zero-to-maximum load repetition, fatigue life estimates could be made. Such assumptions can produce erroneous predictions, in either the conservative or unconservative directions because the load levels never occurred together as expected, or smaller signal magnitudes at some other points in time summed to higher resulting strain levels. Thus, when the load histories of the differing force inputs are complex, and not related in phase, it is usually very difficult to estimate the worst case load sets for all possible critical elements. A better method is to perform an analysis for each input load vector (for example, unit load), find the hot spots for that case, and compute the linear transformation equation between the applied load and hot spot strain, as shown in Fig. 6.

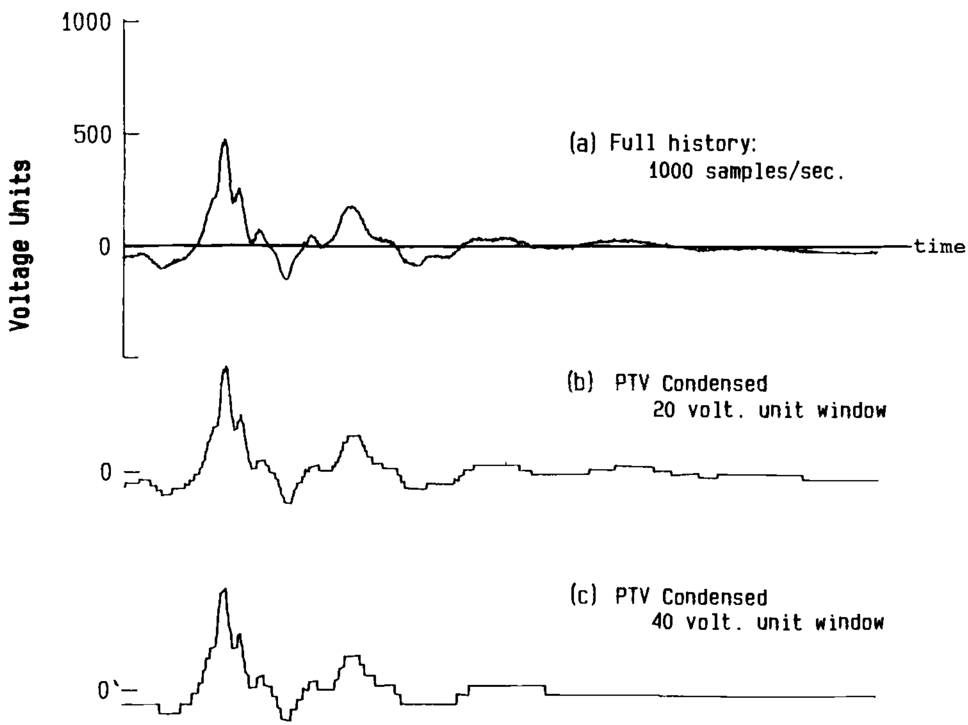

FIG. 5—*Original and condensed history versions of a pothole event.*

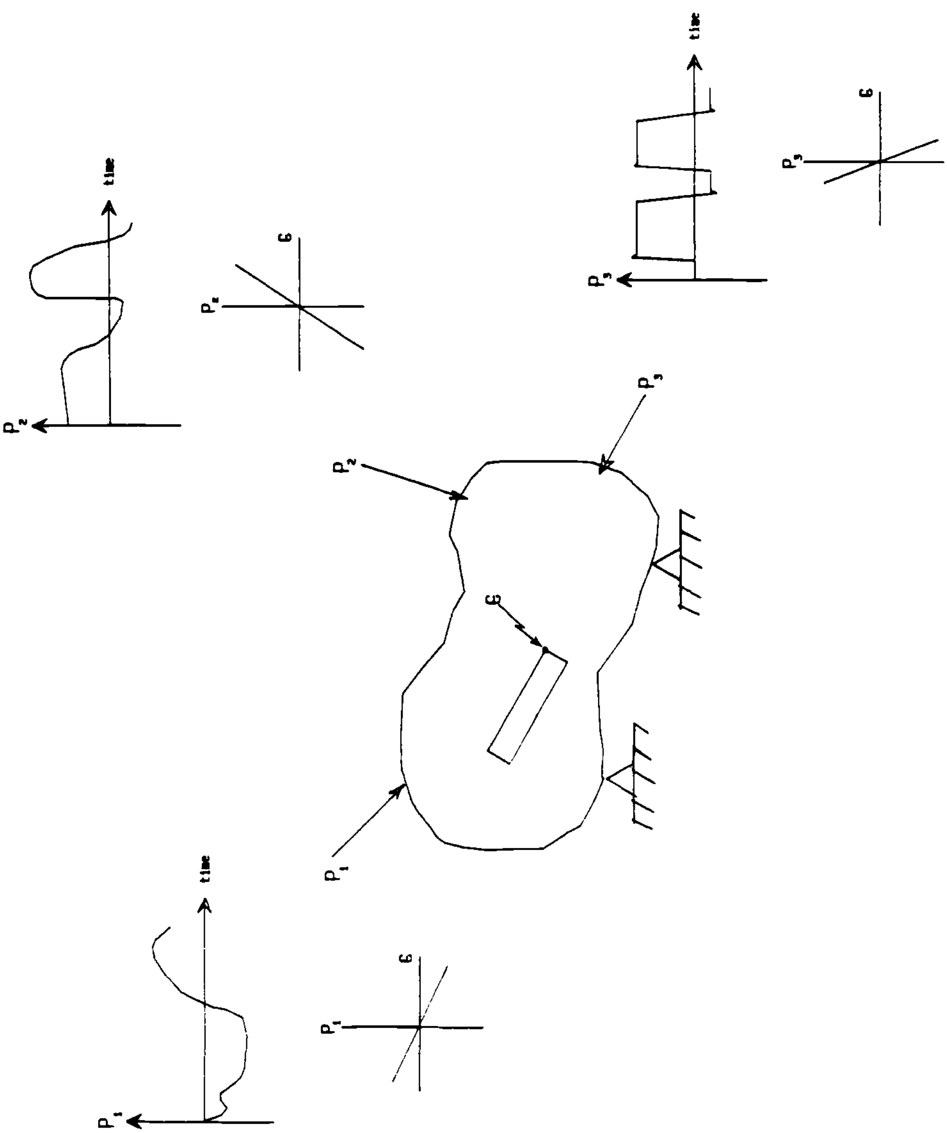

FIG. 6—*Generalized body showing a particular local strain location, the external load history segments, and the external load versus local strain transformations.*

Given that one has the load history (with time) for each input vector, one can then compute the equivalent hot spot strain history, and using superposition, add all the histories together to obtain the full composite service strain history of each hot spot.

A spindle arm, schematically depicted in Fig. 7, was subjected to three orthogonal force vectors applied at the tire patch during a traverse of a section of the durability test track. In this preliminary case, a simple elastic static analysis was used to compute the force to critical load strain transforms. The bending stresses are

$$S_1 = 13.0 \cdot F_{lat}$$

$$S_2 = 4.3 \cdot F_{vert}$$

$$S_3 = 3.5 \cdot F_{long}$$

The scaling equations used to convert the section stresses to elastic strains required the addition of a material modulus factor when other materials were substituted. By changing

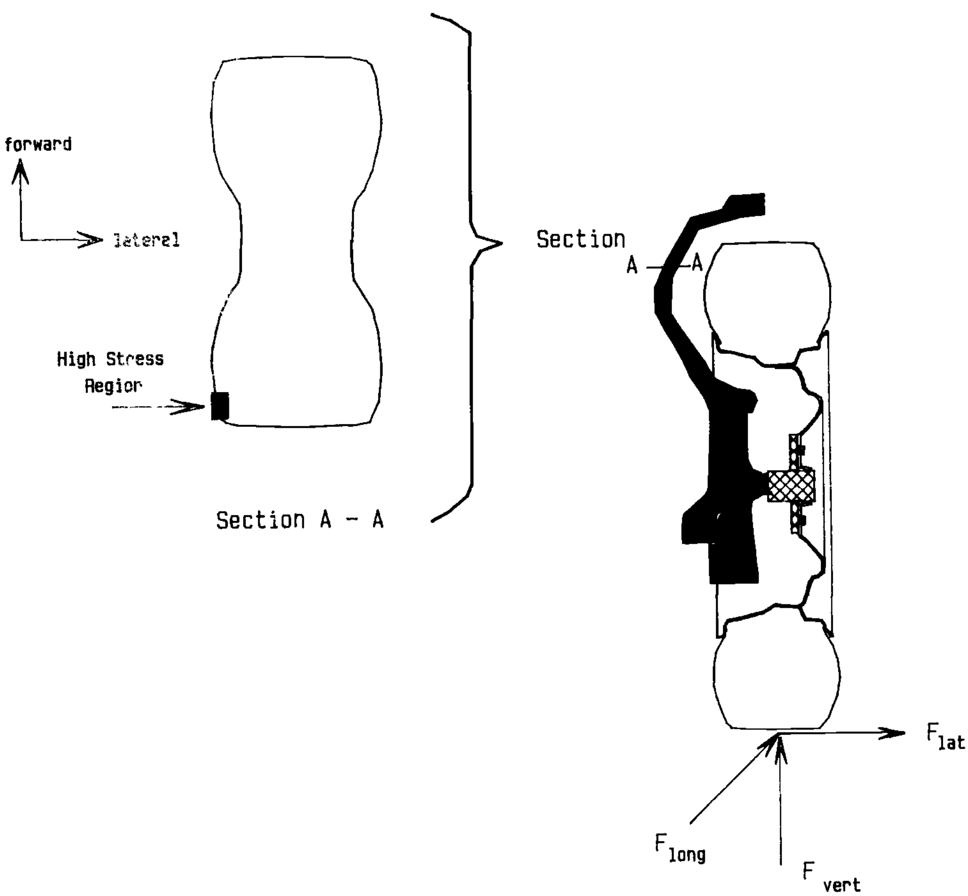

FIG. 7—*Spindle component with selected section and critical local strain location.*

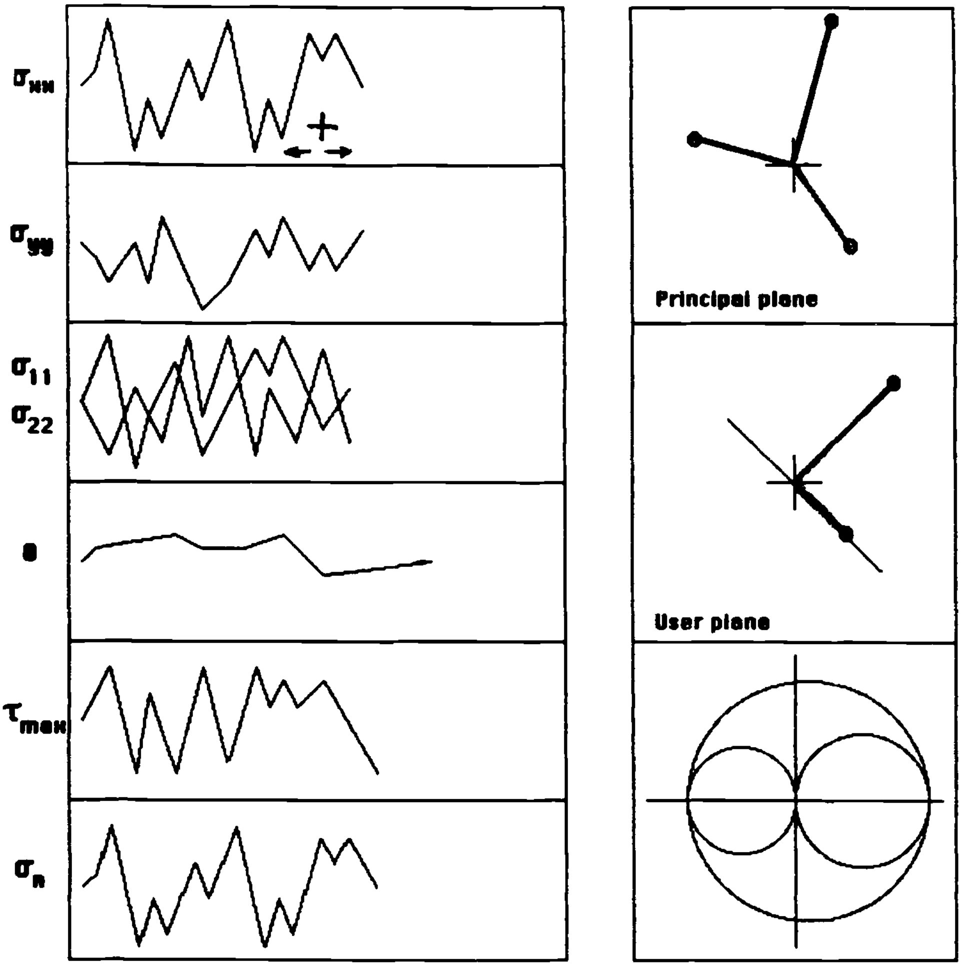

FIG. 8—*Black and white schematic of color raster image of biaxial stress history, equivalent stress traces and dynamic display of principal stresses, user selectable normal stresses, and Mohr's circle.*

signs and a magnitude factor of the transformation equations, it was also possible to estimate the strain histories at other locations on the section.

Multiaxial Extensions

In many design situations, the assumption of a uniaxial strain or stress state is of sufficient accuracy to model the fatigue process. Uniaxial based life assessment techniques are well developed and reasonably reliable. Because of the availability of finite element analysis models, more biaxial or triaxial stress states can be described or observed at component locations. At present, it is impractical to estimate fatigue life using multiaxial stress or strain histories. There is still a great deal of discussion amongst researchers [5] about how to count fatigue damage in multiaxial cases, and only a very few multiaxial plastic deformation

DO YOU WANT AN ANALYSIS THAT TIES THE SMALLER LOOPS
TO THE TENSILE 1/2 CYCLE OF THE LARGEST LOOP ?: Y
4-PASSES OF BLOCKS & COBBLE STONES.

XXXXXX HISTORY FACT. NO. 2 = .2000000E+01

				SIMPLE STRAIN		SMITH-WATSON-TOPPER		MORROW	
	RANGE	MEAN	REVS	DAMAGE	%	DAMAGE	%	DAMAGE	%
1	.540E-02	.880E-03	2	.680E-03	82.0	.880E-03	83.8	.734E-03	82.8
2	.418E-02	.650E-03	2	.884E-04	11.6	.128E-03	11.5	.104E-03	11.8
3	.360E-02	.480E-03	2	.319E-04	4.2	.373E-04	3.5	.341E-04	3.9
4	.300E-02	.190E-03	2	.109E-04	1.4	.768E-05	.7	.800E-05	.9
5	.274E-02	.480E-03	2	.140E-05	.2	.290E-05	.3	.240E-06	.3
6	.274E-02	-.283E-04	4	.293E-05	.4	.134E-05	.1	.212E-06	.2
7	.229E-02	.190E-03	4	.353E-06	.0	.436E-06	.0	.431E-06	.0
8	.229E-02	-.257E-03	4	.353E-06	.0	.424E-07	.0	.164E-06	.0
9	.183E-02	-.283E-04	122	.850E-06	.1	.338E-06	.0	.607E-06	.1
10	.137E-02	.190E-03	184	0.	0.0	0.	0.0	0.	0.0
11	.137E-02	-.257E-03	78	0.	0.0	0.	0.0	0.	0.0
12	.913E-03	.420E-03	36	0.	0.0	0.	0.0	0.	0.0
13	.913E-03	-.943E-03	4	0.	0.0	0.	0.0	0.	0.0
14	.913E-03	-.480E-03	46	0.	0.0	0.	0.0	0.	0.0
15	.913E-03	-.283E-04	2372	0.	0.0	0.	0.0	0.	0.0
16	.456E-03	.257E-03	2	0.	0.0	0.	0.0	0.	0.0

BLOCK LIFE PREDICTED= 1300.8 942.2 1128.8

DO YOU WANT LOCAL STRESS-STRAIN PLOTS NOW?: Y

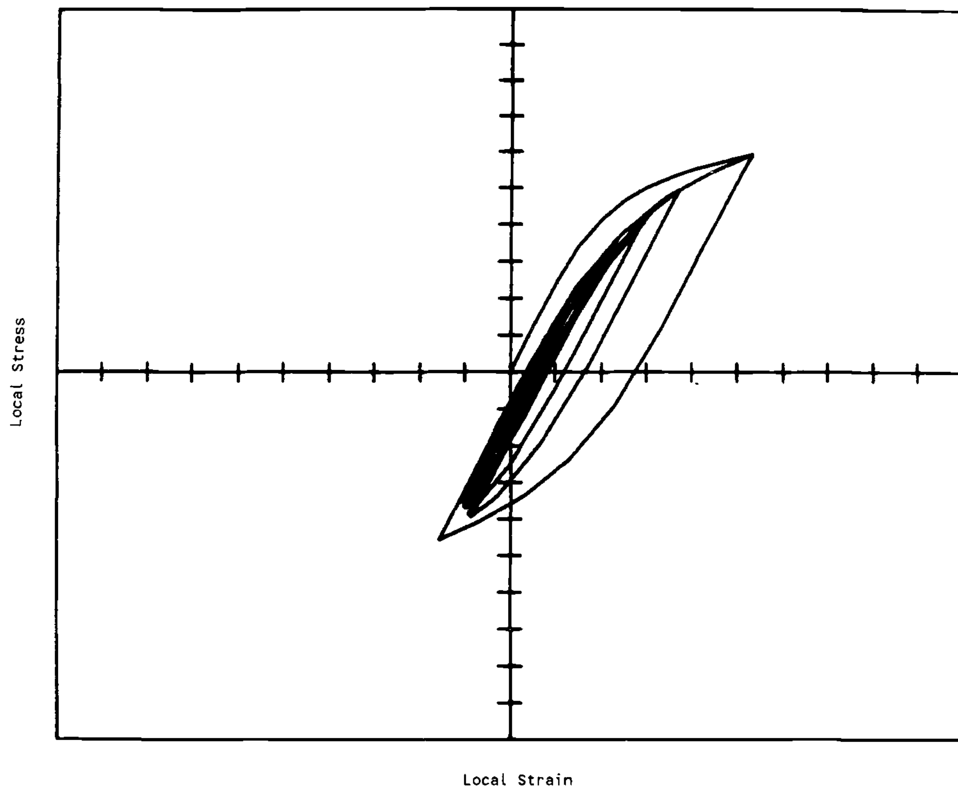

FIG. 9—*Numerical display of rainflow histogram damage for three mean stress assumptions above graphical output of the associated local stress-strain behavior.*

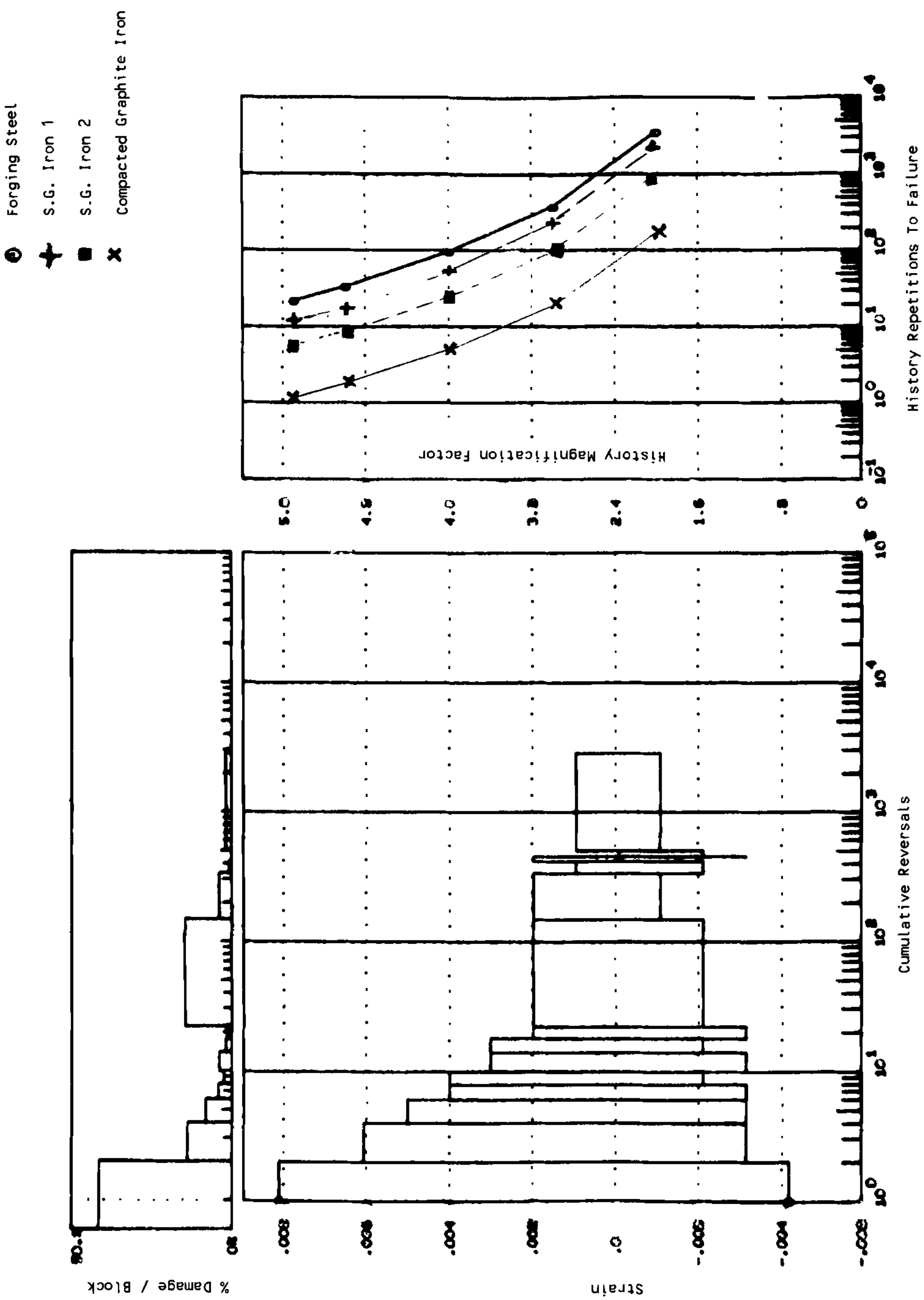

FIG. 10—Graphical display of the rainflow range-mean histogram along with the associated percent damage per block of history, and the expected

behavior models (for example, Ref *6*) can reliably follow the stress-strain locus for complex multiaxial stress or strain histories. As an interim means of approximating the effects of multiaxial stress conditions, it was decided to adapt the uniaxial superposition routines to perform the same function using the 3 × 3 matrix stress description at each point in time and to subsequently derive uniaxial histories based on various equivalencing criteria. The superposition routines simply add the critical location stress (or strain) matrices caused by each load input. In cases where matrices do not exist at the exact instant of superposition, interpolation is applied for each element of the nearest two matrices.

At another section on a similar spindle component, the vertical and longitudinal spindle forces are the primary cause of a biaxial stress condition that can be described by the transformation coefficients A_{ij} in the following equations.

$$S_{xx} = P_1 \cdot A_{xx1} + P_2 \cdot A_{xx2}$$

$$S_{xy} = P_1 \cdot A_{xy1} + P_2 \cdot A_{xy2}$$

$$S_{yy} = P_1 \cdot A_{yy1} + P_2 \cdot A_{yy2}$$

Figure 8 shows a segment of the combined history of matrices created by the superposition of the two individual histories. This history of matrices can be scanned by interactive cursor movement on the Masscomp graphics terminal, and the principal stress directions and Mohr's circle of stress observed. The user can decide upon some form of equivalencing of the history to uniaxial conditions; typically von Mises equivalent stress, maximum shear, or, in this case, normal stress on a user-defined plane (the history shown in the bottom window of Fig. 8). Resulting uniaxially equivalenced histories can be processed in several ways by the analysis software. The most commonly used method is to rainflow count the sequence and send the set of range-mean-occurrence observations to models that determine the local stress-strain behavior and count fatigue damage [*7*]. Figure 9 displays the numerical output and a local stress-strain simulation generated from a simple subset of the complete range-mean-occurrence data set. Several mean stress assumption options are available in the program and Fig. 10 depicts the blocked input load history (rainflow counts), the associated damage per block (top of graph), and the life predictions at several scaled history magnification factors. Prediction curves for several potential materials have been superimposed on the predicted life plots. The procedure thus provided, in this case, a quick relative materials comparison prior to the construction of actual hardware.

Summary

Engineers are becoming aware of the utility of displaying multi-channel, time-synchronized histories that also can be easily manipulated and analyzed. Use of such information depends upon easy storage and retrieval, quick display and analysis routines, and reliable multiaxial stress-strain and fatigue life prediction models. The present study has demonstrated the effectiveness of extracting peak-time values and using them as the building block of load history data storage. Because almost all other previously utilized summarization methods can be derived from time-sequenced load histories, no significant objections are incurred by other analysis technique users. As computer technology continues to improve, this summary method is increasingly practical and allows better insights into the behavior of components subjected to complex load environments.

References

[1] Conle, A. and Topper, T. H., "Fatigue Service Histories: Techniques for Data Collection and History Reconstruction," *Transactions,* Society of Automotive Engineers, Vol. 91, Section 1, Paper No. 820093, 1982, p. 299.

[2] Scherschel, R., "Description of a Peak-Valley Counting Program," *Proceedings,* Ford Motor Company Fatigue Workshop VIII, Dearborn, MI, Dec. 1969.

[3] Conle, F. A., "A Computer Simulation Assisted Statistical Approach to the Problem of Random Fatigue," M.S. thesis, University of Waterloo, Waterloo, Ontario, Canada, March 1974.

[4] Haibach, E., Fisher, R., Schutz, W., and Huck, M., "A Standard Random Load Sequence of Gaussian Type Recommended for General Application in Fatigue Testing: Its Mathematical Background and Digital Generation," *Fatigue Testing and Design,* Vol. 2, Society of Environmental Engineers International Conference, 5–9 April 1976, City University, London, pp. 29.1–29.21.

[5] *Multiaxial Fatigue, STP 853,* Miller and Brown, Eds., American Society for Testing and Materials, Philadelphia, 1985.

[6] Chu, C. C., "The Analysis of Multiaxial Cyclic Problems with an Anisotropic Hardening Model," *International Journal of Solids and Structures,* Vol. 23, No. 1, 1987.

[7] Conle, A. and Landgraf, R. W., "A Fatigue Analysis Program for Ground Vehicle Components," *Digital Techniques in Fatigue,* Society of Environmental Engineers Conference Proceedings, City University, London, 1983.

R. Sunder[1]

Compilation of Procedures for Fatigue Crack Propagation Testing Under Complex Load Sequences

REFERENCE: Sunder, R., "**Compilation of Procedures for Fatigue Crack Propagation Testing Under Complex Load Sequences,**" *Development of Fatigue Loading Spectra, ASTM STP 1006,* J. M. Potter and R. T. Watanabe, Eds., American Society for Testing and Materials, Philadelphia, 1989, pp. 211–230.

ABSTRACT: A review is made of procedures, developed at the National Aeronautical Laboratory for fatigue crack propagation testing under flight spectrum loading. They include K-control and on-line spectrum editing that were found to have a significant impact on spectrum load testing. Techniques are described for unambiguous assessment of crack closure stress and for binary-coded marker loading.

KEY WORDS: fatigue crack, spectrum loading, K-control, dK/da, net stress, on-line spectrum editing, binary-coded loads, fatigue (materials), testing

The service load environment for most engineering structures is random in nature. This induces numerous load interaction effects that restrict the applicability of fatigue crack propagation (FCP) data obtained under constant stress amplitude loading [*1*]. The advent of servohydraulic testing machines followed by developments in service data acquisition and realtime computer control permit laboratory simulation of the complex service load environment on specimens, ranging from simple coupons to full-scale structures. However, while the testing technology is highly developed, it is yet to be streamlined by standard procedures such as ASTM Test Method for Constant-Load-Amplitude Fatigue Crack Growth Rates Above 10^{-8}m/cycle (E 647-83).

Between 1981 and 1986, many FCP tests under constant amplitude, programmed, and combat aircraft spectrum loading were carried out at the National Aeronautical Laboratory (NAL), Bangalore, India [*2–8*]. Procedures were developed to enable automated FCP testing under a variety of load sequences. This paper describes certain salient features of these procedures:

1. K-control under spectrum loading,
2. on-line fatigue cycle analysis (spectrum editing),
3. crack closure measurement, and
4. binary-coded marker loading.

It is generally accepted that under constant amplitude loading, crack growth rate is uniquely related to stress intensity, K. The results reported in this paper indicate that under spectrum

[1] Scientist, National Aeronautical Laboratory, Bangalore 560017, India; presently, NRC research associate, Air Force Wright Aeronautical Laboratories (AFWAL/MLLN), Wright-Patterson Air Force Base, OH 45433.

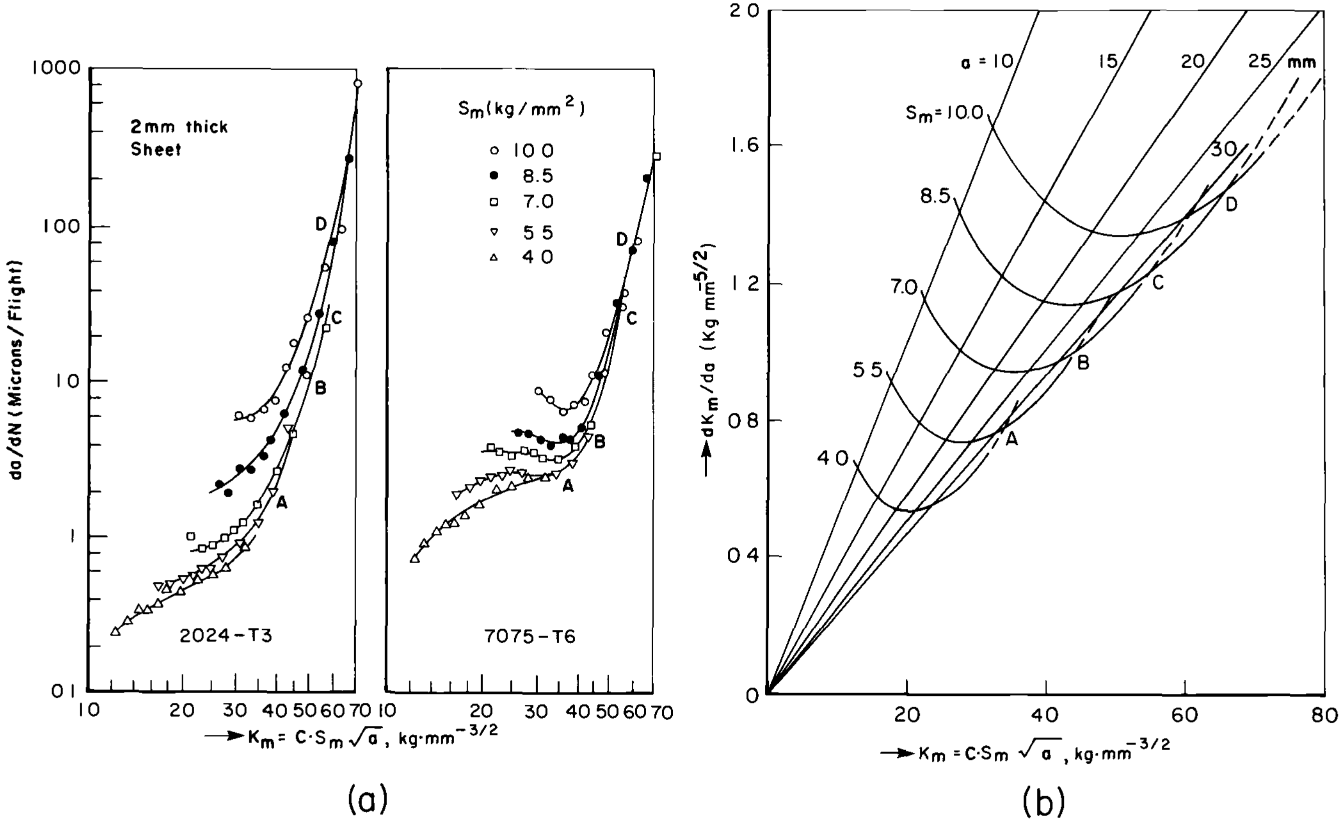

FIG. 1—(a) *Crack propagation rates under transport aircraft wing spectrum loading. Data for two aluminum-alloy sheet materials from 2-mm-thick center-cracked specimens tested at different design stress levels* [1]. (b) *Rate of change of stress intensity versus stress intensity for the different design stress levels* [1]. *Points A, B, C, and D correspond to points with similarity in both* K *and* dK/da.

loading, growth rate can be sensitive to *dK*/*da* (*K*-history), and also to net stress. The procedures described in the paper are intended to assist in conducting spectrum load FCP tests with *K*-control, on-line spectrum editing, and crack closure measurement. They also open up the possibility of studying threshold conditions under spectrum loading.

K-Control Under Spectrum Loading

Significance of dK/da *and Net Stress Effects*

Under constant amplitude loading, crack growth rate, *da*/*dN* is essentially a unique function of stress intensity range, ΔK, given the same stress ratio, material thickness, microstructure orientation, etc. ASTM E 647-83 assumes a *da*/*dN* versus ΔK relationship independent of stress level and crack geometry. Indeed, this is the basis of the fracture mechanics approach to FCP. Under spectrum loading, *da*/*dN* can be stress level dependent. Schijve et al. [9] found that *da*/*dN* under spectrum loading does not uniquely correlate with a characteristic stress intensity. At a given *K*, *da*/*dN* was found to be consistently higher in tests at higher design (1 g) stress (Fig. 1). This figure shows growth rates under a transport aircraft spectrum in 2-mm-thick 2024-T3 and 7075-T6. It was observed that similar growth rates occurred when both stress intensity as well as its derivative, *dK*/*da*, coincided (Points A, B, C, D).

Results from stress and *K*-controlled tests at NAL under combat aircraft spectrum loading [7] appear in Fig. 2 for 5-mm-thick aluminum-copper (Al-Cu) and 1-mm-thick aluminum-

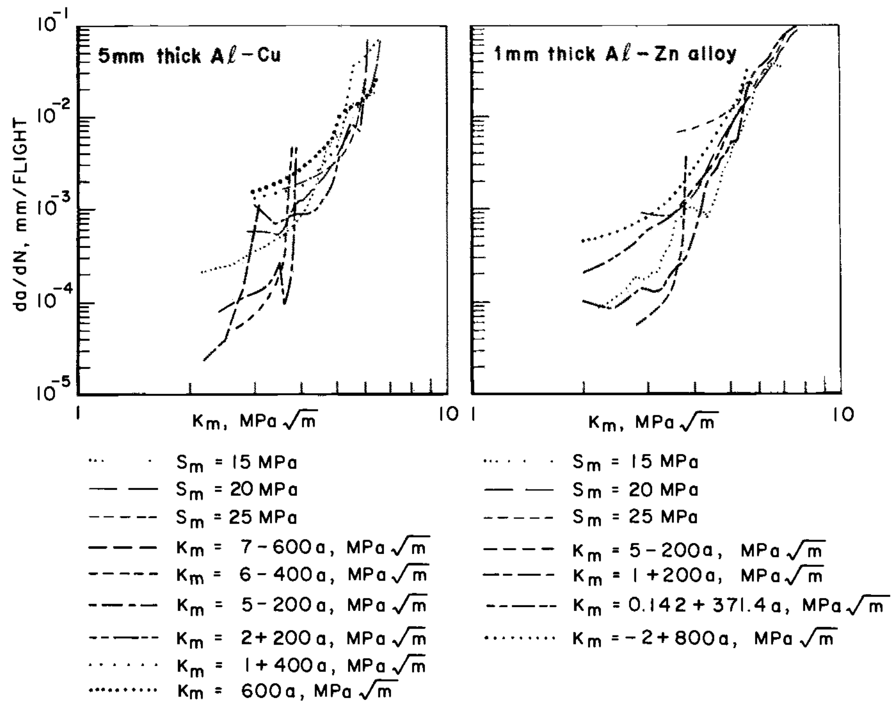

FIG. 2—*Crack growth rates in aluminum-alloy sheet material under combat aircraft spectrum loading* [7]. *Data for different conditions of stress and* K-*controlled spectrum loading.* K_m *and* S_m *refer to 1-*g *load.*

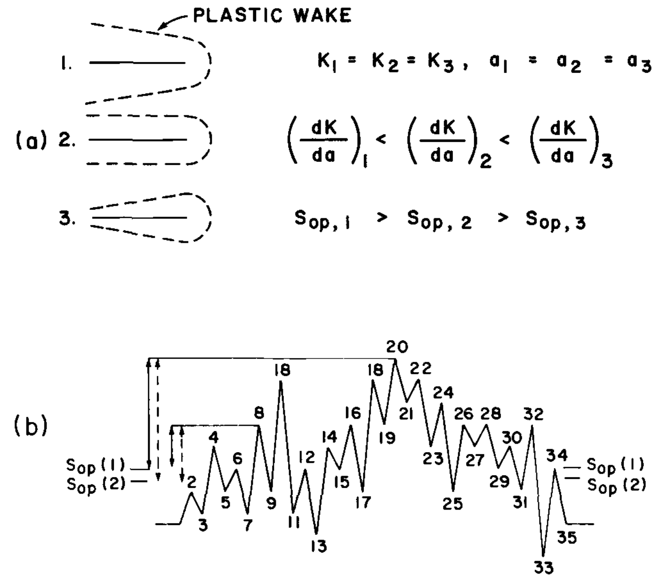

FIG. 3—(a) *Schematic of* dK/da *effect on plastic zone and wake (dotted line), which in turn will affect crack closure.* (b) *Even a small variation in closure stress,* S_{op}, *will cause a noticeable change in effective range of smaller cycles.*

zinc (Al-Zn) alloy sheet materials. The conventional stress-controlled tests were carried out at constant 1-g stress, S_m. Tests under K-control were under linear variation of 1-g stress intensity, K_m, with crack length, a (m), as described by the equations in the figure. These data show that da/dN at a given characteristic K can vary by up to an order of magnitude depending on the K-function simulated in the test. At similar stress intensity, crack growth rates under increasing stress intensity are as a rule greater than those under decreasing stress intensity. These variations were related to fatigue crack closure, which was found to be sensitive to the rate of change of stress intensity, dK/da, and even net section stress. Such effects are likely to go unnoticed under constant amplitude loading. Figure 3 schematically explains why they become significant under spectrum loading. Figure 3*a* is a schematic of the plastic wake for the three possible situations of decreasing, constant, and increasing stress intensity. At any given stress intensity (crack tip plastic zone size), the crack that saw a decreasing K would experience greater closure (due to the larger plastic wake). Figure 3*b* illustrates how a small closure variation can become significant under spectrum loading. Crack closure is controlled by the relatively large overloads like No. 20. Let us assume that it can change between S_{op} (1) and S_{op} (2), depending on dK/da and net stress (whose effect is discussed later in the paper). This variation will affect the effective range of individual cycles in a nonuniform fashion. In the relative sense, larger excursions like 9–10 and 17–18 will not be affected as dramatically as the more frequent smaller ones like 3–4, 5–6, and 7–8. Even a small change in closure stress can either totally "open up" or "eclipse" the large number of small load cycles. If these account for a large proportion of crack extension, growth rate becomes more sensitive to changes in closure stress.

If crack geometry and stress level sensitivity of FCP is related to fatigue crack closure, one should expect considerable variations in that sensitivity depending on the specific material and load spectrum being studied. This observation is supported by results from an analytical study on the sensitivity of predicted FCP life to small variations in closure stress

[10]. It was estimated that depending on the crack geometry and stress level, one can expect a 10 to 20% variation in closure stress level. The study used a closure—based crack growth life prediction model to compute the effect of small changes in crack closure stress on FCP life under different aircraft load spectra. The baseline material properties and load spectra were from an earlier ASTM sponsored study [11]. Some results are summarized in Fig. 4. Figure 4*a* shows how a 10 and 20% change in crack closure stress affects predicted life under constant amplitude, Instrumentation/Navigation (I/N) fighter spectrum, and transport aircraft spectrum loading. The data in Fig. 4*a* are for the 2219 alloy studied in [11]. Figure 4*b* contains results for the hypothetical case of higher baseline closure stress (50%). We find that the material baseline closure level and load spectrum determine the extent to which variations in closure stress (real or computed in models) will affect FCP life.

The I/N spectrum has a large number of smaller load cycles (less severe maneuvers and gusts) whose contribution to crack growth is controlled in much the same fashion as explained earlier in Fig, 3*b*. The transport spectrum also contains a large number of gust loads. The closure level, however, lies below these cycles and therefore does not affect their effective range.

An important implication of *dK*/*da* and net stress effects under spectrum loading concerns extrapolation of laboratory data. It reemphasizes an old question: Can FCP data and models

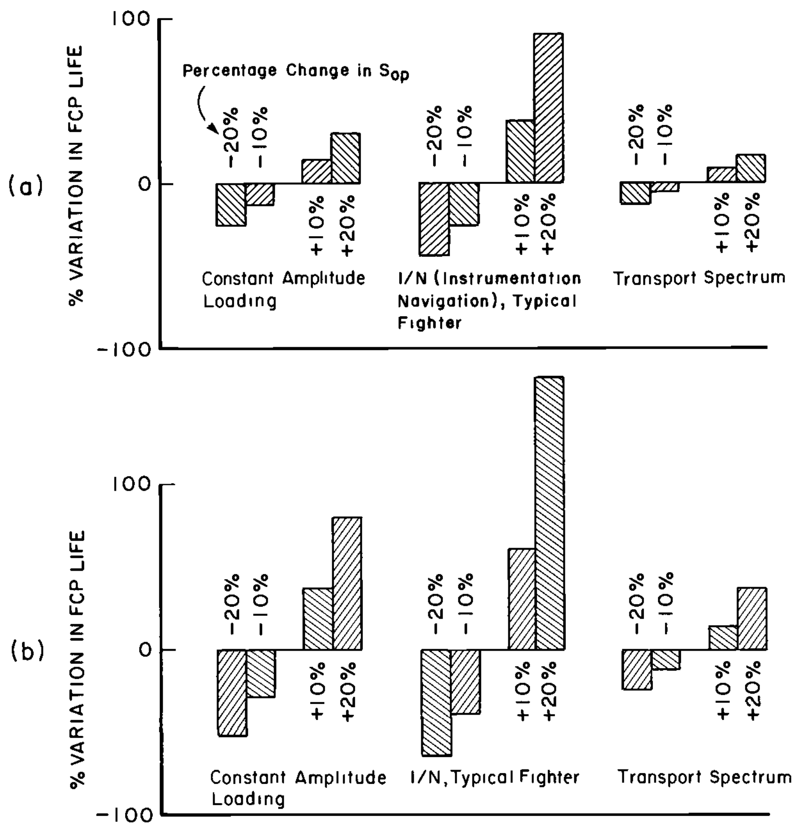

FIG. 4—*Effect of small variations in closure stress on FCP life predictions* [10]. *Load spectra from* [11]. *Data for 2219-T851 alloy sheet material* (S_{op}/S_{max} ~ *0.3*) (top) *and for a hypothetical case of higher closure level,* S_{op}/S_{max} = *0.5* (bottom).

obtained and evaluated on simple laboratory coupons be used to predict the endurance of more complex structural components?

The foregoing discussion points to a requirement for spectrum load FCP data on a variety of crack geometries and stress levels. Setting up a system with grips and fixtures to handle a variety of specimen geometries can be expensive. The exercise of studying FCP in larger and more complex geometries like stiffened panels is often beyond the means of smaller laboratories. This problem can be overcome by introducing the capability for *K*-controlled testing under spectrum loading.

Procedure for K-*Control*

K-controlled testing is common practice under constant amplitude loading and is a recommended procedure to determine *K*-threshold. Under spectrum loading, one has to deal with the problem of scaling each successive load reversal to achieve a preassigned charac-

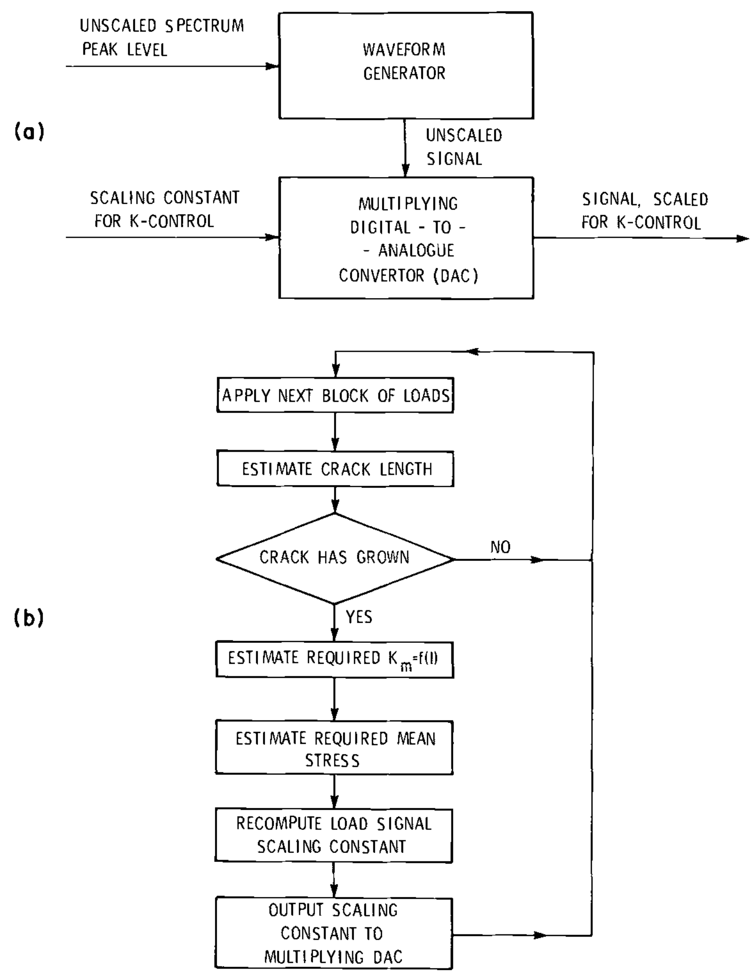

FIG. 5.—*Hardware circuit* (a) *and algorithm* (b) *for* K-*control under spectrum loading.*

teristic K-function. Many microcomputers used in realtime control may not be powerful enough to handle this, particularly at higher load frequencies. A hardware solution to this problem is described in Fig. 5*a*. It involves the attenuation of a "nondimensionalized" load signal to achieve the desired characteristic K. The attenuation factor requires recomputation only when the crack grows, thereby eliminating a major realtime overhead. The algorithm for a flight-by-flight K-controlled test appears in Fig. 5*b*. The test results shown in Fig. 2 were obtained using this procedure for K-control.

With K-control, any desired K-function can be simulated on standard laboratory test specimens. A rivet loaded geometry (decreasing K) can be simulated using center cracked specimens (increasing K). Large stiffened panels can be modeled using smaller specimens through K-function segmentation as shown in Fig. 6. The thick broken line in this figure is a schematic representation of stress intensity variation with crack length in a centrally cracked panel stiffened by stringers, whose axes are marked by dotted vertical lines. The half crack length interval from 10 to 175 mm is broken into eight 20-mm segments marked by the continuous vertical lines. Each of these segments can now be simulated on a smaller laboratory specimen through K-control. A small overlap of about 5 mm as shown by the vertical broken lines provides some continuity in data from consequent specimens. The overlap should be selected to ensure stabilization of the FCP process under spectrum loading.

Tests were conducted using the preceding "segmentation technique" to simulate crack growth in stiffened panels under spectrum loading. The results of these tests are in the process of consolidation. In these tests, growth rates in intervals with negative or low positive dK/da were two to five times less than at identical stress intensity in tests under conventional stress-controlled tests on single edge notch coupons. The ultimate validation of the simulation would be through comparison with a full-scale test on a stiffened wing panel. This exercise is yet to be carried out. A study was carried out at NLR [12] to evaluate various FCP life prediction models under transport wing spectrum loading. The one proposed by de Koning [13] provided the best predictions. The model showed good correlation with experimental data for center-cracked specimens. Interestingly, the FCP life for a stiffened panel (from the same material, subjected to the same type spectrum) was 3.5 times greater than that

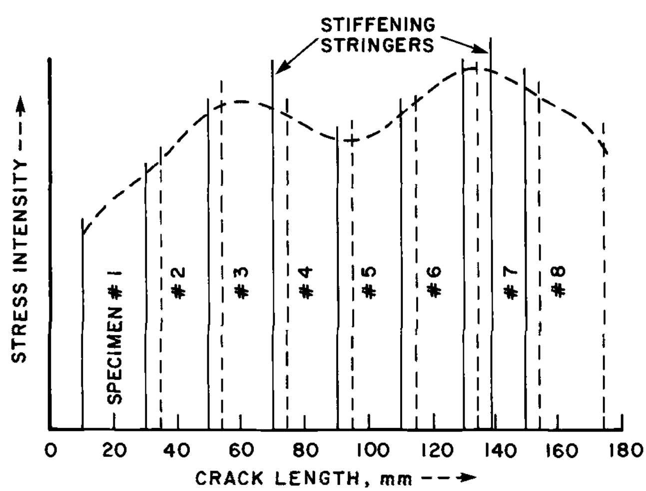

FIG. 6—*Schematic of how FCP in a stiffened panel can be modeled on multiple laboratory specimens of smaller size using* K-*control. A segment of the required* K-*function is simulated on each specimen, with an overlap to ensure continuity in data.*

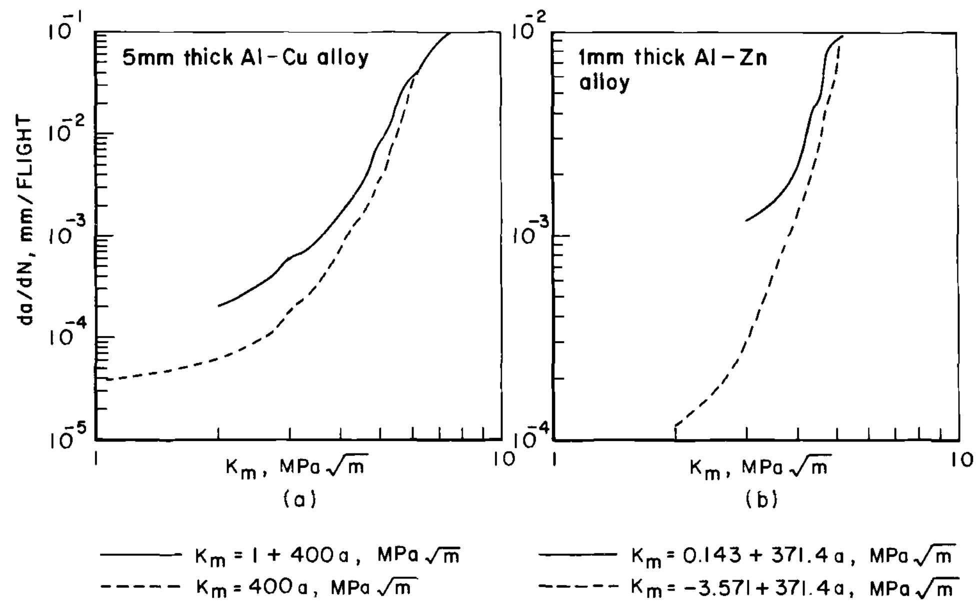

FIG. 7—*Effect of net stress on spectrum load* da/dN *in specimens of different thickness* [7]. *In these tests, the* K*-control functions were of identical slope, but with an offset to ensure identical* K *and* dK/da *and different net stress.*

predicted by the same model. There was no obvious inaccuracy in determining the *K*-function for the panel as evidenced by the correlation between prediction and experiment for constant amplitude loading.

K-control as described in Fig. 5 permits precise simulation of both *K* as well as *dK/da*. It however cannot ensure similarity in net stress. Figure 7 shows crack growth rates obtained from two *K*-controlled tests. In both, *K* and *dK/da* values were identical, but at different crack lengths due to an offset in the *K*-function. This provided similar *K* and *dK/da* with dissimilar net stress. We notice that given identical *K* and *dK/da, da/dN* is greater at higher net stress. This points to a drawback of the *K*-control procedure in Fig. 5.

Let us consider the relationship between stress level and crack closure. Maximum stress intensity, K_{max}, determines the size of the plastic zone that forms the stretched wake through which the crack will grow. The greater the stretch, the higher the load level at which the crack can close. Note hohwever, that once the crack is closed, the applied stress intensity becomes irrelevant—the crack tip stress field is now controlled by the wedge opening forces in the wake, residual stresses ahead of the crack tip, and the applied stress. Further downward excursion in load leads to compression of the crack tip region including the wake, with the material finally yielding in compression, thereby reducing the load at which the crack will subsequently open. Thus, while maximum stress intensity determines the extent to which crack closure can possibly occur, it is minimum stress (not minimum stress intensity) that finally limits closure to some level.

The preceding observations are supported by the results of analytical modeling performed by Newman [*11*] and also by analytical and experimental studies at the German Aerospace Research Lab (DFVLR) [*14*]. In the latter study, net stress rather than applied stress is identified as the controling variable. At small crack lengths, the difference between the two is negligible. However, a long crack experiencing closure cannot close over its entire length due to the wedge opening action of the crack tip area. Strictly speaking, the extent of wake transferring load through bearing will depend on prior K-history. One may observe from Fig. 3*a* that a larger section of the wake will transmit stress in compression if dK/da was negative. Specimen rotation in edge cracked specimens would also affect stress distribution in the wake. The influence of K-history and crack geometry on the behavior of a closed fatigue crack requires further study. At this point, one may assume that in compression, net section stress rather than applied (gross) stress will control crack opening load.

Combined Net Stress and K-*Control*

From the foregoing discussion, it follows that K-control alone is not adequate to ensure accurate simulation of the crack geometry and stress level of interest. To ensure similarity in the crack tip region in laboratory FCP tests using a standard geometry, two control functions are required. The K-function serves as the control function while the crack is open. Once the crack is closed, the net stress function needs to be simulated. This is an impractical proposition considering that prior information on closure is unavailable. For airframe load spectra, a fairly accurate approximation can be achieved by implementing K-control for tensile loads and net stress control for compressive loads (see Fig. 8). This ensures a more faithful simulation at least for the extreme loads. Experience shows that it is such loads that control closure behavior. Further, with the minimum stress of the (compressive) Ground-to-Air Cycle (GAC) occurring after each flight, a continuous net section stress simulation is assured. It must be noted that net stress control will be effective only when the crack is closed. This ensures that the feature will not directly affect stress intensity history experienced by the crack. Rather, the effect will be through crack closure.

On-Line Fatigue Cycle Analysis

Aircraft service load spectra are often characterized by load cycles whose frequency of occurrence is inversely proportional to magnitude. The load spectrum to be used in the test is obtained after some editing of the service load sequence. This includes load truncation and deletion of insignificant cycles. The load omission range is a critical parameter. A smaller omission range may considerably extend test duration without affecting test results. A larger range may noticeably reduce the severity of the load spectrum and lead to unconservative life estimates. Spectrum editing based on fatigue limit data for a given material can largely optimize load sequences used in crack initiation studies [*15,16*]. In such an exercise, one assumes that such time-dependent processes as corrosion and fretting are not present, that fatigue is cycle dependent and largely frequency independent. A growing crack precludes spectrum editing prior to the test. Any omission criteria would have to be stress intensity based and thereby related to crack length and so would have to change not only from material to material, but also with crack length in the same test. Specifically, one may proceed on the premise that a fatigue crack will not grow if the stress intensity range is below K-threshold, or, if K_{max} is below K_{op}.

Over the years, rainflow analysis has proved to be a powerful tool in cumulative damage analysis under random loading. Its physical basis stems from the link between closed fatigue cycles in a random sequence and their associated stress-strain hysteresis loops at the notch root. Such an analysis can be carried out on a realtime basis during an FCP test, to delete load cycles unlikely to contribute to crack extension.

Rainflow evolved around crack initiation studies and its validity was never established for

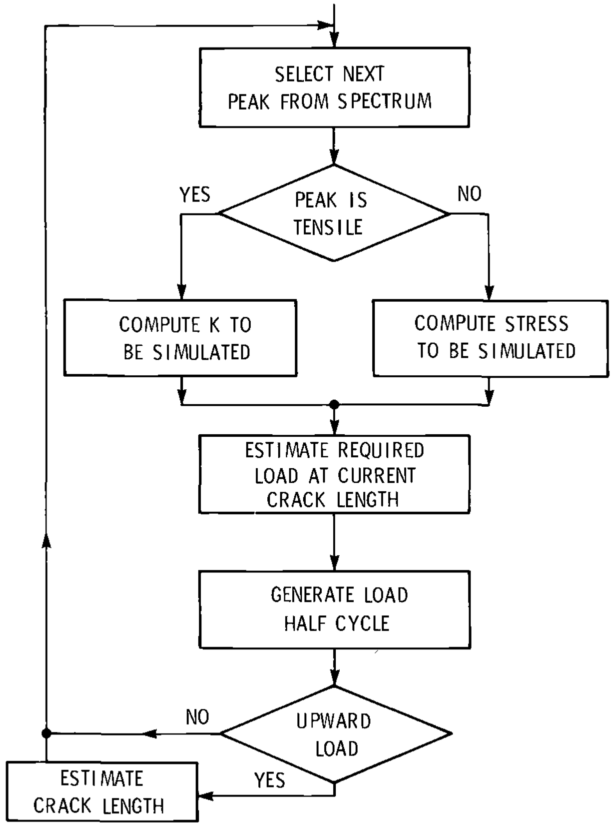

FIG. 8—*Algorithm for combined* K *and net stress control.*

FCP analysis. Experiments were carried out at NAL to evaluate different cycle counting techniques for FCP analysis [*6*]. The study provided conclusive fractographic evidence in support of the rainflow technique. Typical results appear in Fig. 9. Figure 9*a* shows a block of one of the load sequences used. Segments A and B are variations in load for which calculation of crack extension is complicated by the small cycles superimposed on large ones. Rainflow helps reduce such a sequence to one of independent "closed" fatigue cycles. Segments C and D actually contain multiple constant amplitude cycles. The mean and amplitude of these cycles were selected to be similar to each of the rainflow counted cycles from Segments A and B. Multiple cycles were used to ease fractography. Crack extension in one cycle could now be estimated by dividing that over many cycles by the number of cycles.

Figure 9*b* contains a typical fractograph covering three complete blocks of loads. The striations corresponding to individual segments are marked alphabetically. Striation D_0 was caused by the rising half cycle immediately after Segment B. To permit quantitative analysis, each fractograph was digitized as shown in Fig. 9*c*. Then, on the basis of area between striations, an "equivalent digital fractograph" was obtained (Fig. 9*d*).

Rainflow analysis would indicate identical crack extension over Segments A and B. Fur-

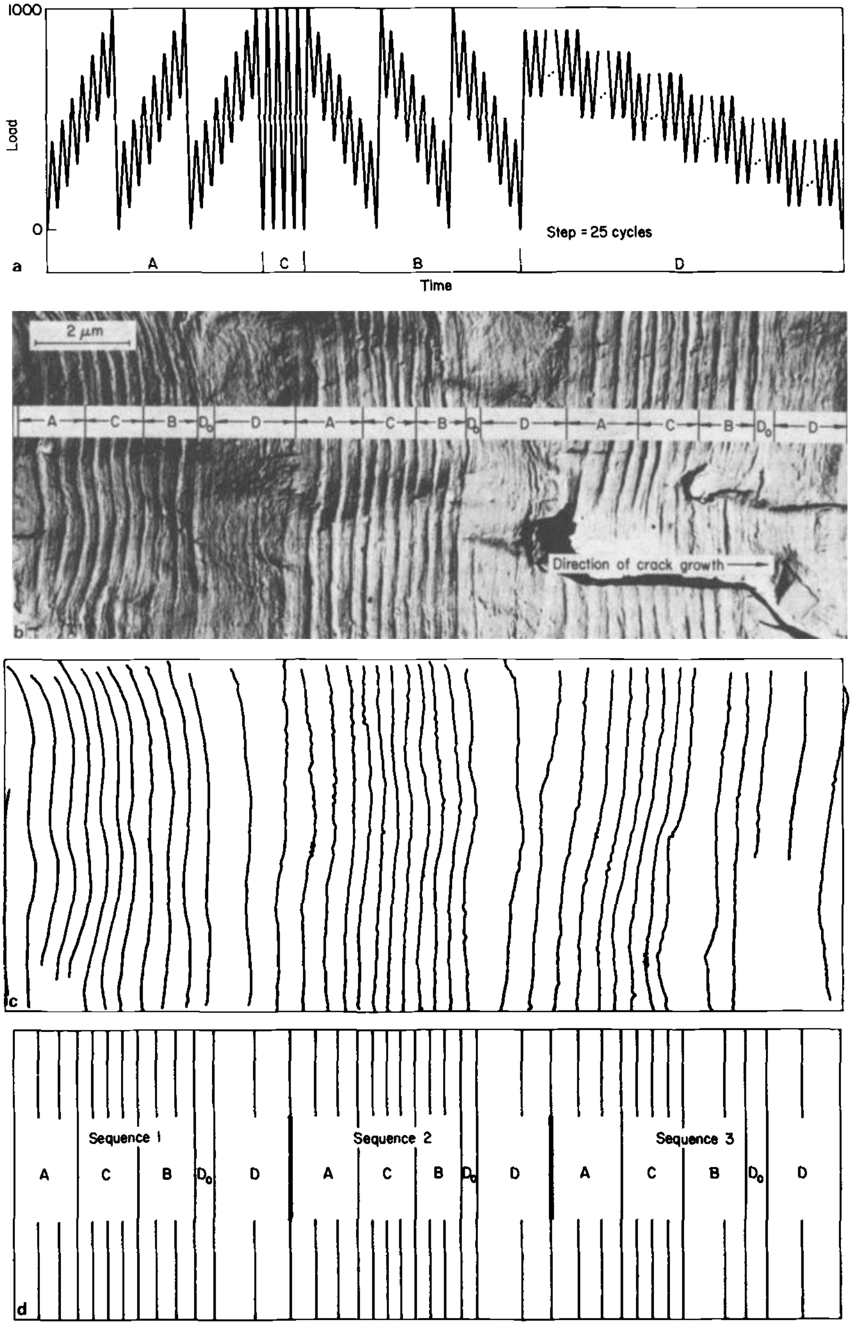

FIG. 9—*Fractographic validation of rainflow analysis.* (a) *Load sequence,* (b) *typical fractograph,* (c) *digitized image, and* (d) *averaged striation spacing.*

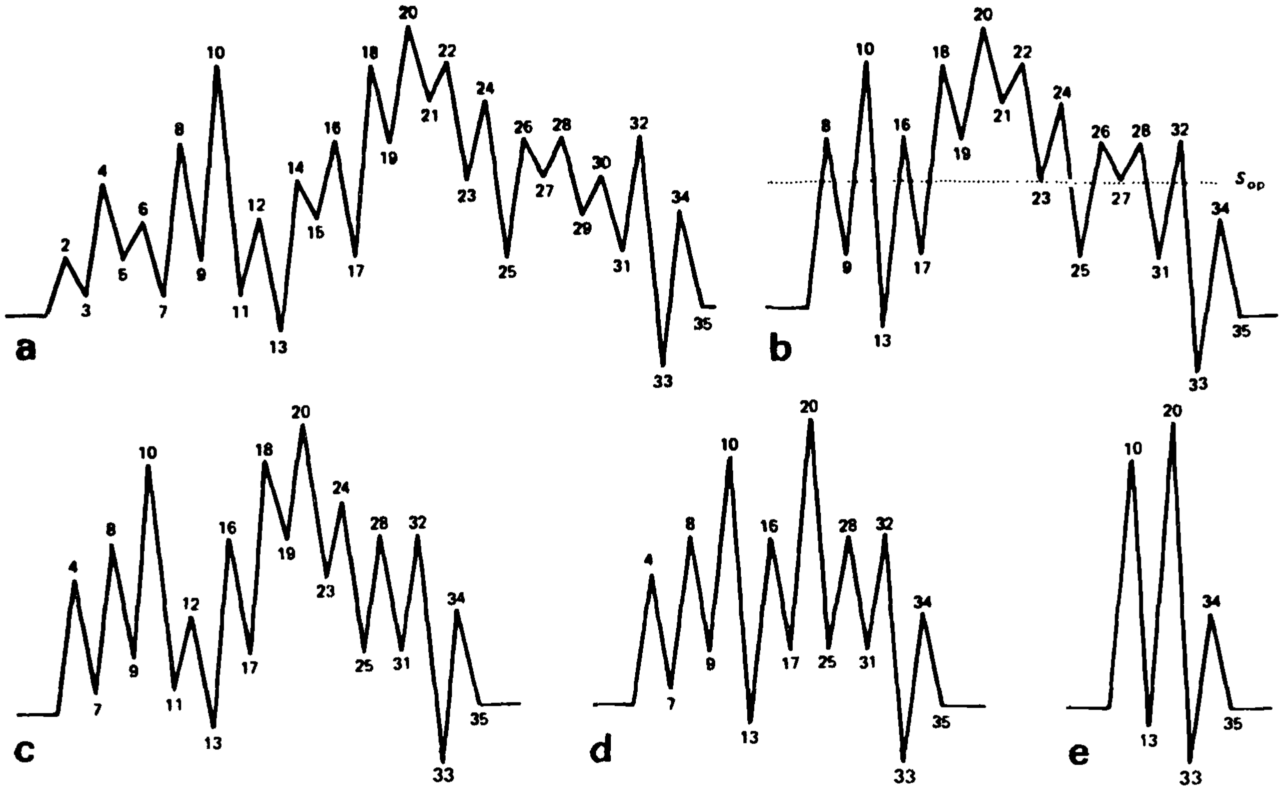

FIG. 10—*Consequences of on-line rainflow-based spectrum editing:* (a) *initial load sequence,* (b) *cycles below crack closure load omitted, and* (c,d,e) *cycles of progressively larger range omitted. Sequence cannot be condensed any further.*

ther, the crack extension in each of the three major cycles in Segments A and B would be equal to the cumulative extension due to one each of the load cycles in the steps in C and D (a total of seven counted cycles). The averaged data from the digitized fractographs support these conclusions, pointing to the validity of rainflow analysis of stress intensity history under random loading.

The significance of on-line rainflow analysis is schematically illustrated in Fig. 10. Consider the block of load cycles in Fig. 10*a*. If crack closure is known to occur at S_{op}, cycles whose maxima lie below this level are unlikely to contribute to crack extension and therefore could be deleted from the test (Fig. 10*b*). Cycles can also be omitted on the basis of threshold stress intensity range. Figures 10*c*–*e* show sequences with cycles of progressively larger range deleted (but no omission based on closure). In a decreasing K test, the sequence in Fig. 10*c* would be for a smaller crack length, the one in Fig. 10*e* for a larger length. Interestingly, the sequence in Fig. 10*e* cannot be condensed further due to the nature of the rainflow algorithm. This feature provides for an inherent safeguard. The service load history can be broken into blocks representing basic operational cycles, for example, one flight for an aircraft. If Rainflow analysis is performed on a flight-by-flight basis, at least the extreme reversals in each flight will always be applied on the specimen, irrespective of the omission criteria.

Basically, two different omission criteria are used in the test. The omission level refers

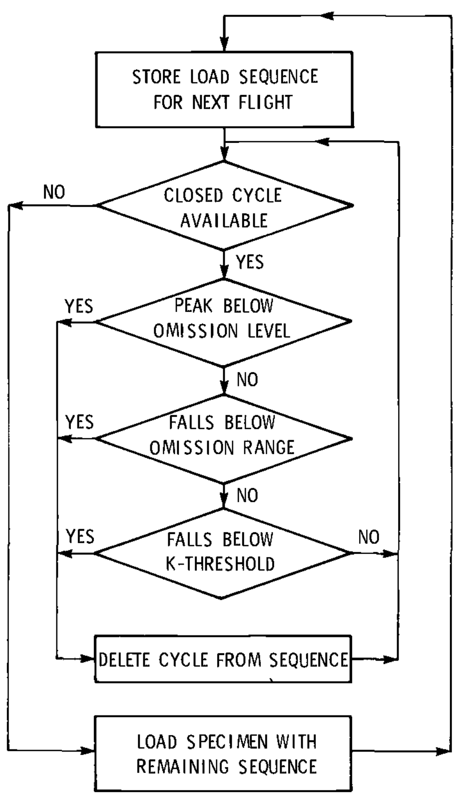

FIG. 11—*Algorithm for flight-by-flight rainflow-based load spectrum editing.*

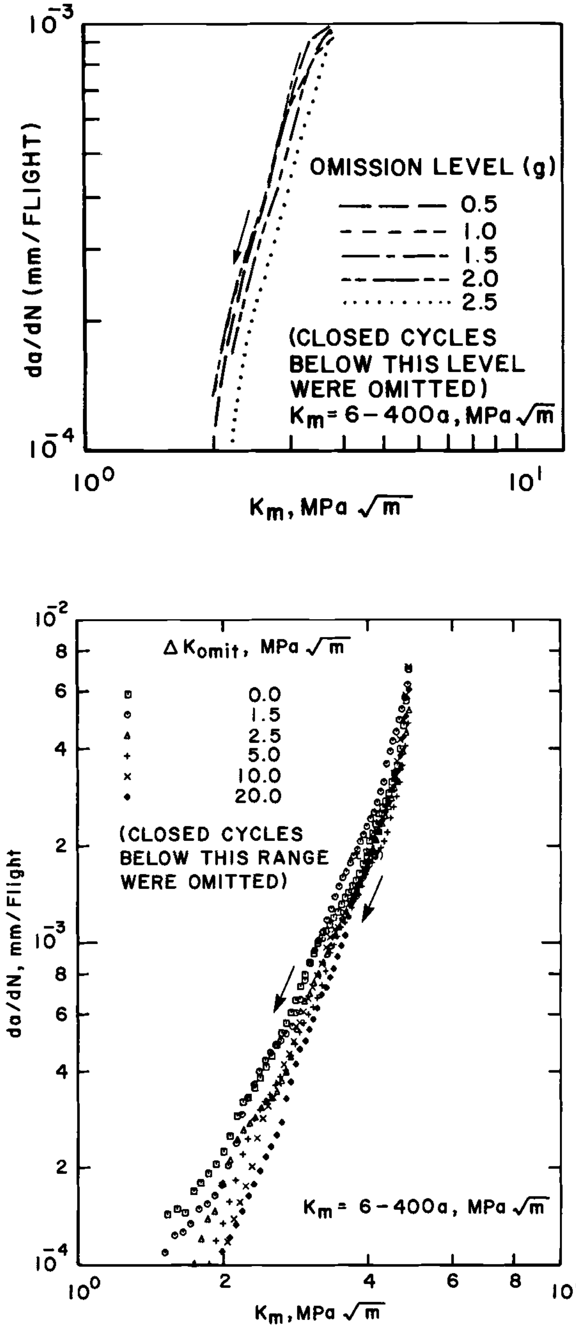

FIG. 12—*Results from tests on aluminum-alloy sheet specimens with on-line spectrum editing* [5]: (top) *tests with different omission level, and* (bottom) *tests with different omission* K-*range. All tests used the same linearly decreasing* K-*function. Spectrum clipped at 6* g. *The* K_m *relates to 1*-g *load.*

to a load level. Cycles whose maxima are below this level are omitted. The omission range looks at the (rainflow counted) range of a cycle. To be applied in the test, the cycle should occur above the specified omission level and further, its range should exceed the specified threshold. The clipping (truncation) level does not lead to cycle omission—loads exceeding this value are simply reduced to the specified level.

On-line rainflow analysis was implemented in automated FCP tests with *K*-control [5]. The algorithm for flight-by-flight spectrum editing appears in Fig. 11. Tests under combat aircraft spectrum loading showed that by omitting inconsequential cycles, test duration can be reduced by almost an order of magnitude with no change whatsoever in growth rates. The test control software caused a pause of about 100 ms between flights due to the overhead for rainflow analysis of the next 70 load reversals. The software would at this stage delete cycles meeting omission criteria. Frequency correction was carried out for each load excursion, taking crack length into account to ensure a more or less constant average load rate (large load excursions at lower frequency, smaller ones at higher frequency). This feature ensured a stable flow requirement on the servohydraulics and thereby reduced power requirements by achieving an average test frequency of 15 to 20 Hz using a low capacity (6 L/min) power pack. Conventional test systems require much greater flow rates to achieve high load rates during overload cycles.

The tests showed that even conservative omission criteria provided noticeable reduction in test duration. More importantly, on-line rainflow analysis opens up new avenues in spectrum load FCP testing. Consider the results in Fig. 12. These are from tests with *K* decreasing linearly with crack length. Figure 12 (*top*) shows growth rates from tests with different omission levels (closed cycles below which were omitted). The data fall into a single narrow band for omission levels up to 1.5 *g*. The 2-g omission level caused a small drop in growth rates. The omission level of 2.5 *g* caused a more noticeable drop. One may conclude from these data that crack closure occurred around 2 *g*—at about one third the clipping level used in the tests. Figure 12 (*bottom*) shows da/dN curves for different omission ranges specified in terms of stress intensity range. These data show that even an omission range close to threshold stress intensity (4 MPa/m) caused a drop in growth rates, indicating that the "true" threshold was closer to zero.

From the results in Fig. 12, one may conclude that on-line rainflow analysis can be used to determine the effective crack closure levels and threshold stress intensity for a given material and load spectrum. The latter is of particular significance. Threshold studies have hitherto been largely restricted to constant amplitude loading. The validity of constant amplitude threshold data for spectrum loading FCP is questionable. Near threshold constant amplitude, FCP is characterized by the predominance of such factors as oxide layer thickness and surface roughness. Spectrum loading involves a wide amplitude bandwidth of loads. Even at average growth rates in the threshold region or lower ($\sim 10^{-10}$ m/cycle), the (infrequent) overloads can cause crack extension in the so-called Paris regime (10^{-7} m/cycle or greater). Such cycles cause crack tip deformations that will overshadow the effect of oxide layer and even surface roughness. These loads can also cause crack branching that is very untypical of near threshold behavior. Further, the frequent compressive load excursions are likely to reduce any possible "build up" of closure normally attributed to near threshold FCP.

Essentially, there is little similarity between constant amplitude and spectrum load threshold behavior. It does not come as a surprise therefore that FCP prediction models tend to give unconservative results as growth rates approach the threshold region. Thresholds estimated from iterative tests with on-line rainflow-based spectrum editing will permit better understanding of near threshold spectrum loading FCP behavior.

Crack Closure Measurement

Development of standard procedures for measuring crack closure stress in laboratory tests under spectrum loading appears to be an attractive prospect in view of the significance of closure. An automated technique for closure measurement under spectrum loading was developed [5]. A schematic of the procedure appears in Fig. 13. It uses compliance measured from a crack mouth displacement gage. The algorithm does not involve subjective elements due to operator involvement or specification of an arbitrary percentage deviation in compliance as a criterion of closure. It yielded closure values that always correctly reflected the trends observed under both stress as well as *K*-controled loading [7]. However, accuracy and consistency in measurements remains an unresolved problem. To be of practical value (for example, in life predictions) crack closure stress intensity has to be determined with an error not exceeding a few percent of maximum stress intensity. As pointed out earlier, even small variations in closure stress have a dramatic effect under spectrum loading (see Fig. 4).

A closure measurement technique was developed for precision estimates of crack closure stress. It involves tests under specially designed programmed loading, followed by electron fractography [2]. Typical results appear in Fig. 14. The method assumes that striation spacing under a sequence of loads with constant maximum stress intensity can vary only if the minimum stress intensity or crack closure stress intensity or both change between cycles. For the block of loads in Fig. 14, the only plausible explanation for equally spaced striations is a constant closure level, lying above the minimum stress intensity. By counting off the number of equally spaced striations and relating them to the cycles in the load sequence, crack closure stress intensity is determined—with a known margin of error, equal to the

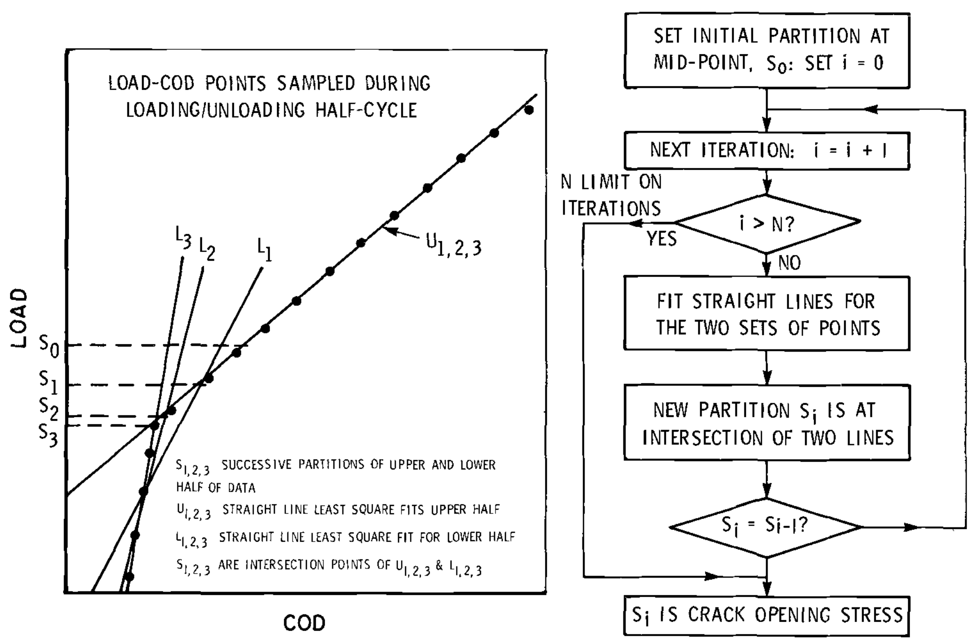

FIG. 13—*Schematic and algorithm for automated estimates of crack closing and opening load. The result of the iterative least square analysis gives the best bilinear fit for sampled crack opening displacement (COD) versus load data. Points close to maximum and minimum load can be deleted to avoid the effect of gage backlash and plasticity/crack extension.*

difference in minimum stress intensity between two successive cycles. The method gives a microscopically localized value of closure stress intensity. It can therefore be used to study closure variation across the crack front (thickness effects), in part-through cracks, etc.

The proposed method has its limitations. It cannot be used if the material, load sequence or environment is not conducive to striation formation. If too many cycles are introduced into the block to improve resolution, a subjective element can be introduced as views may differ on the exact number of equally spaced striations. The technique has been used successfully in a number of studies [*2,17–19*] on closure of through and part-through cracks at notches in aluminum alloy sheet material. This method is currently being used along with back face strain, COD-gage, and laser interferometry at the Air Force Materials Laboratory to study transitional crack closure behavior after an overload. Preliminary results indicate that none of the other three methods are able to detect crack closure variations, consistent with retardation after an overload. The fractographic observations of closure provide unique data on how closure varies across the crack front and with crack extension after an overload. The consistency and accuracy of the proposed method suggest that it can be used as a reference for other, more convenient techniques for closure measurement.

Binary-Coded Marker Loading

Load spectra simulated in the fatigue laboratory are a statistical representation of service conditions. Their duration, however, usually covers only a fraction of the total expected service life. A fatigue test often involves repeated application of the same block of load cycles representing the spectrum. This is convenient for purposes of studying the FCP process. The fracture surface shows successive bands (beach marks) that reflect repetition of the load block. These are macroscopic markers that show up under an optical microscope.

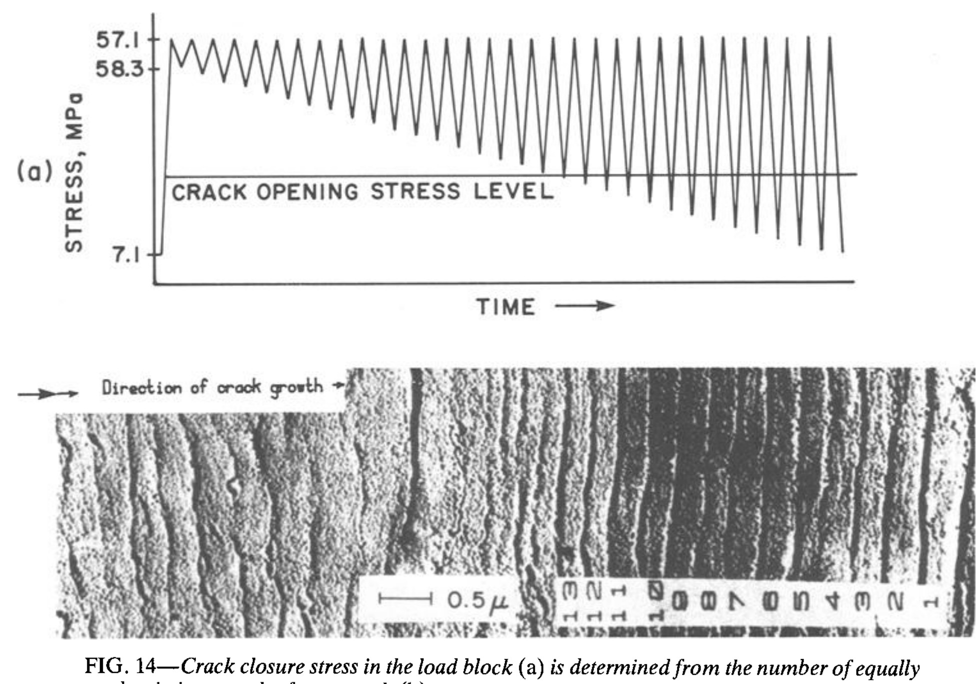

FIG. 14—*Crack closure stress in the load block* (a) *is determined from the number of equally spaced striations on the fractograph* (b).

A procedure was developed for microscopic marking of the fracture surface for subsequent event identification under the electron microscope [3]. The method uses blocks of binary-coded loads designed to leave behind digitally encoded striation patterns. A typical example appears in Fig. 15. It essentially consists of a sequence of cycles, each with either a "Hi" or "Lo" range, designed to leave behind either a wide (Hi) or narrow (Lo) fatigue striation. By suitably encoding the load sequence, information, is microscopically "punched" onto the fracture surface.

The binary-coded event marking technique proved to be indispensable in a recent study of crack closure in part-through cracks growing from a notch [17]. The crack closure load block coupled with a binary coded block carrying the encoded incremental block number (block counter reading) was used to initiate and propagate a corner crack. Different prior overloads were applied on the specimens to evaluate residual stress effects on closure. The fracture surfaces did not contain any macroscopically discernible features like beach marks. However, by studying fracture replicas under a transmission electron microscope, it was possible to map the crack front using block numbers punched on the fracture surface that

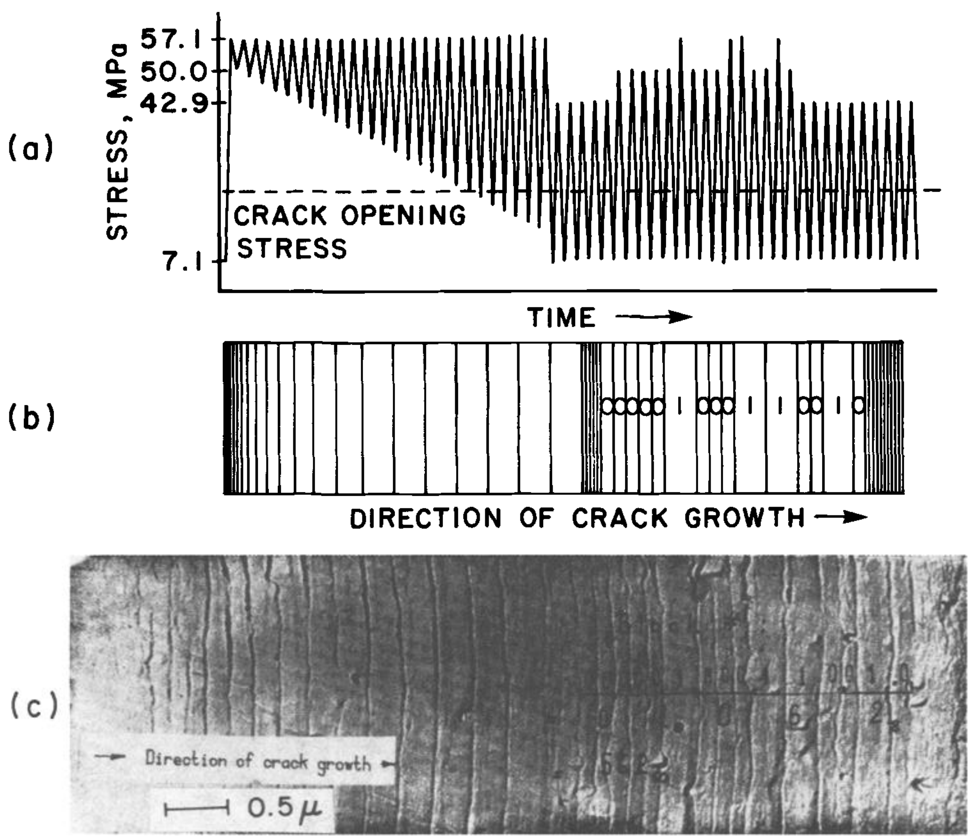

FIG. 15—*Typical results from a test using binary-coded loading.* (a) *Load block No. 562 with the left half containing the closure measurement sequence and the right half representing the binary code for 562. Spacer loads of smaller range were added before and after the binary coded sequence for identification. Expected striation pattern* (b) *after Elber equation for growth rate and* (c) *fractograph.*

recorded the progress of the crack. More importantly, the closure load blocks yielded information on the development of closure stress and its sometimes dramatic variation across the crack front.

Binary-coded marking has the same limitations as the fractographic closure measurement technique. It is unlikely to be of much use in tests with a broad amplitude band load spectrum that is likely to obliterate any useful striation patterns. Further, in using the closure and binary-coded blocks, one must ensure that they by themselves do not change the nature of the FCP process. This can be achieved by suitably ordering loads from the spectrum itself, rather than introducing new load cycles. Experience shows that sequence alterations within blocks (for example, flights) will not affect crack growth rate [*20,21*].

Summary

Experiments confirm the existence of noticeable dK/da (K-history) and net stress effects in spectrum load fatigue crack growth, which restrict the use of laboratory test data. These effects are related to fatigue crack closure and therefore imply that if the material does not develop significant closure stress (at least 20% of maximum applied stress), crack growth rates are likely to correlate uniquely with characteristic K. On the other hand, where closure is significant, appropriate stress levels and specimens have to be selected to ensure similarity with the crack geometry and service stress levels of interest. As this can often be impractical, it is proposed that procedures be standardized for K and net stress controlled testing on standard laboratory specimens under spectrum loading. The study points to the significance of closure measurements and its precise simulation in life prediction models. Models that are not closure-based have limited potential for success if closure effects are significant. Even closure-based models that are insensitive to dK/da and net stress effects can fail under more complex conditions.

On-line fatigue cycle analysis using the rainflow cycle counting technique provides a physical basis to edit load sequences in the course of a fatigue crack growth test. It can considerably reduce test duration without distorting results. More importantly, the procedure provides a unique opportunity to study crack closure and threshold stress intensity under spectrum loading. Spectrum loading threshold is an area of interest for future work in view of its impact on both Safe-Life and Fail-Safe design.

Specially designed program load sequences enable accurate measurements of fatigue crack closure. They can also serve as microscopic event markers on the fracture surface.

Acknowledgment

This paper was prepared while the author was a National Research Council Associate with the Air Force Materials Laboratory (AFML). The experimental work was carried out at the National Aeronautical Laboratory, Bangalore, India. The author is grateful to Dr. Theodore Nicholas at AFML for stimulating discussions and also to the ASTM reviewers for their constructive criticisms.

References

[*1*] Schijve, J. in *Fatigue Crack Growth under Spectrum Loads, ASTM STP 595,* American Society for Testing and Materials, Philadelphia, 1976, pp. 3–23.

[*2*] Sunder, R. and Dash, P. K., "Measurement of Fatigue Crack Closure Through Electron Microscopy," *International Journal of Fatigue,* Vol. 4, April 1982, pp. 97–105.

[*3*] Sunder, R., "Binary Coded Event Registration on Fatigue Fracture Surfaces," Technical Memorandum NAL-TM-MT-8-82, Bangalore, 1982; also, *Proceedings,* SEECO'83, B. J. Dabell, Ed.,

Society of Environmental Engineers, London, March 1983, p. 197.

[4] Sunder, R., "Automated Batch Processing of Fatigue Crack Propagation Tests," NAL-TM-MT-10-83, Bangalore, 1983; also, in *Advances in Fracture Research,* S. R. Valluri, et al., Eds., Pergamon, 1984, Vol. 5, pp. 3523–3531.

[5] Sunder, R., "System for Automated Crack Growth Testing under Random Loading," *International Journal of Fatigue,* Vol. 7, No. 1, 1985, pp. 3–12.

[6] Sunder, R., Seetharam, S. A., and Bhaskaran, T. A., "Cycle Counting for Fatigue Crack Growth Analysis," *International Journal of Fatigue,* Vol. 6, 1984, p. 147.

[7] Sunder, R., "Fatigue Crack Propagation under Stress and *K*-controlled Spectrum Loading," NAL-TM-MT-2-84; also, *Fatigue '84,* C. J. Beevers, Ed., Engineering Materials Advisory Services Ltd., Vol. 2, 1984, pp. 881–892.

[8] Sunder, R., "Crack Growth under Random Loading—Fatigue Cycle Analysis for Testing and Life Predictions," NAL TM-MT-9-84, Bangalore, 1984; (also, in Prochnost materialov i elementov konstruktsij pri zvukovykh i ultrazvukovykh chasthothakh nagruzheniya (V. A. Kuz'menko, Ed.,), Naukova Dumka, Kiev, 1986, pp. 93–102.

[9] Schijve, J., Jacobs, F. A., and Tromp, P. J., "Fatigue Crack Growth in Aluminium Alloy Sheet Material under Flight-Simulation Loading. Effect of Design Stress Level and Loading Frequency," NLR TR 72018, National Aerospace Laboratory, Amsterdam, 1972.

[10] Sunder, R., "Significance of Fatigue Crack Closure under Spectrum Loading," *Fatigue '87–Proceedings,* 3rd International Conference on Fatigue and Fatigue Thresholds, R. O. Ritchie and E. A. Starke, Eds., Engineering Materials Advisory Services Ltd., Vol. 1, 1987, pp. 185–194.

[11] *Methods and Models for Predicting Fatigue Crack Growth under Random Loading, ASTM STP 748,* J. B. Chang and C. M. Hudson, Eds., American Society for Testing and Materials, Philadelphia, 1981.

[12] Vlieger, H., "Damage Tolerance of Stiffened Skin Structures: Prediction and Experimental Verification," presented at 19th Annual Fracture Mechanics Symposium, American Society for Testing and Materials, San Antonio, June 1986.

[13] de Koning, A. U. in *Fracture Mechanics—13th Conference, ASTM STP 743,* Lane and Otten, Eds., American Society for Testing and Materials, Philadelphia, 1980, pp. 63–85.

[14] Marissen, R., Trautman, K. H., and Nowack, H., "The Influence of Compression Loads and of *dK/da* on the Crack Propagation under Variable Amplitude Loading," *Engineering Fracture Mechanics,* Vol. 19, No. 5, 1984, pp. 863–879.

[15] Conle, A. and Topper, T. H., "Evaluation of Small Cycle Omission Criteria for Shortening of Fatigue Service Histories," *International Journal of Fatigue,* Vol. 1, No. 1, 1979, pp. 23–28.

[16] Socie, D. F. and Artwohl, P. J. in *Effect of Load Spectrum Variables on Fatigue Crack Initiation and Propagation, ASTM STP 714,* D. F. Bryan and J. M. Potter, Eds., American Society for Testing and Materials, Philadelphia, 1980, pp. 3–23.

[17] Anandan, K. and Sunder, R., "Closure of Part Through Cracks at the Notch Root," Project Document MT8625, National Aeronautical Laboratory, Bangalore, 1986 (to appear in *International Journal of Fatigue,* 1987).

[18] Brahma, K. K., Sunder, R., and Dattaguru, B., "Automated Estimation of Fatigue Crack Length and Closure/Opening Stress," *International Journal of Fatigue,* Vol. 9, No. 1, 1987.

[19] Brahma, K. K., Dattaguru, B., and Sunder, R., "Effect of Temperature Exposure on Fatigue Crack Propagation," *Fatigue '87—Proceedings,* 3rd International Conference on Fatigue and Fatigue Thresholds, R. O. Ritchie and E. A. Starke, Eds., Engineering Materials Advisory Services Ltd., Vol. 11, 1987, pp. 1027–1036.

[20] Schijve, J., "Effect of Load Sequences on Crack Propagation under Random and Program Loading," *Engineering and Fracture Mechanics,* 1973, Vol. 5, pp. 269–280.

[21] Abelkis, P. R. in *Effect of Load Spectrum Variables on Fatigue Crack Initiation and Propagation, ASTM STP 714,* D. F. Bryan and J. M. Potter, Eds., American Society for Testing and Materials, Philadelphia, 1980, pp. 143–169.

Author Index

Subject Index

D

E

F

G

U

V

W